

INVESTIGATING A SYSTEMS APPROACH TO THE PREDICTIVE MODELING AND
ANALYSIS OF TIME-VARYING WOUND PROGRESSION AND HEALING

A Dissertation Presented
by

Jessica Chin

to

The Graduate School of Engineering

In partial fulfillment of the requirements
for the degree of

Doctor of Philosophy
in
Industrial Engineering



Northeastern University

Boston, Massachusetts

August 2013

UMI Number: 3594652

All rights reserved

INFORMATION TO ALL USERS

The quality of this reproduction is dependent upon the quality of the copy submitted.

In the unlikely event that the author did not send a complete manuscript and there are missing pages, these will be noted. Also, if material had to be removed, a note will indicate the deletion.



UMI 3594652

Published by ProQuest LLC (2013). Copyright in the Dissertation held by the Author.

Microform Edition © ProQuest LLC.

All rights reserved. This work is protected against unauthorized copying under Title 17, United States Code



ProQuest LLC.
789 East Eisenhower Parkway
P.O. Box 1346
Ann Arbor, MI 48106 - 1346

© Copyright 2013 by Jessica Selina Cho Chin
All Rights Reserved

ABSTRACT

Chronic wound is an important national healthcare problem, compounded by the fact that patients with chronic diseases, such as diabetes, are always vulnerable to developing chronic wounds. Wound care research has two strands: clinical and computational. On the clinical side, research has been focusing on how to effectively treat wounds. This includes measuring wounds, tracking their progression with time, and assessing their health. On the computational side, little has been done to treat a wound as an engineering system that needs to be modeled and analyzed with the ultimate goal of predicting the progress of wound healing and determining the factors that influence wound healing.

This dissertation presents three predictive statistical models: multiple linear regression, nonlinear regression, and neural networks and compares their performance. These models take wound parameters such as length, width, and depth as inputs and produce the remaining time to heal as an output. These predictive models also allow us to determine the wound parameters that are most influential on wound healing. These models are developed and analyzed with insight gained from four major wound clinics across the country.

The first predictive modeling technique that we analyze is multiple linear regression. We produce various linear regression models from the inputs, such as length, width, depth granulation, and necrotic tissue. The response variable is the time to heal for the respective wound. Since the data being analyzed deviated considerably from the linearity, the prediction results are poor, and confidence in the observations is weak.

The second type of predictive model constructs the foundation equation using survival analysis and Cox regression, a form of nonlinear regression relative to time-to-event situations. Survival analysis and Cox regression allows us to assess the relationship between the covariates and the probability of survival. The inputs for the Cox regression algorithms were length, width, depth, and granulation.

The output is the probability that a wound will “survive” until time t . This model provided the most accurate prediction results.

The third and final type of predictive model is based on neural networks. We design multiple feed-forward multilayer perceptron neural networks. They are all trained with a backpropagation algorithm. We used the same set of inputs that are used in the nonlinear regression models. The network output is the time it takes the wound to heal. Unlike Cox regression, the neural network model could not be individualized and therefore gave less accurate predictions. Further, we believe that patient demographics would have a considerable impact on the accuracy of the neural network models.

In conclusion, the research presented in this dissertation aims to offer a framework toward predicting chronic wound healing time. The outcomes of this project are beneficial to building a chronic wound predictive modeling system with the capabilities of integrating two-dimensional imaging and three-dimensional modeling with predictive analytics to provide patients and clinicians with an estimated time to wound closure. Two important extensions of this research are to further test and validate the assessment capabilities of using wound three-dimensional modeling by finding and selecting high-quality wound images and to incorporate wound imaging and statistical predictive models in an easy-to-use system for clinical practice.

ACKNOWLEDGMENTS

The past four years have been an incredible experience that allowed me to grow and mature both academically and professionally. I would like to take this opportunity to convey my gratitude to my PhD dissertation advisors, Dr. Abe Zeid and Dr. Sagar Kamarthi. Dr. Zeid and Dr. Kamarthi gave me the opportunity to pursue and develop parallel research interests in science/technology/engineering/mathematics (STEM) education and engineering. With their guidance, I developed the skills that are necessary to teach and solve complex problems. The combination of two uniquely separate research experiences provided me with a more rounded experience in how to conduct research. Through their tutelage, I learned how to approach and analyze intricate scientific problems and leverage past literature to generate new out-of-the-box ideas. Dr. Zeid and Dr. Kamarthi worked continuously to help me become a better critical thinker, a more scientific writer, and a better problem solver. I cannot thank them enough for their guidance and expertise.

There are individuals in this world who are kind enough to give their time to help a lone graduate student. I would like to thank a handful of individuals without whose help I would not have been successful. I would like to thank Dr. Tucker Marion for being on my committee. His insight into product design and development helped shape my research and future career. Dr. Scott Swain provided me with great insight beyond the world of basic statistics. Without his help, time, effort, and energy, I would not have understood how to use statistics and analytical modeling to develop my predictive models. His knowledge and expertise regarding how to analyze data and give meaning to numbers is uncanny, and I could not have found a nicer, smarter individual to guide me through the statistical analysis. Additionally, I would like to thank the wound care facilities: Tufts Vascular, Wound, and Hyperbaric Center; John Leopold, clinical manager at Morganti Wound Care Center; Dr. Shark Bird and Vohra Wound Care Physicians; and Andrew Citron, Dr. Michael Sears, Dawn Johnson, RN, and the staff at Raritan Bay Medical Center. Without these wound care facilities, I would not have been able to gather data, learn, and understand the intricacies of wound

care clinics and all that they do for their patients. Last, I would like to thank Flir Systems for providing me with a thermal imaging camera.

Without an incredible support network behind me, I would not have been able to pursue or complete my PhD. The core of my network is my parents. I would like to thank my parents, Tom and Joan, for their unbelievable love, unconditional support, and continued guidance. I thank my parents for teaching, guiding, and loving me throughout my years of education. They have offered endless inspiration and inspired confidence for me to pursue my next challenge.

I would also like to offer my special thanks to Frank Salcie. Without his humor and emotional support, my journey to PhD completion would have been much harder and a lot less fun. He was there for me when I needed to brainstorm and conceptualize problems. He has taught me the skills to approach, analyze, and solve problems from different perspectives. His support and endless encouragement have pushed me until the end! I would also like to thank Dr. and Mrs. Francisco and Diane Salcie, whose medical knowledge and encouragement, helped me to reaffirm my thoughts and analysis about chronic wound care.

I would also like to thank all my friends for all their support through the years. Special thanks to Keenan McLaren and Martha Legocki, my two very best friends since high school. I would also like to thank John and Arlene McLaren for their constant love, support, and encouragement! And I would also like to thank Dr. and Mrs. Brian and Maria Coan for their continued friendship and support!

Finally, I would like to thank the individuals in the Modeling, Analysis, and Prediction Laboratory: Amal Al-Husseini, Ilke Boyaci, Arjun Duvvuru, Srinivasan Radhakrishnan, Gulam Moeen Uddin, and Tony Sultornsanee. It has been a great pleasure to work with you and be your colleague.

TABLE OF CONTENTS

ABSTRACT	IV
ACKNOWLEDGEMENTS	VI
TABLE OF CONTENTS	VIII
LIST OF FIGURES	XI
LIST OF TABLES	XV
1 CHAPTER 1 INTRODUCTION	2
1.1 OVERVIEW	2
1.2 MOTIVATION	4
1.3 OPEN RESEARCH ISSUES	5
1.4 PROBLEM DEFINITION AND OBJECTIVE	7
1.5 PROPOSED SOLUTION	7
1.6 DISSERTATION CONTRIBUTION	9
2 CHAPTER 2 LITERATURE REVIEW	14
2.1 INTRODUCTION	14
2.2 WOUND TOPOLOGY MODELING	15
2.3 PREVIOUS STUDIES: A REVIEW OF WOUND ASSESSMENT TECHNIQUES	15
2.4 NONINVASIVE WOUND MEASUREMENT TECHNIQUES	20
2.5 SUMMARY	20
3 CHAPTER 3 CHRONIC WOUNDS	24
3.1 BIOLOGY OF A WOUND	24
3.2 WOUND HEALING	26
3.3 WOUND CLASSIFICATIONS	27
3.4 CHRONIC WOUNDS ON LOWER APPENDAGES	28
3.5 WOUND TREATMENTS	29
3.6 ISSUES IN WOUND CARE CLINICAL PRACTICE	30

4	CHAPTER 4 WOUND ASSESSMENT METHODS	36
4.1	CURVATURE-MAPS-BASED METHOD	36
4.2	THREE-DIMENSIONAL CONSTRUCTION-BASED METHOD	37
4.3	DIGITAL CONSTRUCTION-BASED METHOD	37
4.4	COMMERCIAL SYSTEMS	38
4.5	TELEMEDICINE WOUND MANAGEMENT	40
4.6	EXISTING PREDICTIVE METHODS	42
4.7	SUMMARY	43
5	CHAPTER 5 WOUND PARAMETERS	45
5.1	TUFTS VASCULAR, WOUND, AND HYPERBARIC CENTER	45
5.2	MORGANTI WOUND CENTER AT DANBURY HOSPITAL	46
5.3	RARITAN BAY MEDICAL CENTER: THE CENTER FOR WOUND CARE	48
5.4	VOHRA WOUND CARE PHYSICIANS	48
5.5	WOUND CARE CLINIC SUMMARY	49
5.6	INDEPENDENT PARAMETER CORRELATIONS AND RELATIONSHIPS	50
5.7	PARAMETER CORRELATION	53
5.8	SUMMARY	53
6	CHAPTER 6 PRELIMINARY STUDY	55
6.1	DATA COLLECTION	55
6.2	STATISTICAL IMPLICATIONS	59
6.3	MODEL VALIDATION AND VERIFICATION	62
6.4	SUMMARY	64
6.5	LIMITATIONS	64
6.6	PRELIMINARY STUDY ANALYSIS	65
7	CHAPTER 7 WOUND HEALING MODELING METHODOLOGY	67
7.1	METHODOLOGY OVERVIEW	67
7.2	REGRESSION ANALYSIS	69
7.3	NONLINEAR-REGRESSION ANALYSIS	71
7.4	NEURAL-NETWORK ANALYSIS	73
7.5	THREE-DIMENSIONAL CAD GEOMETRIC MODEL	77
7.6	THERMAL-IMAGING (THERMOGRAPHY) MODEL	79
7.7	SUMMARY	84
8	CHAPTER 8 WOUND DATA COLLECTION, PREPROCESSING	86
8.1	DATA COLLECTION	86
8.2	DATA-MINING METHOD SELECTION	88
8.3	DATA PREPROCESSING: STAGE I	90
8.4	GEOMETRICAL ANALYSIS	99

8.5	DATA PREPROCESSING: STAGE II	114
8.6	SUMMARY	150
9	CHAPTER 9 WOUND HEALING PREDICTIVE MODEL	153
9.1	MULTIPLE LINEAR REGRESSION	153
9.2	NONLINEAR REGRESSION: SURVIVAL ANALYSIS	154
9.3	NEURAL-NETWORK ANALYSIS	173
9.4	VALIDATION	188
10	CHAPTER 10 MODEL VALIDATION AND VERIFICATION	196
10.1	OVERVIEW	196
10.2	DATA COLLECTION	198
10.3	THREE-DIMENSIONAL SURFACE PLOTS	203
10.4	VALIDATING PREDICTIVE MODELS AND THE METHODOLOGY	216
11	CHAPTER 11 ANALYSIS OF WOUND COMPUTATIONAL MODELS	231
11.1	IMPLICATIONS	231
11.2	ASSUMPTIONS AND LIMITATIONS	240
12	CHAPTER 12 CONCLUSIONS AND FUTURE WORKS	242
12.1	CONCLUSION	242
12.2	FUTURE WORK	243
	APPENDIX	245
	APPENDIX A: PRELIMINARY STUDY RAW DATA	246
	APPENDIX B: RARITAN AY MEDICAL CENTER AFFILIATION AGREEMENT	247
	APPENDIX C: VOHRA WOUND CARE PHYSICIANS DATA AGREEMENT	251
	APPENDIX D: THERMACAM S65 TECHNICAL SPECIFICATIONS	255
	APPENDIX E: MATLAB CODE, DATA CLEANING	256
	APPENDIX F: MATLAB CODE, IMAGE ANALYSIS AND EDGE DETECTION	269
	REFERENCES	273

LIST OF FIGURES

FIGURE 1.1: INPUT – ANALYSIS - OUTPUT.....	10
FIGURE 2.1: EXAMPLE OF WOUND MODELING IN SOLIDWORKS™ SOFTWARE	15
FIGURE 2.2: BARONE ET AL. WOUND IMAGES FROM DIFFERENT IMAGING MODALITIES [22]	17
FIGURE 2.3: APPROXIMATE GEOMETRIC SHAPE ESTIMATIONS OF WOUNDS [52].....	19
FIGURE 3.1: EARLY PHASE OF WOUND HEALING.....	27
FIGURE 3.2: EARLY PHASE OF WOUND HEALING.....	27
FIGURE 3.3: SCHEMATIC DIAGRAM OF ANATOMY OF SKIN [2, 71].....	28
FIGURE 3.4: WOUND DIAGNOSTIC TRIANGLE DILEMMA	32
FIGURE 3.5: SUMMARY OF RBMC PATIENT PROCEDURE.....	34
FIGURE 4.1: VISITRAK TRACING METHODOLOGY [80]	39
FIGURE 4.2: VERG WOUND MEASUREMENT SYSTEM [52].....	39
FIGURE 4.3: MAVIS-II THREE-DIMENSIONAL WOUND MEASUREMENT INSTRUMENT [48, 53]	40
FIGURE 4.4: WOUNDSMART® APP USER INTERFACE [83].....	41
FIGURE 4.5: WOUND ANALYZER APP USER INTERFACE [84]	42
FIGURE 5.1: CORRELATION PLOT DISPLAYED AS HEAT MAP	51
FIGURE 5.2: CORRELATION SCATTER PLOT.....	52
FIGURE 6.1: WOUND IMAGES OF A PATIENT’S HEEL WOUND	57
FIGURE 6.2: GRAPH OF RAW DATA AND THEIR ESTIMATED REGRESSION EQUATIONS	58
FIGURE 6.3: DISTRIBUTION OF TIME TO HEAL IN WEEKS	64
FIGURE 7.1: TIME TO HEAL CHRONIC METHOD	68
FIGURE 7.2: NEURON MODEL [100].....	74
FIGURE 7.3: LEARNING WITH A TEACHER [100]	75
FIGURE 7.4: LEARNING WITHOUT A TEACHER, REINFORCEMENT LEARNING [100]	76
FIGURE 7.5: UNSUPERVISED LEARNING [100].....	76
FIGURE 7.6: EDGE DETECTION TO SPLINE CREATION METHODOLOGY	78
FIGURE 7.7: CIELAB COLOR SPACE [105, 106].....	79
FIGURE 7.8: IMAGE PROCESSING FOR THERMAL IMAGING IN MEDICINE [53].....	82
FIGURE 7.9: CALCULATION OF TI/WOUND INFLAMMATORY INDEX [14] AT BASELINE FOR THE TEST SUBJECT [109].	83
FIGURE 8.1: IRB PROCESS FOR RBMC AND VOHRA.....	88
FIGURE 8.2: DATA-PREPARATION METHODOLOGY	89

FIGURE 8.3: INDEPENDENT VARIABLE-DATA PREPARATION	90
FIGURE 8.4: MATLAB® METHODOLOGY TO CLEAN DATA	91
FIGURE 8.5: BOX PLOTS OF LENGTH 1	93
FIGURE 8.6: BOX PLOTS OF LENGTH 2	93
FIGURE 8.7: BOX PLOTS OF LEFT AND RIGHT DOPPLER	94
FIGURE 8.8: BOX PLOTS OF PREALBUMIN AND ALBUMIN	95
FIGURE 8.9: SUBNEURAL-NETWORK METHODOLOGY FOR MISSING DEPTH VALUES	97
FIGURE 8.10: BOX PLOTS OF DEPTH AFTER PREDICTED VALUES	99
FIGURE 8.11: IMAGE-ACQUISITION AND -ANALYSIS METHODOLOGY.....	100
FIGURE 8.12: PATIENT 11 IMAGE ANALYSIS.....	101
FIGURE 8.13: PATIENT 11: WOUND EDGE	102
FIGURE 8.14: PATIENT 2: RGB IMAGE AND BINARY IMAGE WITH SCALE.....	103
FIGURE 8.15: PATIENT 2: WOUND EDGE.....	104
FIGURE 8.16: PATIENT 2: WOUND-EDGE TWO-DIMENSIONAL MATRIX OF XY COORDINATES	104
FIGURE 8.17: PATIENT 4: IMAGE ANALYSIS	105
FIGURE 8.18: PATIENT 4: WOUND EDGE.....	106
FIGURE 8.19: PATIENT 4 FINAL WOUND OUTLINE ANALYZED IN MATLAB.....	106
FIGURE 8.20: FLIR THERMACAM S65 THERMAL-IMAGING SYSTEM	107
FIGURE 8.21: PATIENT 15 IMAGE COMPILATION	108
FIGURE 8.22: PATIENT 2 PIXEL-TO-CENTIMETER CONVERSION	109
FIGURE 8.23: SCANTO3D METHODOLOGY	111
FIGURE 8.24: BOUNDARY-TRACE PROCESS	112
FIGURE 8.25: VARIOUS VIEWS OF PATIENT 11'S WOUND SHAPE AND BOUNDARY	113
FIGURE 8.26: ASPECT RATIO OF LESS THAN 1, VOLUME VERSUS TIME	116
FIGURE 8.27: ASPECT RATIO OF LESS THAN 1, VOLUME VERSUS TIME.....	117
FIGURE 8.28: ASPECT RATIO OF LESS THAN 1, LENGTH 1 VERSUS TIME	118
FIGURE 8.29: ASPECT RATIO OF LESS THAN 1, LENGTH 1 VERSUS TIME	119
FIGURE 8.30: ASPECT RATIO OF LESS THAN 1, LENGTH 2 VERSUS TIME	120
FIGURE 8.31: ASPECT RATIO OF LESS THAN 1, LENGTH 2 VERSUS TIME	121
FIGURE 8.32: ASPECT RATIO OF LESS THAN 1, DEPTH VERSUS TIME	122
FIGURE 8.33: ASPECT RATIO OF LESS THAN 1, DEPTH VERSUS TIME.....	123
FIGURE 8.34: ASPECT RATIO OF 1 TO 2, VOLUME VERSUS TIME.....	124
FIGURE 8.35: ASPECT RATIO OF 1 TO 2, VOLUME VERSUS TIME.....	125
FIGURE 8.36: ASPECT RATIO OF 1 TO 2, LENGTH 1 VERSUS TIME.....	126
FIGURE 8.37: ASPECT RATIO OF 1 TO 2, LENGTH 1 VERSUS TIME.....	127
FIGURE 8.38: ASPECT RATIO OF 1 TO 2, LENGTH 2 VERSUS TIME.....	128
FIGURE 8.39: ASPECT RATIO OF 1 TO 2, LENGTH 2 VERSUS TIME.....	129
FIGURE 8.40: ASPECT RATIO OF 1 TO 2, DEPTH VERSUS TIME.....	130
FIGURE 8.41: ASPECT RATIO OF GREATER THAN 2, VOLUME VERSUS TIME.....	131
FIGURE 8.42: ASPECT RATIO OF GREATER THAN 2, LENGTH 2 VERSUS TIME.....	132

FIGURE 8.43: ASPECT RATIO OF GREATER THAN 2, DEPTH VERSUS TIME.....	133
FIGURE 8.44: WOUND-HEALING TRAJECTORY APPROACHING AN ASYMPTOTE OF 0	135
FIGURE 8.45: VOLUME BOX PLOT FOR AN ASPECT RATIO OF 1	136
FIGURE 8.46: VOLUME BOX PLOT FOR ASPECT RATIO OF 2	140
FIGURE 8.47: LENGTH 1 BOX PLOT FOR ASPECT RATIO GREATER THAN 1 AND LESS THAN 2	143
FIGURE 8.48: LENGTH 2 BOX PLOT FOR ASPECT RATIO GREATER THAN 1 AND LESS THAN 2	143
FIGURE 8.49: DEPTH BOX PLOT FOR ASPECT RATIO OF GREATER THAN 1 AND LESS THAN 2.....	144
FIGURE 8.50: VOLUME BOX PLOT FOR ASPECT RATIO=3	145
FIGURE 8.51: LENGTH 1 BOX PLOT FOR ASPECT RATIO > 2	148
FIGURE 8.52: LENGTH 2 BOX PLOT FOR ASPECT RATIO > 2	148
FIGURE 8.53: DEPTH BOX PLOT FOR ASPECT RATIO OF GREATER THAN 2	149
FIGURE 9.1: SURVIVAL FUNCTION AT MEAN OF COVARIATES.....	157
FIGURE 9.2: ONE MINUS SURVIVAL FUNCTION AT MEAN OF COVARIATES	158
FIGURE 9.3: HAZARD FUNCTION AT MEAN OF COVARIATES	159
FIGURE 9.4: SURVIVAL FUNCTION AT MEAN OF COVARIATES.....	160
FIGURE 9.5: SURVIVAL FUNCTION DIFFERENTIATED BY ASPECT RATIOS	161
FIGURE 9.6: BASELINE CUMULATIVE HAZARD	162
FIGURE 9.7: SURVIVAL FUNCTION AT MEAN OF COVARIATES.....	168
FIGURE 9.8: LOG-MINUS-LOG PLOT.....	169
FIGURE 9.9: BASELINE CUMULATIVE HAZARD	170
FIGURE 9.10: NEURAL-NETWORK MODEL FOR DATA WITH ASPECT RATIO OF LESS THAN 1	174
FIGURE 9.11: LIFT CHART FROM NEURAL-NETWORK MODEL FOR DATA WITH AR < 1, TRAINING DATASET	176
FIGURE 9.12: LIFT CHART FROM NEURAL-NETWORK MODEL FOR DATA WITH ASPECT RATIO OF LESS THAN 1, VALIDATION DATA SET	177
FIGURE 9.13: NEURAL NETWORK MODEL FOR DATA WITH AR < 1 AND RBMC	178
FIGURE 9.14: NEURAL-NETWORK MODEL FOR DATA WITH ASPECT RATIO GREATER THAN 1 AND LESS THAN 2	179
FIGURE 9.15: NEURAL NETWORK MODEL FOR DATA WITH $1 < \text{ASPECT RATIO} \leq 2$ AND RBMC.....	181
FIGURE 9.16: NEURAL-NETWORK MODEL FOR DATA WITH ASPECT RATIO 1 AND RBMC.....	183
FIGURE 9.17: NEURAL-NETWORK MODEL FOR DATA WITH ASPECT RATIO GREATER THAN 2, RBMC.....	187
FIGURE 9.18: EXAMPLE OF SURVIVAL FUNCTION VS. TIME FOR SAMPLE WOUNDS (VARIABLES: LENGTH 1, LENGTH 2, DEPTH, GRANULATION).....	190
FIGURE 9.19: EXAMPLE OF SURVIVAL FUNCTION VERSUS TIME FOR SAMPLE WOUNDS (ALL VARIABLES)	191
FIGURE 10.1: BOX PLOTS FOR RBMC DATA	197
FIGURE 10.2: LENGTH 1 VERSUS TIME.....	199
FIGURE 10.3: LENGTH 2 VERSUS TIME	200
FIGURE 10.4: DEPTH VERSUS TIME	201
FIGURE 10.5: VOLUME VERSUS TIME	202
FIGURE 10.6: SURFACE PLOT: TIME TO HEAL AGAINST LENGTH 1, LENGTH 2 (QUADRATIC FIT)	204
FIGURE 10.7: SURFACE PLOT: TIME TO HEAL AGAINST LENGTH 1, LENGTH 2 (SPLINE FIT).....	205
FIGURE 10.8: SURFACE PLOT: TIME TO HEAL AGAINST LENGTH 1, LENGTH 2 (LINEAR FIT).....	206

FIGURE 10.9: SURFACE PLOT: TIME TO HEAL AGAINST LENGTH 1, LENGTH 2 (QUADRATIC FIT)	207
FIGURE 10.10: SURFACE PLOT: TIME TO HEAL AGAINST LENGTH 1, LENGTH 2 (SPLINE FIT).....	208
FIGURE 10.11: SURFACE PLOT: TIME TO HEAL AGAINST LENGTH 1, DEPTH (LINEAR FIT).....	209
FIGURE 10.12: SURFACE PLOT: TIME TO HEAL AGAINST LENGTH 1, DEPTH (SPLINE FIT).....	210
FIGURE 10.13: SURFACE PLOT: TIME TO HEAL AGAINST LENGTH 1, DEPTH (LINEAR FIT).....	211
FIGURE 10.14: SURFACE PLOT: TIME TO HEAL AGAINST LENGTH 1, DEPTH (LINEAR FIT).....	212
FIGURE 10.15: SURFACE PLOT: TIME TO HEAL AGAINST LENGTH 2, DEPTH (QUADRATIC FIT).....	213
FIGURE 10.16: SURFACE PLOT: TIME TO HEAL AGAINST LENGTH 2, DEPTH (SPLINE FIT).....	214
FIGURE 10.17: SURFACE PLOT: TIME TO HEAL AGAINST LENGTH 2, DEPTH (LINEAR FIT).....	215
FIGURE 10.18: SURVIVAL FUNCTION AT MEAN OF COVARIATES	219
FIGURE 10.19: HAZARD FUNCTION, RBMC	220
FIGURE 10.20: ONE MINUS SURVIVAL FUNCTION AT MEAN OF COVARIATES	221
FIGURE 10.21: LOG MINUS LOG FUNCTION	222
FIGURE 10.22: EXAMPLE OF SURVIVAL FUNCTION VS. TIME FOR SAMPLE WOUNDS (VARIABLES: L1, L2, D), RBMC.....	223
FIGURE 10.23: EXAMPLE OF SURVIVAL FUNCTION VS. TIME FOR SAMPLE WOUNDS (VARIABLES: L1, L2, D), RBMC.....	224
FIGURE 11.1: VARIOUS IMAGING ISSUES	234

LIST OF TABLES

TABLE 2.1: SUMMARY OF ONE-, TWO-, AND THREE-DIMENSIONAL MEASUREMENT ASSESSMENT TECHNIQUES [33]	22
TABLE 5.1: WOUND ASSESSMENT, PHYSICAL ASSESSMENT PARAMETERS PROCEDURES FOR PRACTITIONERS [2]	47
TABLE 5.2: SUMMARY OF WOUND-ASSESSMENT PROCEDURES FOR PRACTITIONERS [2].....	48
TABLE 5.3: SUMMARY OF ASSESSMENT PROCEDURES FOR PRACTITIONERS	49
TABLE 6.1: DATA-COLLECTION COMPONENTS.....	56
TABLE 6.2: INPUT FACTORS FOR ALGORITHM	59
TABLE 6.3: CORRELATIONS AMONG VARIABLES	61
TABLE 6.4: SUMMARY OF PARAMETER ESTIMATES FOR MULTIPLE-REGRESSION MODEL.....	61
TABLE 6.5: MODEL TEST DATA	63
TABLE 7.1: CALCULATION OF THERMAL INDEX/WOUND INFLAMMATORY INDEX RESULTS [109]	84
TABLE 8.1: SUMMARY OF BOX-PLOT STATISTICS OF INDEPENDENT VARIABLES	95
TABLE 8.2: COMPUTATION OF INDEPENDENT VARIABLES FOR LOWER AND UPPER WHISKERS OF BOX PLOTS.....	96
TABLE 8.3: NEURAL-NETWORK PREDICTION VARIABLES AND PARAMETERS	97
TABLE 8.4: INTERLAYER CONNECTIONS WEIGHTS	98
TABLE 8.5: TRAINING AND VALIDATION DATA-SCORING REPORT	98
TABLE 8.6: TRAINING AND VALIDATION DATA-SCORING REPORT	98
TABLE 8.7: FIGURE 8.12 GEOMETRIC ANALYSIS RESULTS	101
TABLE 8.8: IMAGE STATISTICS	102
TABLE 8.9: FIGURE 8.14 GEOMETRIC ANALYSIS RESULTS	103
TABLE 8.10: IMAGE STATISTICS.....	103
TABLE 8.11: FIGURE 8.12 GEOMETRIC ANALYSIS RESULTS.....	105
TABLE 8.12: IMAGE STATISTICS.....	105
TABLE 8.13: FIGURE 8. GEOMETRIC ANALYSIS RESULTS	109
TABLE 8.14: GEOMETRIC ANALYSIS RESULTS.....	110
TABLE 8.15: PATIENT 11 HUMAN WOUND MEASUREMENTS.....	112
TABLE 8.16: PATIENT 11 SOLIDWORKS WOUND MEASUREMENTS	112
TABLE 8.17: COMPUTATION OF INDEPENDENT VARIABLES FOR LOWER AND UPPER WHISKERS OF BOX PLOTS.....	136
TABLE 8.18: NEURAL-NETWORK PREDICTION VARIABLES AND PARAMETERS	137
TABLE 8.19: NEURAL-NETWORK PARAMETERS, ASPECT RATIO LESS THAN 1	137
TABLE 8.20: TRAINING- AND VALIDATION-DATA SCORING REPORT	138

TABLE 8.21: COMPUTATION OF INDEPENDENT VARIABLES FOR LOWER AND UPPER WHISKERS OF BOX PLOTS.....	138
TABLE 8.22: NEURAL-NETWORK PREDICTION VARIABLES AND PARAMETERS	139
TABLE 8.23: NEURAL-NETWORK PARAMETERS, ASPECT RATIO OF LESS THAN 1	139
TABLE 8.24: TRAINING- AND VALIDATION-DATA SCORING REPORT	139
TABLE 8.25: COMPUTATION OF INDEPENDENT VARIABLES FOR LOWER AND UPPER WHISKERS OF BOX PLOTS.....	140
TABLE 8.26: NEURAL-NETWORK PREDICTION VARIABLES AND PARAMETERS, FOR AN ASPECT RATIO GREATER THAN 1 AND LESS THAN 2	141
TABLE 8.27: TRAINING- AND VALIDATION-DATA SCORING REPORT	141
TABLE 8.28: NEURAL-NETWORK PARAMETERS, ASPECT RATIO OF GREATER THAN 1 AND LESS THAN 2	142
TABLE 8.29: COMPUTATION OF INDEPENDENT VARIABLES FOR LOWER AND UPPER WHISKERS OF BOX PLOTS.....	144
TABLE 8.30: NEURAL-NETWORK PREDICTION VARIABLES AND PARAMETERS	144
TABLE 8.31: TRAINING AND VALIDATION DATA SCORING REPORT	145
TABLE 8.32: COMPUTATION OF INDEPENDENT VARIABLES FOR LOWER AND UPPER WHISKERS OF BOX PLOTS.....	146
TABLE 8.33: NEURAL NETWORK PREDICTION VARIABLES AND PARAMETERS, $1 < \text{ASPECT RATIO} < 2$	146
TABLE 8.34: NEURAL NETWORK PARAMETERS, $1 \leq \text{ASPECT RATIO} \leq 2$	147
TABLE 8.35: TRAINING AND VALIDATION DATA SCORING REPORT	147
TABLE 8.36: COMPUTATION OF INDEPENDENT VARIABLES FOR LOWER AND UPPER WHISKERS OF BOX PLOTS.....	149
TABLE 8.37: NEURAL NETWORK PREDICTION VARIABLES AND PARAMETERS	150
TABLE 8.38: TRAINING- AND VALIDATION-DATA SCORING REPORT	150
TABLE 8.39: SUMMARY OF PREDICTED THRESHOLD VALUES (DAYS) TO CALCULATE TIME TO HEAL	150
TABLE 8.40: SUMMARY OF PREDICTED THRESHOLD VALUES (DAYS) TO CALCULATE TIME TO HEAL	151
TABLE 9.1: STATISTICS OF MULTIPLE LINEAR-REGRESSION MODEL (FOUR DEGREES OF FREEDOM)	154
TABLE 9.2: TRAINING- AND VALIDATION-DATA SCORING REPORT, MULTIPLE LINEAR REGRESSION (FOUR DEGREES OF FREEDOM)	154
TABLE 9.3: COVARIATE MEANS.....	155
TABLE 9.4: OMNIBUS TESTS OF MODEL COEFFICIENTS.....	163
TABLE 9.5: SURVIVAL TABLE.....	164
TABLE 9.6: VARIABLES IN THE EQUATION AND CORRESPONDING STATISTICS	166
TABLE 9.7: RATIO OF HAZARD RATES	166
TABLE 9.8: RATIO OF HAZARD RATES	167
TABLE 9.9: COVARIATE MEANS.....	168
TABLE 9.10: SURVIVAL TABLE.....	171
TABLE 9.11: NEURAL-NETWORK PREDICTION VARIABLES AND PARAMETERS, ASPECT RATIO LESS THAN 1	174
TABLE 9.12: TRAINING- AND VALIDATION-DATA SCORING REPORT, ASPECT RATIO LESS THAN 1.....	175
TABLE 9.13: NEURAL-NETWORK PREDICTION VARIABLES AND PARAMETERS, ASPECT RATIO OF LESS THAN 1 AND RBMC. 178	
TABLE 9.14: TRAINING- AND VALIDATION-DATA SCORING REPORT, ASPECT RATIO LESS THAN 1 AND RBMC	179
TABLE 9.16: TRAINING- AND VALIDATION-DATA SCORING REPORT, ASPECT RATIO GREATER THAN 1 AND LESS THAN 2	180
TABLE 9.17: NEURAL-NETWORK PREDICTION VARIABLES AND PARAMETERS, ASPECT RATIO GREATER THAN 1 AND LESS THAN 2 AND RBMC.....	181

TABLE 9.18: TRAINING- AND VALIDATION-DATA SCORING REPORT, ASPECT RATIO GREATER THAN 1 AND LESS THAN 2 AND RBMC	181
TABLE 9.19: NEURAL-NETWORK PREDICTION, INTERLAYER CONNECTION WEIGHTS.....	184
TABLE 9.20: NEURAL-NETWORK PREDICTION, OUTPUT-LAYER CONNECTION WEIGHTS.....	185
TABLE 9.21: NEURAL NETWORK PREDICTION VARIABLES AND PARAMETERS, ASPECT RATIO GREATER THAN 2.....	186
TABLE 9.22: TRAINING- AND VALIDATION DATA-SCORING REPORT, ASPECT RATIO GREATER THAN 2.....	186
TABLE 9.23: NEURAL-NETWORK PREDICTION VARIABLES AND PARAMETERS, ASPECT RATIO GREATER THAN 2, RBMC	187
TABLE 9.24: TRAINING- AND VALIDATION-DATA SCORING REPORT, ASPECT RATIO GREATER THAN 2, RBMC.....	187
TABLE 9.25: SUMMARY OF TRAINING- AND VALIDATION-DATA SCORING REPORT	192
TABLE 9.26: SUMMARY OF TRAINING- AND VALIDATION-DATA SCORING REPORT	193
TABLE 9.27: SAMPLE VALIDATION SCORE.....	194
TABLE 10.1: LOWER AND UPPER WHISKERS OF BOX PLOTS FOR RBMC DATA.....	197
TABLE 10.2: SAMPLE PATIENT DATA.....	198
TABLE 10.3: VARIABLE COMBINATIONS OF SURFACE PLOTS	203
TABLE 10.4: MULTIPLE LINEAR-REGRESSION MODEL VARIABLES, RBMC DATA	216
TABLE 10.5: MULTIPLE LINEAR-REGRESSION MODEL PARAMETERS, RBMC DATA.....	216
TABLE 10.6: MULTIPLE LINEAR-REGRESSION MODEL PARAMETERS, RBMC DATA.....	216
TABLE 10.7: TRAINING AND VALIDATION DATA SCORING REPORT FOR RBMC DATA	217
TABLE 10.8: RATIO OF HAZARD RATES.....	218
TABLE 10.9: COVARIATE MEANS.....	218
TABLE 10.10: WOUND DATA THAT CORRESPONDS TO PLOT IN FIGURE 10.23	227
TABLE 10.11: NEURAL-NETWORK PREDICTION VARIABLES AND PARAMETERS, RBMC DATA.....	228
TABLE 10.12: TRAINING- AND VALIDATION-DATA SCORING REPORT FOR RBMC DATA	229

CHAPTER ONE INTRODUCTION

CHAPTER ONE

Introduction

1.1 OVERVIEW

A wound can occur anywhere, at any time, either by accident or from constant pressure. A wound is an injury to living tissue caused by an extrinsic agent and comes in various shapes and sizes [1-3]. Wounds typically develop in physical locations that are difficult to see, difficult to reach, or lack feeling and nerve endings due to disease. Unfortunately, those who are susceptible to certain diseases, such as diabetes, are more prone to the development of wounds. However, regardless of the tendency of a person to develop wounds, the common wound locations remain the same. Wounds are more likely to develop in the appendages of the human body than anywhere else. Areas of the body such as the hands, buttocks, and feet, which experience continuous and repetitive pressure, are most susceptible to the development of wounds.

Wound healing represents a critical healthcare issue. Wounds are difficult and expensive to treat and to heal. The length of time it takes for a wound to heal is dependent on multiple factors, such as optimal moisture ratio, wound depth, and necrotic (dead) tissue. Naturally forming wounds tend to occur when there is unrelieved pressure or friction over a distributed area for a period of time. For this study, we will investigate the robustness and accuracy of predictive models to estimate the time to heal for chronic, nonhealing wounds.

According to the Mayo Clinic, wounds tend to develop quickly and are often arduous to treat [4]. A recent cross-sectional study that measured pressure wound pain in an acute care setting showed that 33.3% of patients were unable to respond to the evaluation tools. This study used the Faces Rating Scale [5]. After a wound has developed, the concern for clinicians and patients is the probability of infection. The infection rate of traumatic wounds varies from about 1% to 31%. The likelihood of infection is based on the wound characteristics, such as the nutrition of the patient,

whether the patient is obese or smokes, and the genetic predispositions of the patient [6]. Previous studies have involved bacterial counts and moisture levels to measure the infection of the wound bed. Both of these types of measurements require invasive techniques to the patient and the wound bed. Pressure wounds in particular are due to extended stays in one position. Millions of people are in jeopardy for developing a disease such as diabetes, and as many as 25% of these patients are at moderate to high risk for wounds during their lifetimes [7].

Small wounds and blisters can cause catastrophic issues, such as lower limb amputations. Besides the physical consequences of an amputation, there are psychological consequences, as well. Preventing wounds will, in all likelihood, reduce infection and amputation, but preventive measures and devices need to be emplaced to give patients the proper tools [8]. At least 85% of lower extremity amputations are preceded by a diabetic foot wound [7]. Research shows that the incidence of amputations has not significantly decreased despite new technology [9, 10].

A Dutch study found that the cost associated with the care of wounds are the third highest after those treated for cancer and cardiovascular diseases [11, 12]. In addition to the time and pain of treating a pressure wound, the price of a single full-thickness wound is estimated to be as much as \$70,000. The U.S. alone has been estimated to spend \$11 billion per year for wound expenditures [13, 14].

As the epidemic of wounds increases, wounds, blisters, sores, and cuts become inherent problems [15]. Decubitus wounds are worldwide health concerns [16]. Consequently, there is a growing need, both in the research and the commercial market for early detection systems and preventive tools. Diabetes is the leading cause of nontraumatic lower extremity amputations [17, 18]. Approximately 60% of nontraumatic lower-limb amputations occur in diabetic patients. And approximately 14% to 26% of patients with diabetes develop foot ulcers that will require amputation of the foot [17]. Worldwide, there is a diabetic amputation every 30 seconds [19]. Regrettably, 50% of amputees will develop a wound or infection in the contralateral (other) limb within 18 months, and 58% will have a contralateral amputation three to five years after the first amputation [20].

Approximately 2% of the U.S general population suffer from chronic, nonhealing wounds [21]. Conservatively, the cost of treating these nonhealing wounds is estimated to exceed \$50 billion per year, approximately 10 times more than the annual budget of the World Health Organization [21-24]. The prevalence of wound healing is similar to that of heart failure and cardiac diseases [25].

However, unlike cardiac diseases, little is known regarding the comparative treatments of wounds and their respective outcomes [21, 25]. Additional factors that contribute to the healing time of a wound are patient characteristics, such as diet, exercise, average blood flow, and living environment [26]. These unrelated but patient-controlled factors can greatly impact the healing time of a wound. For patients who suffer from chronic wounds, there are a number of methods to heal and alleviate wound conditions. However, there are no systems that assist in diagnostic measures.

There are few methodologies to help affect the decision for clinicians regarding wound care, how wounds are evaluated, and how wounds are treated. The epidemiology of wounds have varied incident rates ranging from 0.4% to 38% in acute care, 2.2% to 23.9% in long-term care, and 9% to 17% for in-home care [27]. In the U.S. alone, an estimated 2.5 million ulcers are treated each year in acute care facilities [27]. Monitoring wound progression over time is the main purpose of this research. A wound can be a tear, a scrape, or a cut — simply anything that damages the protective layer of the skin [28]. Wounds can occur anywhere on the body and range anywhere from a small paper cut to a large gash. Similarly, traumatic wounds are a greater challenge to heal without infection due to their nature, size, depth, and moisture. Despite the range of severity and commonalities of wounds, there are no predictive modeling systems to assist physicians in quantifying and diagnosing wound progression. Given the magnitude of the problem of nonhealing chronic wounds and the lack of a robust system to assess them, we investigate the clinical evaluation and predictive modeling of chronic, nonhealing wounds.

1.2 MOTIVATION

There is great interest in understanding chronic wound care assessment. There is also great interest in standardizing the process of wound care and wound analysis. The baby-boomer generation is redefining many aspects of the healthcare industry. Baby boomers are people who were born during the post-World War II baby boom between 1946 and 1964 [29]. As baby boomers enter the next phase of their lives, this population of people (approximately 79 million in the U.S.) are, on average healthier and have longer life expectancies than were previous generations [30]. This population remains more active and more independent than their predecessors. Due to the size of this population, it has developed and attracted multiple disciplines in studying gerontology from a psychological, biological, and engineering perspective. The boomer population has redefined aspects of the society, the culture, and now healthcare.

Approximately 6.5 million people suffer from chronic wounds in the U.S. [31] . This number is expected to exponentially rise due to this aging boomer population [32]. Wound care assessment has many limitations — specifically, budgets, equipment, and tools. These limitations make it challenging to consistently treating wounds across multiple clinics. Wound care assessment and healing depends heavily on the capability of clinicians and the systems at their disposal to handle the development and treatment of chronic wounds. These tasks involve understanding and adapting chronic wound assessments to handle the variability within each patient.

Using predictive modeling systems to predict for such a diverse group of patients is challenging. To build a robust and adaptive predictive system, we suggest that certain control systems must integrate common properties of wounds, such as surface area, volume, and temperature through the systems' emergent behavior. From a complex systems engineering perspective, the systems approach for wound care and the development of a predictive modeling and analysis for time-varying wound progression and healing represent a promising path using the common properties of wounds.

1.3 OPEN RESEARCH ISSUES

A distinct difference exists between ideal wound assessment methods and the current common practice. There is still a debate among researchers about the effectiveness of measurable wound parameters, such as size, shape, and color, and what measures best reflect accurate wound healing [33, 34]. However, there seems to be a common agreement that there is no established best-practices assessment and treatment for wound healing. There are, nevertheless, comparatively better practices than others [33, 35, 36]. Currently, most wound evaluation methods use typical physical properties, such as size, shape, and color, that manifest themselves externally. In this study, we examine the issues associated with assessing wound health. More specifically, we look at the aspects of wound data collection, such as the difficulty of acquiring wound depth as part of wound assessment.

To date, there have been extensive studies performed on best wound healing practices [22, 28, 33, 37-39], evaluation of wound analysis tools, and wound healing measuring properties. However, most of these practices are limited to physical and visual properties of the wound rather than internal properties. We assume that this limitation is due not to a lack of investigation but to a lack of appropriate tools in clinical practice. In the study, we focus on methodologies that are relevant to obtaining wound measurements, such as size, shape, color, and necrotic tissue. Unfortunately, most of these methods are still subjective when it comes to forming conclusions about the data.

The methodology that we present in this study is applicable and transferable as assessment techniques improve to include both biological and physical wound characteristics.

Width, length, depth, surface area, and volume measurements are the most frequently obtained physical wound characteristics [33]. St-Supery et al. [33] have published a study on 29 wound healing evaluation methods in which the authors extensively reviewed one-dimensional and two-dimensional wound analysis tools [33]. From their review, the authors found that the most common limitation of these evaluation methods is the subjectivity and lack of sensitivity of the users and the tools [33]. Area measurements are among the most frequently used methods for assessing wounds in a clinical setting [33, 40]. For many of the current processes in clinical and research settings, the primary limitations are the sensitivity of the shape, contact with the wound, and the inability to have accurate manual or digital planimetry — measurement of plane surfaces — due to the size of the tablet acquiring the wound boundary.

Surface area measurements are most common in wound condition observations due to ease of measurements [41]. Individuals in research and clinical practice can use the principal imaging methods: planimetry, digital imaging, or stereophotogrammetry. Digital images provide full-scale imaging of the wounds but are limited to visibility and contour shape. Many instances exist of two-dimensional digital images in which the wound of a patient is on a curved surface, resulting in a distorted photo [33, 40, 42]. The digital image of a curved surface can lead to an overestimation or an underestimation of wound size. Another issue in wound photography arises when a wound exceeds the size of the image frame. The inability to photograph the full wound in a single frame can also lead to problematic size estimations. Stereophotogrammetry photography uses two or more images from slightly different perspectives to create a composite image using triangulation to allow for linear, area, and volume estimations [33, 43]. Stereophotogrammetry is a hybrid between one-dimensional and three-dimensional imaging. Two-dimensional images of wounds are beneficial for gathering surface data, but much of the healing takes place underneath the visible wound bed.

Many factors influence wound healing, specifically with regard to wound volume. Factors that primarily influence wound volume and wound healing are wound debridement; patient positioning; and edema, an abnormal accumulation of fluid. We have not found previous literature that documents successful wound volume measurement methodologies that accurately account for wound healing. Currently, only a few general methods can measure wound volume. The first method is a generalized linear approximation that uses basic geometrical shapes and volume

formulas to estimate the volume of the wound [21, 44]. The limitation of this method is that it bases all measurements on an approximation, which has a tendency to produce an overestimation or underestimation of wound volume. Similarly, the second most common method of measuring wound volume is to use various types of saline-gel fillings to physically measure the wound volume by injecting fluids into an open, sensitive area [45]. These injectable fluids have a high probability of contamination and leaking, and they may cause an overestimation of the wound volume. The most crucial aspect of these fillings is the unnecessary contact with the wound bed.

Currently available three-dimensional wound imaging systems use techniques such as light reflection, laser optics, compilation of standard images, and stereophotogrammetry [24, 38, 46-48]. Some of these techniques are noncontact methods. Many of these systems take into account irregular wound shapes and are portable. There are, however, some limitations to these systems. For example, the structured light-based method is limited to wounds that “are not very small and not very large” [24, 38, 48]. Additionally, the accuracy of the measurement depends on the accuracy of the quality of calibration. Furthermore, the operator defines the edge of the wound rather than the system. The limitations were common with most other three-dimensional wound imaging systems. The restriction of a stereophotogrammetric system is that the accuracy of measurements depends on the training of the operator. Further, measurements using this system are cumbersome, time-consuming, and costly.

1.4 PROBLEM DEFINITION AND OBJECTIVE

Treating and monitoring wounds vary with each patient and with each wound. Tracking wound progression is even more difficult. With various levels of standards of care, tracking wound progression is inconsistent across wound clinics. The purpose of this dissertation is threefold. First, it contributes to the understanding of chronic, lower appendage wound assessment tools and techniques. We look to contribute to the understanding of how various wound characteristics impact the length of wound healing time. Second, it identifies certain wound traits that can be characterized quantitatively and that provide indication of overall wound health. Third, it investigates and formulates an accurate algorithm and system model to predict the amount of time left to heal for lower appendage chronic wounds.

1.5 PROPOSED SOLUTION

In this dissertation, we explore and investigate chronic wound healing practices and their tools and instruments for the purpose of developing models that contribute to the prediction of wound

healing time. This dissertation contribution has three main components: 1) retrospective and current patient two-dimensional and three-dimensional image analysis; 2) predictive models and algorithms; and 3) recommendations for routine chronic wound management.

The objective of this research is to develop a methodology that can accurately predict the amount of time remaining for a chronic, wound during the healing process. This research has five primary objectives:

Objective 1. Identify deficiencies within current wound progress tracking methods. The main deficiency is the lack of accurate clinical assessment tools.

Objective 2. Identify input parameters

Working with physicians at various wound care clinics, we identified potential input parameters for wound characterization. The common criteria for the input parameters are that they are measured using noninvasive methods and technologies. The objective is to determine the most efficient, effective combination of inputs to produce a reliable and useful output.

These parameters include but are not limited to [49]:

- Moisture content: In a wound that is too wet or too dry, moisture facilitates bacterial growth. It is possible to include this parameter quantitatively.
- Necrotic (dead) tissue: the measure of necrotic tissue in a wound bed
- Wound depth/depth of tissue damage: There is always the possibility that a wound has “dead space” that must be harnessed and “filled.”
- Size (length by width by depth)
- Periwound skin (skin around the wound): The condition of the periwound skin around the wound directly affects wound healing.
- Wound margin or edges
- Wound odor: It is unknown whether the wound odor is a quantifiable value but is something to consider.

By correctly identifying the underlying etiology and respective parameters of the wound, we can develop a better baseline for the development of the predictive algorithms.

Objective 3. Development of Predictive Algorithms

These algorithms are based on robust predictive methods, such as regression analysis, neural networks, and survival statistics.

Objective 4. Modeling a Wound

With accurate and reliable data, three-dimensional wound modeling is a possible incorporation into the overall system. We will produce a three-dimensional model of the shape and volume of a wound to provide an accurate representation of the current stage of the wound.

Objective 5. Data Analysis

The data analysis includes a comprehensive understanding and development of the predictive algorithms. We determine through the data analysis the robustness and accuracy of each of the modeling techniques.

The overall goals of this dissertation is to design a methodology that standardizes assessment of wound with three main focus points: 1) develop a methodology to predict model prototype to estimate wound healing time; 2) support the predictive algorithm with a three-dimensional wound model; and 3) recommend adaptations to the model prototype, including parameters, such as patient characteristics and risk factors, that are known to be associated with wound healing. We hope the model will provide the initial framework and support for continued research in developing a more comprehensive predictive modeling system that can lead to a standard approach to the routine management of chronic wounds.

1.6 DISSERTATION CONTRIBUTION

The primary contribution of this dissertation is the development of predictive models and algorithms to estimate the time to heal of chronic, lower appendage wounds. This contribution consists of three components: predictive algorithms, the system components, and the overall methodology.

Predictive algorithms are the developments of a mathematical formulation that uses a combination of specific wound characteristics to predict the number of weeks left to heal. The importance of each wound characteristic is determined through statistical analysis. More specifically, the significance of each wound characteristic input is determined through the correlation between each wound characteristic input, as well as each input with the output. Various correlation metrics

determine each wound characteristic inputs' importance. Figure 1.1 shows a basic overview of the respective input/output diagram.

There are three components of Figure 1.1: the inputs, the algorithm, and the output that have a unique contribution to the overall predictive model. The inputs were chosen based on a series of statistical analysis and statistical correlations that determine the ideal set of inputs for the predictive algorithm. Based on the analysis, we determine the archetype set of inputs for each of the predictive algorithms: regression and neural networks. Similarly, within the predictive algorithms, we contribute two algorithm analyses to compare their accuracy and robustness. Last, the output contribution will be twofold: 1) Primary output will be the predictive quantitative value of the time left to heal for a wound; and 2) A three-dimensional model of the wound shape and depth. The three-dimensional model of the wound will provide the ability to view and track the change in volume of the wound.

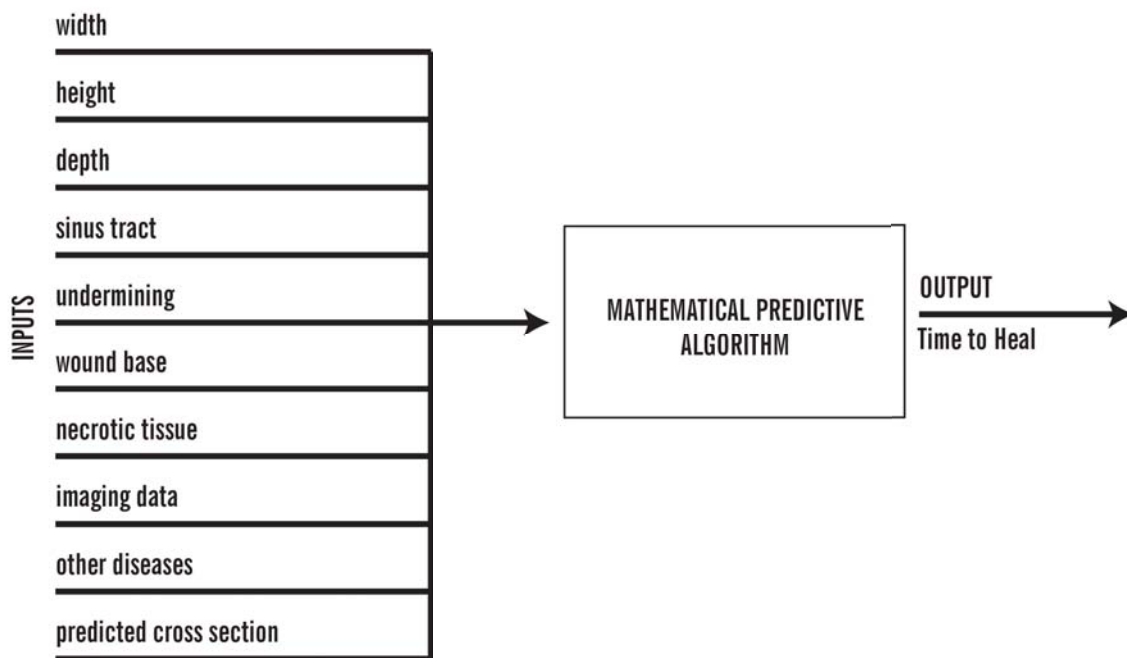


FIGURE 1.1: INPUT – ANALYSIS - OUTPUT

The quantitative value of time to heal is the primary contribution of this dissertation. However, the secondary contributions add complementary value to this overall research. The second complementary contributions to this research are the development of three-dimensional models of chronic wounds and overall methodology that includes image analysis and routine chronic wound management analysis. Three-dimensional virtual modeling is used primarily in product design and

development to prevent unnecessary prototype creations due to minor changes. Recently, three-dimensional modeling has become more mainstream in medical devices. However, in many past publications for chronic wound modeling, three-dimensional modeling does not provide a true three-dimensional model, as we show in Chapter 2.

Three-dimensional modeling is heavily used in other areas of medical imaging, such as cancer and tumor detection, but is rare in wound care and assessment. Three-dimensional modeling provides the methodology with the ability to track the changes in the surface area of the wound and the subtle changes in the volume of the wound below the surface. The changes in volumetric data will contribute to the knowledge that understanding and tracking the volume will assist in understanding how the wound is healing.

Part of understanding and appropriately using three-dimensional modeling for chronic wounds also includes gaining the necessary information to input accurate data into a three-dimensional modeling system. Our contribution also includes the imaging component of the overall system, which integrates still and thermal imaging over a length of time. These images provide us with the ability to photograph the wound with a ruler, trace the spline of the wound, and import that data into the three-dimensional modeling program. In this research, we use Solidworks™ as the three-dimensional modeling program, thus allowing us to accurately determine the perimeter of the wound. By using computerized planimetry, we are able to more accurately define the wound perimeter without human measurement and ultimately construct a virtual model the wound. Similarly, thermography provides us with the respective temperature difference between the wound and the surrounding skin to monitor how wound healing impacts the temperature of the wound.

The third contribution of this dissertation research is the development of recommendations of routine chronic wound management for wound clinics. This is based on the observations at wound clinics that range from community to large teaching facilities. We have spent significant time in various wound clinics and wound treatment centers observing, recording, and analyzing the individual treatment of patients and their wounds.

Routine medical practice has long had a varying definition of “standard.” As common with any industry with multiple entities, each entity defines its standards and expectations according to what it believes are the needs and wants of its customers — that is, the patients. This research on developing a predictive wound care assessment methodology and system has extended a branch of inquiry into the routine care of wound clinics. Through the research for the predictive model

systems development, we noticed among between all the clinics that were visited. The scope of this inquiry evaluates the observed wound care practice and routine wound care treatment. The purpose of this inquiry is to determine whether a common practice can be developed to better streamline chronic wound care, regardless of the type and size of the hospital. The purpose of this contribution is to compare and contrast the clinic practices, tools, and resources at various community and teaching hospitals. This exploration determines a proposed combination of tools and technique that could be most beneficial to patient wound care. This contribution focuses on three wound care clinics, a major teaching hospital, a midsized teaching hospital, and a community hospital, and a wound care provider, each with its own methods of patient wound care. On that basis, we provide recommendations of “Routine chronic wound management from an engineering perspective, which is based on the observation and interactions with these hospitals.

CHAPTER TWO LITERATURE REVIEW

CHAPTER TWO

Literature Review

2.1 INTRODUCTION

The underlying pathophysiology, which drives the development of chronic wounds, is still poorly understood [50]. The ability to measure wound progression is critical to the healing of wounds. Wounds either progress in healing or deteriorate in health; the health of wounds rarely remains the same. A wound bed that stagnates is generally the same as medical treatment that is not effective in treatment. Proper tools for measuring the effect of an intervention are critical to properly healing the wound. There has been recent progress in modeling and evaluating wounds [22]. Wounds are most prevalent in elders. However, as the population becomes more active, people must take more precautions to prevent wounds. The analysis of the geometric and chromatic parameters of a wound is the most crucial and accurate way to evaluate a diabetic wound [22]. No currently available technologies integrate all peculiarities and issues pertaining to a pressure wound [22]. Researchers and supporting clinicians have combined geometrical, thermal, and chromatic data capture using three-dimensional optical scanners and computer-vision techniques.

Innovative research has defined a robust segmenting tool that enables discrimination of wounds to accurately classify lesions at different stages using textual information [22]. Two-dimensional processes lack the detail of wounds larger than 1 to 2 microns, as well as the necessary information of a wound [22]. The newest technologies have attempted to automatically detect a wound edge by analyzing curvature maps [51]. Because the topology of each wound varies so significantly, tracing methods must be tremendously adaptable. Current tracing methods are inaccurate and unreliable for wounds that exceed a certain depth. Noninvasive, full-field technologies are necessary to effectively measure and assess the severity of a wound. The grand challenge is to integrate image acquisition and computer vision to monitor the wound with respect to area, volume, color, and temperature without physical contact with the patient [22]. Currently,

the development and analysis of this research is performed using off-the-shelf cameras and equipment. The goal of our research is that the methodology we have developed will be the foundation in pursuing a full-field, practicum-enabled wound assessment core technology that can be integrated in current wound care clinics.

2.2 WOUND TOPOLOGY MODELING

In most wound clinics, wound progression is monitored by charts, diagrams, and measurements. Some wound clinics have standard protocols to photograph the wound during each visit. However, this practice is not standard across all wound clinics. Despite good wound tracking procedures, wound monitoring, in general, concentrates on the surface measurements of the wound. This study, however, also supports the ability to take those surface measurements and measured depth to create a three-dimensional model of a wound. A three-dimensional model of the wound allows more accurate calculation and monitoring of wound health using the volume of the wound rather than just the surface area. Figure 2.1 is an example of the wound shape, dimensions, and depth based on dimensions from a patient wound.

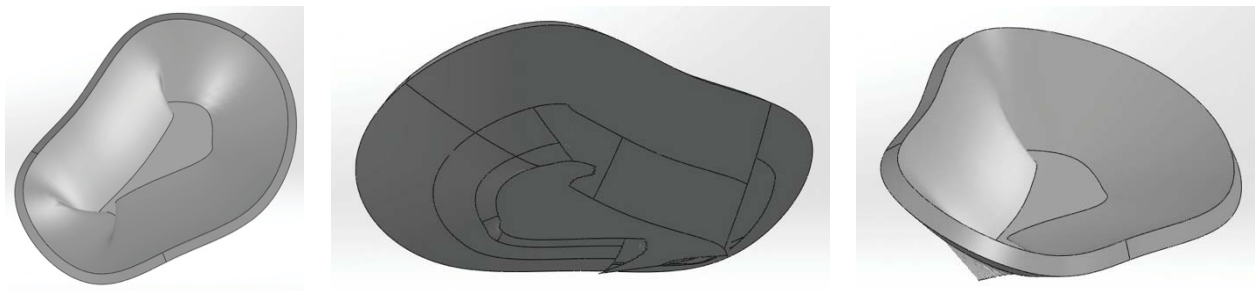


FIGURE 2.1: EXAMPLE OF WOUND MODELING IN SOLIDWORKS™ SOFTWARE

2.3 PREVIOUS STUDIES: A REVIEW OF WOUND ASSESSMENT TECHNIQUES

Previous research is and has continually performed in the area of reducing the healing time of chronic wounds in patients. Still, most previous research converges on using the surface of the wounds rather than the underlying geometry of chronic wound development [52]. These methodologies can be classified in terms of the measurement process, the measurement techniques, and the completeness of the data [22, 52]. These systems include traditional imaging techniques, including point-and-shoot digital cameras, and range to stereophotographic systems, which use two cameras to create depth perception to calculate and create a three-dimensional map of the wound surface [22, 52]. Despite these imaging advances, most previous research lacks

the ability of a comprehensive chronic wound assessment system that enables real-time tracking and prediction of wound progress. In most cases, the performance of previous wound assessments are fragmented, focusing on one aspect of chronic wound assessment.

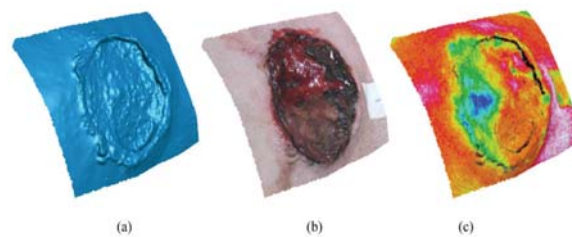
The University of Pisa in Pisa, Italy, conducted one study on chronic wound assessment that used three-dimensional optical imaging based on integrating geometrical, chromatic, and thermal data [22]. This study focused on the development of a noninvasive system to automatically measure chronic wounds, with little human intervention or assistance. By analyzing both the visible and the thermal imaging data, Barone et al. [22] hypothesized that their imaging system can determine the size, shape, and depth of ulcers on human legs.

Barone et al. [22] determined that clinical treatments should be validated through constant and consistent monitoring of the progression of wound size and wound healing. Previous research supports the claims of Barone et al. [22] that ischemic wounds present a lower temperature than core body temperature. This discrepancy could indicate healing or nonhealing. This discrepancy would be similar to biological characteristics, such as a change in blood flow, an increase or a decrease in oxygen, or a regrowth of skin [53-55]. The study of Barone et al. [22] focuses on a noninvasive wound assessment method that monitors the healing process using three types of surface data: geometrical, thermal, and chromatic data. Their research uses a three-dimensional optical scanner and an infrared (IR) detector to capture the color and thermal images of the wounds.

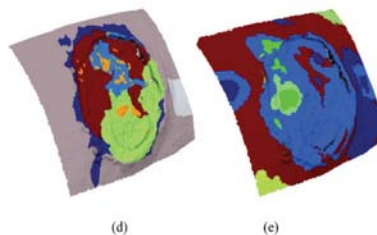
In short, Barone et al. [22] created an optical configuration that recorded three-dimensional images based on image configuration. This optical configuration was composed of a color digital video camera, a digital thermal video camera, and a standard video projector. The three cameras were mounted at three slightly different perspectives to provide the “depth,” which is similar to a stereo camera. To acquire accurate data, this study used light plane projects to obtain the shape measurements. The light plane projects provided a sequence of images that represented parallel vertical light planes. This study generated three-dimensional chromatic and thermal representations of the wound by automatically mapping the visible and infrared images onto three-dimensional geometries generated by the scanning process. This information allowed researchers to view the three-dimensional coordinates of the points on the vertically projected lines. This research produced success in the detection of wound regions and computing their relative areas and volumes. The accuracy of this study was tested by measuring the shape of a reference object of known dimensions. The precision was evaluated by comparing the point clouds of single scans

that corresponded to best-fit surfaces. Figure 2.2 is an example of results observed by Barone et al. [22]; they present results of a singular wound acquired from each imaging modality. This study provided validation in the need for more comprehensive wound care systems. This study had a few limitations: 1) the complexity of calibration and integration of the three cameras; 2) a three-dimensional mesh surface contains very little depth along the Z-axis; and 3) the cost effectiveness of the technique in clinical practice.

Despite the limitations of the study of Barone et al. [22], their research validated the need for better chronic wound assessment systems. Furthermore, this study was among the first studies to use three-dimensional imaging to create a three-dimensional map of the wound's surface. What differentiates the study by Barone et al. [22] from the previous studies is its ability to use geometric and thermal imaging data in addition to chromatic data. Most of the previous methodologies and acquisition systems support only chromatic data. Additionally, most previous systems are considered strictly two-dimensional systems without any possibility of collecting and tracking the volume of the chronic wound.



(a) three-dimensional geometrical wound model, (b) three-dimensional colour texture map,
(c) three-dimensional thermal map



(d) three-dimensional segmented data using wound detection on the chromatic image
(e) three-dimensional segmented data using wound detection on the thermal image

FIGURE 2.2: BARONE ET AL. WOUND IMAGES FROM DIFFERENT IMAGING MODALITIES [22]

In 2008, the University of Pennsylvania School of Medicine published a review article on current methodologies of wound care assessment. The article reviewed the techniques for measuring and documenting wound geometries with an emphasis on multidimensional computerized wound documentation [52]. The prominence of this article focused on more computerized wound documenting systems rather than typical length and width measurements.

Computerized wound-documenting systems are rare, and the techniques have yet to be standardized. Various methods exist to trace, calculate, and record the two-dimensional surface measurements. Chapter 4 discusses the most common of these methods. The details extracted from this article focus on the three-dimensional assessment because wound volume is the most frequently reported desired metric.

Ultrasound sonography provides a visualization and quantitative assessment of deeper imaging modalities below the epidermis, dermis, and hypodermis layers and allows clinicians to view into the muscle, should a wound penetrate that far. Similar to the surface approximation of two-dimensional wound measurements, wound volume measurements involve some limitations.

For many current wound volumetric measurement techniques, the initial three-dimensional shape of the lesion is approximated based on known, typical geometric shapes, such as rectangles, spheres, and domes [52]. For example, if a wound shape is approximated to be similar to a rectangular parallelepiped, the volume is:

$$volume = length * width * height \quad (2.1)$$

versus a spheroid

$$volume = \frac{\pi}{6} * length * width * height \quad (2.2)$$

Many similar studies have reported methods to approximate the volume of a wound and the approximation with traditional geometric shapes with three degrees of freedom [52]. For similar studies, researchers have typically used some type of approximation for the footprint of the wound, relying on already known objective measurements (Figure 2.3). Although this technique is sufficient, the method is both inaccurate and unreliable in determining the change in surface area and depth.

Geometries with different shapes and areas can have the same lengths and widths and will be judged to be of the same severity.

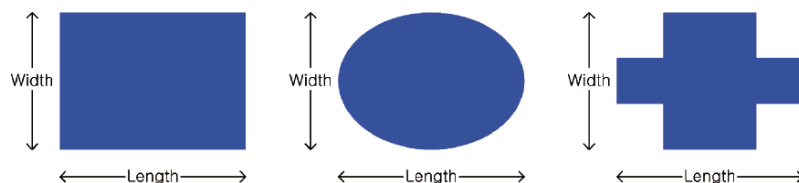


FIGURE 2.3: APPROXIMATE GEOMETRIC SHAPE ESTIMATIONS OF WOUNDS [52].

Similarly, other studies have showed that the combination of standard photography, transparency tracing, and video camera recording produce acceptable results of diabetic wounds and venous ulcers [44]. Combining these techniques still yields inaccurate results for estimating healing rates. Mayrovitz et al. [44] used the ratio of the surface area of a wound (S) to its perimeter (P) to characterize healing rates. The study [44] has provided an effective ratio to assess healing rates in venous ulcers and a suitable indicator of linear healing rate per day. It has also been used to predict time to wound closure based on nonlinear delayed exponential models that offer some predictive capabilities but have not been verified.

The Mayrovitz et al. [44] model developed a study consisting of 20 nursing students using six test images of various wounds. Using provided images, students were required to determine the actual areas, the weight (W_i) of each target, and the weight (W_k) of the cutout square of each target shape to compare it with a computer-generated and computer-drawn square of known area (A_k). The area (A_i) was determined by

$$A_i = \frac{W_i}{W_k} * A_k \quad (2.3)$$

For this study, students were required to measure and calibrate the imaging device to the wound and trace the wound three times in succession using a mouse. The purpose of multiple tracing was to obtain a perimeter calibration factor to use for obtaining the area and perimeter. Researchers used a standard error equation to determine the accuracy and reliability of their results:

$$Error = Weight - Area Determined - Area Planimetry \quad (2.4)$$

The area planimetry was determined through the average of the three tracings for each image. Overall, this study supported the hypothesis that the characterization of wound shapes is possible, but accuracy and reliability are questionable based on the techniques used. Mayrovitz et al. [44] found that the standard consensus of estimating the correct weight-determined area among other factors could contribute to the inconsistent measurements. Furthermore, the results were heavily dependent on the student measurement process, image calibration, and the identification of wound margins. The repeatability proved to be challenging. However, this study does support the desire to use software algorithms to determine the perimeter of chronic wounds. The study also suggests that further research and further training of wound care specialists can successfully use computerized planimetry of digitized wound photographs to determine wound surface area.

2.4 NONINVASIVE WOUND MEASUREMENT TECHNIQUES

There are currently only a handful of noninvasive wound measurement techniques in both research and clinical practice [22, 38, 56, 57]. These methods include a variety of techniques, but the most prevalent are forms of imaging, laser, and light refraction. In Chapter 4, we will discuss the four most common methods. including curvature-map-based method, three-dimensional construction, digital construction, and a few currently available commercial systems.

St-Supery et al. [33] developed a review article that questioned whether an ideal methodology for tracking chronic wounds exist. They discovered a series of methods organized into one-, two-, and three-dimensional techniques. Table 2.1 [33] shows modified results from St. Supery et al. [33] to show only the noninvasive techniques of wound assessment. Chapter 4 will discuss in more detail the primary and current methodologies used in current chronic wound care management⁴.

2.5 SUMMARY

We have explored various methods of measuring the surface area and volume of chronic wounds. By fully understanding past research, we can determine the niche of chronic wound measurement techniques. St-Supery et al. [33] is the most similar study we have found that uses both thermography and three-dimensional modeling to reconstruct the behavior and topology of a chronic wound. However, as Figure 2.2 shows, their techniques involved more inverted models of the wound by creating a negative impression. The methodology uses the surface area shape with the corresponding depth measurements to create a positive three-dimensional model.

Additionally, the planimetry of digitized wound photographs and approximate geometric shapes (Figure 2.3) allows clinicians to estimate wound shape in real time. We believe that, with the decline of cost for digital cameras, digital photography, and the storage of medical record photography, the consistency of photographing wounds should become more standard. Wound surface area should grow beyond the approximate bounding box.

Table 2.1 is a compressive summary that we have determined from literature that summarizes two- and three-dimensional chronic wound measurements. However, most of the methods have significant limitation in determining irregularly shaped wounds. We believe the methodology, when refined, could eliminate some human variation in measurements and discrepancy between measurements. This elimination would allow for additional accurate tracking of wound surface size using digital planimetry.

TABLE 2.1: SUMMARY OF ONE-, TWO-, AND THREE-DIMENSIONAL MEASUREMENT ASSESSMENT TECHNIQUES [33]

Degree of Freedom	Methodologies	Descriptions	Advantages	Limitations
One-dimensional	Perimeter	Measured directly on wound, on acetate tracings, or on photography tracings	Sensitive to wound contour variations	Measure is taken on wound edges, which are often hard to delimitate precisely
Two-dimensional	Linear measurements	Calculation using width (W) and length (L) measures Wound approximated by regular geometric shapes	Simple and quick No special material needed Convenient Cheap	Highly observer dependent Approximation of wound size using regular geometric shapes Many widths and lengths possible on a single wound Not sensitive to all shape variations
Two-dimensional	Direct manual planimetry	Rectangle: $W \times L$ Ellipse: $W \times L / 4$ Wound contour traced on an acetate Squares within contour counted manually Inclusion of squares over-crossing wound boundaries is variable	No need for an approximation by geometric shapes No expensive material needed Simple	Squares crossing boundaries are source of error Square counting is time consuming Exudate can blur wound edges Contact with wound needed
Two-dimensional	Direct digital planimetry	Wound contour retraced on digital tablet Software calculates area	No ambiguity with crossing squares No tabulation errors possible	Problematic when wound is bigger than the tablet Contact with wound needed Exudate can blur wound edges
Two-dimensional	Manual or digital planimetry on photos	Full-scale wound images taken Wound contour retraced on an acetate or on a digital tablet	Simple and quick No direct contact with wound needed No blurring of wound edges by exudate	Expensive Wound edges less clear on a photo Curved surface distorted on photo which leads to underestimation of real area Problematic when wound is bigger than the photo Images calibration is time consuming and a source of error
Three-dimensional	Linear measures	Width (W), length (L) and depth (D) measures Volume approximation by regular geometric shape formula Parallelepiped: $W \times L \times D$ Spheroid: $(W \times L \times D)/6$	Simple and quick Low cost No special material needed	Approximation of wound size using regular geometric shapes Not sensitive to shape variation outside the measured axes Undefined wound edges and wound base irregularities can affect the measure
Three-dimensional	Barber Measuring Tool	Software calculates volume from linear measurements Shows % of volume variation and its graphic representation	No tabulation errors possible Data storage Simple and quick Calculates volume variation as a percent of baseline	Deep sinuses skew the results Errors due to manual measures are present One formula for all wound shape Deep sinuses skew the results
Three-dimensional	Kundin	Three calibrated perpendicular axes reproducing the Cartesian system Width, length, and depth measures in a formulas: $W \times L \times D \times 0.327$ Area measurement also possible: $W \times L \times 0.785$	Simple Low cost Disposable Overcomes the variation due to ruler positioning Portable	Approximation of irregularly shaped wound volume or area with only one formula Not sensitive to shape variation occurring outside the measured axes

CHAPTER THREE CHRONIC WOUNDS

CHAPTER THREE

Chronic Wounds

Two primary, outermost layers of the skin protect the human body. The outermost layer is the epidermis (75 to 150 microns thick), and the innermost layer is the dermis. The two layers are separated by the basement membrane [2]. When human skin is broken by anything from a small cut to a traumatic wound, the normal regenerative healing process allows new skin to grow over the damaged area. Unfortunately, those who suffer from chronic wounds lack the ability to properly heal.

3.1 BIOLOGY OF A WOUND

Wounds occur in all shapes and sizes. Clinicians often need to try multiple treatment options to determine the most effective one for a wound [24]. Wounds are typically defined as disruptions to the integrity of the skin. Simple wounds are those that remove or damage the first layers of skin. A complex wound is deeper, often causing injury to nerves, blood vessels, or muscles [24]. The underlying pathology of a wound determines the approximate treatment route; however, the primary goal of wound management is rapid wound closure [24].

Pressure wounds impact the deeper tissues of a patient and are due to unrelieved pressure, shear forces, frictional forces, or a combination of these factors [58]. The susceptibility of a person for a pressure wound depends on a number of internal and external factors [16]. It is, however, generally agreed that the accumulation of bacteria and bacteria colonization contribute to the tissue breakdown and delay of healing [58-60]. Bacteria, although it typically prolongs healing, can provide information on how well a wound is healing [58]. For many clinicians, the diagnosis of wound health and eventual wound treatment depends on the diet of the patient and the nutrients the patient commonly consumes. There also could be a discrepancy in the thickening of skin and

bone changes in the feet. Known wound factors include ischemia, or the restriction of blood supply; perfusion; oximetry, or the oxygenation of hemoglobin; and hardening of the surrounding skin.

According to biology literature, impaired blood supply and tissue malnutrition cause wounds [16]. The combination of prolonged pressure and tissue compression can lead to capillary bed occlusion and local ischemia, contributing to the rate of cell death [16]. People can sustain, decubitus, or “lying-down,” wounds in any part of the body in which pressure and compressive forces continue for a prolonged period [16]. Areas of the body that are more easily susceptible to decubitus wounds are the heels, sacrum, occiput, helices, elbows, and lower extremities [16]. The morphology of wounds occurs when the subcutaneous tissue breaks down. Epidermal necrosis occurs later during morphology because epidermal cells can withstand a lack of oxygen for a longer period. The prolonged absence of oxygen often contributes to pressure wound morphology [16]. Various classification systems exist for decubitus wounds, such as the National Pressure Ulcer Advisory Panel (NPUAP), the most widely accepted system.

The NPUAP has four stages of classification for pressure wounds [61]: Stage 1, nonblanchable erythema; Stage 2, partial thickness loss of dermis, Stage 3, full thickness skin loss; and Stage 4, full thickness tissue loss with exposed bone, tendon, or muscle.

Wound management is a multidisciplinary concern, but nurses primarily care for and manage wounds [62]. Wound management should not be treated in isolation but should be considered in respect to the body of each patient [62]. In many cases, assessment of the wound area is the responsibility of both the patient and the clinician, and regular intervals of wound assessment is generally important during the healing process [62]. According to literature, wound care is dynamic, and the assessment, treatment, and wound progression is vital. Once a wound has formed, key aspects of wound management, such as cleaning, effective drainage, and absorption [16], are necessary to ensure effective healing. A typical path of treatment of pressure wounds is common across all wounds. They are dependent upon four primary modalities [16]:

- Pressure reduction and prevention of additional ulcers,
- Wound management,
- Surgical intervention, and
- Nutrition.

Few diseases exist for which so many treatments have been attempted as there have been for wounds. Treatment attempts include various chemicals, poultices of vegetables, enzymes,

vitamins, cod-liver oil, dried blood plasma, various precious and nonprecious metals, sugar, and salt [16, 63]. Mechanical treatments include electric lamps, ultraviolet light, hyperbaric oxygen, rubber rings, sawdust beds, and a variety of pressure beds and padding [16, 63].

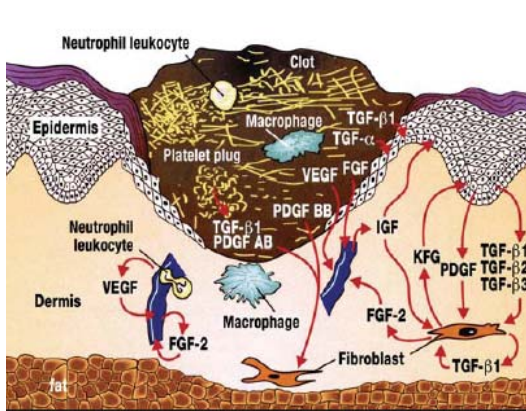
3.2 WOUND HEALING

Wound healing is a complex biological process that differs with every patient. Many factors contribute to the health and healing rate of a wound, and we thus focus only on the basics of wound healing and major procedures in clinical practices [64-66]. Chronic wounds stem from an inability of the body to heal a damaged area. As expected, each wound is unique, which causes wound assessment to be nonstandard. Common procedures for each patient occur in wound clinics, but the course of treatment is extremely customized. Major systemic parameters, such as blood pressure, temperature, and pulse rate, affect wound healing [3]. According to literature [66], wounds [in general] have been relegated either undeserving or too difficult to measure.”

The wound healing phenomenon comprises multiple processes. all of which must function in perfect harmony to properly and fully work [67]. The biological aspects of wound healing occur in most wound repair and include inflammation; epithelization, or the formation of new skin; angiogenesis, or the formation of new blood vessels; granulation, or the formation of connective tissue; and tissue formation [3, 67]. The difficulty in accurately measuring wound healing is the unknown information that is occurring but unseen at the surface of the wound. For example, the healing of pressure ulcers has previously been linked to angiogenesis and the deposition of extracellular matrix; this situation ultimately leads to the wound’s filling up with new tissue and contracting over time [3, 67]. In particular, pressure wound healing consists mostly of new tissue formation and contraction of the skin. Epithelization is especially important in wound healing and involves four stages: keratinocyte, proliferation, migration, and differentiation. These stages allow for new epithelials to make their way across the surface of the wound. These stages make it cumbersome to accurately measure wound depth. Further, techniques that work in exploratory research do not necessarily work in practice. Unfortunately, new skin growth causes more uncertainty in the accurate measurement of wound depth because the reliability of the measurements have yet to be established.

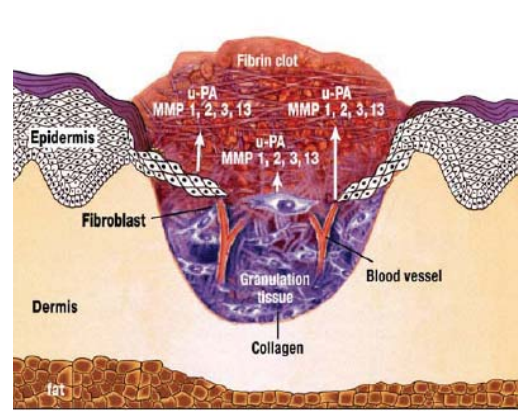
A significant amount of progress in understanding wound healing and wound anatomy has occurred in the past century [68]. Wound healing has traditionally been divided into four distinct and sometimes overlapping phases: exudative, resorptive, proliferative, and regenerative [68]. Some discussion has occurred on whether wound healing is a three- or a four-phase process. But,

given the consequences of unpredictable wound healing, most literature states that a four-phase process is more accurate [68]. During the exudative phase, a visible clot forms. The resorptive phase occurs 24 to 48 hours after the wound has formed. Macrophages migrate toward the wound, causing visible inflammation. The proliferative phase typically occurs between the third and the seventh day of healing. During this phase, the body forms granulation tissue, new epidermal cells begin to grow, and a visible delicate border around the wound begins to form [68]. During the regenerative phase, which can last more than a year, maturation of collagen occurs, reinforcing the resistance of the wound to future damage [68]. Regardless of the complexity of the wound, if the skin integument becomes damaged, bleeding and coagulation is inevitable [68]. Figure 3.1 and Figure 3.2 represent two of the four stages through of a wound healing in its third day and third to seventh days, respectively.



(Third day) (Kujath and Michelsen 2008)

FIGURE 3.1: EARLY PHASE OF WOUND HEALING



(Third to seventh days) (Kujath and Michelsen 2008)

FIGURE 3.2: EARLY PHASE OF WOUND HEALING

Although we cannot understand all the parameters and factors that contribute to the “normal” wound healing process, we are certain that particular physiological parameters, such as oxygen perfusion and tissue bacteria levels, influence the microenvironment of the wound bed. Nonetheless, there is only so much time per patient, and a battery of tests cannot be conducted in every patient visit. At best, clinicians take wound measurements; perform debridement of the wound bed, depending on the severity of the wound; and judge the health of the wound bed to assess the extent of healing compared with its condition during the patient’s previous visit.

3.3 WOUND CLASSIFICATIONS

There are two categories of wound classification: partial and full thickness and acute or chronic wounds. Partial- and full-thickness wounds infer a partial or full loss of the epidermis and dermis.

Full-thickness wounds frequently involve a loss of deeper tissue layers, including subcutaneous tissue, muscle, and bone [2]. Figure 3.3 shows a schematic diagram of the anatomy of the skin, showing the depths of penetration of human skin and tissue when a wound occurs. Surgery or trauma typically causes acute and chronic wounds. Acute wounds are unexpected, sudden wounds [2]. Chronic (acute) wounds fail to follow the expected wound healing process. In many instances, other issues, such as vascular compromise and imbalances in the body, including those that diabetes creates, perpetuate chronic wounds [2, 69, 70].

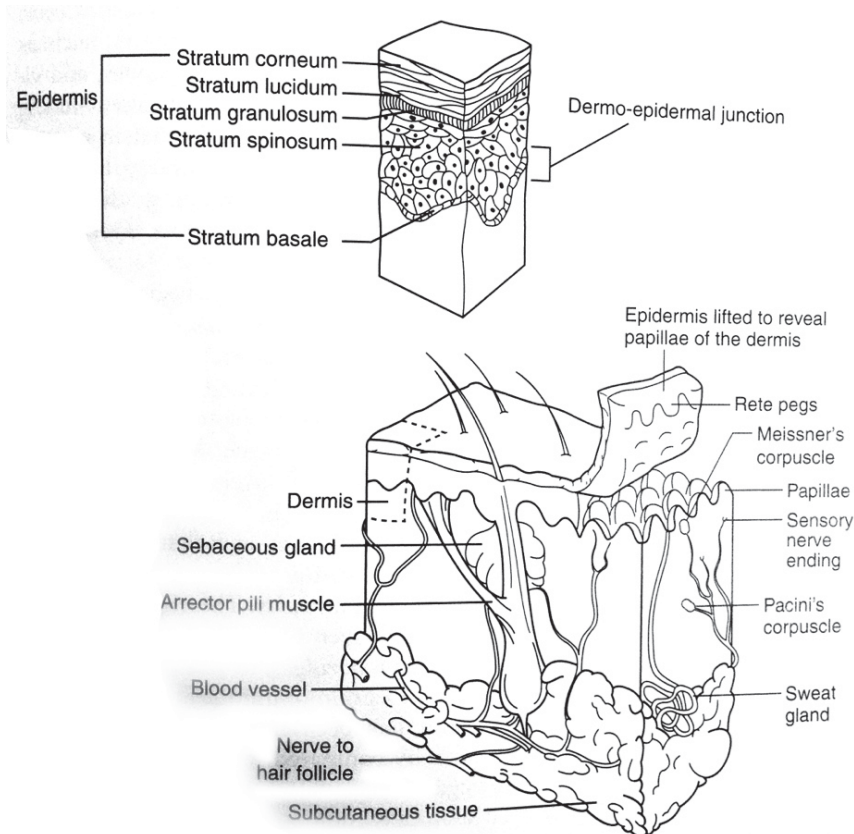


FIGURE 3.3: SCHEMATIC DIAGRAM OF ANATOMY OF SKIN [2, 71]

3.4 CHRONIC WOUNDS ON LOWER APPENDAGES

Chronic wounds on the lower appendages account for 70% of most wounds at typical wound clinics [72]. They fail to heal in a timely manner. Prolonged inflammation, failure to epithelialize, and defective reconstruction of the extracellular matrix typically cause chronic and nonhealing wounds [73]. They are most often associated with abnormal wound odor, inability to properly drain, and patient discomfort [73]. Furthermore, chronic wounds that occur on the lower appendages historically are more slower to heal because of their location on the body. Lower appendages are

the last to receive circulation, to receive oxygen, and to receive nutrients. The circulatory system cycles from top to bottom, which inherently causes the lower appendages, including the, calves, feet, and toes, to bear the constant forces and pressures of walking.

Patients develop chronic, nonhealing wounds for many reasons. For many patients, their body lacks proper blood circulation; without adequate blood supply to an injured area, healing becomes more difficult. Similarly, blood pressure, blood flow, pulse volume, capillary perfusion, and the amount of oxygen near a wound are also wound healing indicators. These indicators are especially important for lower appendage wounds because the lower legs, feet, and toes are the last to receive circulation.

Particular characteristics are attributed to the development of chronic wounds. For example, they generally have a prolonged inflammatory phase and deficiency of growth factor receptor sites [2]. Additionally, many chronic wounds do not have an initial bleeding event. This initial bleeding is significant in the process of wound healing because it triggers fibrin production and the release of growth factors. What is more, individuals who develop chronic wounds have a high level of proteases. However, the greater biological impact on individuals with chronic wounds is the deficiency of growth factor receptor sites and cellular senescence — a decrease in proliferative potential and the loss of ability to respond to growth factors, typically in elderly patients [2].

3.5 WOUND TREATMENTS

The treatment of chronic wounds is important because proper treatment affects the length of time to heal. Although understanding various wound treatments is important, we will detail only a few of the most common treatments. The predictive model does not directly take into account the treatments between each visit. Therefore, we do not provide substantial detail pertaining to various treatments. However, it is important to document the most common chronic wound treatments.

One type of treatment is a three-layer high-compression system, which 3M developed. The use of a Class 3, high-compression system is common in lower extremity chronic wounds specific to patients with venous and arterial diseases [74]. Compression of the wound works in much the same way as stitches work. When a wound is compressed, the epidermis and dermis layers of the skin that comprise the wound perimeter squeeze together in an attempt to stimulate skin growth. For many patients with venous disease and venous hypertension, some degree of compression should continuously be used [74].

For diabetic wounds, treatments involve more maintenance of the wound from infection. The second type of treatment involves the use of topical antimicrobials that can be effective in healing chronic wounds. However, diabetic wounds are more prone to infection. As a result, the most common treatment for these wounds is the use of antibiotics. Neuropathy, or nerve damage, is among the most common problems that individuals with diabetes experience. Neuropathy causes a lack of feeling in the damaged nerve endings, which are typically in the lower appendages. This lack of feeling results in the development of wounds.

The balance of moisture and good bacteria to heal a chronic wound is the third type of treatment. This balance is a key component in the success or failure of the wound healing process. Various types of dressings for chronic wounds can have a great impact on wound healing. Various types of dressings maintain certain levels of moisture in the wound healing environment. Similarly, different types of wound dressing manage and protect periwound skin [74]. Clinicians look for wound dressings that maintain their position on the body, minimize shear and friction, and do not contribute to additional tissue damage [74].

3.6 ISSUES IN WOUND CARE CLINICAL PRACTICE

Many influences affect the efficiency of the heavily regulated healthcare industry. Limited federal and state regulations exist to control the quality of wound care clinics, which must comply not only with federal and state regulations, but also with insurance companies and payment regulations to receive reimbursement for their services. Figure 3.4 provides an overview of the “Wound Care Diagnostic Triangle Dilemma,” in which all wound clinics try to balance fast wound healing, the quality of wound care, and reimbursement.

In the medical industry, a number of components are involved in the quality of patient care. These components include not only well-educated and trained physicians but also procedures, tests, reimbursements, financial management. The diagnostics of a wound are challenging because each procedure on a wound needs to be reimbursed somewhere down the treatment pipeline. If a nurse underestimates the size of a wound or the length of treatment, the institution loses money. However, if a nurse overestimates the size of a wound, insurance companies can question documentation, records, and procedures. These situations occur because centers receive part of their reimbursements based on their measurements and outcomes. In essence, wound state determination is a triangle of conflicting obligations, with medical insurance companies on one side, quality of wound care on another side, and determination of wound depth and shape on the third. Figure 3.4 shows an explanation behind the three thematic sides of the triangle.

The quality of patient wound care should be the first and foremost concern of wound care facilities. However, with any situation, we question the right balance of care, cost, and reimbursement. One of the major issues between wound assessment and medical insurance is the process of wound measurement. The double-edged sword is that wound measurements are prone to human inconsistencies but insurance companies reimburse on the accuracy and size of the surface area. Unless an improved imaging device with a built-in measurement system becomes standard in wound clinics, measurement variability is unavoidable.

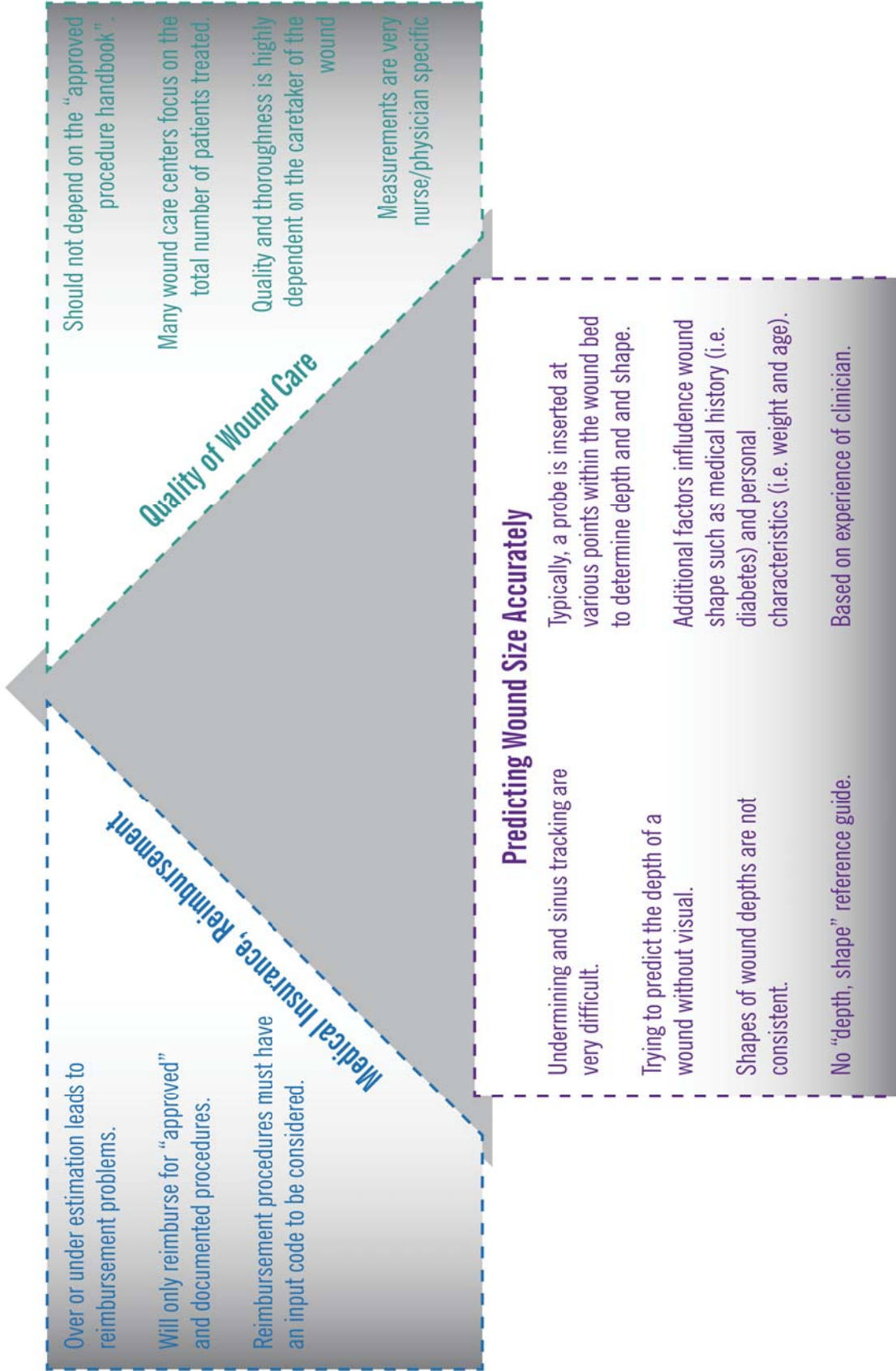


Figure 3.4: Wound Diagnostic Triangle Dilemma

Even with improved technology, we discovered that not every wound clinic uses photographic evidence to document the progress of wound healing. Photography of wounds is a basic, simple, and logical assessment technique that should be common across all wound clinics. Unfortunately, we have observed that photographing wounds is not routine.

The previously mentioned issue has been discussed with various practicing clinicians. Those who do photograph patient wounds to follow their progress, reason that Medicare and Medicaid require photographic evidence for reimbursement. Those facilities that do not photograph on a regular basis have various reasons for not doing so. Some facilities state that photographic evidence is unnecessary to judge the health of the wound. Other facilities submitting the photographs with the insurance claim puts them in the hands of inexperienced, nonexpert wound care specialists — insurance agents. Further, nonspecific-wound care clinicians may judge photographs by deeming wounds as not healed when in fact they are looking at photos of healthy wound beds. Similarly, wound care treatment is a delicate process, and the body sometimes requires stimulation to facilitate wound healing. In many instances, the necessary treatment of a wound is to increase its size to promote healing because of the patient's healing trajectory.

With the implementation and initiative of electronic medical record systems across all wound clinics, a discrepancy exists between a general EMR system and a wound care-specific (electronic medical records) EMR system. Figure 3.5 displays the overall general patient wound care procedure. In Figure 3.5, the last three steps illustrate what occurs during a small window of time between patients when the nurses input their notes into the EMR system. If nurses do not input their notes during this small time window, a backlog of paperwork occurs. The nurses have approximately five minutes to input their assessments before retrieving the next patient. For those clinics that see approximately 30 to 40 patients a day, time is critical for maintaining on-time patient satisfaction. There were many instances in which we observed the nurses waiting 30 to 60 seconds for the system to load the appropriate patient page. Although this amount of time is insignificant in many situations, for operational efficiency of a wound clinic, such a system wastes time and tests patient satisfaction.

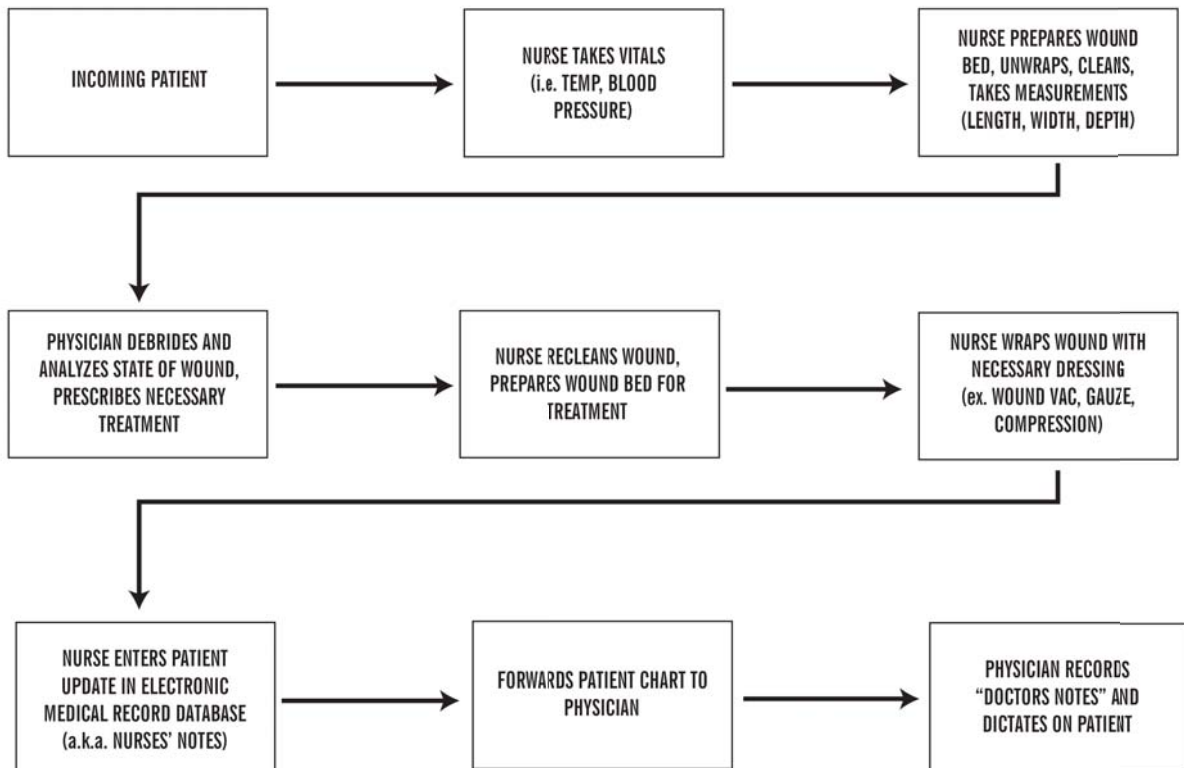


FIGURE 3.5: SUMMARY OF RBMC PATIENT PROCEDURE

Similarly, additional unpredicted and unforeseen factors may appear, including training and retraining the staff to use the selected EMR system. Many physicians and nurses work at a collection of hospitals and facilities. Each facility has a different EMR system that physicians – some of whom travel to three or four facilities per week – and nurses must learn.

A major and noticeable observation during the clinic visits was the use of an incorrect EMR system for many wound clinics. In view of the Obama Administration’s EMR initiative, many facilities are “scrambling” to implement and meet the federal government timelines. We observed that most facilities needed wound care-specific EMR systems that allow the inclusion of photographs in medical records. Many wound care-specific centers are using general EMR systems that are not appropriate for chronic wound care. EMR systems for wounds promote patient safety and reduce costs through routine chronic wound management [75].

CHAPTER FOUR WOUND ASESMENT METHODS

CHAPTER FOUR

Wound Assessment Methods

A number of noncontact, three-dimensional wound surface modeling techniques have been developed. However, none have been widely accepted by practitioners due to their low accuracy, high cost, and complicated calibration procedures [51]. Researchers have also posed other techniques, such as a tracing paper system in which a plastic film is placed over the wound and physically traces it with a stylus — an obtrusive procedure with a potential for infection.

Previous studies focus on the three-dimensional modeling of a wound based on geometrical data, chromatic data, thermal data, or all of these types of information [22]. Similarly, some studies imply that tools provide a better quantitative understanding of the state of a wound. However, nonhospital systems promote the direction of telemedicine and at-home medical aids or that link high-quality three-dimensional modeling and quantitative diagnostic tools to aid monitoring of wound progress. An ideal technique is to employ a method that does not require contact but is able to measure blood flow and other internal characteristics of a wound. The most common methods for quantifying wound progression rely on antiquated techniques of physically measuring the length and width of a given area. Moreover, the reliability and accuracy of physical measurements are problematic because these techniques can be cumbersome and prone to human error.

4.1 CURVATURE-MAPS-BASED METHOD

Wound surface modeling has become a popular method in determining wound contours. A previous study focused on wound measurement using curvature maps and a laser scanning system. The curvature maps provide some vital data on the topology of the wound; it is simply a noncontact measurement system to acquire a physical model of the injured area [51]. FastSCAN is

a common three-dimensional laser-scanning tool used to acquire the topology of a wound to create curvature maps but does not collect any medical data.

Other studies have focused on the use of a nonuniform, rational B-spline (NURBS) surface technique to measure the ulcerated region and respective wound boundary. Computer graphics and imaging analysis use NURBS to create, generate, and represent nonuniform curves [76]. Overall, this method uses numerous modalities that assist in the management of chronic wounds. However, the method lacks reliability and standardized wound measurement techniques to better assess the healing process of a wound [51].

4.2 THREE-DIMENSIONAL CONSTRUCTION-BASED METHOD

Only a few methods can acquire a three-dimensional model reconstruction of wounds. The most common methods are extremely invasive and potentially painful to the patient. Alternative wound measurement techniques include molds and saline infusions, similar to dental molds [22]. Jeltrate measures wound volume as an alternative method to planimetry. Jeltrate is inserted and injected into wounds to reproduce their three-dimensional shape [22, 77]. Its volume is then calculated by weighing the mold. Although dated, Jeltrate is still in use. This method is more susceptible to cross-contamination and time-consuming; it is also uncomfortable for the patient [22, 77]. A similar method to Jeltrate is injecting a saline infusion into the wound using an amount of liquid dispensed from the syringe that is equal to the volume of the wound. This process is less accurate than a mold due to the possibility of absorption by wound tissue into the body [22]. Moreover, this method is also uncomfortable for the patient.

The Advanced Topometric Sensor II (ATOS II) optical measuring technique uses stereophotographic systems to calculate a three-dimensional map of the wound surface. ATOS II uses dual charge-coupled-device (CCD) cameras and a central projection. This technique uses various fringe patterns on the object of measurement and images are captured by software. These fringe patterns allow for a three-dimensional coordinated map of the wounds surface. However, ATOS II was originally developed for forensic medical use and provides no quantitative surface measurements, such as height, width, and depth.

4.3 DIGITAL CONSTRUCTION-BASED METHOD

There is also research on three-dimensional model reconstruction using a traditional digital camera. This technique uses noncalibrated photography using the Iterative Closest Point (ICP) algorithm

[78]. The ICP algorithm is the dominant method of aligning two- and three-dimensional models based purely on geometry and, periodically, color [79]. The ICP algorithm is used to minimize the distance between two points in space. It performs this process by looking at local neighbors to estimate the transformation parameters using mean-square cost function. ICP is an iterative process for acquiring an accurate estimation of the points [79]. Unfortunately, the ICP algorithm is prone to accumulative errors that can lead to mapping failures. However, its primary purpose of aligning two matrices, two meshes, or two photographs is the relevant aspect to this study.

The use of three-dimensional modeling for wound surfaces and wound depth is not new. A 2007 study focused on a three-dimensional measuring device using a photometric camera and modified laser retrofitted to a digital camera [76]. Researchers in Austria developed this technique, which integrates digital photography and a three-dimensional laser-based analysis. The digital camera acquires the focal length, exposure time, and shutter time, and the laser acquires depth of the wound. The rapid photography technique requires limited calibration. This method has limitations with precise measurements of flat wounds and irregularities in wound boundaries. Although the precision is inconsistent, it is one of the more compact methods developed to model a wound.

4.4 COMMERCIAL SYSTEMS

Commercial systems for wound modeling exist, but no system is singularly above the rest. Many of the commercial systems are contact-invasive, awkwardly intrusive, or two-dimensional in data acquisition. These techniques are prone to cross-contamination and secondary wound infection [52]. The computations of wound areas are made by approximating the contour regions. Systems that estimate wound contouring base their approximation on conventional shapes, such as rectangles; ellipses; and length and width — also known as ruler-based methods [22]. More common approaches exist in acquiring two-dimensional measurements from different angles and extracting a three-dimensional model. Several digital planimetry systems are commercially available, each unique in its own right; however, none are ideal.

The commercially available Visitrak wound measurement system was developed to “standardize the approach of wound measurement” [80]. There is no standardization regarding the system itself. Visitrak is a portable tablet that measures the wound dimensions and wound area in an extremely invasive manner [80]. It requires the patient to place tracing paper on the wound and trace the wound boundary. This method exposes the patient to unnecessary risk for infection and cross-contamination. Figure 4.1 displays the Visitrak Tracing Methodology. Visitrak also does not produce a three-dimensional model.

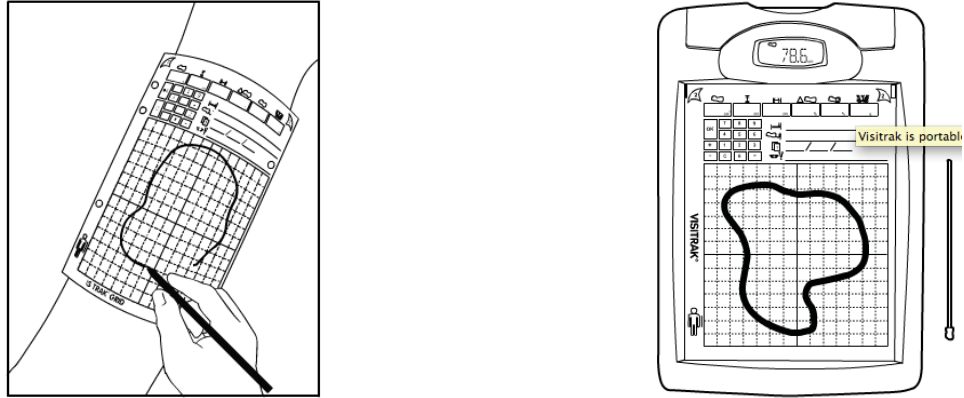


FIGURE 4.1: VISITRAK TRACING METHODOLOGY [80]

A similar system, from Vision Engineering Research Group (VERG), uses a 3x3-cm reference that is placed on the same plane as the wound for calibration. The VERG system is also based on a manual tracing technique following the wound periphery. Unlike Visitrak, in which the tracing is performed against the wound, the VERG system traces based on a photographic image projected on the computer. This software allows the clinician to trace on the computer rather than on the patient (Figure 4.2) [52].



FIGURE 4.2: VERG WOUND MEASUREMENT SYSTEM [52]

Although there has been recent progression in wound diagnostics, three-dimensional wound modeling is still in its infancy, and there has yet to be a system to incorporate all the components

we are proposing. In Europe, there is more research being performed in this area, resulting in systems such as Measurement of Area and Volume Instrument System (MAVIS) (Figure 4.3). MAVIS uses a camera to create a three-dimensional contour of a wound using the area and volume. Similar to the VERG system, this system lacks the ability to measure the true depth of the wound [48, 53].



FIGURE 4.3: MAVIS-II THREE-DIMENSIONAL WOUND MEASUREMENT INSTRUMENT [48, 53]

Mephedos is another system that has been documented as similar to the method proposed in this research. Mephedos uses four optical cameras mounted on a tripod. The ability to see and perceive a scene at slightly different angles creates depth. Human beings can perceive depth because they have two eyes. The loss of sight in one eye limits depth perception. Similar to human eyes, Mephedos uses the four optical cameras to create a single triangular frame, allowing the combination of images to create three-dimensional image [47]. This system is extremely sensitive to accurate calibration and light reflectivity. Wounds provide a moisture bed for both good and bad bacteria, resulting in reflective pus. This unpredictable situation causes the Mephedos system to fail due to specular reflections and misinterpretation of wound parameters [47].

4.5 TELEMEDICINE WOUND MANAGEMENT

More recently, telemedicine, a new technique for medical imaging and health monitoring has been developed. Telemedicine allows patients to receive diagnoses and health-related advice through the Internet. This new wave of medical treatment allows physicians to diagnose and assess the management of wound care using electronic communication rather than physical appointments. Several clinical studies showed positive results with telemedicine assessment and patient satisfaction [81]. Furthermore, another study supported the use of telemedicine for wound care assessment to the extent of determining wound condition and possible treatment options [82].

With the exponential growth of smartphones, consumers have more access to health self-monitoring resources. With the growth of the smartphone market, consumers can now download apps to their phones that allow self-health responsibility. Various companies now offer wound management and wound tracking applications that enable patients to photographically monitor the progress of their wounds.

The WoundSmart® documentation tool allows patients to document their wound healing progress from their smartphones. This app was developed by wound care specialists for personal or professional wound documentation. The application allows a user to track multiple patients or one patient with various demographic information [83]. This app is specific to wound management and wound tracking rather than wound analysis. Figure 4.4 provides screenshots that show the limitations of WoundSmart®.

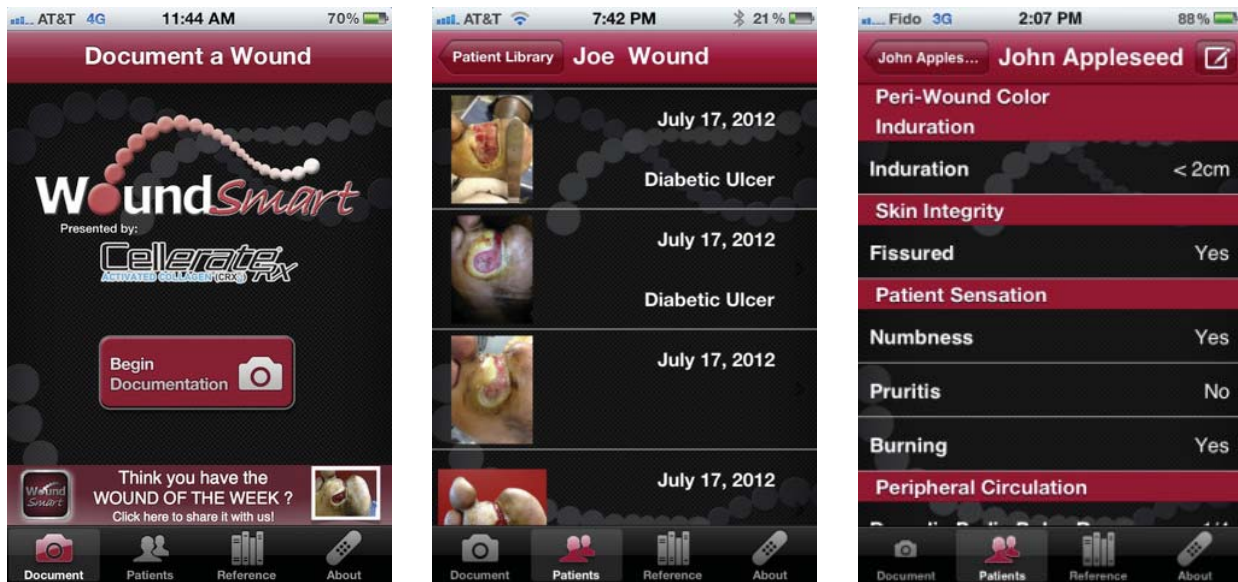


FIGURE 4.4: WOUNDSMART® APP USER INTERFACE [83]

A more comprehensive wound management app was developed to analyze pressure wounds. Wound Analyzer® allows patients to view the region of interest and to take images using smartphone cameras [84]. The Wound Analyzer® application differs from WoundSmart® in that Wound Analyzer® allows users to segment the images into red, yellow, or black segments and thus more accurately estimate the health of the wound. The app itself is intended for wound care providers rather than personal wound tracking management. Figure 4.4 provides screenshots that show the limitations of Wound Analyzer.

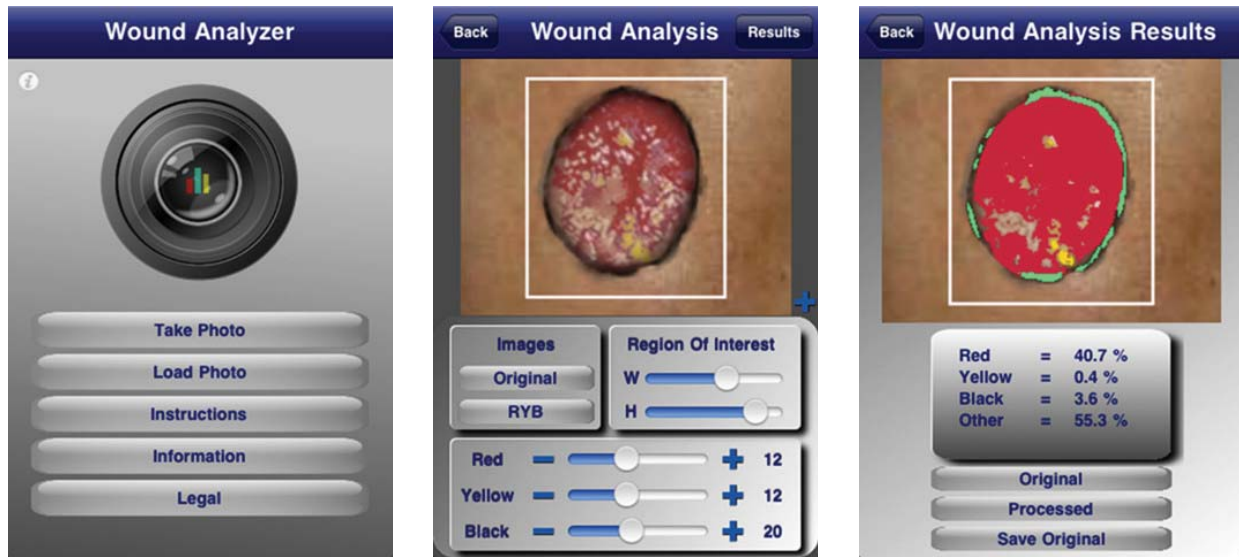


FIGURE 4.5: WOUND ANALYZER APP USER INTERFACE [84]

The previously mentioned wound management applications are the only two relevant electronic health apps that allow clinicians and patients to track and monitor their own wounds. There are, however, limitations to these apps. Both apps are recommended for use with wound clinician expertise and do not promote the ability to diagnose wounds. Furthermore, the apps have not been scientifically validated through clinical studies and do not currently abide by the same Food and Drug Administration (FDA) laws.

4.6 EXISTING PREDICTIVE METHODS

Predictive models have existed for years in areas such as the stock market or real estate market. Yet, predictive models have recently become more prevalent in medicine. For example, numerous genetic studies and tests can predict a patient's susceptibility to cancer based on presence of certain proteins or certain biomarkers within the body [34, 36]. Predictive models also exist for the prediction of consumer behavior and why people buy what they buy [40, 85]. In other words, prediction is a popular method of trying to anticipate and monitor actions and reactions. However, in wound healing and treatment, scarce research exists for predictive quantification.

Based on the literature review, no wound predictive models truly predict. As mentioned, they focus primarily on cancer and tumor detection rather than wounds [42]. Azimi [42] focused his research methodology to monitor and predict daily tumor volume and surface changes of head and neck

tumors. His method used regression analysis to effectively predict models for tumor geometry and analysis of results. The Azimi model generated two kinds of prediction — one dependent on tumor volume and the other based on tumor surface variations [42]. However, the significant difference in his model is its dependency on the quantitative amount of chemotherapy a patient receives. The method relies on the feedback of a visual analysis to determine whether a treatment is working.

4.7 SUMMARY

Although wound systems exist in research and commercial applications, none encompasses ideal functionality for measuring or modeling a wound. Furthermore, none of these systems applies a quantitative determination of the wound progression state. Although modeling of a wound is significant in understanding wound pathology, a model simply does not help in quantifying its state of healing in the shortest time, which is the ultimate goal. The existing research and commercial methods have progressed chronic wound analysis but lack the ability to be used in real-time clinic settings. We must better determine the appropriate and relevant patient and wound parameters to establish which characteristics indicate proper wound healing.

CHAPTER FIVE WOUND PARAMETERS

CHAPTER FIVE

Wound Parameters

Wound evaluation, treatment, and analysis vary depending on the institution, the hospital, or medical facility. A chronic wound is one that is nonhealing or that does not follow the healing stages within 12 weeks of acquisition [21, 64, 68]. This section will discuss four wound centers, Tufts Vascular, Wound, and Hyperbaric Center (Tufts) in Boston; Morganti Wound Center (Morganti) in Danbury, CT; Raritan Bay Medical Center (RBMC) in Perth Amboy, NJ; and Vohra Wound Care Physicians (Vohra) in Mirimar, FL. These sites typically receive patients whose wounds have not progressed in healing for a substantial amount of time. These wounds usually have existed for approximately eight to 12 weeks, and the patients' primary care physician cannot achieve healing. Unlike the other three clinics, Vohra is a private company that provides wound care nurses and physicians to patient rehab facilities and nursing homes.

The purpose of sharing the clinic experiences in this thesis is to show examples that currently occur in medical practice and in the general practice of wound care. Understanding what currently exists in practice helps us to better understand how to integrate the methodology in the least disruptive manner.

5.1 TUFTS VASCULAR, WOUND, AND HYPERBARIC CENTER

Tufts Vascular, Wound, and Hyperbaric Center focuses on multidisciplinary treatment for chronic wounds, including diabetic, venous, and pressure ulcers [86]. The focus and wound classification is based on arterial, venous, and diabetic wounds. We observed clinical practice and treatment of wounds to gain a perspective and understanding of chronic wound care treatments and daily activities. Additionally, we developed a sense of what physicians and nurses record pertaining to wounds.

At Tufts, we were exposed to how a toe amputation debridement differs from a callous, large heel wound. Furthermore, the clinic experience at Tufts allowed us to understand how nurses measure the surface area of a wound and understand patient characteristics that are vital to chronic wound healing. We began to understand how patients develop chronic wounds. For some, the chronic wounds occur after a stubbed toe, and, for others, nonhealing results from the patient's failure to comply with doctor's orders.

5.2 MORGANTI WOUND CENTER AT DANBURY HOSPITAL

Morganti Wound Center is in Danbury Hospital. Similar to our experience at Tufts, we observed Morganti for patient care and wound care treatment. Additionally, we worked with the center's clinical manager and learned from his expertise pertaining to wound care-specific training, resources, and hyperbaric medicine. Morganti is wound-care-specific; 50% of its patients' wounds are a result of surgical wounds; and 75% to 80% are wounds below the knee [72]. Morganti primarily tracks surface measurements, such as width and length; however, like most other clinics they use the wooden ends of wooden Q-tip swabs to measure depth.

Bryant et al. [2] has supported the idea that common and accessible wound assessment is important to the management of nonhealing wounds. Their literature has documented procedures for the ulcer assessment, physical assessment parameters, and assessment cofactors. Table 5.1 summarizes this information [2]. A common practice among wound care clinics follow the Bryant et al. [2] procedural assessment in Table 5.1 and Table 5.2. Nurses and physicians track surface measurements, including length, width, and depth of a wound. Using the assessment parameters in Table 5.1 and Table 5.2, wound treatment begins with a patient first seeing a nurse, then the clinical manager, then the physician, and then the nurse again to apply a dressing to the wound.

TABLE 5.1: WOUND ASSESSMENT, PHYSICAL ASSESSMENT PARAMETERS PROCEDURES FOR PRACTITIONERS [2]

Wound Assessment Parameters	Anatomic location of wound
	Extent of tissue loss
	Characteristics of wound base
	Type of tissue
	Percentage of wound containing each type of tissue observed
	Dimensions of wound in centimeters (length, width, depth, tunneling, undermining)
	Exudate (amount, type)
	Odor
	Wound edges
	Periwound skin
	Presence or absence of local signs of infection
	Wound pain
Physical Assessment Parameters	Wound etiology and differential diagnosis
	Duration of wound
	Cofactors
	· Comorbid conditions (diabetes, cardiac)
	· Medications
	· Host infection
	· Pressure ulcer risk factors
	· Decreased oxygenation and tissue perfusion
	· Alteration in nutrition and hydration
	· Psychosocial barriers
· Past therapies	

Table 5.2 summarizes the skin-assessment parameters that literature has acknowledged as the most important in the indication of wound health.

TABLE 5.2: SUMMARY OF WOUND-ASSESSMENT PROCEDURES FOR PRACTITIONERS [2]

Skin-Assessment Parameters
Color
Moisture
Temperature
Olfaction
Texture
Turgor
Lesions
Skin Injury
Nails
Hair

5.3 RARITAN BAY MEDICAL CENTER: THE CENTER FOR WOUND CARE

The Center for Wound Healing at RBMC is in a small, community hospital. Wound care procedures at RBMC are similar to those at both the Tufts and Morganti clinics. RBMC schedules patients at intervals of 30 to 45 minutes. The wound clinic rotates four patient rooms with four nurses and one physician. Typically, the wound clinic sees 25 to 40 patients per day, depending on the analysis of the patients' previous week. RBMC observation provided us insight into their hospital's operational procedure and allowed us to use a thermal imaging camera to photograph patient wounds over a short period. Furthermore, RBMC takes photographs of wounds throughout a patient's duration at the wound clinic as documentation of wound change over time. This documentation allows us to compare changes over time, such as color, size, and temperature. Figure 3.5 summarizes the patient/nurse/doctor procedure at RBMC.

Over three weeks, we visited the same 18 patients, documenting their wound temperature with a thermal imaging camera. The thermal imaging camera provided us the temperature difference between the surrounding environment and their wounds. Chapter 9 documents three of these patients.

5.4 VOHRA WOUND CARE PHYSICIANS

Vohra Wound Care Physicians, a private company, acts as a liaison between wound care physicians and facilities such as nursing homes. Vohra maintains a database of patients and their

respective wounds. This company supplied us with an enormous amount of data to analyze. The data analysis concentrated on 6,600 unique wounds that were treated by a physician a minimum of five times, resulting in approximately 860 unique patient visits and their corresponding wound measurements.

Vohra Wound Care Physicians provided us with data strictly detailing the attributes of the patient wounds. Unfortunately, the company did not provide any patient demographic data due to strict Health Insurance Portability and Accountability Act (HIPAA) privacy laws. The data provided by Vohra included the following wound attributes:

TABLE 5.3: SUMMARY OF ASSESSMENT PROCEDURES FOR PRACTITIONERS

Wound Attribute	Attribute Measurement Unit
Etiology	Arterial, venous, diabetic
Location	Body part code
Date of Service	Date
Length 1	Centimeters
Length 2	Centimeters
Depth	Centimeters
Undermining	Percentage
Granulation	Percentage
Yellow Necrotic Tissue	Percentage
Black Necrotic Tissue	Percentage
Slough	Percentage
Left Doppler	Frequency
Right Doppler	Frequency
Nutrition	Grams/deciliter

5.5 WOUND CARE CLINIC SUMMARY

Based on observations, most wound clinics emphasize detail, thoroughness, and consistency. According to the practices we observed, wound measurement accuracy and reliability is highly clinician-dependent. Swelling, especially in wounds, creates physical tension within the body, potentially causing inaccurate measurements. Similarly, all the practices we observed reinforced the idea that a red wound can heal; if the wound bed is not red and granulation does not expose red tissue, the wound is dead. Moreover, all practices had a general consensus that the wound

bed can support granular tissue only if the wound bed is viable and active. For the wound to properly heal, granulation must occur because it allows new, healthy skin to grow across and close the wound.

5.6 INDEPENDENT PARAMETER CORRELATIONS AND RELATIONSHIPS

Through chronic wound care data analysis, we used a series of correlation plots (Figure 5.1 and Figure 5.2) to determine the importance, relevance, and impact each variable had on the final algorithm. Additionally, we used correlation plots and correlation matrices to determine variable relationship and whether each variable was truly independent of one another.

The final algorithms do not provide every provided input variable. Figure 5.1 shows the relationship between each input variable to each other. It also shows whether any redundancy exists within the input variables by using color to represent the strength of their relationship to each other. The only variables that have a strong enough correlation with each other are the right and left Doppler values. This is expected because the Doppler readings represent the level of circulation in the right and left legs, respectively. We would expect this strong relationship because if a patient has poor circulation in one leg, the probability is greater that he or she would have poor circulation in the other leg.

Figure 5.2 shows a better visual representation of the directionality of each of the input variables and that they are visually correlated, not just that they are correlated. For example, we observe that the right and left Doppler are positively correlated.

Color map of correlations (13.03.16 Training+Test+Cleaned in 130316 Correlation Plots and Heat Maps)

N=27955 (Casewise deletion of missing data)

Variable	Length_1	Length_2	Depth	Undermining	Granulation	YellowNecrotic	BlackNecrotic	Slough	Left Doppler_Numerical	Right Doppler_Numerical	PreAlbumin	Albumin
Length_1	1.000000	0.724686	0.332056	-0.011468	-0.022502	0.056677	-0.010554	-0.031871	0.014016	0.000381	0.003243	0.016069
Length_2	0.724686	1.000000	0.312731	-0.007492	0.009540	0.045145	-0.058718	-0.017166	0.010175	-0.008588	-0.005894	0.018622
Depth	0.332056	0.312731	1.000000	0.042464	-0.172547	0.123580	0.088718	0.032690	0.071920	0.058597	0.010637	0.008263
Undermining	-0.011468	-0.007492	0.042464	1.000000	0.029192	-0.006731	-0.018195	-0.007099	-0.007499	-0.004375	-0.004132	-0.005684
Granulation	-0.022502	0.009540	-0.172547	0.029192	1.000000	-0.278830	-0.045289	-0.190532	-0.110901	-0.091228	-0.031991	-0.031726
YellowNecrotic	0.056677	0.045145	0.123580	-0.006731	-0.278830	1.000000	-0.246136	-0.086363	0.043906	0.040906	0.001971	-0.002612
BlackNecrotic	-0.010554	-0.058718	0.088718	-0.018195	-0.045289	-0.246136	1.000000	-0.197655	0.075310	0.057590	0.017735	0.013311
Slough	-0.031871	-0.017166	0.032690	-0.007099	-0.190532	-0.086363	-0.197655	1.000000	0.028320	0.014659	0.015162	0.028460
Left Doppler_Numerical	0.014016	0.010175	0.071920	-0.007499	-0.110901	0.043906	0.075310	0.028320	1.000000	0.772814	0.006681	-0.032508
Right Doppler_Numerical	0.000381	-0.008588	0.058597	-0.004375	-0.091228	0.040906	0.057590	0.014659	0.772814	1.000000	0.005517	-0.028458
PreAlbumin	0.003243	-0.005894	0.010637	-0.004132	-0.031991	0.001971	0.017735	0.015162	0.006681	0.005517	1.000000	-0.032942
Albumin	0.016069	0.018622	0.008263	-0.005684	-0.031726	-0.002612	0.013311	0.028460	-0.032508	-0.028458	-0.032942	1.000000

FIGURE 5. 1: CORRELATION PLOT DISPLAYED AS HEAT MAP

Correlation (Scatter) Plots

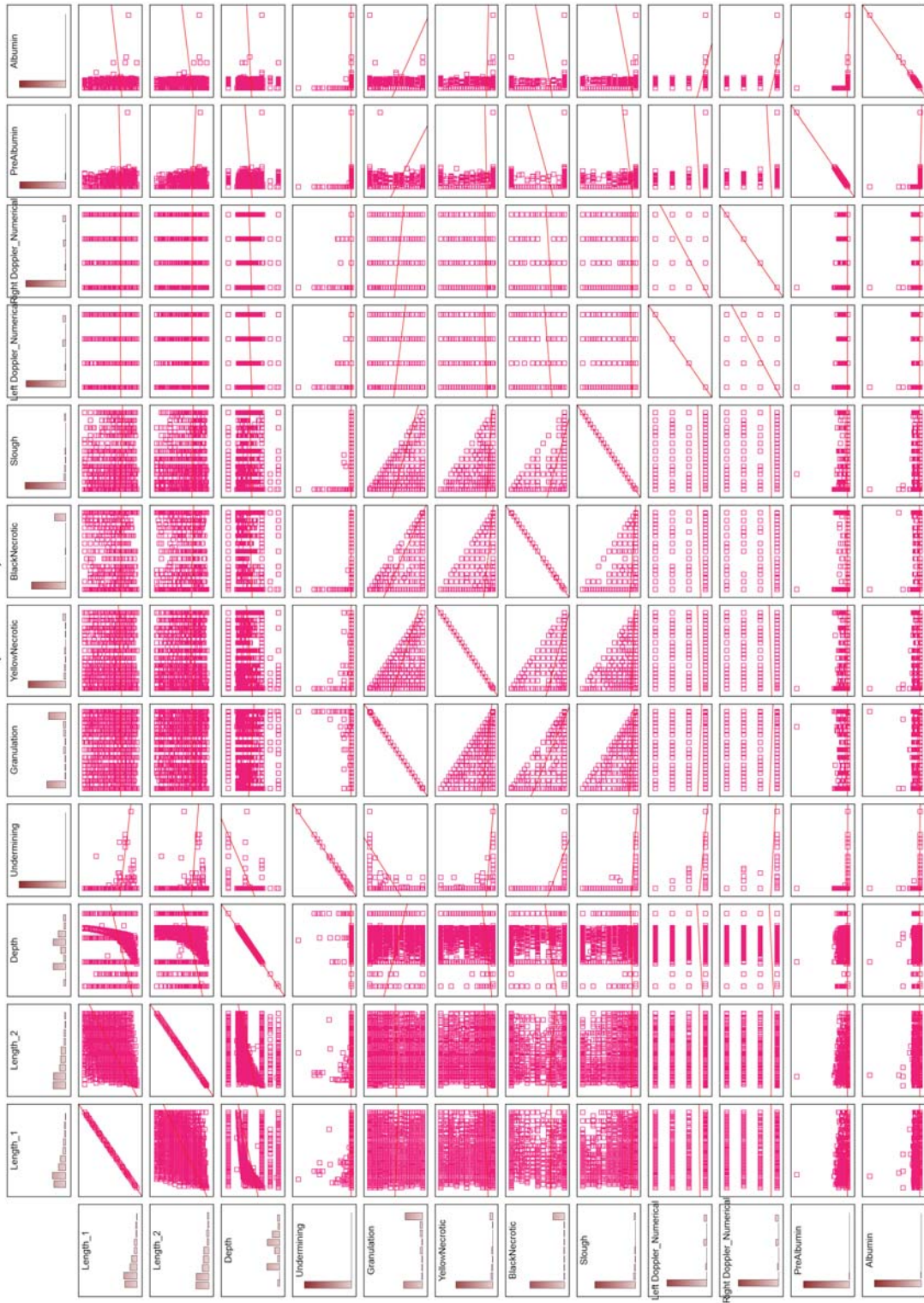


FIGURE 5.2: CORRELATION SCATTER PLOT

5.7 PARAMETER CORRELATION

By understanding the behavior of the data, we were better able to determine the relevant input variables of the algorithms. We determined these variables through a combination of correlation plots and an understanding of recorded wound characteristics that seem to be consistent across wound care facilities. Although some facilities may have a more comprehensive patient and wound data collection than others, we focused on the characteristics that were consistent across facilities or that we could determine through patient's medical records. We have determined that four wound attributes in Table 5.1 and Table 5.2 statistically impact the accuracy and precision of the proposed methodology, as Chapter 9 shows. These four variables are length 1, length 2, depth, and granulation.

5.8 SUMMARY

Through discussions with all facilities, we found that wound care practices lack adequate and consistent tools. This lack hinders their ability to provide consistent and concise standards of care. Furthermore, the tools that are currently being developed to supplement the quality of wound care are for research purposes only, are too expensive for clinical practice, or are inadequate and awkward for clinical use in real time. The variety of wounds these practices experience only propels and reinforces the theory that there is a need for a more efficient system that assists in determining an accurate wound healing methodology.

CHAPTER SIX PRELIMINARY STUDY

CHAPTER SIX

Preliminary Study

To support the pursuit of a larger study, we have performed a smaller study with fewer patients and a limited number of variables. The purpose of this preliminary study is to determine the efficacy of the hypothesis. Based on the visits to these wound clinics, we identified three common issues: 1) lack of consistent measurement tracking; 2) lack of reliable data collection; and 3) lack of monetary funds to purchase equipment. However, the primary observation noticed among all practices is the lack of a standard procedure for care across the respective visited clinics. Although we do not believe that a modeling system can predict healing time for all types of wounds, we expect to see a common system that would encourage more consistent data collection of a common set of wound parameters. This preliminary study focused on three common wound parameters: width, length, and depth. In the larger study, we will add parameters such as granulation as covariate inputs.

The preliminary study focused on the development of an algorithm to predict the number of weeks before lower appendage wounds heal. We present, in this section, 37 original, chronic, nonhealing wounds to examine how the width, length, and depth affect the amount of time to heal.

6.1 DATA COLLECTION

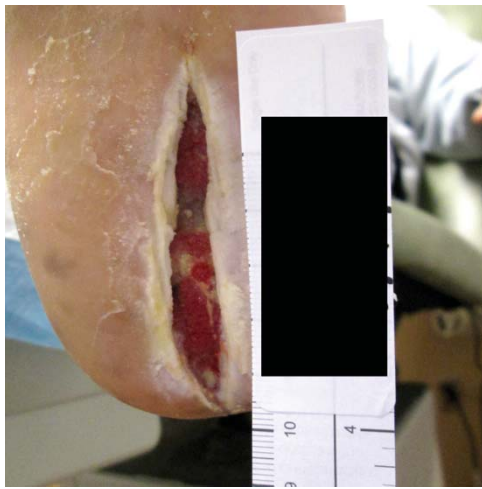
After much investigation, we have identified three primary characteristics in the data collection. Table 6.1 articulates the ideal set of characteristics that we deemed necessary to establishing a reliable predictive model for wound healing time. The extensiveness of details characterizing wounds made data collection and information gathering challenging tasks. We had planned to photograph patients' wounds, and we also verified that data collection, recordings, and clinician measurements on a given patient were reliable and consistent. We noticed that hospital practices use a great variety of techniques in measuring patients' wounds and that this variety has resulted in

inconsistent measurements. Based on these observations, we deemed the retrospective measurements too inaccurate to use in a predictive modeling system.

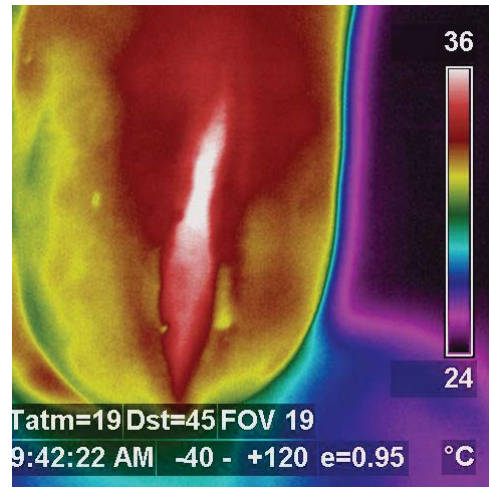
TABLE 6.1: DATA-COLLECTION COMPONENTS

Patient History	<ul style="list-style-type: none"> • Age • History of chronic wounds • Overall health • Arterial disease (yes or no) • Venous stasis disease (yes or no) • Diabetes (yes or no) • Ankle brachial index (ratio)
History of Chronic Wounds	<ul style="list-style-type: none"> • Initial wound development • Time without healing • Historical photos • Previous dimensions
Current State of Wounds	<ul style="list-style-type: none"> • Current dimensions • Depth • Temperature profile • Substantial change (yes or no)

To understand what data to collect, we spent time in wound clinics observing their daily practices. After observing multiple wound clinics, we decided to develop a predictive modeling system that uses both still photography and thermography (Figure 6.1) to allow for more consistent wound tracking and assessment over a long period. From the wound image (Figure 6.1a), we can acquire the respective surface dimensions of the wound. The surface measurements are the typical measured and recorded wound attributes [87] by the previous researchers. The wound thermal image (Figure 6.1b) provides the heat map of the wound to confirm proper healing. Ultimately, images provide qualitative and quantitative data about the wound to help us estimate the length of healing time.



(a) Still Photograph



(b) Thermal Photograph

FIGURE 6.1: WOUND IMAGES OF A PATIENT'S HEEL WOUND

Appendix A shows the data of multiple wounds from multiple patients. The weight variable indicates whether a patient had multiple wounds and thus a predisposition for chronic wound development. For the preliminary study, we used a healing rate of $0.15 \text{ cm}^2/\text{week}$ to estimate the time to heal in weeks. This healing rate was confirmed through clinicians and previous studies that examined whether healing rates were a reliable early predictor [88, 89]. Furthermore, this wound-healing rate was an acceptable consensus among the collaborators at the various wound clinics. Figure 6.2 provides a graphical representation of the data and their corresponding estimated regression lines to provide the initial curvature of the data in Appendix A. The data in Appendix A allows us to further develop a predictive algorithm for wound progression over time. Table 4 provides additional input factors for algorithm exploration. The data will be useful to statistically determine whether the variables are relevant to the time to heal for a patient's wound.

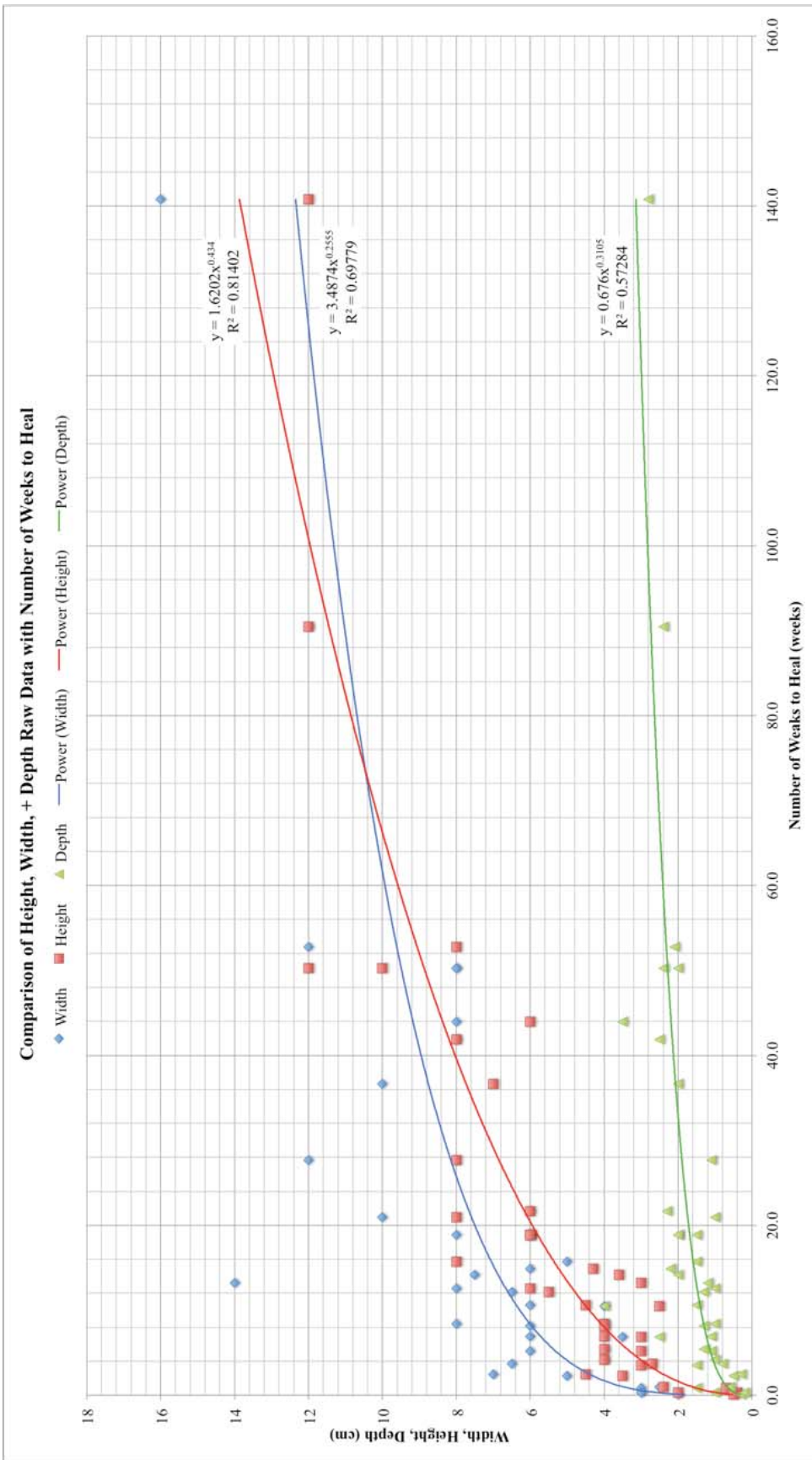


FIGURE 6.2: GRAPH OF RAW DATA AND THEIR ESTIMATED REGRESSION EQUATIONS

TABLE 6.2: INPUT FACTORS FOR ALGORITHM

Administrative Data	<ul style="list-style-type: none"> • Patient reference number • Date of observation
Patient Attributes	<ul style="list-style-type: none"> • Ankle brachial index (ratio) • Diabetes (yes or no) • Venous stasis disease (yes or no) • Arterial disease (yes or no) • Wound location on body
Wound Characteristics	<ul style="list-style-type: none"> • Width (centimeters) • Height (centimeters) • Depth (centimeters) • Wound base (color) • Undermining • Wound shape • Necrotic tissue • Photos (still photography) • Photos (thermal photography) • Predicted cross-section

6.2 STATISTICAL IMPLICATIONS

To establish a reliable and accurate predictive model, we divided the data into two groups: training and testing data points. We used the training data to develop the predictive algorithm (Appendix A) and the testing data to confirm the accuracy of the algorithm.

We performed two analyses on the raw data. Using the original data, we developed a single predictive algorithm that was dependent on width, height, and depth. The second analysis involved the transformation of the raw data to the natural log. The purpose of this transformation was twofold: 1) to determine whether the data could be linear; and 2) whether the natural log transformation simplify the algorithm. The natural log transformation could approximate a linear-regression predictive model and displayed the data as a traditional decay model. The equation of the natural log predictive algorithm is given by:

$$\ln(\text{Time to Heal}) = -1.301 + 1.332\ln(\text{Width}) + 0.414 * \ln(\text{Height}) + 0.805 * \ln(\text{Depth}) \quad (6.1)$$

To determine the validity of the algorithm, the correlation and redundancy of the variables were verified to ensure the reliability of the model. The correlations in Table 6.3 show the strength of the positive and negative relationship among all the variables. This measurement includes the relationships between each input variable to each other and then each input variable to the output variable. For example, width has a strong positive correlation with height and the number of weeks to heal. Similarly, height has a positive relationship with depth and weeks to heal, and depth has a strong positive correlation with weeks to heal. The Pearson Correlation, or correlation coefficient, measures the strength and direction of the linear relationship between two variables. The strongest relationships are among width, height, and the number of weeks to wound closure. Height and width also have a strong correlation, indicating that only one of the variables may need to be in the final predictive model. Although the relationship between these two variables is statistically strong, it is not strong enough to eliminate a variable from the final algorithm.

To create and establish a mathematically accurate algorithm, each variable of the algorithm needs to be evaluated in comparison to the algorithm output. Table 6.4 provides the model summary coefficients for each variable: width, height, and depth. The model summary presents the results of the statistical analysis of the original data to determine the equation parameters. This model summary helps us determine a model fit of the regression equation to the respective variable data and their corresponding parameter estimates. Based on the model summary results and the parameter estimates, the best-fit regression model is selected. Table 6.4 shows the parameters for the best-fit model for width, height, and depth.

TABLE 6.3: CORRELATIONS AMONG VARIABLES

		Width (cm)	Height (cm)	Depth (cm)	Weight	Weeks to Heal (Surface Healing Rate)
Width (cm)	Pearson Correlation					
	P-Value					
	N					
Height (cm)	Pearson correlation	0.676				
	P-Value	.000				
	N	30				
Depth (cm)	Pearson Correlation	0.190	0.360			
	P-Value	0.315	0.050			
	N	30	30			
Weight	Pearson Correlation	0.349	0.160	-0.223		
	P-Value	0.059	0.398	0.237		
	N	30	30	30		
Weeks to Heal	Pearson Correlation	0.713	0.697	0.402	0.150	
	P-Value	0.000	0.000	0.028	0.428	
	N	30	30	30	30	

TABLE 6.4: SUMMARY OF PARAMETER ESTIMATES FOR MULTIPLE-REGRESSION MODEL

Parameter Estimates				
Constant	Width	Height	Depth	
-41.937	5.9885	2.8063	5.7984	
Standard Error				
Constant	Width	Height	Depth	
7.95	1.68597	1.65112	3.372	

The best-fit regression estimate is based on the R^2 value. R^2 indicates the percentage of the variation in time that is explained by the model. The adjusted R^2 makes corrections for the addition of extraneous predictors to the model. Lastly, we use the standard error of estimates to measure the extent at which the data deviates from the best-fit line. We look for the standard error to be small, allowing a good fit of the equation to the data without overfitting the data. The final best-fit linear regression model is given by:

$$\text{Time to Heal (Weeks)} = -41.934 + 5.9885(\text{width}) + 2.8063(\text{height}) + 5.7984(\text{depth}) \quad (6.2)$$

Equation (6.1) allows us to understand the underlying correlation of the variables. It also assists in the determination of whether there is a linear relationship of the input variables and the output variable. Equation (6.2) provides us the actual best-fit linear regression model into which we could input wound characteristics width, height, and depth, and the output will be the number of weeks from wound conception to time to heal.

6.3 MODEL VALIDATION AND VERIFICATION

Appendix A shows 37 wound data points. We use 23 points as training data to develop the model and 15 records to validate the model. The model presented here is a preliminary model to establish the efficacy of the theory and hypothesis. Table 7 shows the model results. The “Actual Output” represents the original data that was received from the patients. The “Theoretical Output” column shows the values of the calculated theoretical time to heal (Weeks) using Equation (6.2). We calculated the error and percent error using the standard error equations in Equation (6.3) and Equation (6.4). For this linear-regression model, the validation data resulted in, on average, a smaller percentage error than the test data (Table 6.5). There are many possible reasons for this discrepancy that we will discuss later in this dissertation.

$$\text{Error} = \frac{\text{Actual Output} - \text{Theoretical Output}}{\text{Actual Output}} \quad (6.3)$$

$$\text{Error} * 100 = \% \text{ Error} \quad (6.4)$$

We believe that, with further refinement of the algorithm and the collection of additional data, the algorithm will be a more comprehensive and robust algorithm. With larger amounts of data, we can better predict a more accurate time to heal of chronic, nonhealing lower-leg wounds.

We recognize that some of the percentage error is high with some of the test records. We hope that, with future studies and more patient information, we will be able to lower the percentage error when testing algorithmic models. With respect to this data, the high percentage error could be attributed to the additional health issues with the patient. For example, the patient could claim compliancy and not be truly compliant. Nutrition also has a big impact on wound healing. As a

result, another factor contributing to the high percent error could be the poor nutrition of the patient. The high percentage error could be the result of a multitude of other, uncontrollable patient issues that we did not have access to for this study.

TABLE 6.5: MODEL TEST DATA

Actual Output	Theoretical Output	Error	Percentage Error
90.5	77.52	0.13	12.98
15.7	19.15	-0.03	-3.45
3.5	-6.85	0.10	10.35
6.9	1.94	0.05	4.96
18.8	22.43	-0.04	-3.63
27.6	58.75	-0.31	-31.15
5.2	8.79	-0.04	-3.59
36.7	49.19	-0.12	-12.49
8.4	22.99	-0.15	-14.59
0.3	-17.05	0.17	17.35
5.4	0.78	0.05	4.62
0.9	-16.75	0.18	17.65
2.3	0.73	0.02	1.57
20.9	46.20	0.25	-25.30

To show that the data is randomly distributed and is not predisposed to a certain number of weeks, we have constructed a histogram of the distribution of the time to heal in weeks (Appendix A). The histogram in Figure 6.3 appears to skew to the left, and we attribute this phenomenon to the fact that most wounds in this data set have similar dimensions. We believe that, with a larger data set, Figure 6.3 will shift from a left-skewed data set to a more normal distribution.

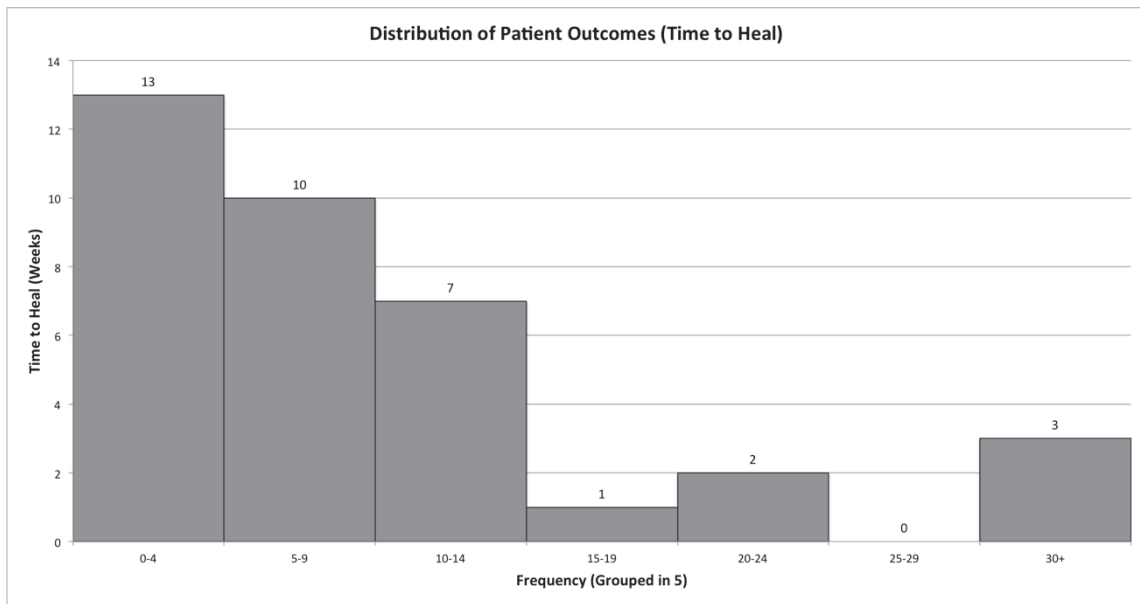


FIGURE 6.3: DISTRIBUTION OF TIME TO HEAL IN WEEKS

6.4 SUMMARY

This study presents preliminary findings on the development of a predictive model for chronic wound healing time. It appears that the length and width appear to have a strong relationship with wound healing time and perhaps re-create redundancy in the algorithm. However, this finding can be confirmed only with additional data collection and analysis. We believe that, with a greater variety of patient data and wound characteristics, the algorithm will become more reliable in its predictive capabilities. The next phase of development for this study is to collect more data and refine the algorithm to incorporate additional wound attributes. It should also focus on additional wound characteristics and photographic evidence to determine whether temperature can be an accurate predictor of wound health and wound viability.

6.5 LIMITATIONS

We recognize that this study has limitations regarding the number of possible inputs for a predictive model for wound healing. Additionally, we recognize that the sample size is not statistically large enough to develop a truly reliable and robust model. We designed this study to ascertain and test the efficacy of the hypothesis in developing a wound healing predictive model. The wound characteristics in Table 5.1 and Table 5.2 would be the ideal set of characteristics to better predict wound healing. In this data sample, we do not have access to additional patient health information. For the preliminary study, we did not know how other factors affect the result of healing time. We hope that, with the larger study, we would have access to more patient

information and health records to determine whether the other characteristics affect the predictive model accuracy. One final limitation of not only this study but also all wound care assessment studies is human variability in wound measurements. The effect of human measurement variability impacts the predictive model at the microscopic level, but when patient data is recorded over a period of months, the macroscopic observations provide a more definitive trend.

6.6 PRELIMINARY STUDY ANALYSIS

This preliminary study presents preliminary findings on the development of a predictive model for chronic wound healing time. It appears that length and width have a strong relationship with wound healing time and perhaps re-create redundancy in the algorithm. We confirmed this finding with the larger data set and analysis in Chapter 8.

CHAPTER SEVEN

WOUND HEALING MODELING METHODOLOGY

CHAPTER 7

Wound Healing Modeling Methodology

7.1 METHODOLOGY OVERVIEW

The core of the method is its ability to use a predictive model to quantify the percentage of a wound healed over a period of time. This method will provide clinicians with a better understanding of what treatments will be successful. Additionally, the wound diagnostic system will further the progression of telemedicine and the ability to monitor wound progression from remote locations. Figure 7.1 shows an overview of the proposed methodology and its respective components.

The uniqueness of this method is determined by the combination of qualitative and quantitative information available to clinicians. The health of a wound is determined in the following order of importance: the health of the tissue, the presence of granulation, the size, and the drainage of the wound. These parameters are the primary components that determine the health of a wound. Further, they are all parameters that are determined by observation — enormously subjective and prone to human judgment. The method uses still photography and thermal photography to accurately measure the size and depth of a wound. By providing the ability to more accurately ascertain the topology of a wound, it will provide a better understanding of the wound's characteristics. Using the combination of still and thermal photography, the method provides us with information on the viability of the wound — that is, whether the wound bed itself can support wound healing.

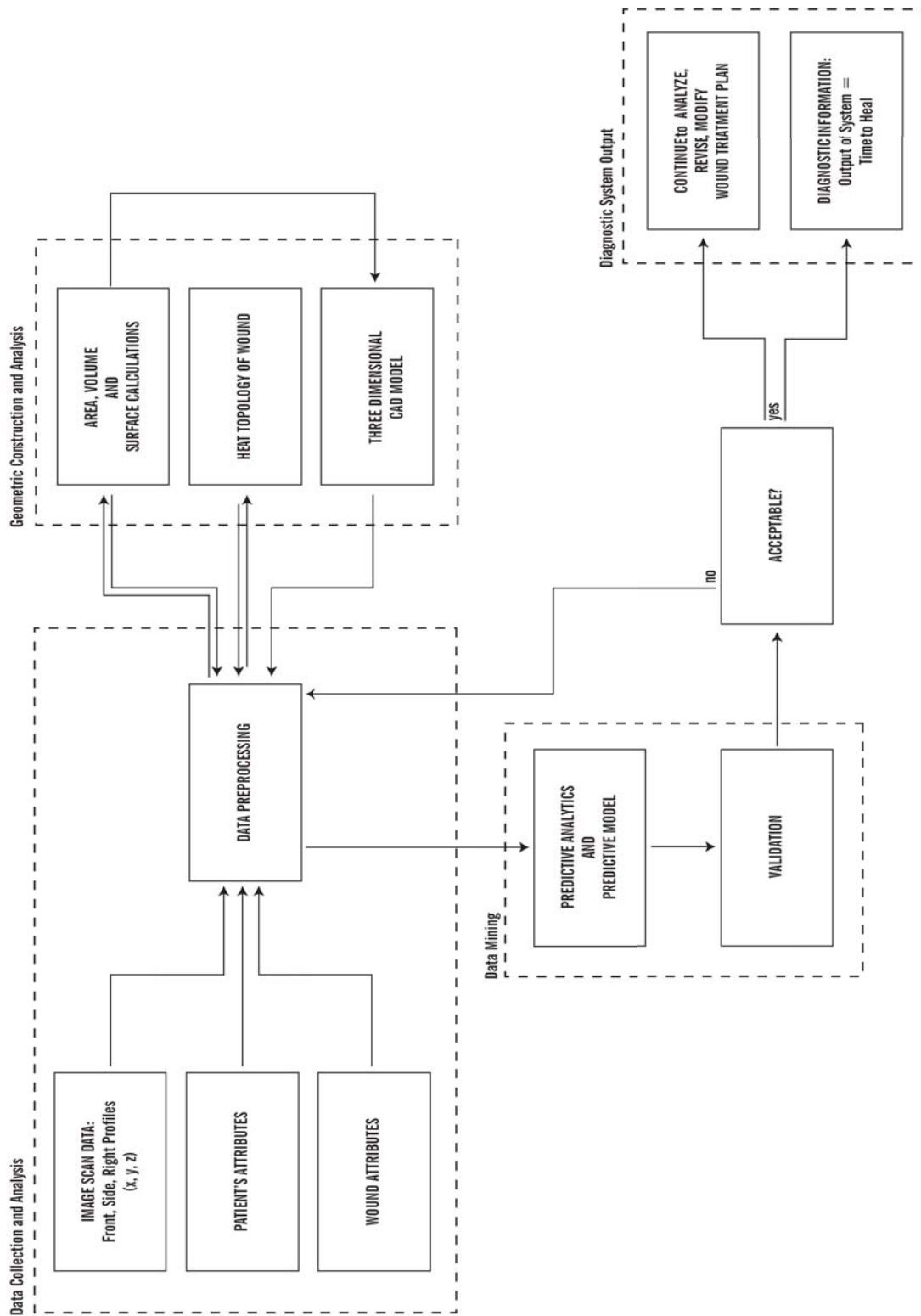


FIGURE 7.1 : TIME TO HEAL CHRONIC METHOD

In further detail, the method will have three overall stages: 1) data acquisition and analysis; 2) image acquisition, geometric construction and analysis; and 3) data mining, predictive models. The first stage will allow us to collect the data and preprocess it to prepare it for data analysis. In parallel, the methodology will perform image acquisition using both optical and infrared cameras. An optical camera will acquire an image of the top of the wound, and the infrared camera will capture an image of the depth and heat dispersion of the wound bed and surrounding area. The image acquisition will allow us to construct a geometric three-dimensional model to enable us to see over time the wound's growth or shrinkage. The method uses more than a three-dimensional model of a wound, like many of its predecessors use. It is a diagnostic method that will assist clinicians in determining the healing state of a wound in a quantitative manner to eliminate some of the subjectivity of wound assessment. Lastly, we will use this information to create a predictive model in which the dependent variable will result in time to heal, which represents the number of weeks left for the healing process provided that the patient is compliant.

The method is based on prognostics and prediction. This model evaluates and analyzes multiple predictive methods techniques to ensure robust and accurate outcomes. By evaluating and analyzing multiple predictive modeling techniques, we then compare the results, accuracy, and precision of each model within itself and then with each other. There is a strong need for various modeling methods, depending on the type of data we are analyzing. The remainder of this chapter describes the two predictive models that best fit this set of data: regression analysis and neural networks.

We designed this experiment to reflect the nature and variability of trying to predict the amount of time left to heal for chronic wounds. We performed a series of correlation and relationship analyses to determine the importance of the independent inputs to the mathematical models. We explored multiple predictive-model techniques and determined that three methods were ideal for this set of data: multiple linear regression, nonlinear regression, and neural networks. In the following sections, we will describe the theory and intent behind each of the predictive modeling methods. In Chapter 9, we apply each model to the data and compare and analyze their respective results to determine the most accurate predictive model.

7.2 REGRESSION ANALYSIS

Regression models are the most widely known and applied analysis methods that can predict both categorical and continuous values. This situation warrants regression analysis that predicts continuous values rather than categorical values. Regression analysis is a methodology that

models a relationship between one or more independent variables to one or more dependent variables. In this case, the independent variables consist of wound characteristics, and the dependent, or response, variables represent the time to heal.

For the purposes of this dissertation, we will provide a brief discussion on linear and nonlinear regression. The linear-regression technique involves one or more predictor variables and a single response variable [90]. Single linear regression is the simplest regression model. The model is a linear function given by:

$$y = \alpha + \beta x + \varepsilon \quad (7.1)$$

Multiple linear regression involves more than one predictor variable and one response variable. Multiple linear regression is a linear function of response variable y of n predictor variables $x_1, x_2, x_3 \dots x_n$. This is expressed in Equation (7.2) where ε represents the error of prediction [90, 91].

$$y = \alpha + \beta_1 x_1 + \beta_2 x_2 + \beta_3 x_3 + \dots + \beta_n x_n + \varepsilon \quad (7.2)$$

Regression analysis requires that we make certain assumptions. Regression analysis assumes that the predictions based on the equation are the best predictions possible, are unbiased, and have a smaller average squared error than do any unbiased estimates. This methodology is further dependent on the assumptions that [92]:

- 1) The error (ε) follows a normal distribution.
- 2) The linear relationship is correct.
- 3) The predictor variables are independent of each other.
- 4) The variability in y values for a given set of predictors has homoscedasticity — that the variability is the same regardless of the values of the predictors (homoscedasticity).

Regression analysis allows us to use and determine a predictive algorithm with as many numbers of predictors as we choose. However, regression analysis may not need every predictor variable. Through correlation matrices and various statistical parameters, we can reduce the number of predictors to only those that are necessary. The most popular criterion, $R_{adj.}^2$, is given by:

$$R_{adj.}^2 = 1 - \frac{n-1}{n-p-1}(1-R^2) \quad (7.3)$$

R_{adj}^2 is a statistic that is used to assist in the selection of ideal number of predictors that minimizes error and maintains best fit [92].

Another popular statistic is Mallows's C_p :

$$C_p = \frac{SSR}{\hat{\sigma}^2} + 2(p + 1) - n \quad (7.4)$$

Mallows's C_p assumes that the predictive model is unbiased. Good models return C_p values near the total number of parameters (p) plus one.

7.3 NONLINEAR-REGRESSION ANALYSIS

Nonlinear regression models contain the same basic form as linear-regression models. Nonlinear regression is used when linearity and a linear pattern do not fit the respective data. Nonlinear regression modeling is another method used to predict outputs based on given predictor (input) variables. Nonlinear regression is also known as curve fitting or the process to determine the best-fit equation to the observed data [93].

Nonlinear regression allows us to specify the approximate function with parameters as a foundation of understanding what model best fits the behavior of the data. In this case, we predict the steady decline of each wound parameter in an exponential or a logarithmic behavior, as given by:

$$y = \alpha + x^\beta + \varepsilon \quad (7.5)$$

7.3.1 SURVIVAL ANALYSIS

Survival analysis is a predictive modeling technique that is used to model time-to-event situations [94]. Unlike linear regression, survival analysis has a dichotomous outcome and analyzes the amount of time to an event [95]. The importance of this type of modeling refers to the ability to predict the amount of time left for an event to occur. In this case, the time left to heal for chronic, nonhealing wounds. Survival analysis provides us with the tools to understand and assess the relationship between the covariates or predictor variables and the survival time.

Survival analysis hinges upon the comparison between the survival probability and the time to event. This analysis is used with situations such as the recurrence of cancer after treatment. In this

case, the analysis refers to the probability of a wound to heal in a specified amount of time. Survival analysis produces two distinct plots: a survival plot and a hazard plot. The survival plot provides a visual representation of the model-predicted time to heal for the average wound. The hazard plot provides a visual representation of the cumulative model-predicted potential to heal for the average wound [95, 96]. The hazard function is the derivative of the survivor function over time:

$$h(t) = \frac{\partial S(t)}{\partial t} \quad (7.6)$$

Cox proportional hazards method of survival analysis is widely employed in time-to-event data analysis [95]. The Cox regression model is the most commonly used multivariable survival method for assessing the effect of multiple covariates on the time to event. The proportional hazards model assumes that the time to event and the covariates are related through the following equation [97, 98]:

$$h_i(t) = [h_0(t)] * e^{b_0 + b_1 x_{i1} + \dots + b_p x_{ip}} \quad (7.7)$$

where

$h_i(t)$	is the hazard rate for the i^{th} case at time t
$h_0(t)$	is the baseline hazard at time t
p	is the number of covariates
b_j	is the value of the j^{th} regression coefficient
x_{ij}	is the value of the i^{th} case of the j^{th} covariate

Similar to the general survival analysis explanation, the Cox regression model works with the hazard model to separate the baseline hazard function and the survival function. The Cox model assists in distinguishing the contribution of each independent covariate on the outcome or survival of time to event [99]. In other words, $h_i(t)$ represents the probability that the chronic wound will survive until time t .

7.4 NEURAL-NETWORK ANALYSIS

Neural network analysis models the adaptive behavior of the human brain. This data-mining process mimics human thinking, adaptation, and modification. Neural networks consists of a set of nodes that are characterized by input, output, and intermediate nodes [100, 101]. More specifically, neural network consists of four distinct components: a neuron; a set of synapses, or connecting links; an adder; and an activation function [100, 102].

A neuron is the overarching model for information processing that is critical to the operation of a neural network (Figure 7.2) [100]. The neuron consists of three basic elements: a set of synapses, or connecting links; an adder; and an activation function. Specifically, input x_j connects to synapse j . The set of synapses carry the respective information from one location to another. Each synapse is characterized by a weight or a strength that is indicative of the impact that a single input will have on the overall system. The weight or strength is represented by w_{kj} . The k subscript represents the specific neuron in question. The adder or the summing junction represents the combiner for the weighted input signals. Finally, the activation function determines the new level of activation or permissible amplitude range based on the input and current activation and converts them to some finite output signal value [100]. In Figure 7.2, b_k is the externally applied bias that can increase or decrease the net input of the activation function depending on whether the output is positive or negative.

In essence, neural network techniques are series of nonlinear nodes that communicate in parallel. The synaptic weights allow the network to adapt without having an analytical solution [101].

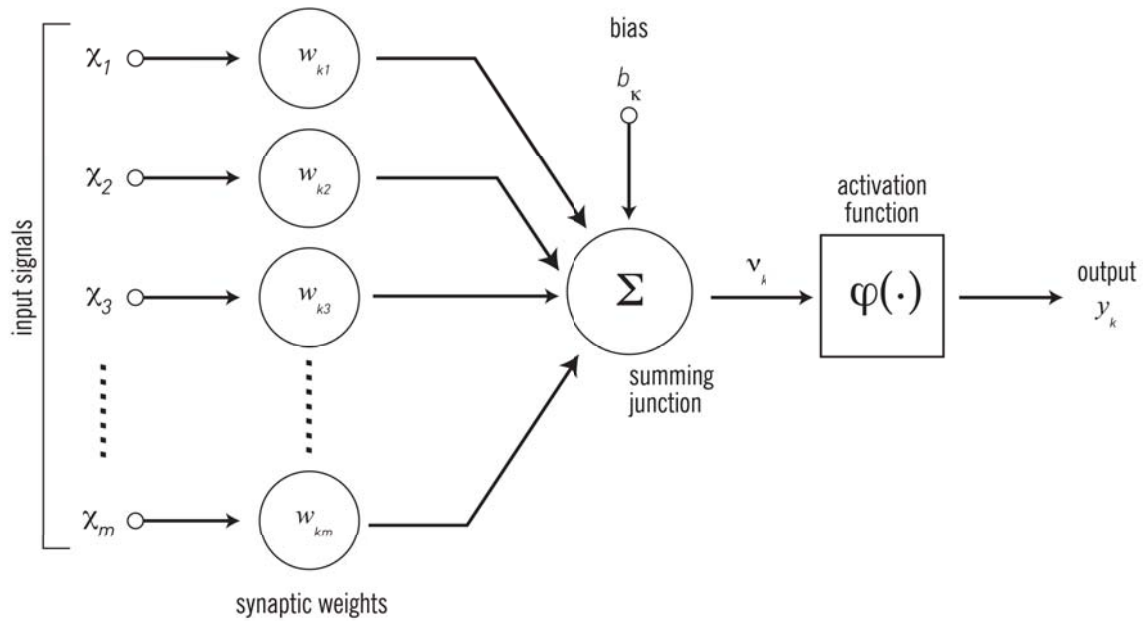


FIGURE 7.2: NEURON MODEL [100]

Figure 7.2 is represented in mathematical terms for neuron k through a pair of equations [100]:

$$u_k = \sum_{j=1}^m w_{kj} x_j \quad (7.8)$$

and

$$y_k = \varphi(u_k + b_k) \quad (7.9)$$

There are two types of learning methods of neural-network analysis: supervised and unsupervised learning. Supervised learning is like learning with a teacher (Figure 7.3). In this situation, the teacher has the knowledge and is able to provide the neural-network environment using various training vectors. The supervised-learning process constitutes a closed-loop feedback system with the

unknown environment outside the loop. Supervised learning is the basis of error-correction learning, in which the neural network is adjusted using an iterative step-by-step process, with the aim of having the neural network emulate the teacher. Emulation is considered optimum when the knowledge of the teacher is transferred to the neural network and the synaptic weights are fixed [100, 101].

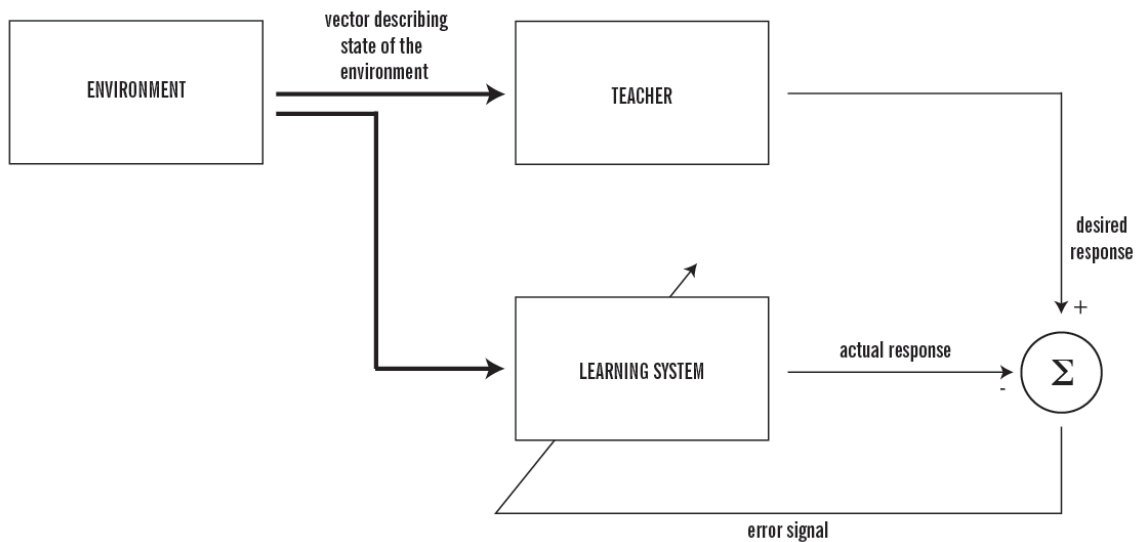


FIGURE 7.3: LEARNING WITH A TEACHER [100]

There are two forms of learning without a teacher: reinforcement learning and unsupervised learning. Reinforcement learning is learning performed through an input-output mapping through continued interaction with the environment to minimize the scalar index of performance. Figure 7.4 provides a block diagram of one form of a reinforcement-learning system. The system in Figure 7.4 learns under delayed reinforcement or an observational temporal sequence of stimuli sent to the environment. This learning ultimately leads to the generation of the heuristic reinforcement signal [100, 101].

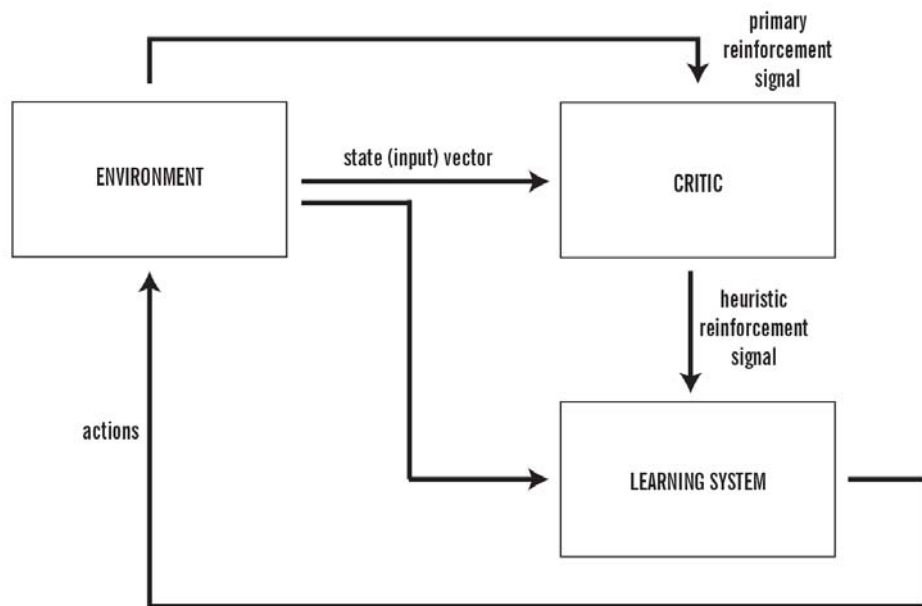


FIGURE 7.4: LEARNING WITHOUT A TEACHER, REINFORCEMENT LEARNING [100]

Unsupervised, or self-organized, learning occurs when a neural network learns without a teacher or critic to oversee the learning process. The unsupervised-learning method requires the network to learn despite not receiving external feedback. This type of neural network can generally extract useful relationships from the input by learning the respective concepts itself [100]. Figure 7.5 provides a block diagram that represents self-organized learning for which there is no external teacher.

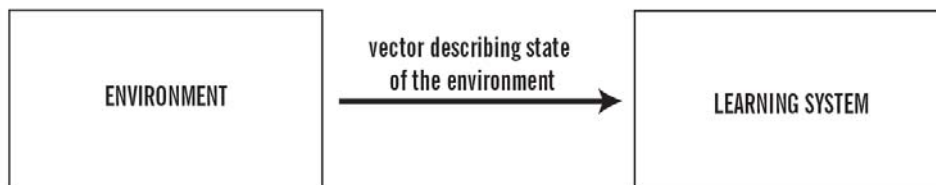


FIGURE 7.5: UNSUPERVISED LEARNING [100]

For the analysis of the data, we used XLMiner, a Microsoft Excel add-on that features both statistical- and machine-learning methods [103]. This software allows us to partition the data and assist in the development of predictive algorithms and outcomes based on various methods of prediction, one of which is neural networks.

7.5 THREE-DIMENSIONAL CAD GEOMETRIC MODEL

Medical imaging has evolved dramatically in the past few decades due to the constant change of digital imaging sensor chips. With multidetector computed geography (MDCT) and magnetic resonance imaging (MRI), three-dimensional imaging has become less invasive and more easily accessible [104]. These machines are large and expensive. For example, three-dimensional imaging is heavily used for viewing, tracking, and monitoring tumor growth. With the cost of three-dimensional imaging decreasing, a corresponding technique, three-dimensional modeling, is becoming more achievable, specifically in medicine. Unlike three-dimensional imaging, three-dimensional modeling involves the creation of a virtual model based on input dimensions. Three-dimensional modeling provides a three-dimensional scan of the geometry of a wound that is then imported into a three-dimensional modeling program, such as Solidworks™.

To acquire an accurate three-dimensional model of a wound, we needed to determine an accurate method of correlating pixels and centimeters. Using the methodology in Chapter 8, we were able to accurately determine the shape and size of the wound. We then proceeded to analyze the image using the process in Figure 7.6 to obtain the final pixel XY coordinates of the edge of the wound using color intensity values in Chapter 8. In essence, a digital image is simply a two-dimensional matrix comprising various intensity, or numerical, values that create a visual image.

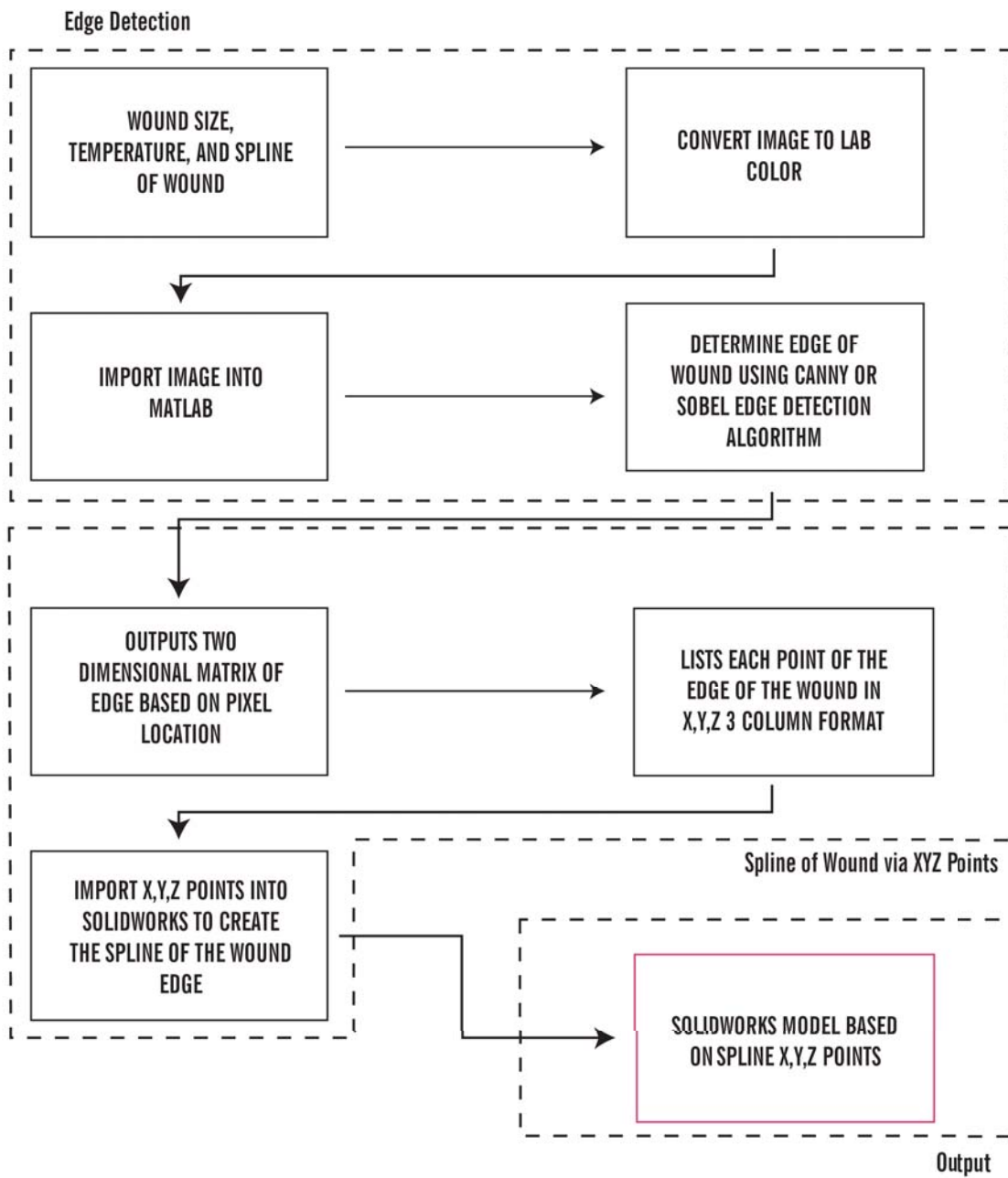


FIGURE 7.6: EDGE DETECTION TO SPLINE CREATION METHODOLOGY

Specifically, the CIELAB — for lightness, Color Channel A, and Color Channel B — color space was the key to wound- and image-boundary analysis. The LAB color offers better digital manipulation than does the traditional RGB (red/green/blue) color space. This is attributed to the luminance of the LAB color space (Figure 7.7). This modification in color profile allowed the algorithms to better detect a precise wound boundary.

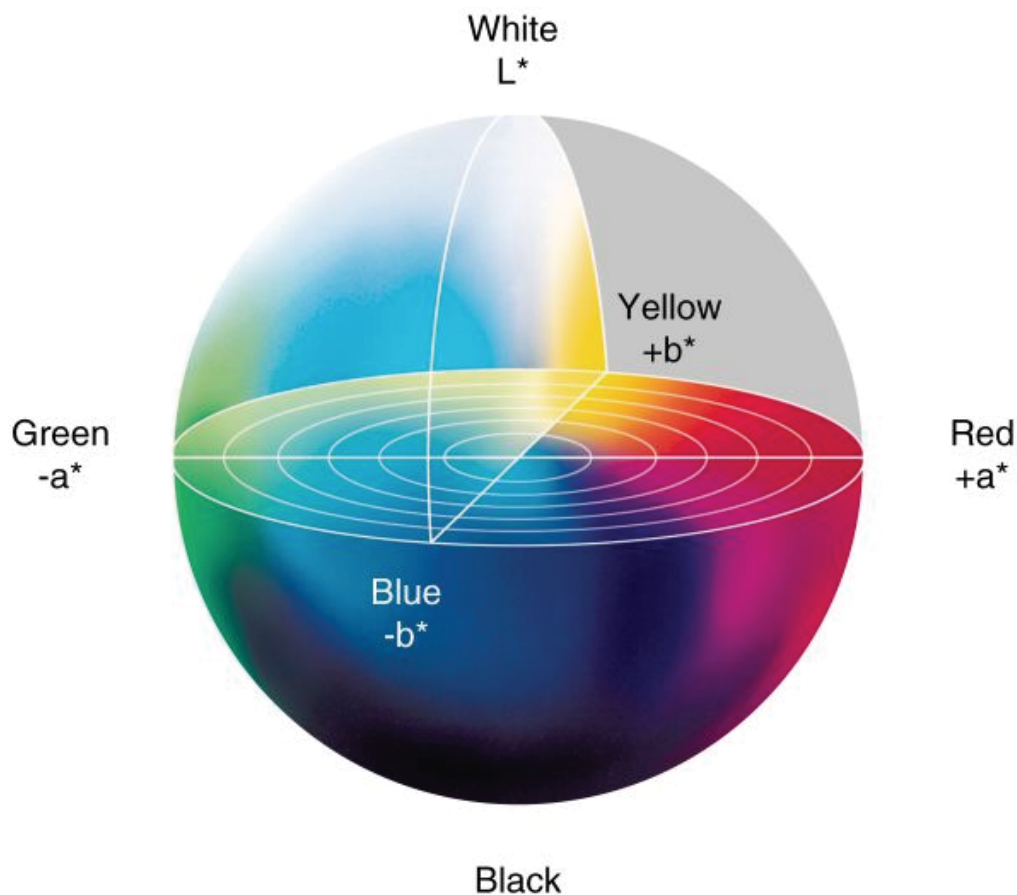


FIGURE 7.7: CIELAB COLOR SPACE [105, 106]

Different parts of the body have different temperatures. As a result, we have the ability to measure the change in temperature using techniques such as thermal imaging.

7.6 THERMAL-IMAGING (THERMOGRAPHY) MODEL

Thermal imaging uses thermal photography to measure natural thermal radiation generated by an object at a temperature above absolute zero [53]. The use of thermal imaging in wound analysis is appealing because it is noninvasive and provides a method of investigating physiological changes. It does not replace X-rays and three-dimensional scanning techniques but rather complements

techniques such as computed-tomography and MRI scanning. Like all other photography techniques, thermal cameras use specialized lenses to absorb infrared wavelengths. Germanium is commonly used to focus thermal radiation onto a focal plane array of infrared detectors [107].

Thermal imaging allows clinicians to examine human organs that are too dense for other imaging techniques to show. Only a few technologies are available on the research and commercial markets. Flir Systems is the primary designer and manufacturer of high-quality, expensive thermal imaging systems. High-quality cameras tend to cost more than equipment for other methodologies. Interpretation of images and erratic temperatures can be difficult to understand. Further, most cameras have an accuracy of only $\pm 2^{\circ}\text{C}$ due to the noncontact methods. Thermography also can detect only surface temperatures and does not offer penetration depth.

7.6.1 TECHNICAL SPECIFICATIONS

In thermal imaging, the feedback of the camera is highly dependent on body temperature. Each person has a core body temperature that typically varies from 35.5°C to 37.7°C [53]. Thermal imaging uses two core principles: radiometry, or the measurement of radiation, and photometry, the measurement of visible radiation. In radiometry, the spectral radiant flux, $F_{e\lambda}$, is the spectral radiant flux. The spectral flux is the power emitted, transferred, or received as radiation per wavelength interval, resulting in the integral [53]. The output, in watts, is expressed by this integral equation:

$$F_e = \int_0^{\infty} F_{e\lambda} d\lambda \quad (7.10)$$

Photometry measures the visible radiation of the system. Photometry's relationship with radiometry weighs the spectral power with the normalized, spectral luminous efficacy of the standard observer, $V(\lambda)$ [53, 108]. Luminous efficacy is the measure of the ability of radiation to produce a visual sensation [53] equating to:

$$F_v = 683 \int_{380}^{780} F_{e\lambda} V(\lambda) d\lambda \quad (7.11)$$

F_v is the luminous flux in lumens (lm). According to [53], radiance is the radiant flux at a point on the surface of the source or receptor. Both radiance and luminance are used substantially in both human and computer vision. By analyzing the radiometry of imaging systems, it allows focused

images to effectively measure radiation. In radiometry, the radiance of an object does not diminish with distance, as it does in spectroscopy. The radiance of an object is not affected by the distance between the object and its receptor in the absence of scattering and absorption [53]. More modern infrared cameras use a focal plane array of detectors to capture the image [107].

Thermal radiation of skin originates from the epidermis and is independent of race; it depends only on the surface temperature [53]. Emissivity varies with wavelength. Skin emissivity is rather constant between 3 and 15 microns at a value of 0.975 ± 0.05 [54]. Figure 7.8 displays the steps in processing infrared thermal imaging for medical applications.

In the latest research, the more robust tools that quantify inflammation and infection of a wound use thermal imaging to easily identify diabetic foot wounds [109]. Bharara et al. [109] have performed numerous studies that support the theories of in-home monitoring using temperature change and thermal technology. Bharara et al. [109] reported approximately fourfold to 10-fold reductions in pressure wounds for patients using home-based thermometry devices. There has been growing interest in simple digital thermometers, liquid-crystal-thermography technology, and the Spectrasole Pro 1000 system for quick diabetic-foot assessment [110]. Previous research has suggested that thermal imaging could facilitate the assessment of wounds and wound healing, but the industry and science lack standard thermal-imaging techniques and analysis to validate this methodology [109].

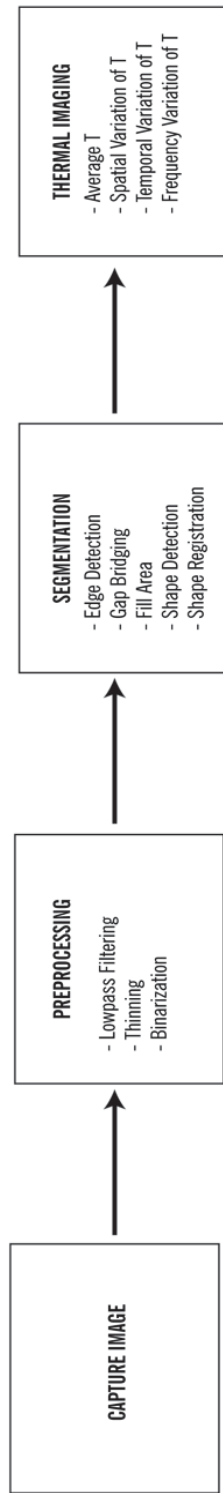


FIGURE 7.8: IMAGE PROCESSING FOR THERMAL IMAGING IN MEDICINE [53].

The temperature difference between the wound and the surrounding environment depends on the size, shape, curvature, and eccentricity of the wound. Understanding the interruption in the skin matrix could lead to better understanding of how wounds form based on shear stress [109]. When a wound forms, excessive vertical and shear stress force on the edges disturb the skin matrix [109]. According to Bharara et al., [109] an objective parameter — that is, an index based on thermal profile — is necessary to track wound healing over time using the Wound Inflammatory Index. Bharara et al. [109] have proposed a new tool for quantifying wound conditions using thermal imaging and wound size as inputs:

$$TI = \frac{\Delta T * a}{A} \quad (7.12)$$

This equation uses the temperature difference (ΔT), the area of the isotherm (a), and the area of the wound bed (A) to calculate the thermal index of the wound (TI). The calculations for Figure 7.9 are currently performed manually to evaluate wound assessment.

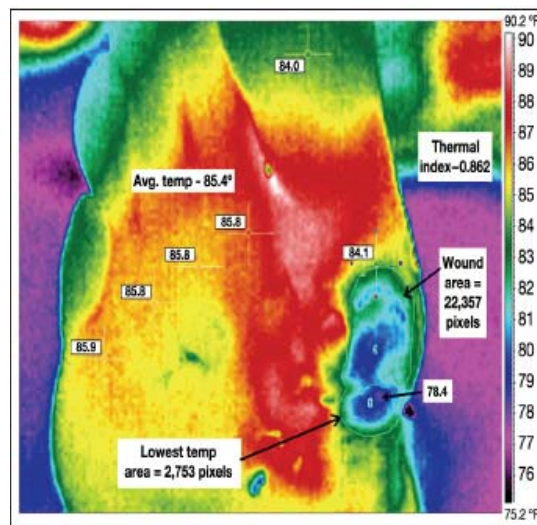


FIGURE 7.9: CALCULATION OF TI/WOUND INFLAMMATORY INDEX [14] AT BASELINE FOR THE TEST SUBJECT [109].

Thermometry is an innovative strategy to treat and manage wounds. This technique facilitates early diagnosis, surgical planning, and preventive actions. Thermography also offers fast, noninvasive, and safe examination of wounds. Table 7.1 shows the results from Bharara et al. [109] as a proof-of-concept study for a wound healing trajectory. Bharara et al. [109] have created preliminary scoring methods to assess wounds on the skin's surface.

TABLE 7.1: CALCULATION OF THERMAL INDEX/WOUND INFLAMMATORY INDEX RESULTS [109]

Day	Average Foot Temperature (°C)	Wound Area (Pixels) - A	Isotherm Area (Pixels)	Wound Temperature (°C)	WII	Wound Area (L x B, cm ²)
0	37.28	20907.00	8216.00	36.39	-0.63	5.44
7	36.56	13949.00	3158.00	35.17	-0.57	5.67
14	38.24	4615.00	2701.00	38.00	-0.26	4.8
21	37.87	1821.00	279.00	40.39	0.70	1.4
35	36.78	1715.00	174.00	36.96	0.03	0.84

Several studies have shown that foot temperature is an important parameter in assessing the state of an wound [111]. The most commonly used current method of monitoring foot temperature is the use of an infrared (IR) thermometer for self-inspection. This method is, however, manually intensive and prone to human error. An IR thermometer also relies on human judgment rather than automation. An IR thermometer also reads only one parameter, temperature, which can provide only so much information. The benefit of this methodology is that it allows for consistent home monitoring of a wound. By using thermography as a component of overall wound health, thermography could provide important insight into further understanding and analysis of wound health.

7.7 SUMMARY

Various predictive-modeling techniques exist. We explored types of models and ultimately settled on multiple linear regression, nonlinear regression, and neural networks. Based on the data, we believe these predictive modeling techniques provide the most consistent, robust, and accurate results. This chapter provides the theoretical understanding for the predictive modeling processes we use to analyze the data and produce the results in Chapter 9.

CHAPTER EIGHT WOUND DATA COLLECTION, PREPROCESSING

CHAPTER 8

Wound Data Collection, Preprocessing

Chapter 8 focuses on data collection and both still and thermal photography to devise an accurate predictor of wound health and wound viability. The proposed research methodology was developed to contribute to the understanding of how various wound health characteristics impact the length of time and quality of chronic wounds in patients. The subsequent data was collected through two wound-care facilities: RBMC, a community hospital, and Vohra, a national wound-care physician group. We compiled data in concert with all state and federal regulations involving each location's Institutional Review Board (IRB) and HIPAA compliance, as well as each location's nondisclosure agreements (NDAs).

8.1 DATA COLLECTION

RBMC provided both retrospective and living patient data for this study. Vohra provided most of the retrospective data.

8.1.1 INSTITUTIONAL REVIEW BOARD

At each institution and each hospital, the process differs for authorizing and complying with the state and federal privacy health laws. For RBMC, the process took approximately nine weeks. For Vohra, the process took approximately two weeks. Figure 8.1 diagrams the process of approval for both institutions.

To pursue research at RBMC, we had to present the research plan to the IRB, which comprised nine individuals. The purpose of the presentation was to ensure the safety and privacy of patients involved. Along with the presentation to IRB, we had to develop an informed consent for patients if

they chose not to participate. This form was developed with the assistance and guidance of Northeastern University's IRB. Once RBMC's IRB approved the plan, the clinic's legal department required an official educational-affiliation agreement to complete the approval process in Appendix B. This approval process allowed us to collect live patient data at RBMC's Care Center. Retrospective data collection differs slightly from live data collection in that retrospective data collection allows those with large patient databases to easily remove patient identities and demographics.

We sent Vohra, the retrospective data source a one-page proposal with a description of the research and a request for the desired data. Follow-up telephone calls further detailed the necessary criteria for selecting patients. Along with the telephone calls, we had to enter into a data-use agreement (Appendix B).

8.1.1.1 Living Human Data Collection

Figure 8.1 details the IRB process at the wound care facilities from which we received the patient data. Vohra physicians supplied us with the training and testing data to develop the predictive model. RBMC allowed us to collect on-site and retrospective data and to observe daily operations in the wound clinic. RBMC also supplied us with photographs of patient wounds from still and thermal imaging. Of the multiple wound care facilities we observed, RBMC was among the few that consistently photographed patient wound progress.

With retrospective data, the data is a collection of numbers. Patients are not identified, and we received no personal information. With on-site patient data collection, however, pain is a reality. For four weeks, we observed the same group of 18 patients attend weekly visits to the wound care center to monitor and determine their wound health, hoping for change in size as small as 0.10 cm. We observed and conversed with all patients who were willing to let us photograph their nonhealing wounds. Most patients suffered from neuropathy and could not feel their wounds.

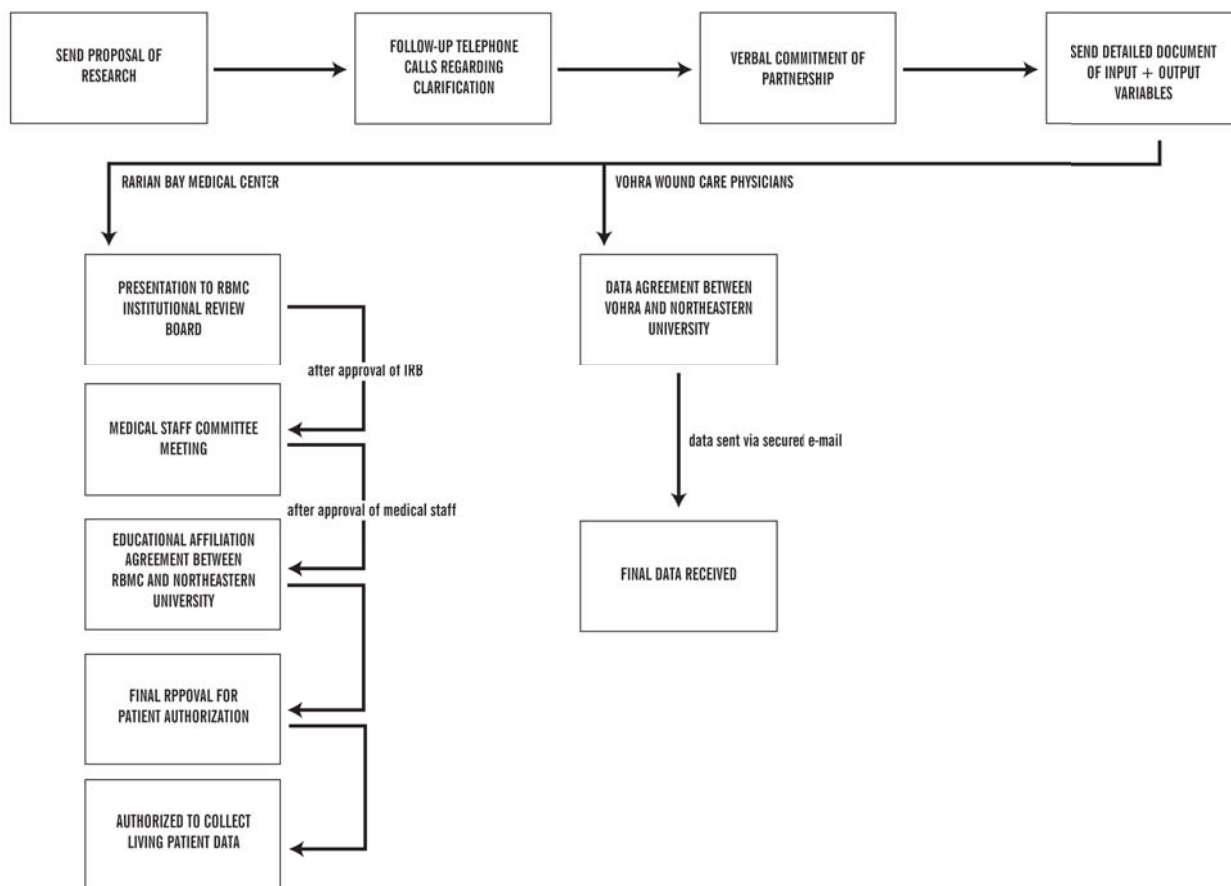


FIGURE 8.1: IRB PROCESS FOR RBMC AND VOHRA

8.2 DATA-MINING METHOD SELECTION

We received data on 19,203 unique wounds, each wound having multiple records over time, from Vohra, and we received data on 18 unique wounds from the RBMC. A variety of statistical analyses were performed on the raw data to ensure a statistically accurate data cleaning of outliers and extreme cases. Figure 8.2 shows an overview of how the data was initially prepared.

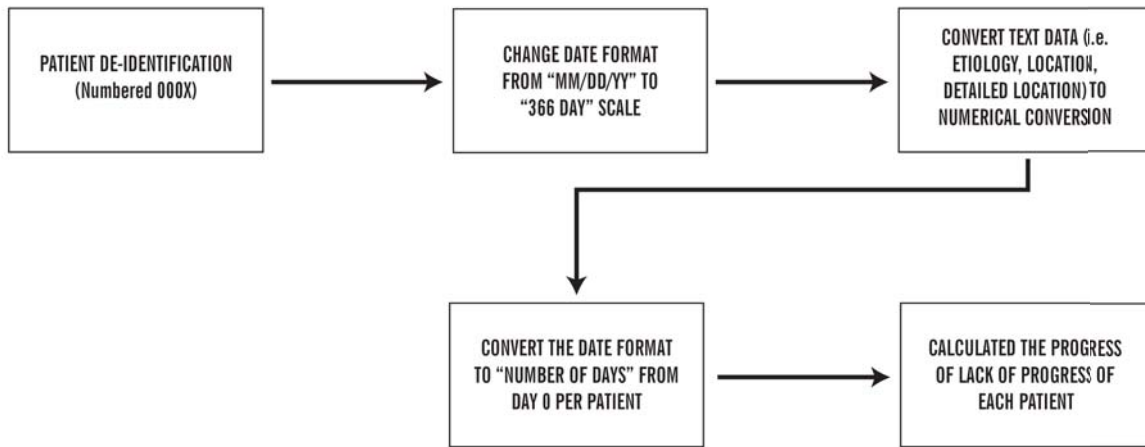


FIGURE 8.2: DATA-PREPARATION METHODOLOGY

Figure 8.3 displays the computational process of determining whether the data and each variable had a normal distribution. The purpose of this data mining was also to discover each variable's best-fit data distribution. Furthermore, histograms, box plots, and scatter plots were used to determine the fit of each variable in preparation for data cleaning.

The purpose of normalization is to show the variability of each variable relative to the other variables. The standard equation was used to normalize the data between zero and one, as given by:

$$\text{Normalize Data } \{0,1\} = \frac{x_i - x_{min}}{x_{max} - x_{min}} \quad (8.1)$$

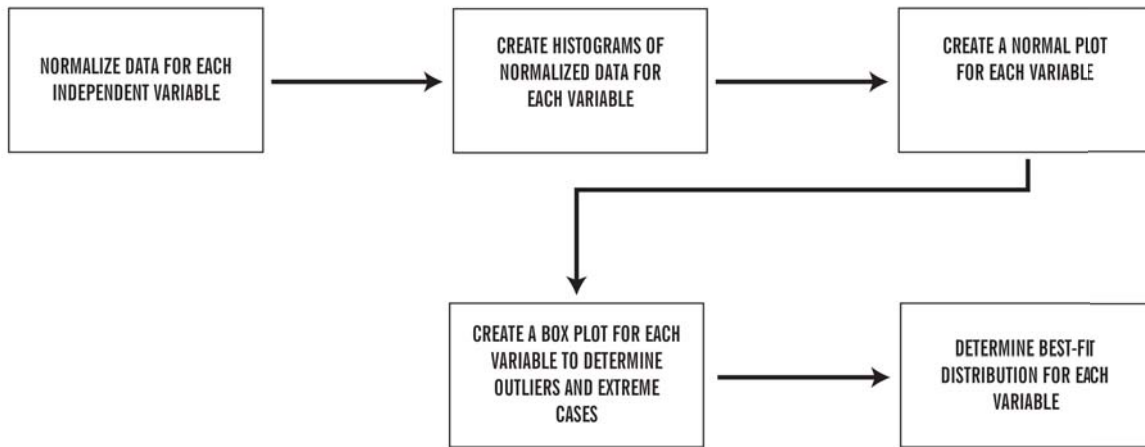


FIGURE 8.3: INDEPENDENT VARIABLE-DATA PREPARATION

8.3 DATA PREPROCESSING: STAGE I

As Figure 8.2 and Figure 8.3 show, the preprocessing of the data included normalizing and cleaning the data set to prepare it for both regression and neural-network predictive modeling. Specifically, Matlab® was used to write small blocks of code to assist in the cleaning of the massive data set. Figure 8.4 shows a visualization of the process the data cleaning with Matlab® code (Appendix E and F).

Box plots assisted in the elimination of outliers and extreme data points from the set of data. The box plot describes the location of the center of the data is, the spread of the data, and the departure from symmetry of the data. Furthermore, box plots identify data points — that is, outliers or extreme outliers — that deviate from the bulk of the data [112].

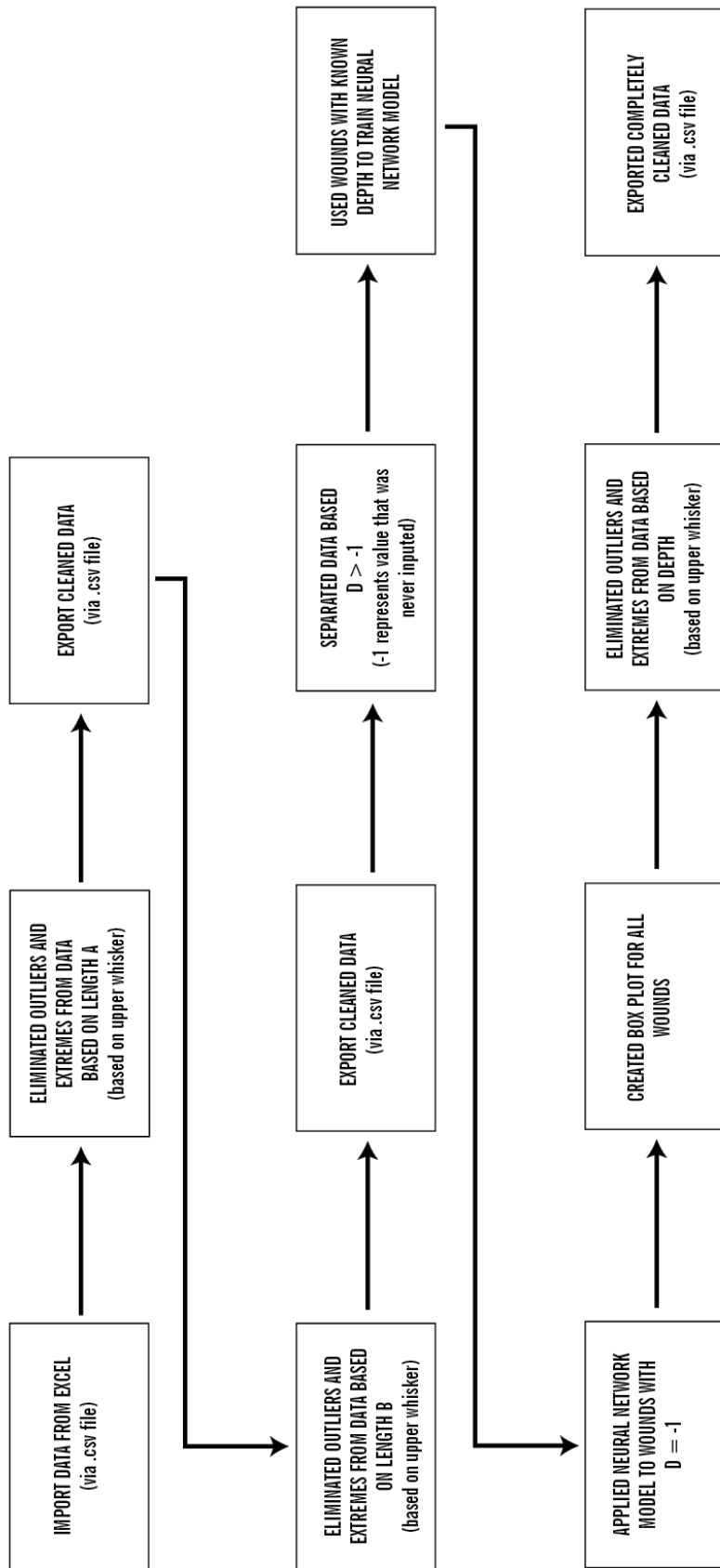


FIGURE 8.4: MATLAB® METHODOLOGY TO CLEAN DATA

Equations (8.2) and (8.3) show how we derived the lower and upper values for each variable to determine the ideal set of input parameters:

$$\text{Lower Whisker of Box Plot} = \max \left\{ \begin{array}{l} \text{Minimum Data Value} \\ Q_1 - R \end{array} \right\} \quad (8.2)$$

$$\text{Upper Whisker of Box Plot} = \min \left\{ \begin{array}{l} \text{Maximum Data Value} \\ Q_3 - R \end{array} \right\} \quad (8.3)$$

For each variable, we created box plots. We eliminated data based only on the box plot information for length 1, length 2, and depth because each wound data sample has a guaranteed value for each of these three variables (Figure 8.5, Figure 8.6, and Figure 8.10). Unlike length 1, length 2, and depth, the independent variables of undermining, granulation, yellow necrotic tissue, black necrotic tissue, and slough are percentages that represent what is occurring within the wound. Not every wound has the previously mentioned characteristics, which results in a value of zero. Due to this fact, we could not eliminate this data based on most values for each of these variables, including undermining, granulation, yellow necrotic tissue, black necrotic tissue, and slough.

Similarly, certain wounds result from physical imbalances within the patient. One of those imbalances occurs because of the blood flow and circulation in the lower appendages. This measurement is recorded via a Doppler tool and measures the flow in both the right and the left lower appendage (Figure 8.7).

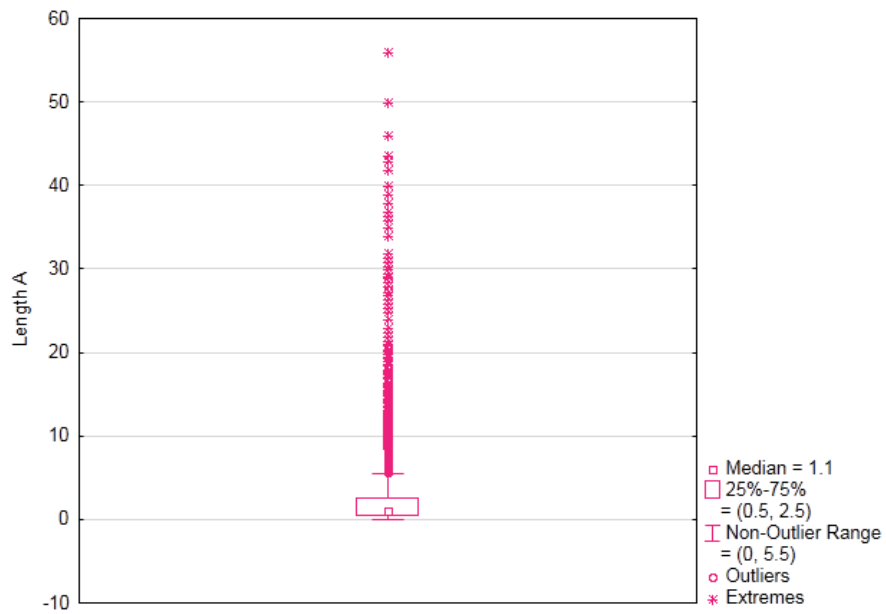


FIGURE 8.5: BOX PLOTS OF LENGTH 1

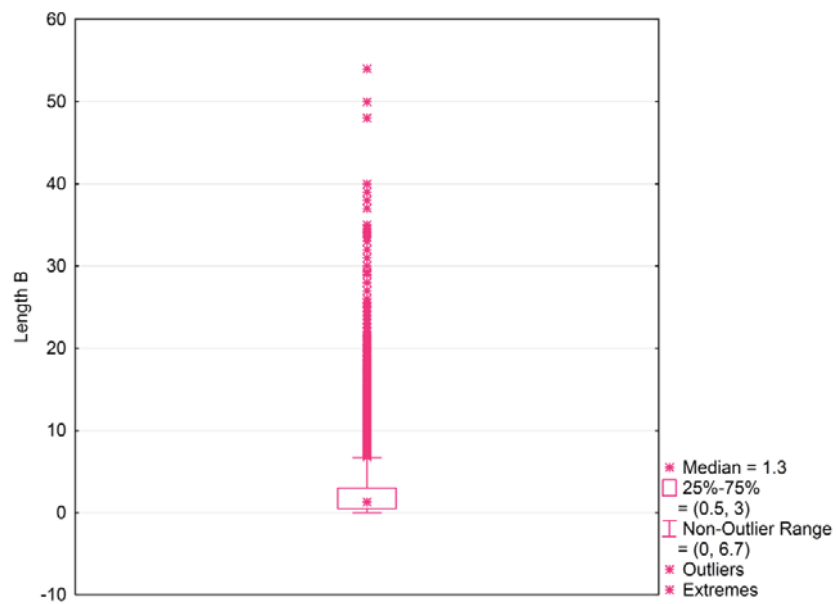


FIGURE 8.6: BOX PLOTS OF LENGTH 2

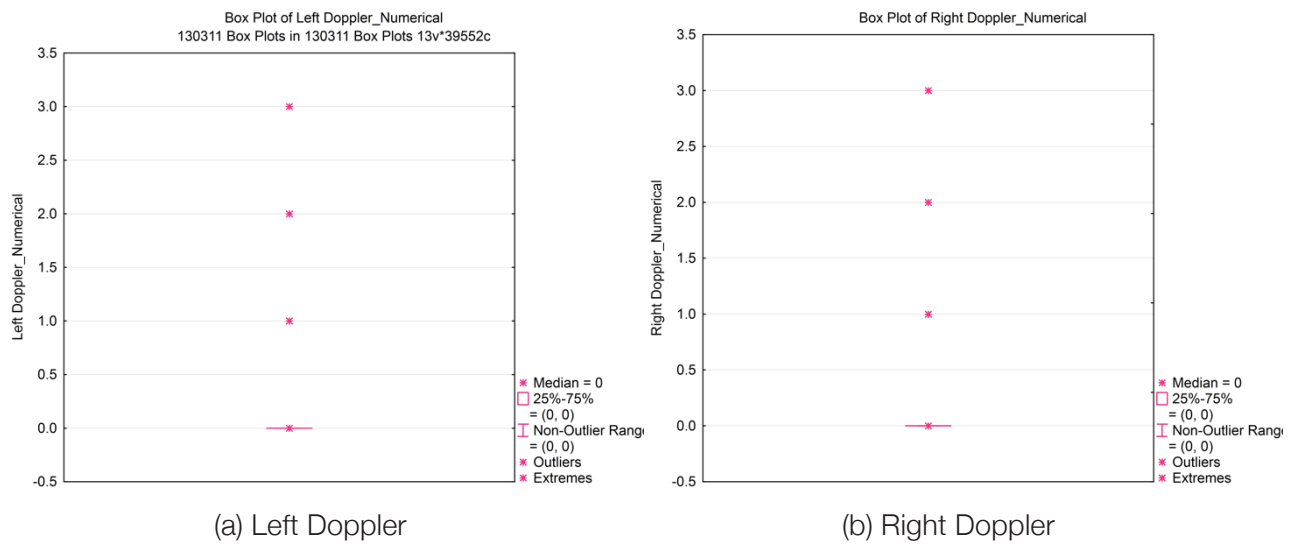


FIGURE 8.7: BOX PLOTS OF LEFT AND RIGHT DOPPLER

Figure 8.8 represents the box plots for both the albumin and prealbumin measurements of each wound. Albumin is a visceral protein that functions as a carrier protein to assist in maintaining oncotic pressure [113]. Clinicians use albumin and prealbumin as measures of the nutritional state of the wound and the patient based on the patient's need for protein. Although albumin and prealbumin are good indicators of morbidity and mortality, some disagreement exists about whether they can be used as measures of nutritional status [114].

Table 8.1 displays each variable and its box-plot properties. Table 8.1 and Table 8.2 show the lower and upper limits of each variable, which provide the values for establishing the threshold for each input parameters. This amalgamation of input parameters is the healed threshold for how we have defined a wound that is healed. In addition, the range between the upper and the lower quartiles is significant because these values define the upper limit to eliminate outliers and extreme values. Although we have calculated both the upper and the lower limits of the data, we use only the upper limits to eliminate the outliers and extreme values. The lower limits represent, within the context of the data and situation, a closed wound. Therefore, we did not eliminate them for the purpose of analysis because the wounds are considered closed.

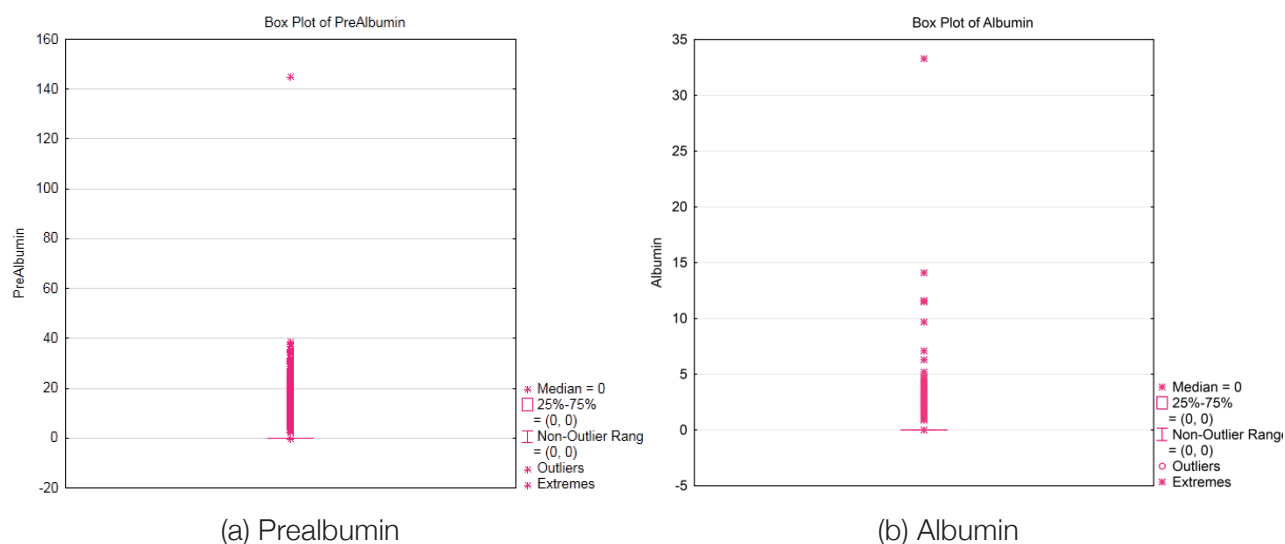


FIGURE 8.8: BOX PLOTS OF PREALBUMIN AND ALBUMIN

TABLE 8.1: SUMMARY OF BOX-PLOT STATISTICS OF INDEPENDENT VARIABLES

Independent Variable	Q1	Q3	Range	Minimum	Maximum
Length 1	0.50	2.50	2.0	0	56
Length 2	0.50	3.0	2.5	0	54
Depth	0.10	0.20	0.10	0	4
Undermining	0	0	0	0	7
Granulation	0	100	100	0	100
Yellow Necrotic	0	0	0	0	100
Black Necrotic	0	100	100	0	100
Slough	0	0	0	0	100
Left Doppler Numerical	0	0	0	0	3
Right Doppler _Numerical	0	0	0	0	3
Prealbumin	0	0	0	0	145
Albumin	0	0	0	0	33.3

Table 8.2 focuses on the upper whisker, or maximum, because it represents the boundary between the included data and the outliers and extreme data points. Although we calculated the lower and upper whiskers for all independent variables, we eliminated outliers and extremes based on length 1, length 2, and depth because these measurements were present in every wound.

TABLE 8.2: COMPUTATION OF INDEPENDENT VARIABLES FOR LOWER AND UPPER WHISKERS OF BOX PLOTS

Independent Variable	Q1-R	Lower Whisker	Q3+R	Upper Whisker
Length 1	-1.5	0	4.5	4.5
Length 2	-2	0	5.5	5.5
Depth	0	0	0.313	0.313
Undermining	0	0	0	0
Granulation	-100	0	200	100
Yellow Necrotic	0	0	0	0
Black Necrotic	-100	0	200	100
Slough	0	0	0	0
Left Doppler Numerical	0	0	0	0
Right Doppler Numerical	0	0	0	0
Prealbumin	0	0	0	0
Albumin	0	0	0	0

Unlike the box plots in Figure 8.5 and Figure 8.6, the box plot for this figure depth was created using combined data from a neural network. In the receipt of the raw data, the clinician did not input some depth values into the electronic medical record to determine some of the missing values, we separated the data based on:

$$depth = -1 \quad (8.4)$$

This approach allowed the wounds to be classified based on their depth. The subneural-network analysis had was necessary for prediction of the missing depth values. Figure 8.9 displays the methodology of how the subneural network predicts the missing depth values. The ideal neural network has minimal average error for training data scoring and a value of nearly zero average error for validation data scoring. To prepare the data for input into the neural network, the data had to be partitioned into 70% (7,000 data points for training) and 30% (3,000 data points for validation) training and validation data, respectively. This partition was achieved by using random algorithms to select the 10,000 maximum number of inputs to train the network. To verify the accuracy of the neural network for the data set, we used multiple random algorithms to partition the same data [115].

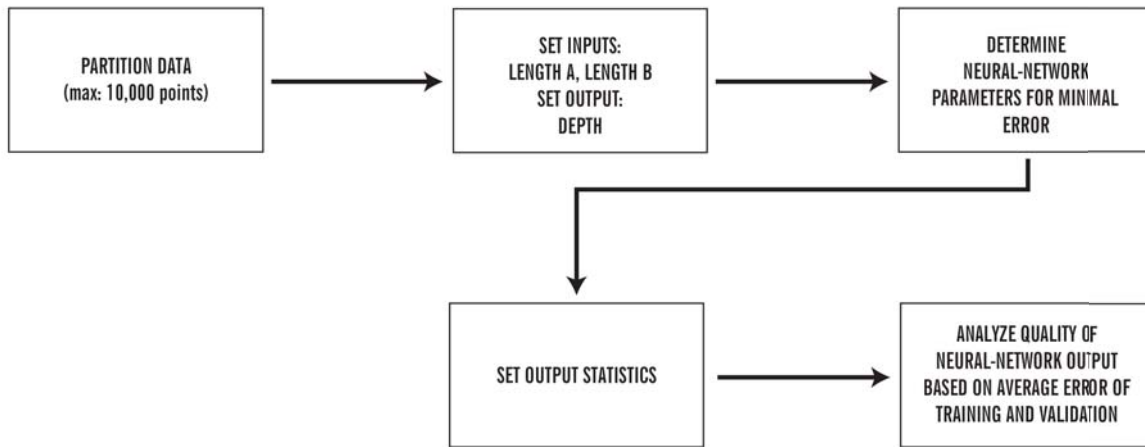


FIGURE 8.9: SUBNEURAL-NETWORK METHODOLOGY FOR MISSING DEPTH VALUES

We designed and analyzed multiple neural networks to ensure the accuracy of the conclusions in Table 8.3. We tested the network’s accuracy against various combinations of parameter options and against various random algorithms for data partitioning. Table 8.3 displays the optimal combination of parameter values that produce minimal average error of training data and validation data [115].

TABLE 8.3: NEURAL-NETWORK PREDICTION VARIABLES AND PARAMETERS

Variables		Parameter/Options	
Number of input variables	2	Number of hidden layers	1
Input variables	Length_A	Number of nodes in hidden layer 1	3
	Length_B		
Output variable	Depth	Number of epochs	3,000
		Step size for gradient descent	0.02
		Weight-change momentum	0.2
		Error tolerance	0.001
		Weight decay	0

Table 8.4 provides the results of the neural-network analysis that provides the respective weights of each node within each hidden layer of the network. Similarly, it provides the weights for the output node, which is depth.

TABLE 8.4: INTERLAYER CONNECTIONS WEIGHTS

Input Layer				
Hidden layer 1	Length 1	Length 2	Bias node	
Node 1	-4.763429826	-3.163800314	-1.083572488	
Node 2	-1.056294408	0.625808772	-0.25194046	
Node 3	0.565769301	-0.977301608	-0.589001043	

Hidden Layer 1				
Output layer	Node 1	Node 2	Node 3	Bias node
Output node	-3.47674292	-0.72515721	-0.478521953	-2.36592218

Table 8.5 shows the quality and accuracy of the neural network and the amount of error within the training data scoring and how accurate the network is when tested against the validation data. To determine the accuracy of the model, we focus on the average error of the training and validation data scoring. The average error for training should be less than 5%. In this case, the average error is 0.26 %. The average error for validation data scoring should be nearly zero. In this case, the average error for validation data is 0.005%, or essentially zero (Table 8.5). This information supports the use of this network to predict the missing depth values for the remaining patient wounds.

TABLE 8.5: TRAINING AND VALIDATION DATA-SCORING REPORT

Training Data Scoring			Validation Data Scoring		
Total sum of squared errors	RMS Error	Average Error	Total sum of squared errors	RMS Error	Average Error
308.21	0.21	0.0026	105.08	0.187	5.22E-05

Table 8.6 provides a summary of statistics pertaining to the depth of the data set. It summarizes the statistics of the depth parameter for the combination of training and predicted data.

TABLE 8.6: TRAINING AND VALIDATION DATA-SCORING REPORT

Valid N	Mean	Mini mu m	Maximum	Q1	Q3	Range	Q Range	Standard deviation
29085	0.179	0.00	4.000	0.100	0.206	4.000	0.106	0.139

Figure 8.10 represents the box plot of both the training data and the tested data to determine the outliers and extreme values based on the depth. Figure 8.10 is the final step in completing the data cleaning to determine the predicted time to heal.

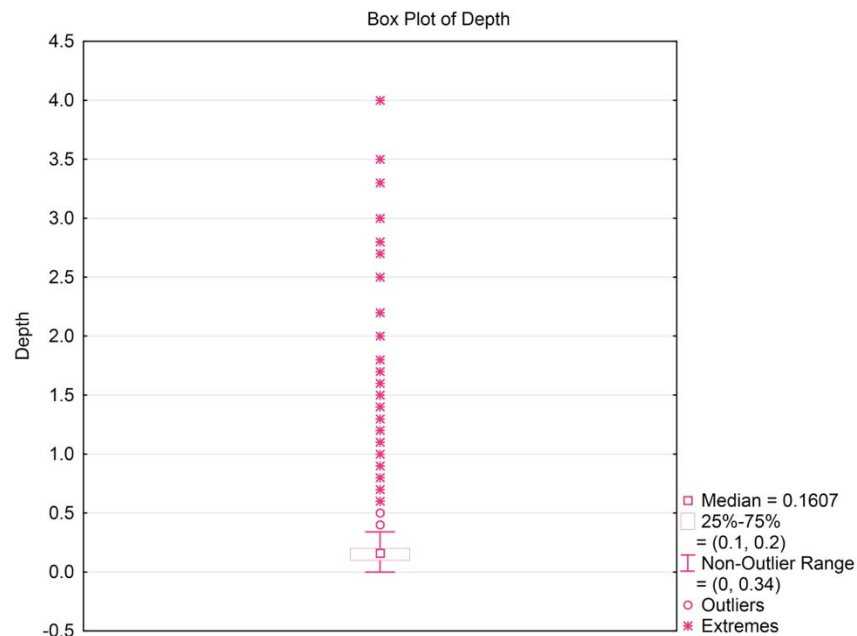


FIGURE 8.10: BOX PLOTS OF DEPTH AFTER PREDICTED VALUES

8.4 GEOMETRICAL ANALYSIS

At most wound clinics, clinicians measure wounds at the point of greatest width and maximum height perpendicular to the measured width [2]. To determine the geometric characteristics of various wounds, we developed an acquisition and analysis methodology that acquires, analyzes, and outputs the necessary wound information for eventual three-dimensional model importing. Figure 8.11 shows the methodology for both still- and thermal-image analysis. For still-image analysis, we used the National Institutes of Health (NIH)-sponsored ImageJ software [116]. For thermal-image analysis, we used the ExaminIR system from Flir Systems.

The Java-based, NIH-sponsored, ImageJ image-processing-analysis software for scientific research assisted the image and geometrical analysis in acquiring the spline of the wound from the wound images. This analysis is necessary to determine the proper wound shape to import into Solidworks and ultimately build a three-dimensional model of the wound [117].

ImageJ's developers conceived the software to analyze problems in the life sciences. The software's developers wanted it to remain accessible to newcomers and powerful enough for complex image analysis and processing. Because the software is open-sourced, anyone can contribute to improvements, ideas, and creation of plug-ins [118].

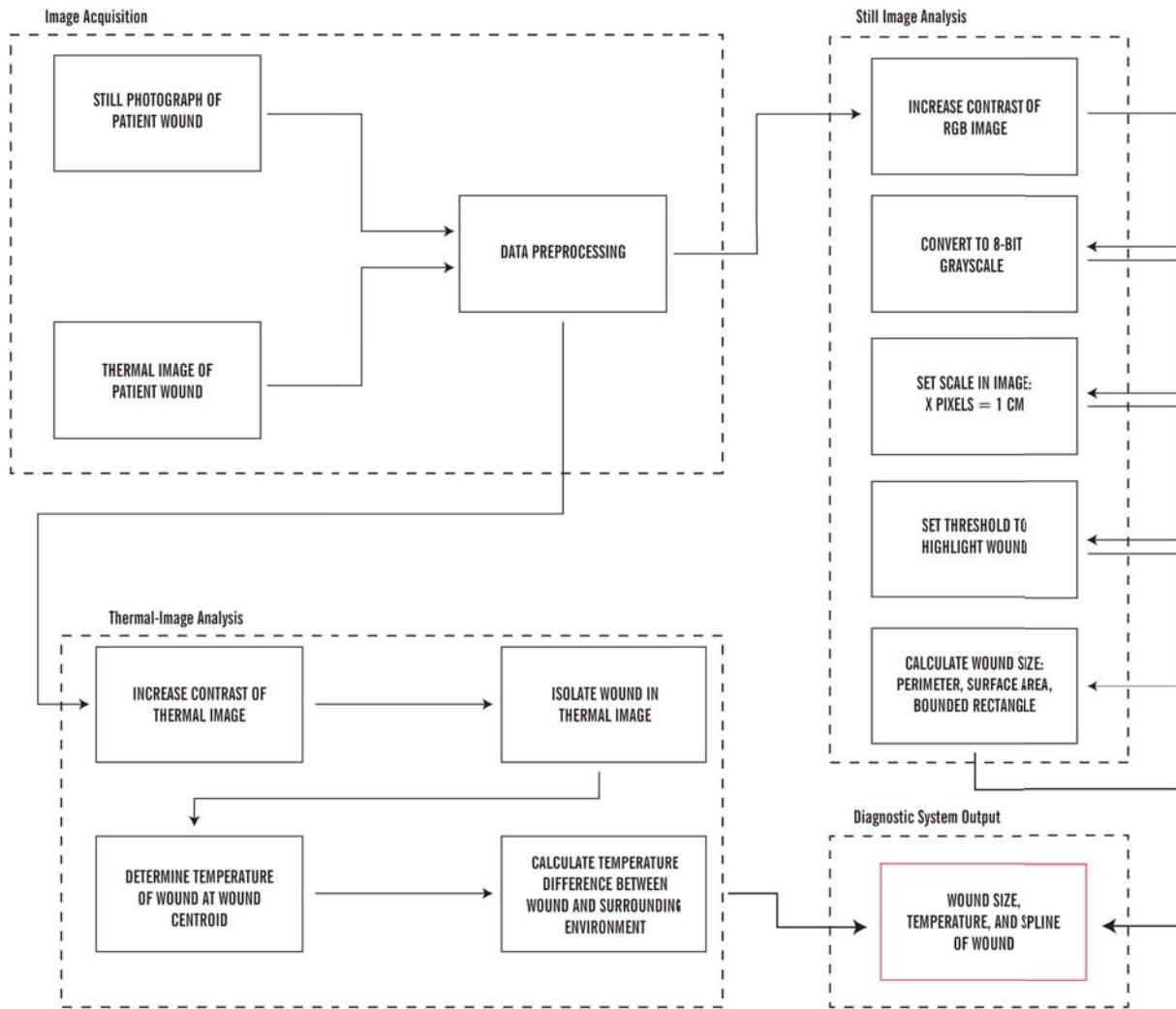


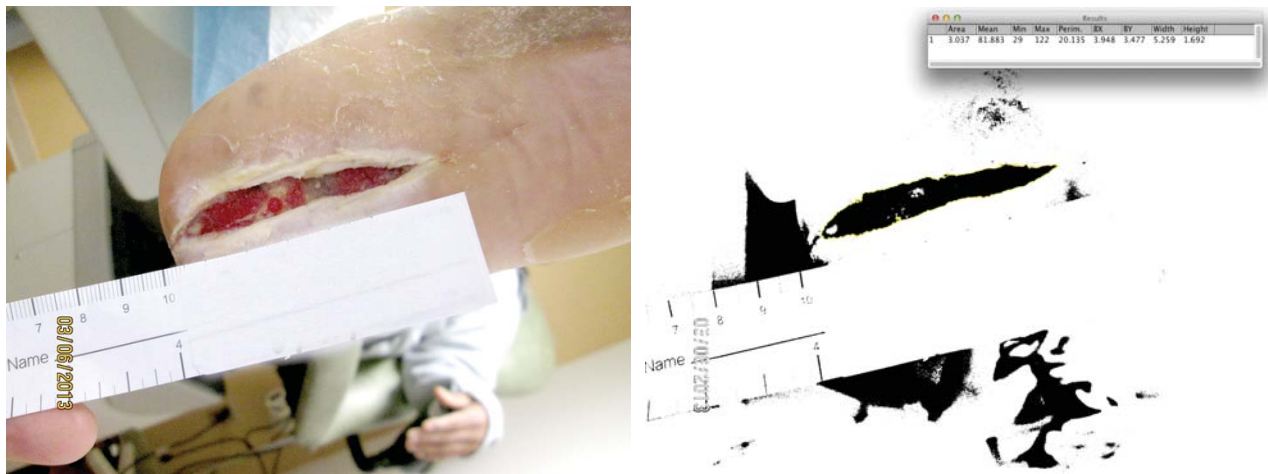
FIGURE 8.11: IMAGE-ACQUISITION AND -ANALYSIS METHODOLOGY

8.4.1 STILL-PHOTOGRAPHY ANALYSIS

Still photography should be a principal tool for the tracking and progress of wound healing. Unfortunately, the photographing of wounds through the course of treatment is not a standard

practice. Therefore, we analyze and evaluate how photographing wounds can assist in the development of wound care and the improvement of wound tracking and progression.

Figure 8.12a shows an example of the original wound image, and Figure 8.12b shows an example of the binary converted image with emphasis on the wound's shape and size. The highlighted yellow area of Figure 8.12b is calculated with ImageJ and calibrated with the corresponding ruler in the photograph. Table 8.7 provides the parameters of the highlighted yellow area of the wound.



(A) RGB IMAGE

(B) BINARY IMAGE WITH SCALE

FIGURE 8.12: PATIENT 11 IMAGE ANALYSIS

Table 8.7 provides the quantitative geometrical information about the respective wound and the calculated respective wound surface area and the wound-bounding rectangle. Note the difference in value between the area and the calculated area of the wounding rectangle. Currently, clinics can measure and calculate using only the bounding rectangle. Every subsequent measurement and comparison uses the change in area of the bounded rectangle.

TABLE 8.7: FIGURE 8.12 GEOMETRIC ANALYSIS RESULTS

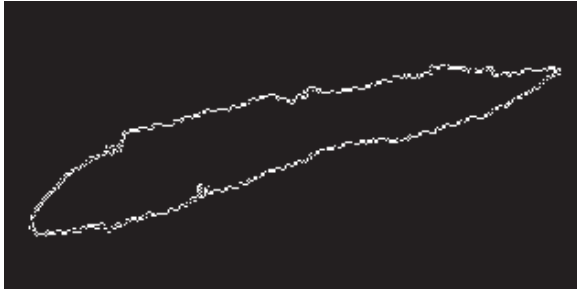
Area	Mean	Minimum (pixel value)	Maximum (pixel value)	Perimeter	Bx	By	Width (bounding rectangle)	Height (bounding rectangle)	Bounding Rectangle Area
3.037	81.883	29	122	20.135	3.948	3.477	5.259	1.692	8.898

Table 8.8 provides reference information about the size of the image and how many pixels equal one centimeter.

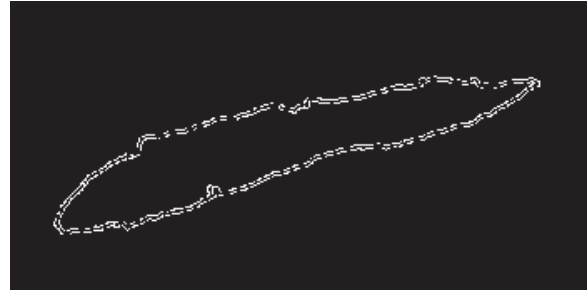
TABLE 8.8: IMAGE STATISTICS

Width (pixels)	Width (cm.)	Height (pixels)	Height (cm.)	Pixels/cm.
857	1145	10.35	13.83	82.765

Table 8.13 shows the wound boundary. The boundary of the wound was provided using both the Sobel and the Canny edge-detection algorithms. The purpose of using both algorithms is to compare the accuracy and precision of the edge detection.



(A) SOBEL EDGE-DETECTION ALGORITHM



(B) CANNY EDGE-DETECTION ALGORITHM

FIGURE 8.13: PATIENT 11: WOUND EDGE

Figure 8.14 provides another example of the image analysis of wound's surface area, perimeter, and shape. Figure 8.14 shows a more traditionally shaped wound, representing nearly circular wounds with 90% granulation. Table 8.9 provides the geometrical analysis of the wound area from Figure 8.14. The product of the width and the height of the bounded rectangle is an approximated calculated area. In the situation of Patient 2, the error is approximately 43% (Figure 8.14). We include this error discrepancy to illustrate the difference between measuring the bounding rectangular box of a wound and measuring the surface area of the wound itself.

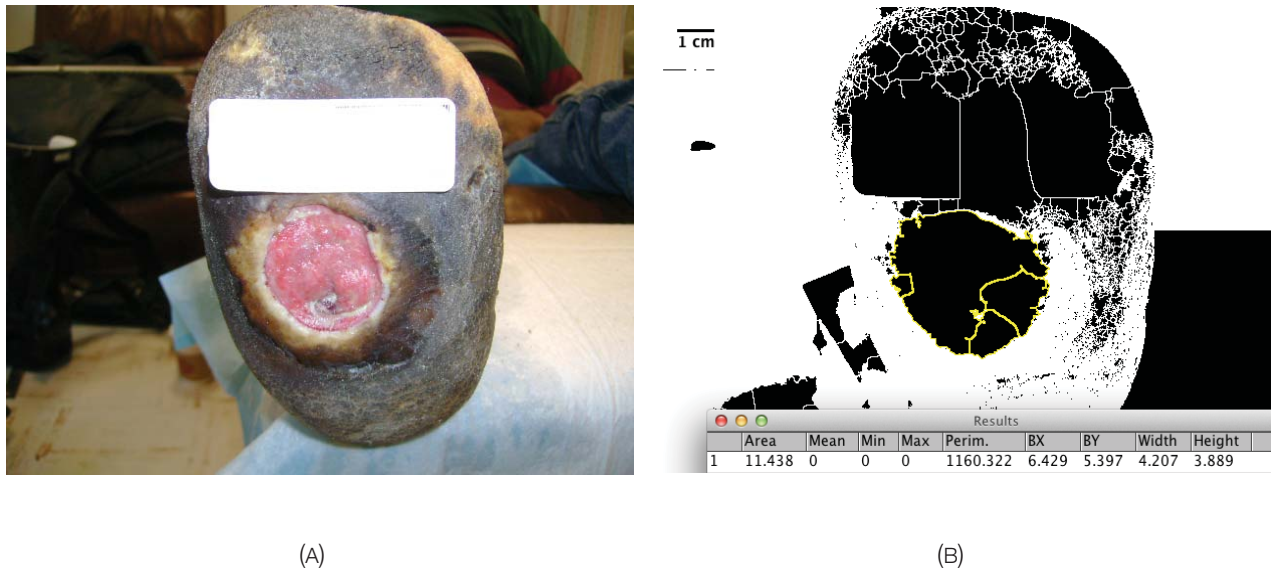


FIGURE 8.14: PATIENT 2: RGB IMAGE AND BINARY IMAGE WITH SCALE

Table 8.9 and Table 8.10 provide the same information for other patients.

TABLE 8.9: FIGURE 8.14 GEOMETRIC ANALYSIS RESULTS

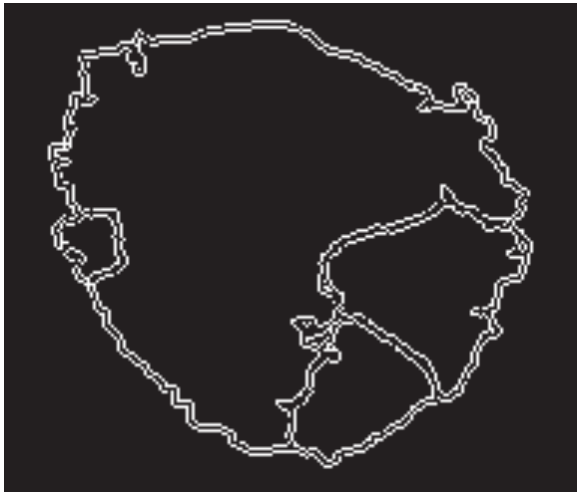
Area	Mean	Minimum (pixel value)	Maximum (pixel value)	Perimeter	Bx	By	Width (bounding rectangle)	Height (bounding rectangle)	Bounding Rectangle Area
11.438	0	0	0	1160.322	6.429	5.397	4.207	3.889	16.36

TABLE 8.10: IMAGE STATISTICS

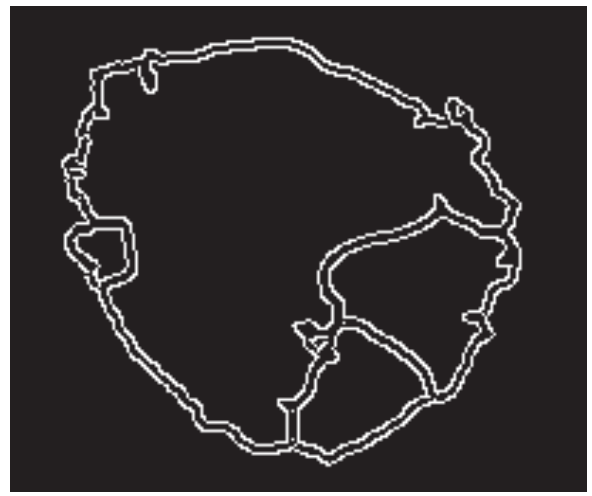
Width (pixels)	Width (cm.)	Height (pixels)	Height (cm.)	Pixels/cm.
463	16.81	622	12.51	37

We used these imaging techniques for all patient photographs to compare them with the actual measurements. ImageJ assists us in determining the outline of the wound. Figure 8.15 and Figure 8.16 show the results of using Matlab to determine the actual XY coordinates of the edge of the wound. These results are a combination of the Sobel and the Canny edge-detection algorithms [119]. We imported those points into Solidworks to create a spline of the wound and, ultimately, a three-dimensional, volumetric model of the wound.

Similarly, Figure 8.15 shows the comparison between the Sobel and the Canny edge-detection algorithms for a patient wound.



(A) SOBEL EDGE-DETECTION ALGORITHM



(B) CANNY EDGE-DETECTION ALGORITHM

FIGURE 8.15: PATIENT 2: WOUND EDGE

Figure 8.16 shows a matrix of the pixel coordinates of the edge from the wound of Patient 2. Figure 8.16 shows successive marks that indicate the edge of the boundary. Each mark indicates the location of a boundary pixel and provides the XY coordinates of each pixel that comprises the wound boundary. The XY coordinates allow us to import the location of each boundary pixel into Solidworks to create a three-dimensional model of the wound.

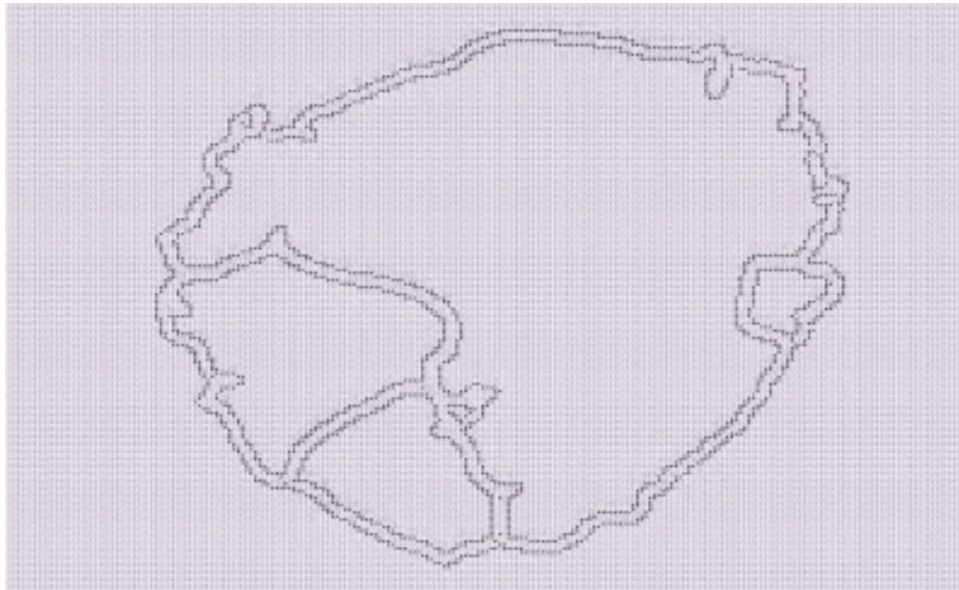
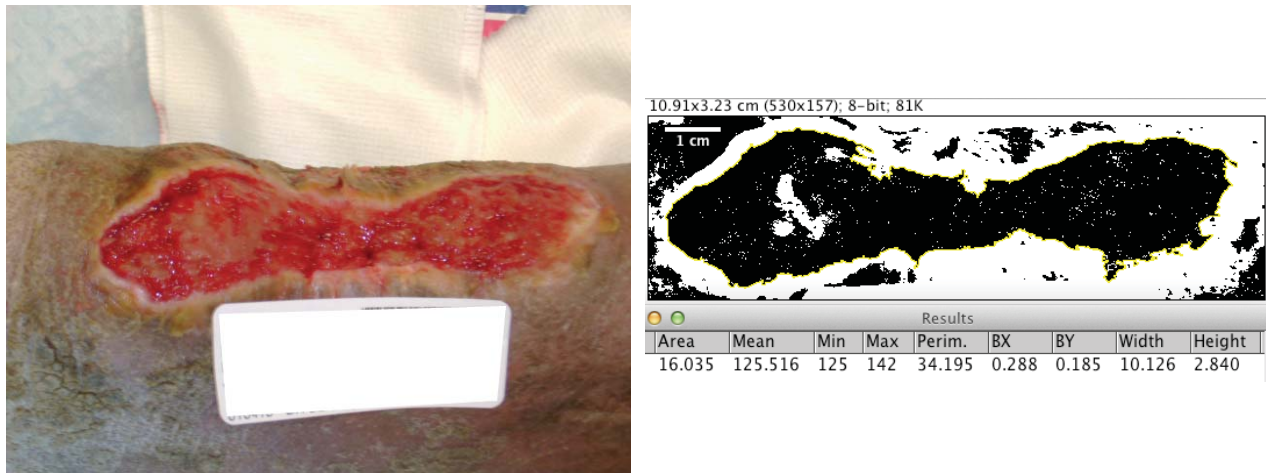


FIGURE 8.16: PATIENT 2: WOUND-EDGE TWO-DIMENSIONAL MATRIX OF XY COORDINATES

Patient 3, with a severe 10-cm.-wide wound on the back of his calf, provides another example of image analysis. This individual has a history of chronic wound problems, is diabetic, and lacks proper nutrition.

Figure 8.17, Table 8.11, and Table 8.12 show another patient example using image analysis.



(A) RGB IMAGE

(B) BINARY IMAGE WITH SCALE

FIGURE 8.17: PATIENT 4: IMAGE ANALYSIS

TABLE 8.11: FIGURE 8.12 GEOMETRIC ANALYSIS RESULTS

Area	Mean	Minimum (pixel value)	Maximum (pixel value)	Perimeter	Bx	By	Width (bounding rectangle)	Height (bounding rectangle)
16.035	125.516	125	142	34.195	0.288	0.185	10.126	2.840

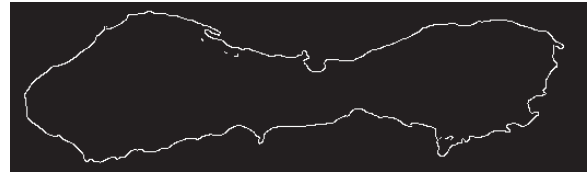
TABLE 8.12: IMAGE STATISTICS

Width (pixels)	Width (cm.)	Height (pixels)	Height (cm.)	Pixels/cm.
530	157	10.91	3.23	123.41

Similarly, Figure 8.18, and Figure 8.19 represent the final wound boundary output for Patient 4. The respective spline in Figure 8.18 was imported into Solidworks



(A) SOBEL EDGE-DETECTION ALGORITHM



(B) CANNY -TECTION ALGORITHM

FIGURE 8.18: PATIENT 4: WOUND EDGE



FIGURE 8.19: PATIENT 4 FINAL WOUND OUTLINE ANALYZED IN MATLAB

The image of Patient 4's wound was analyzed to determine the XYZ pixel coordinates and imported into Solidworks to render a three-dimensional model of the wound.

8.4.2 THERMAL-PHOTOGRAPHY ANALYSIS

Thermal imaging and analysis were performed with a ThermoCAM S65 infrared camera from Flir Systems. The camera has a with a 38.5-micron lens and provides 38.5-micron/pixel resolution (Figure 8.20 and Appendix D). The accuracy of this camera is $\pm 2^{\circ}\text{C}$ or $\pm 2\%$ of the reading — a higher tolerance than we would have chosen. Because the average temperature difference between an ulceration and the surrounding environment is approximately $\pm 2^{\circ}\text{C}$, we would have preferred a camera with a smaller tolerance deviation. The objective of using the ThermoCAM was to collect thermal images of wounds to track the temperature change over time. We measured the center of the wound's temperature and used that measurement to compare changes over time. We photographed the patient's wound approximately three times per visit over a three-week

period and averaged the temperature of the wound's center. We collected the data on live patients rather than retrospective patients.



(A)



(B)



(C)

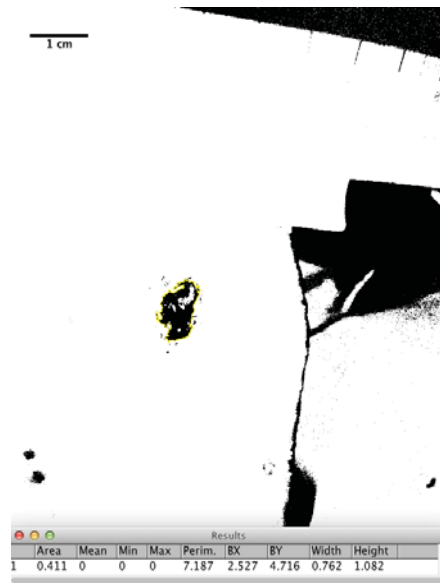


(D)

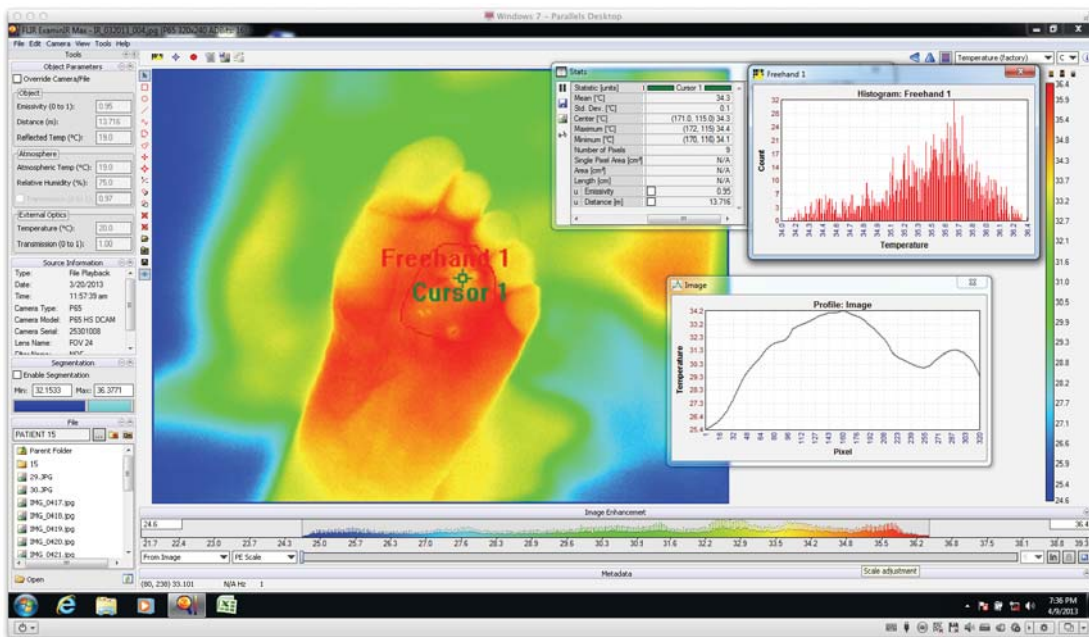
FIGURE 8.20: FLIR THERMACAM S65 THERMAL-IMAGING SYSTEM



(a) RGB Image



(b) Binary Image with Scale



(c) WOUND THERMAL IMAGING

FIGURE 8.21: PATIENT 15 IMAGE COMPILATION

Figure 8.21 documents the full image analysis of patient 15's wounds through RGB image analysis, binary image analysis, and wound thermal imaging. Table 8.13 provides the same image statistics as those for the previous patients. The addition to these geometric results is the inclusion of the wound temperature.

TABLE 8.13: FIGURE 8. GEOMETRIC ANALYSIS RESULTS

Area	Mean	Maximum (pixel value)	Maximum (pixel value)	Perimeter	Bx	By	Width (bounding rectangle)	Height (bounding rectangle)	Thermal Temperature
0.411	0	0	0	7.187	2.527	4.716	0.762	1.082	34.3°C

8.4.3 THREE-DIMENSIONAL CAD-MODEL DEVELOPMENT

To create a three-dimensional CAD Model from a two-dimensional image, we had to develop the proper methodology to prepare the image for processing. That process included image manipulation from the RGB color space to the LAB color space. This slight modification is key in allowing the Sobel and Canny edge-detection algorithms to better detect the shape of the wound. Figure 8.22 shows the final input image to the three-dimensional CAD system. Figure 8.22 allows us to determine the pixel-to-centimeter relationship, allowing us to convert from pixels back to centimeters in preparation for point-cloud importing.

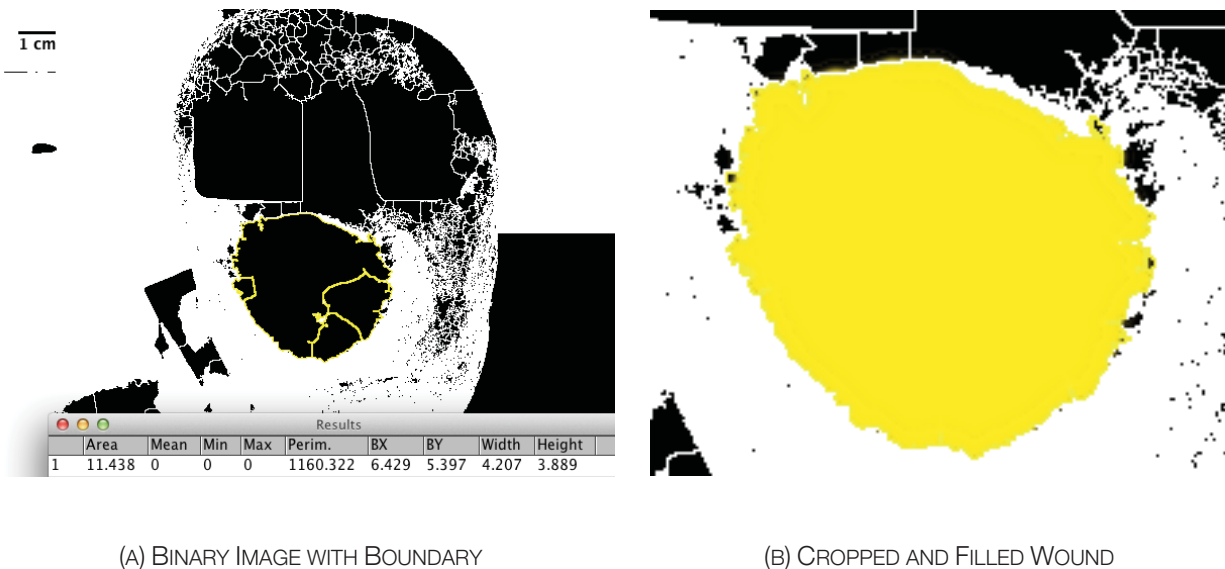


FIGURE 8.22: PATIENT 2 PIXEL-TO-CENTIMETER CONVERSION

This methodology determines the pixel XY coordinates of the boundary of the wound, eliminates duplicates, and cleans the collection of XY coordinates in preparation for Solidworks data importing. Cleaning of this data is of the utmost importance because, in many instances, the boundaries are so complex, that single pixels are on or nearly on top of one another. That situation is acceptable for analysis of a two-dimensional matrix; however, with three-dimensional geometric processing, it creates self-intersecting splines, which prevent two-dimensional-to-three-dimensional geometry. When the data is clean, the methodology exports the table of XYZ points (Table 8.14). This text file allows the three-dimensional CAD system to construct a series of XYZ points to construct the desired shape using point-cloud theory [120, 121].

The XYZ coordinates in Table 8.14 are then converted to centimeters, which allows proper importing of the three-dimensional system. Solidworks has a built-in ScanTo3D, which allows us to import a series of cloud points to create a solid three-dimensional model. ScanTo3D performs a series of reverse-CAD functions that creates a three-dimensional model from a two-dimensional image [120]. Figure 8.23 shows the modified ScanTo3D methodology and details the process of extracting the boundary points of the wound and importing them into Solidworks. Although a variety of ways exist to import XYZ coordinates into Solidworks, one method of inserting a curve through XYZ coordinates does not work for boundary creation. When inserting a curve of XYZ coordinates in Solidworks, the order of the boundary points causes system instability.

TABLE 8.14: GEOMETRIC ANALYSIS RESULTS

X (Pixel)	Y (Pixel)	Z (Pixel)
150	756	0
151	651	0
151	670	0
151	671	0
168	564	0
168	565	0

With edge-detection algorithms, such as the Sobel or Canny, the boundary-trace algorithms outlines an object (Figure 8.24). The boundary-trace algorithm determines the initial starting point, Pixel P, with an assigned start direction — that is, northeast. From there, the algorithm checks the surrounding seven remaining pixels and records the XY coordinates of each nonempty pixel. Although the boundary-trace and edge-detection algorithms acquire the boundary of object, XY

coordinates are repeated due to the innate characteristics of edge- and boundary-detection methods.

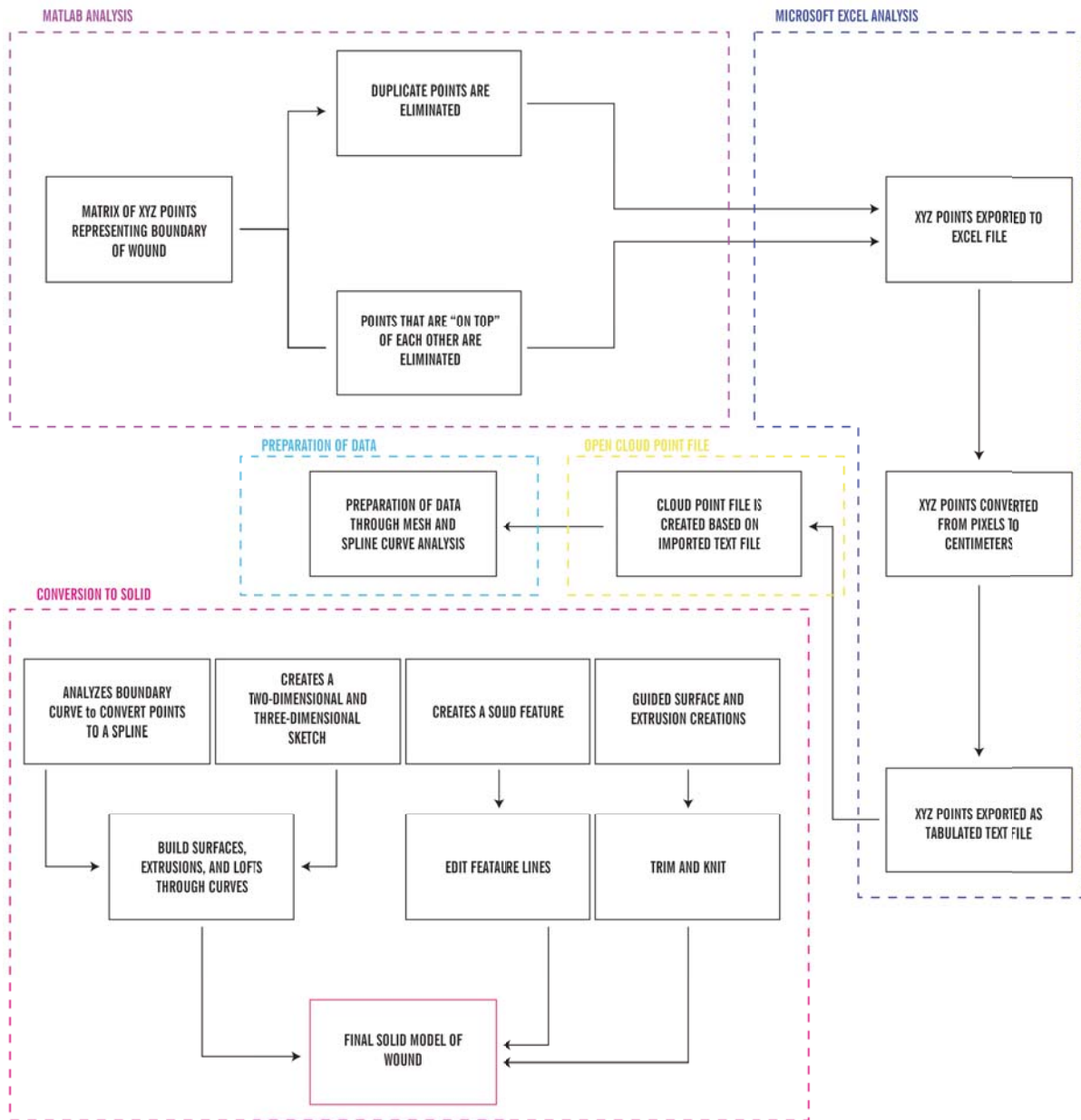


Figure 8.23: ScanTo3D Methodology

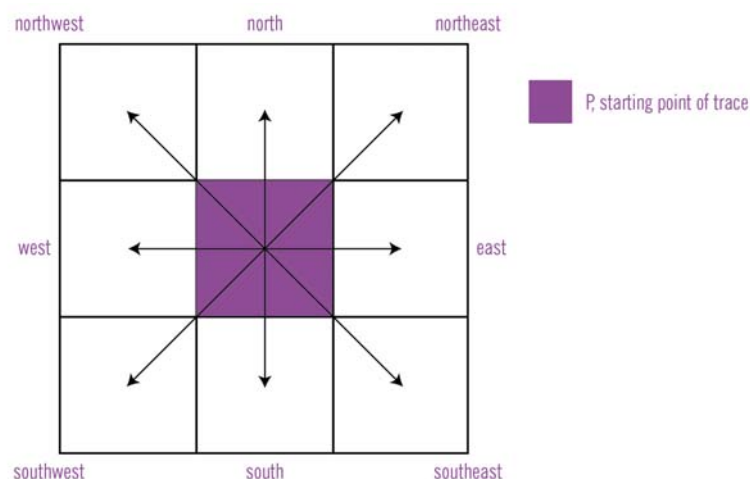


FIGURE 8.24: BOUNDARY-TRACE PROCESS

8.4.3.1 Calculating Wound Volume Through Three-Dimensional Modeling

Using the methodology developed in Figure 8.23, we created multiple three-dimensional models of wounds over time. This time-varying analysis allows us to see the change in mass, volume, and surface area over an observed period.

Using Patient 11, we have documented the wound over a 28-day period.

TABLE 8.15: PATIENT 11 HUMAN WOUND MEASUREMENTS

Day	Length 1 (cm.)	Length 2 (cm.)	Depth (cm.)	Volume (cm. ³)	Surface Area (cm. ²)
0	8.0	1	0.5	4	8.0
7	7.0	1	0.5	3.5	7.0
14	7.0	1	0.5	3.5	7.0
21	6.2	1	0.5	3.1	6.2
28	4.0	0.8	0.5	1.6	3.2

Using the imaging techniques in Figure 8.11, we compared the calculated measure of surface area based on the measurements in Table 8.15 and the calculated wound properties based on image analysis (Table 8.16).

TABLE 8.16: PATIENT 11 SOLIDWORKS WOUND MEASUREMENTS

Day	Length 1	Length 2	Depth	Volume	Surface Area
7	6.35	1	0.1	0.18	6.79
21	4.74	1	0.089	0.13	5.32

One of the necessary assumptions pertaining to the wound healing modeling is that the shape of the wound throughout the course of healing does not drastically change the shape and cross-section of the wound. Thus, we assume that the reduction in size proportionally is based on the dimensions of the wound boundary. The purpose of the inclusion of Solidworks was to show the measurement difference between human wound measurements and computerized measurements. Through Solidworks and image analysis, we were able to acquire a more accurate measurement of the size of the wound, including surface area and volume. This feature enabled us to better monitor the change in wound size over time. Figure 8.25 shows a Solidworks model of a patients' complex-shaped wound.



(A) Isometric View



(B) Top View



(C) Side View

FIGURE 8.25: VARIOUS VIEWS OF PATIENT 11'S WOUND SHAPE AND BOUNDARY

8.5 DATA PREPROCESSING: STAGE II

During The second stage of data processing, we used only those wounds for which we had retrospective data for more than five visits — that is, more than approximately 40 days. This data sorting and cleaning guaranteed that we could build an accurate and robust predictive model. The purpose of the second stage was to categorize wounds based on their aspect ratio during the patient’s initial visit. Equation (8.5) yields the aspect ratio:

$$\text{Aspect Ratio} = \frac{\text{Length 1}}{\text{Length 2}} \quad (8.5)$$

The aspect ratio represents the shape of the wound. For example, if the aspect ratio is 1-to-1, the shape of the wound is most likely circular. If it is 3-to-1, the aspect ratio is more elliptical in shape. We hypothesized that the difference in the wound shape results in different healing patterns and wound behavior.

Based on the aspect ratio, the wound and all of its subsequent measurements were grouped into three groups of smaller data sets:

$$\text{Group 1:} \quad \text{Aspect Ratio} < 1 \quad (8.6)$$

$$\text{Group 2:} \quad 1 \leq \text{Aspect Ratio} \leq 2 \quad (8.7)$$

$$\text{Group 3:} \quad \text{Aspect Ratio} > 2 \quad (8.8)$$

Before building the models, we needed to determine whether we could achieve the same accuracy and precision using calculated inputs rather than raw inputs to the algorithm as predictive variables. In other words, we needed to determine whether volume, the calculated input; length 1; length 2; and depth, the raw inputs, differed in their output accuracy. Unfortunately, we discovered that the small depth measurements drastically skewed the calculated volume. Using volume as an input rather than the raw inputs caused the algorithms to be less accurate in their predictive capabilities. Equation (8.9) illustrates this problem.

$$a(b + c) \neq ab + ac$$

(8.9)

This equation confirmed that we required raw, independent variables as variable. To verify the hypothesis, we graphed a sample of data from each aspect-ratio group in Figure 8.26 to Figure 8.41. Each aspect ratio revealed different wound-healing characteristics based on volume. Figure 8.26 and Figure 8.27 show the wounds with an aspect ratio of less than 1 and show a distinctive pattern and behavior of increasing wound volume before decreasing wound volume. This result differs from that in Figure 8.4 and Figure 8.35, in which wound volume seems to dramatically decrease over time, as opposed to what occurs with wounds having an aspect ratio of greater than 2 (Figure 8.41). This category of wounds showed a steady decrease in volume over time but a smaller gap between starting volume and ending volume. This phenomenon appears to be unique to wounds with an aspect ratio of greater than 2 as opposed to those wounds with an aspect ratio of less than 2.

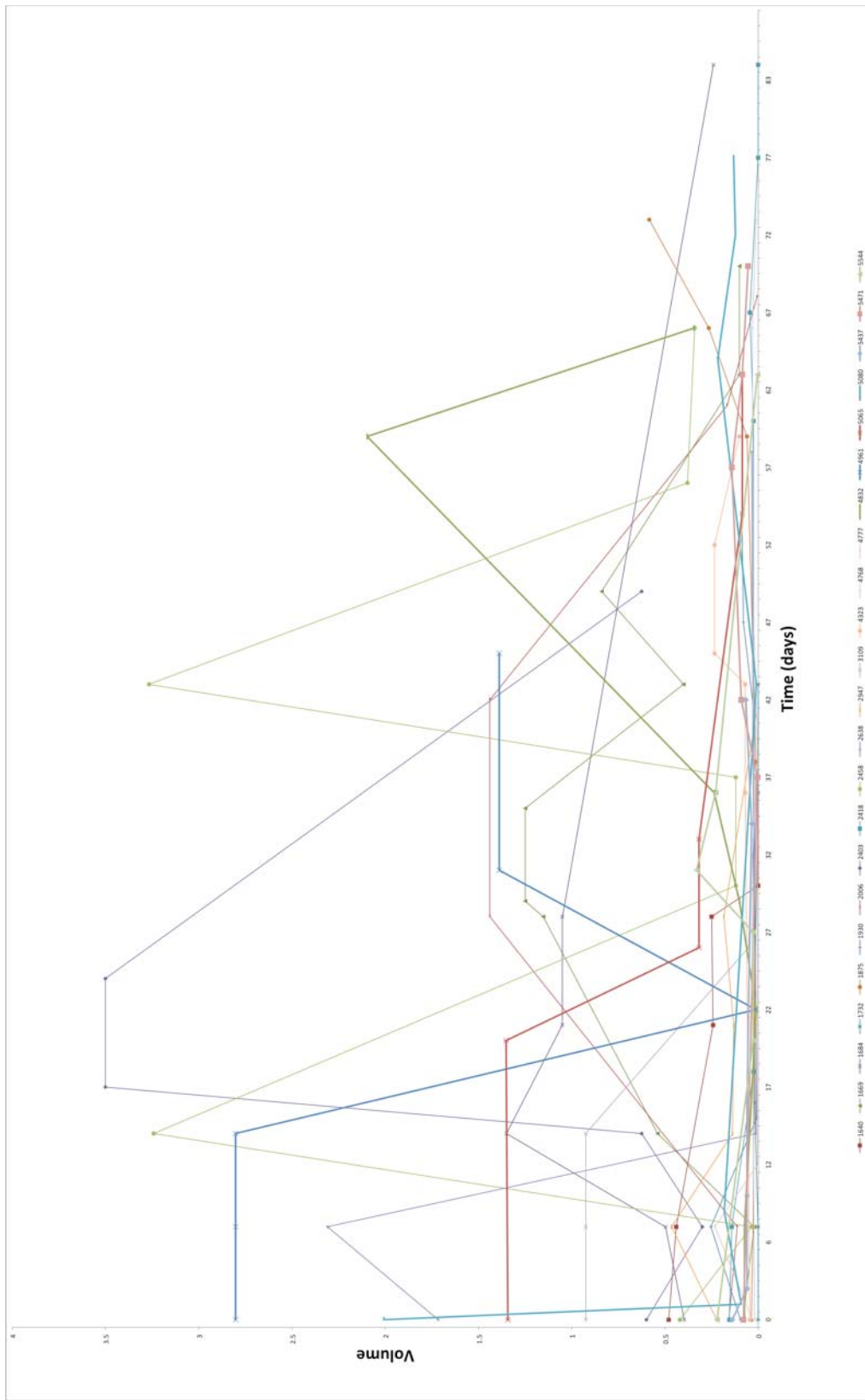


Figure 8.26: Aspect Ratio of Less Than 1, Volume Versus Time

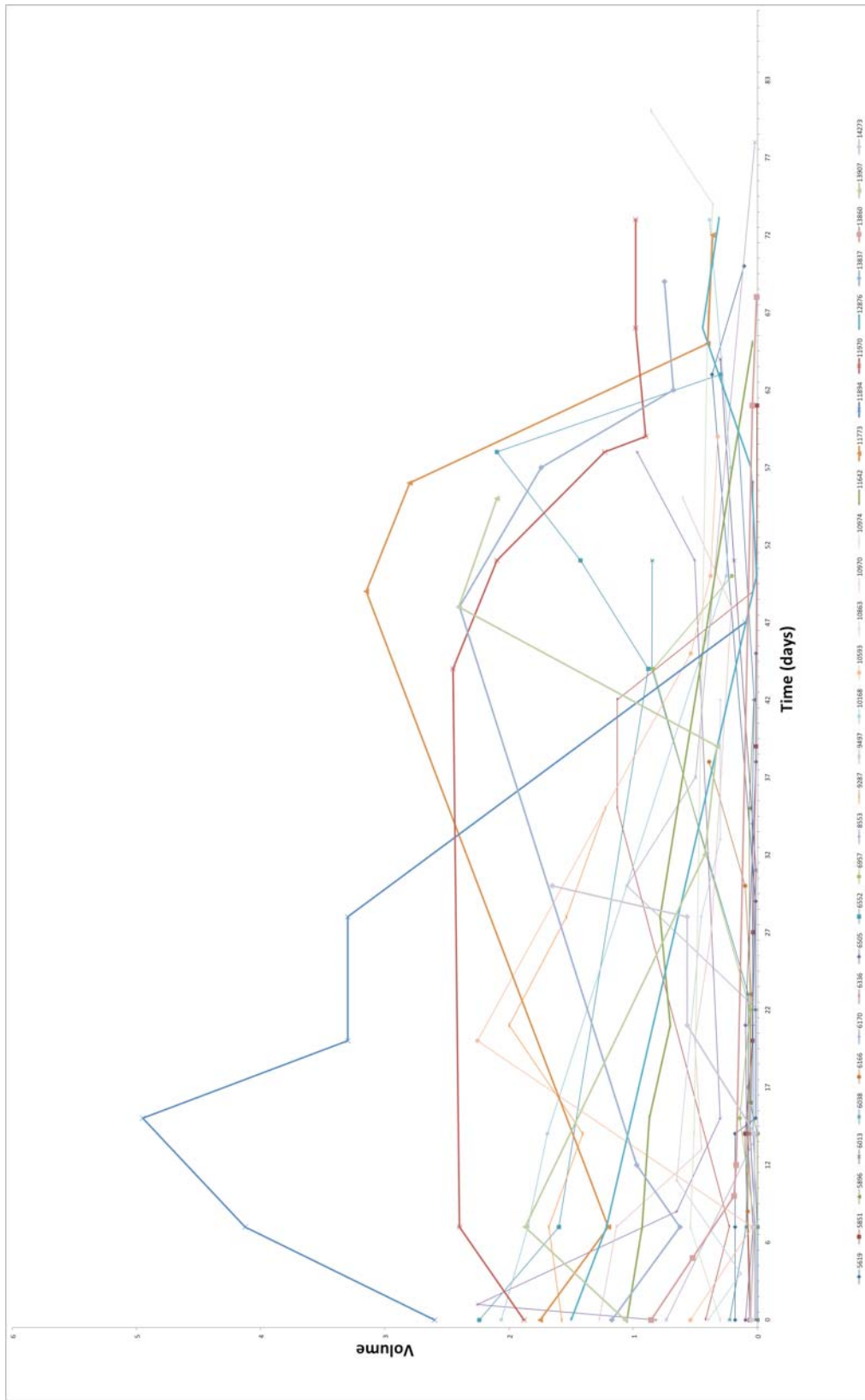


Figure 8.2.7: Aspect Ratio of Less Than 1, Volume Versus Time

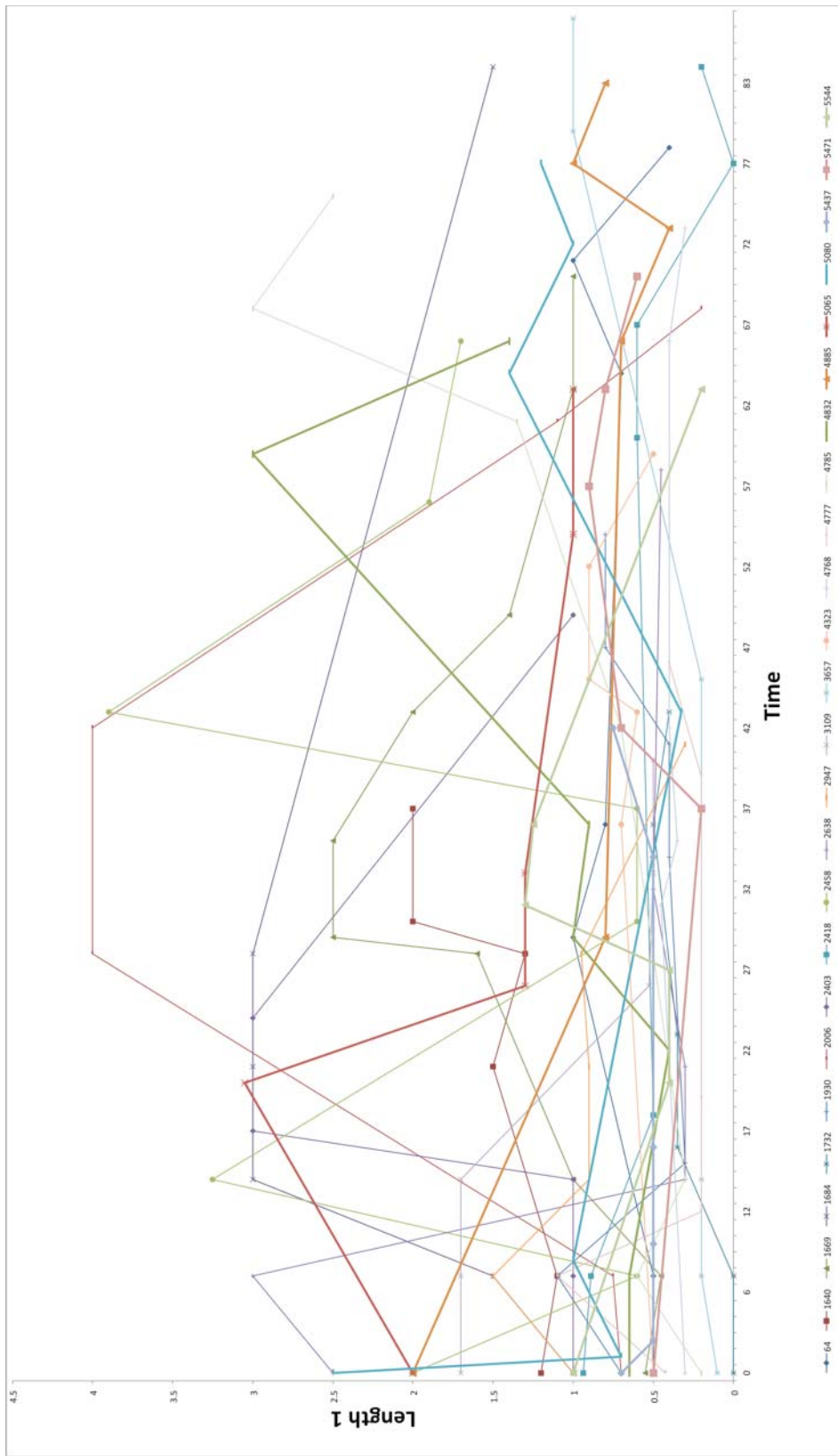


FIGURE 8.28: ASPECT RATIO OF LESS THAN 1, LENGTH 1 VERSUS TIME

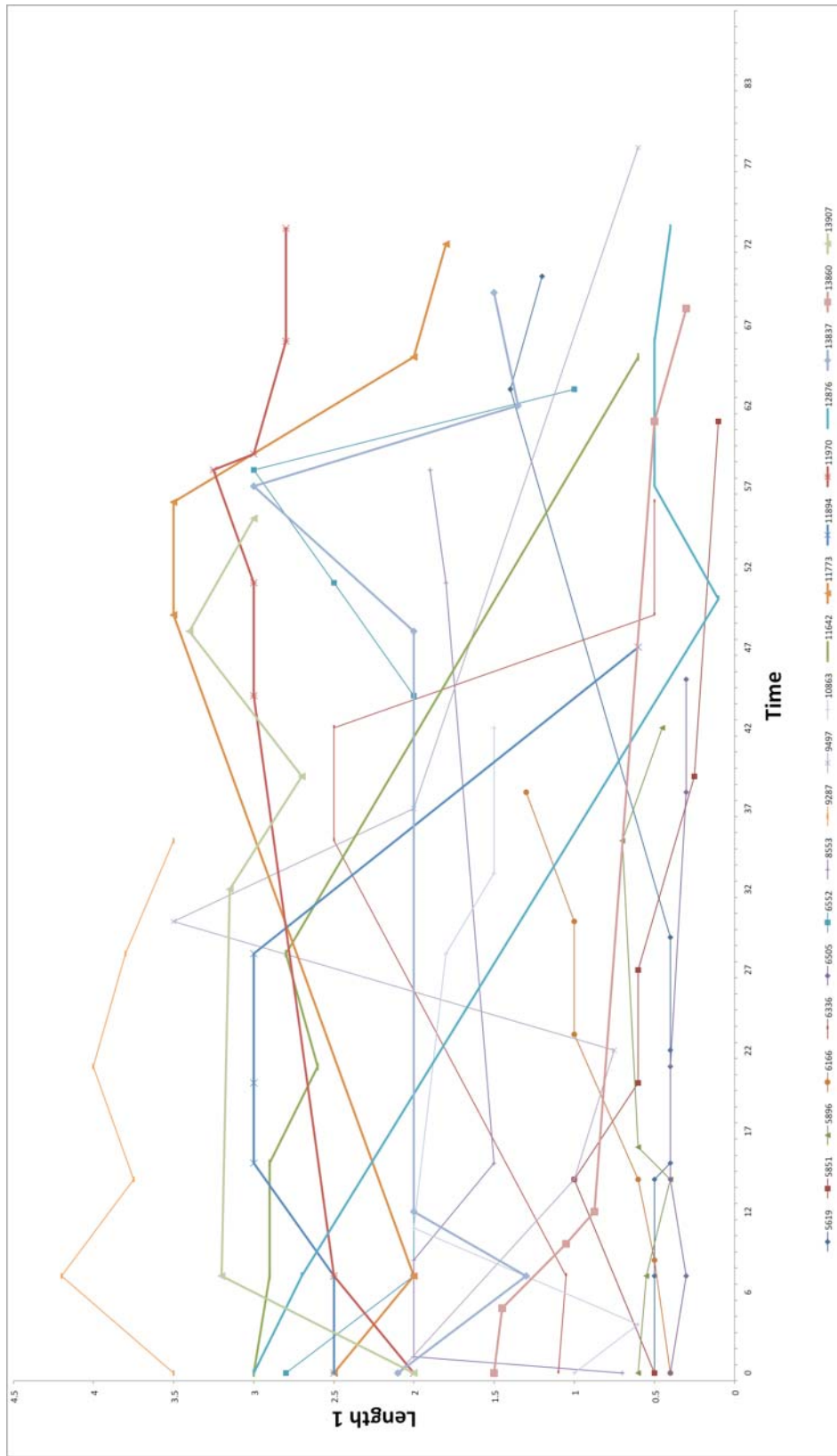


FIGURE 8.29: ASPECT RATIO OF LESS THAN 1, LENGTH 1 VERSUS TIME

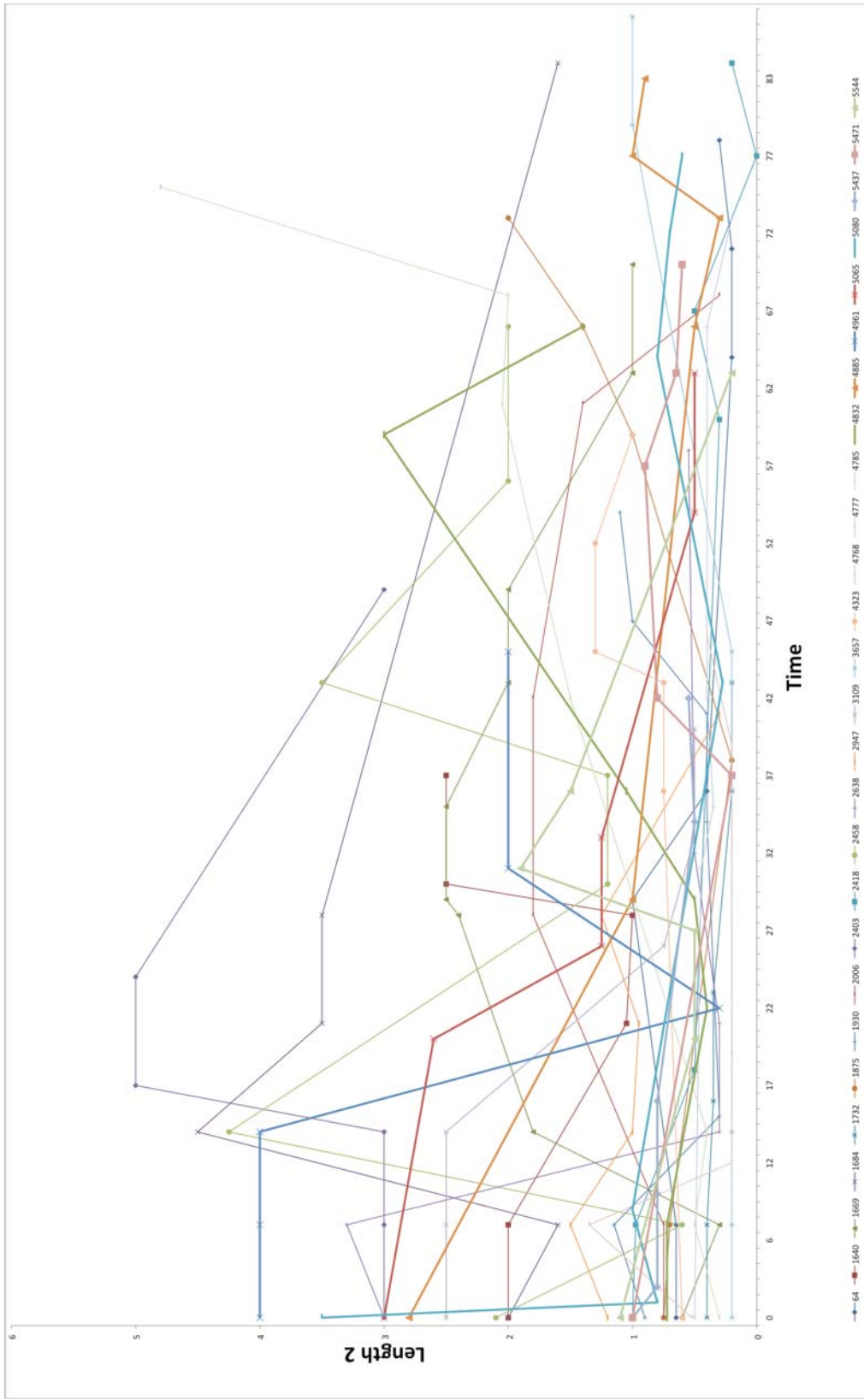


FIGURE 8.30: ASPECT RATIO OF LESS THAN 1, LENGTH 2 VERSUS TIME

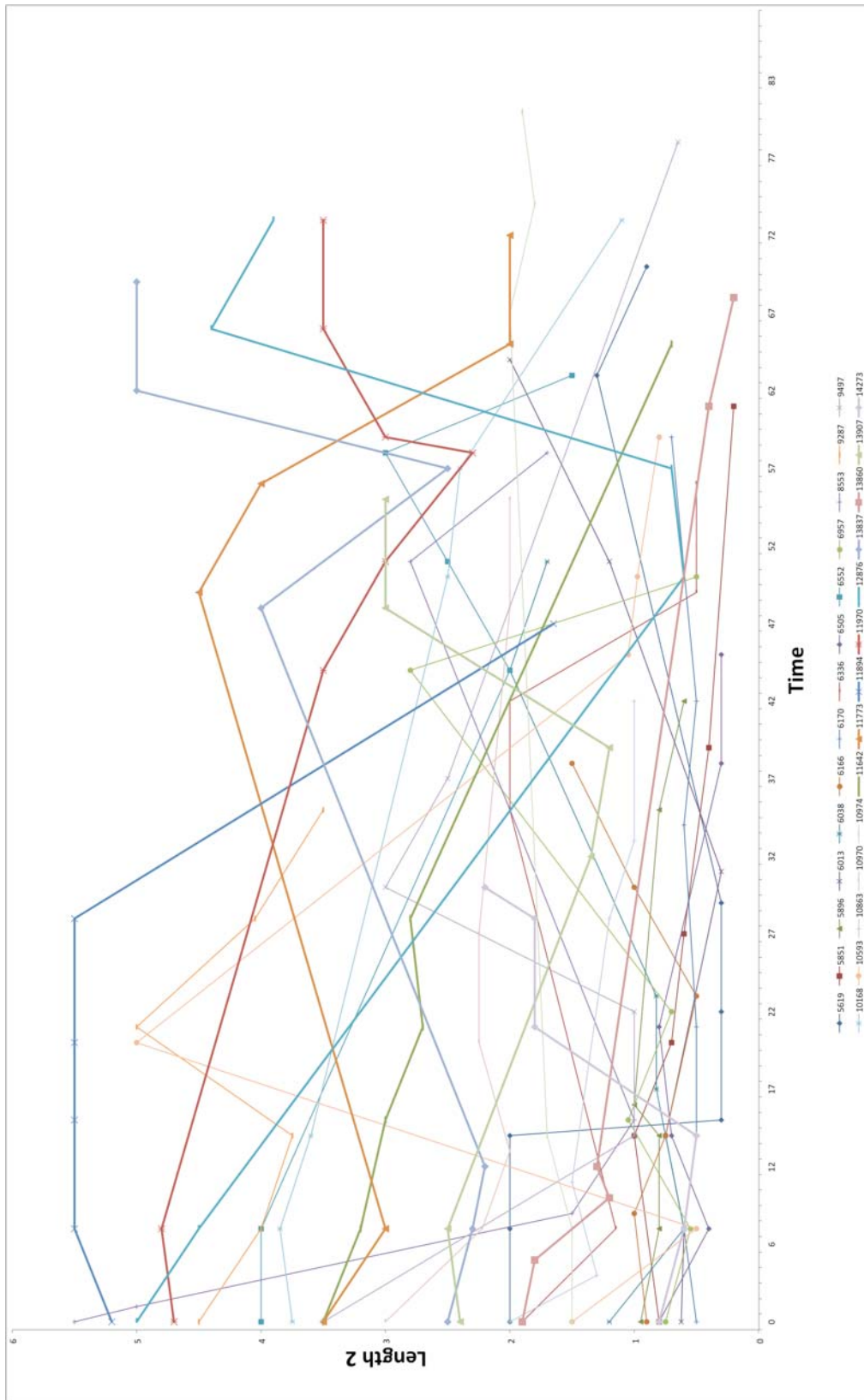


FIGURE 8.31: ASPECT RATIO OF LESS THAN 1, LENGTH 2 VERSUS TIME

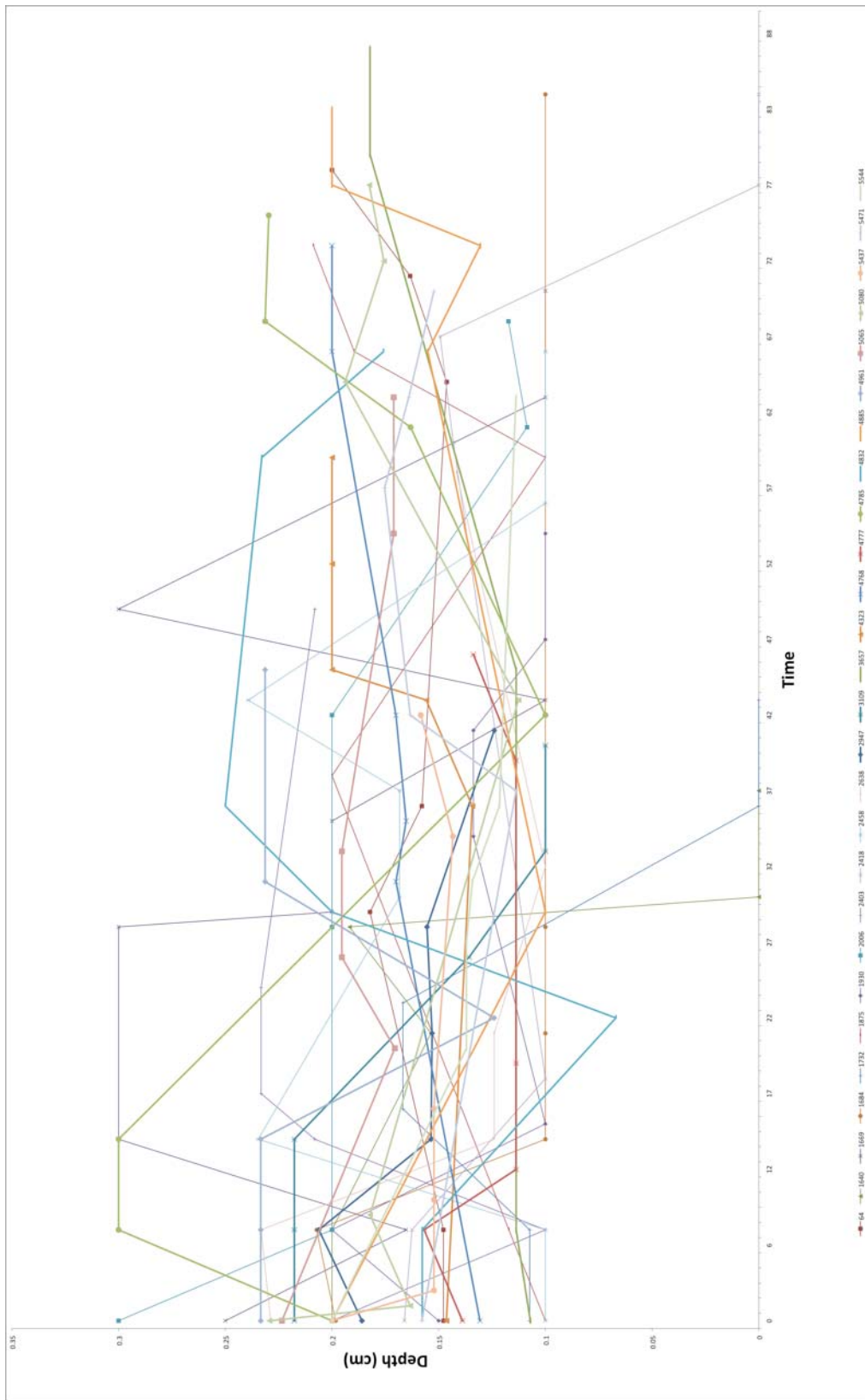


FIGURE 8.32: ASPECT RATIO OF LESS THAN 1, DEPTH VERSUS TIME

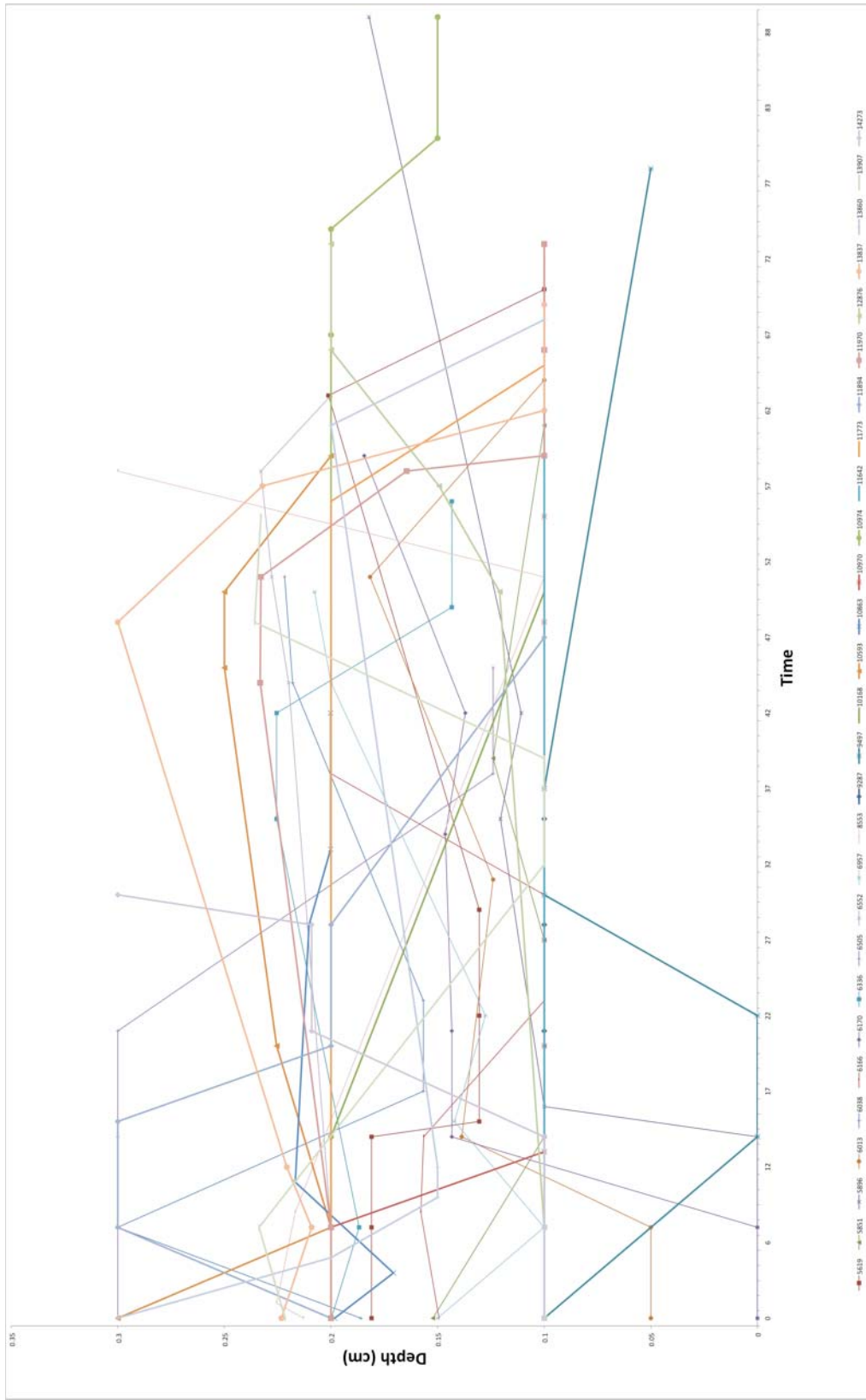


FIGURE 8.33: ASPECT RATIO OF LESS THAN 1, DEPTH VERSUS TIME

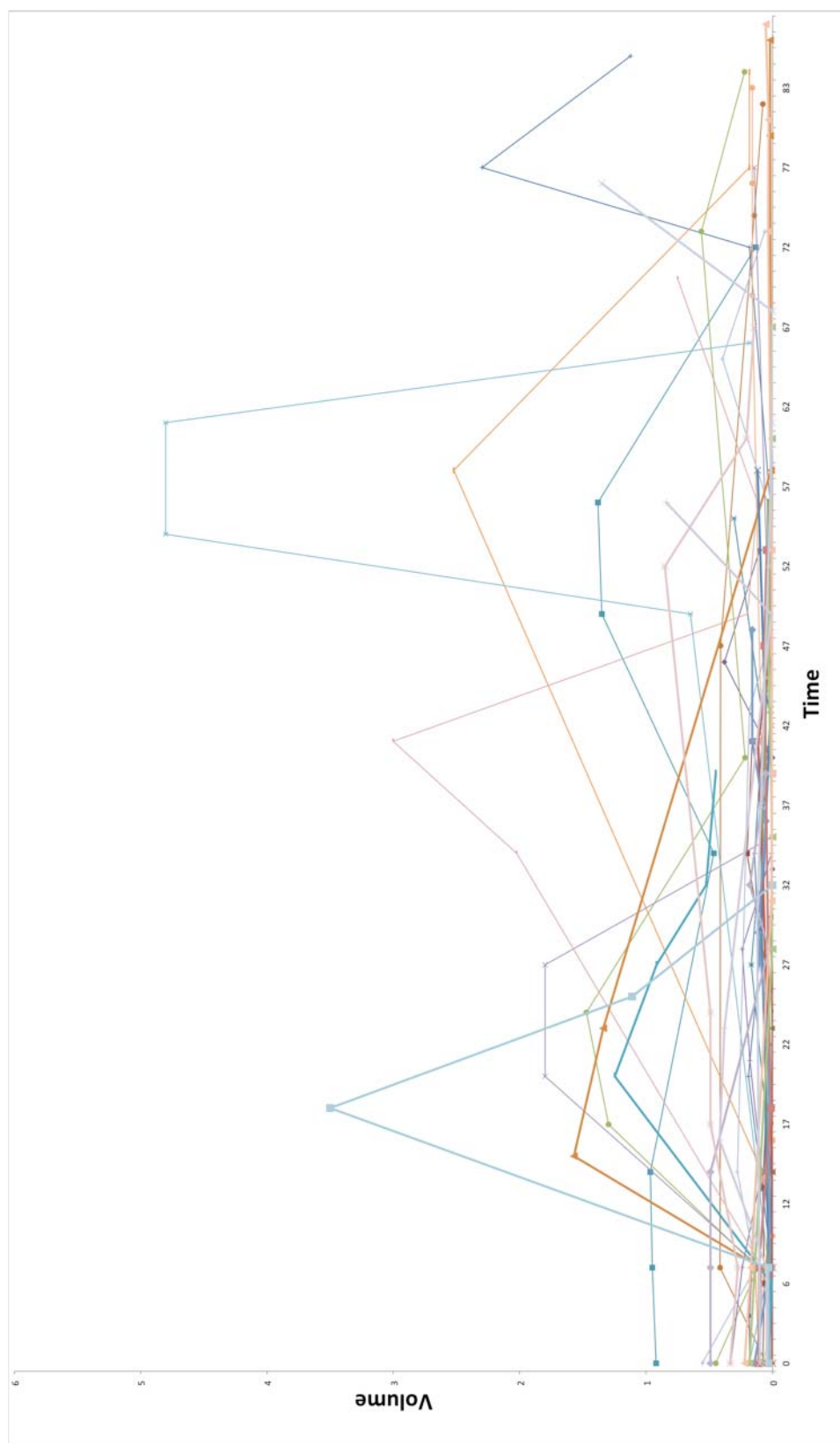


FIGURE 8.34: ASPECT RATIO OF 1 TO 2, VOLUME VERSUS TIME

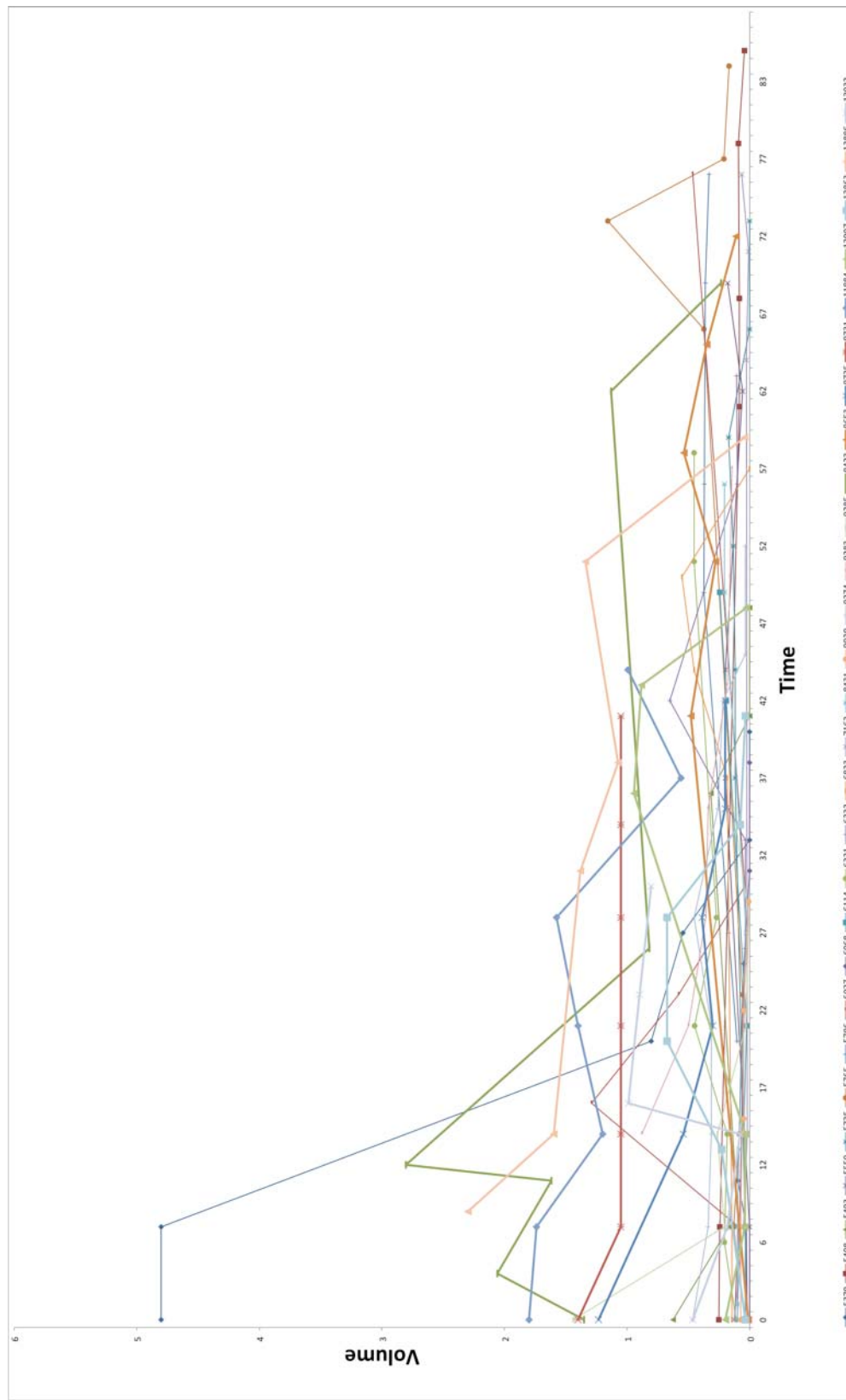


FIGURE 8.35: ASPECT RATIO OF 1 TO 2, VOLUME VERSUS TIME

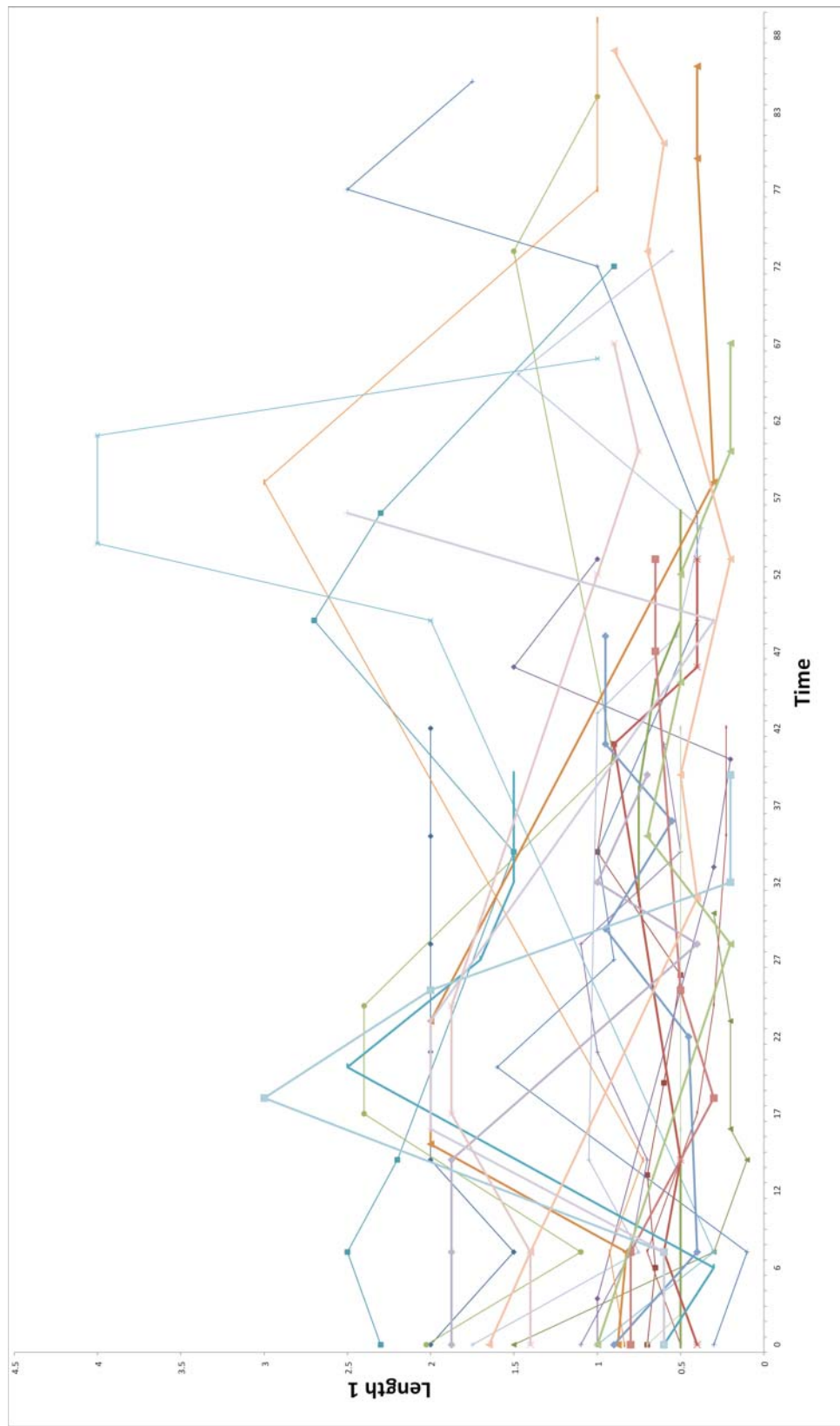


FIGURE 8.36: ASPECT RATIO OF 1 TO 2, LENGTH 1 VERSUS TIME

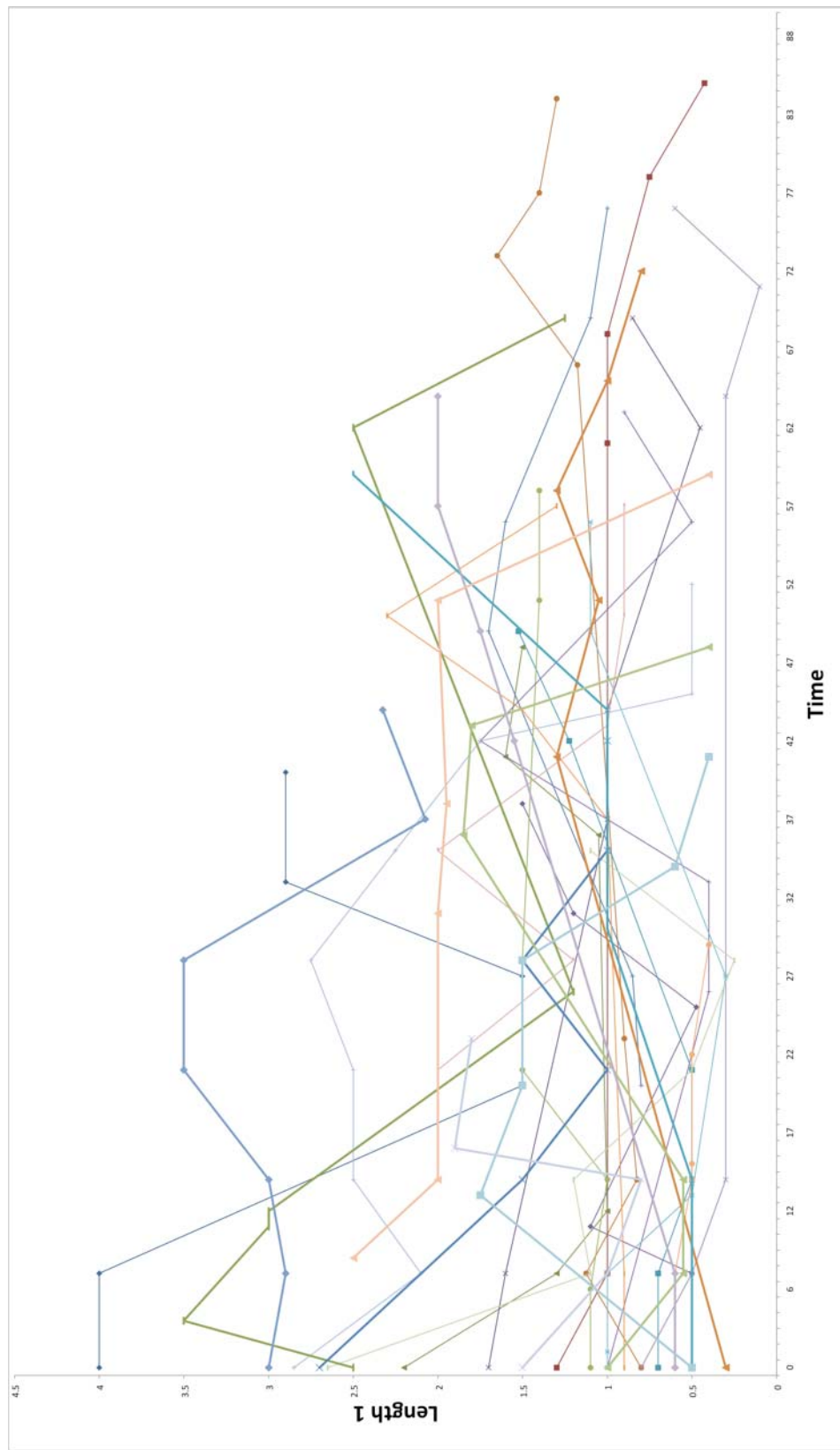


FIGURE 8.37: ASPECT RATIO OF 1 TO 2, LENGTH 1 VERSUS TIME

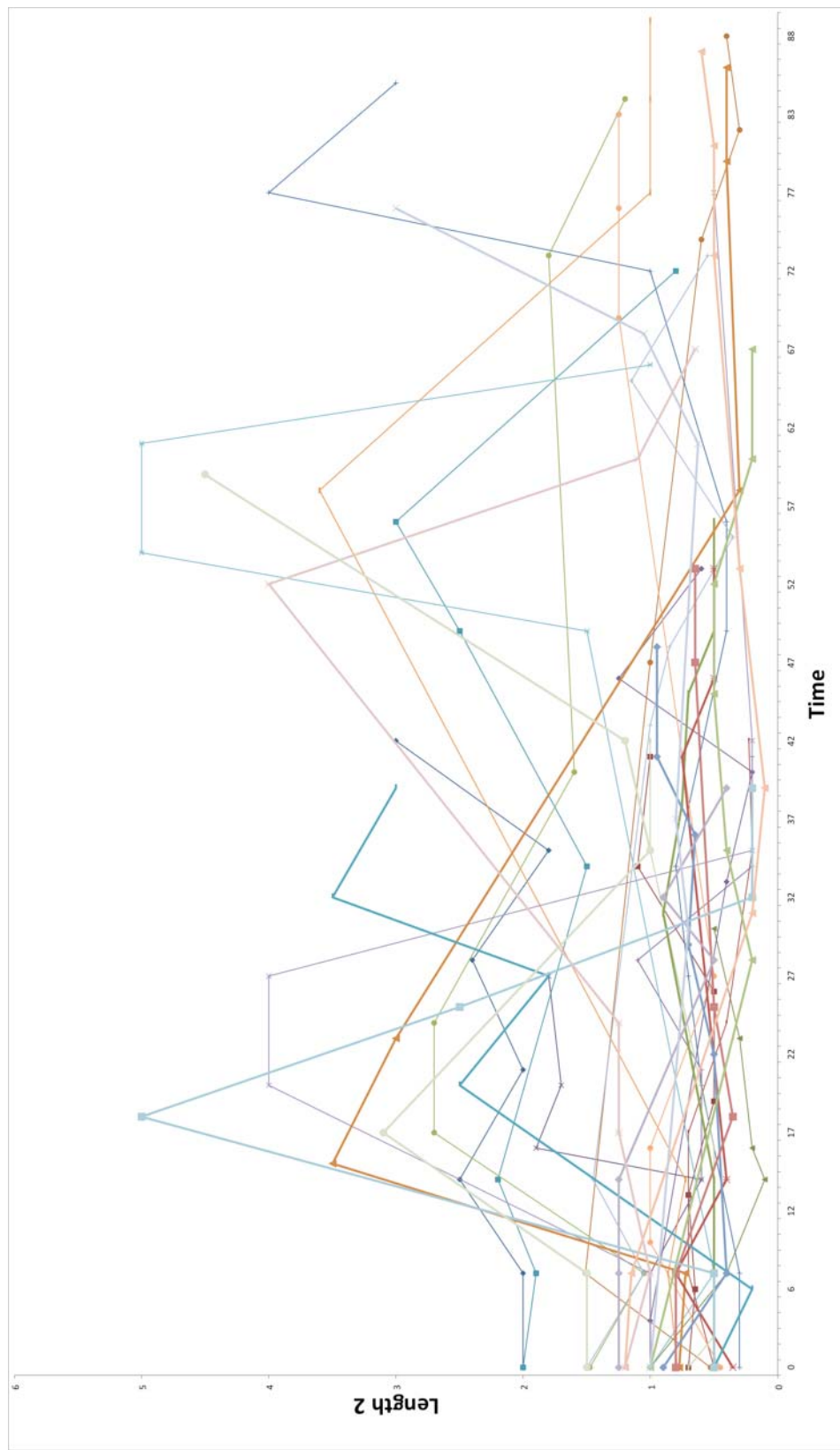


FIGURE 8.38: ASPECT RATIO OF 1 TO 2, LENGTH 2 VERSUS TIME

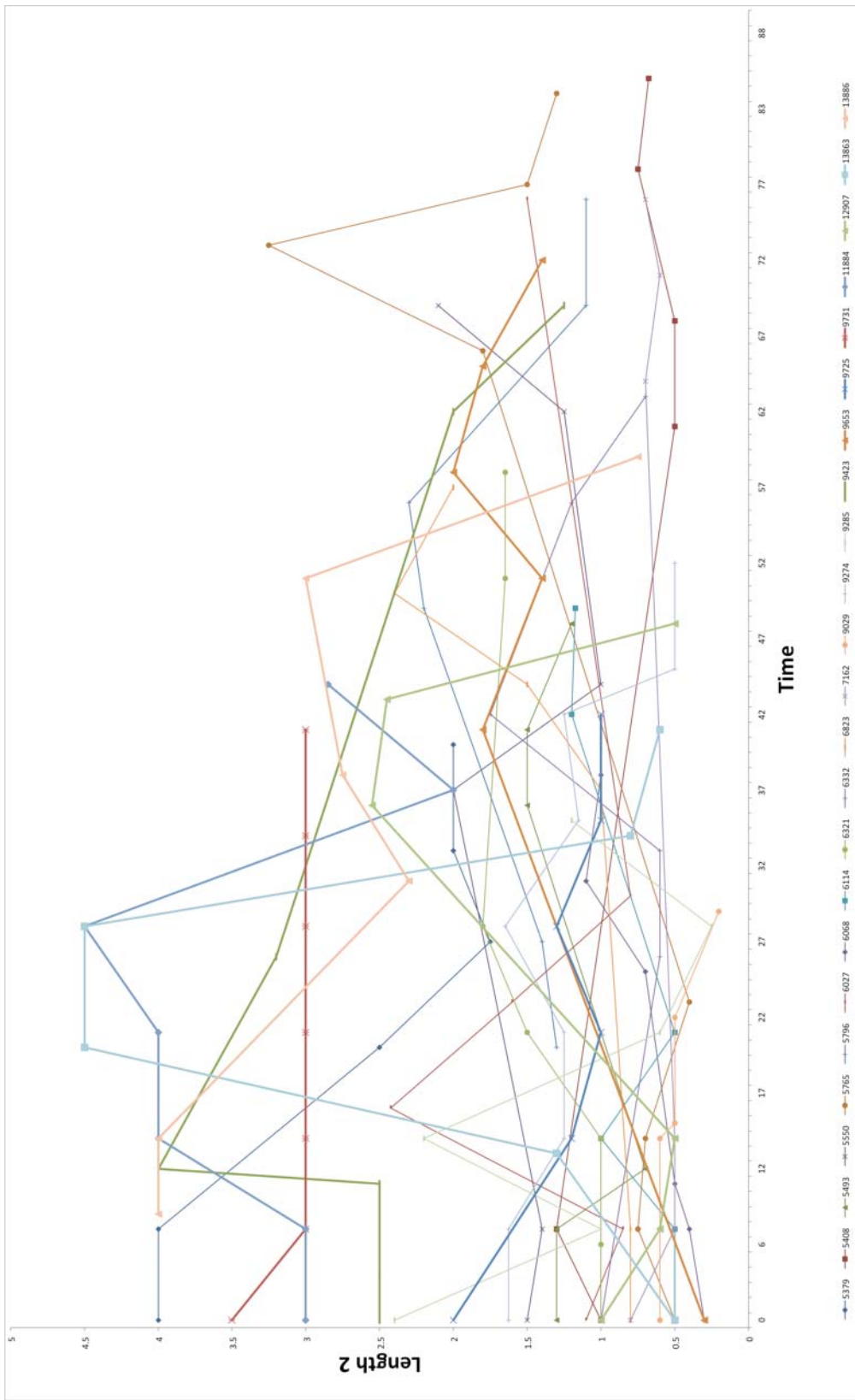


FIGURE 8.39: ASPECT RATIO OF 1 TO 2, LENGTH 2 VERSUS TIME

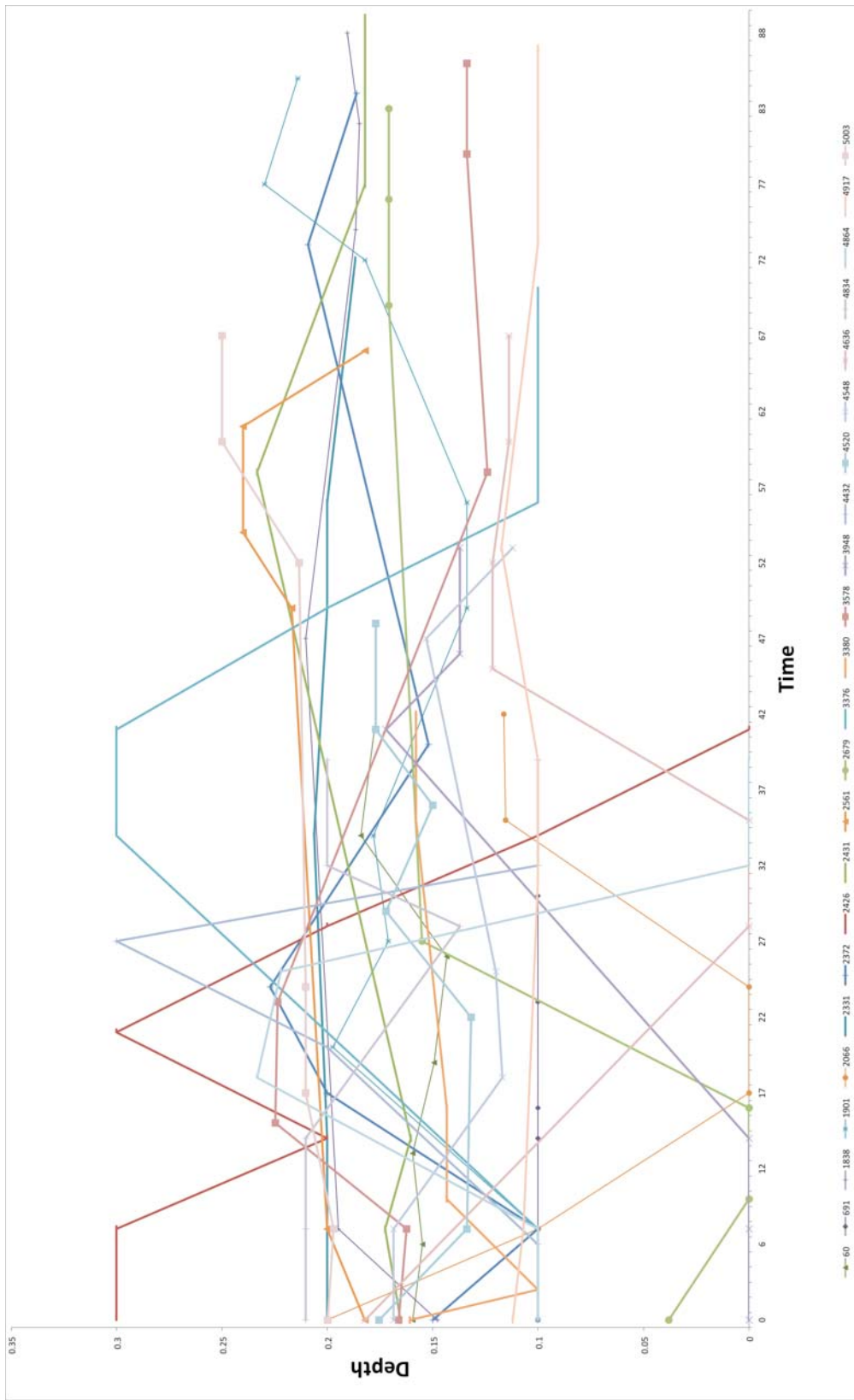


FIGURE 8.40: ASPECT RATIO OF 1 TO 2, DEPTH VERSUS TIME

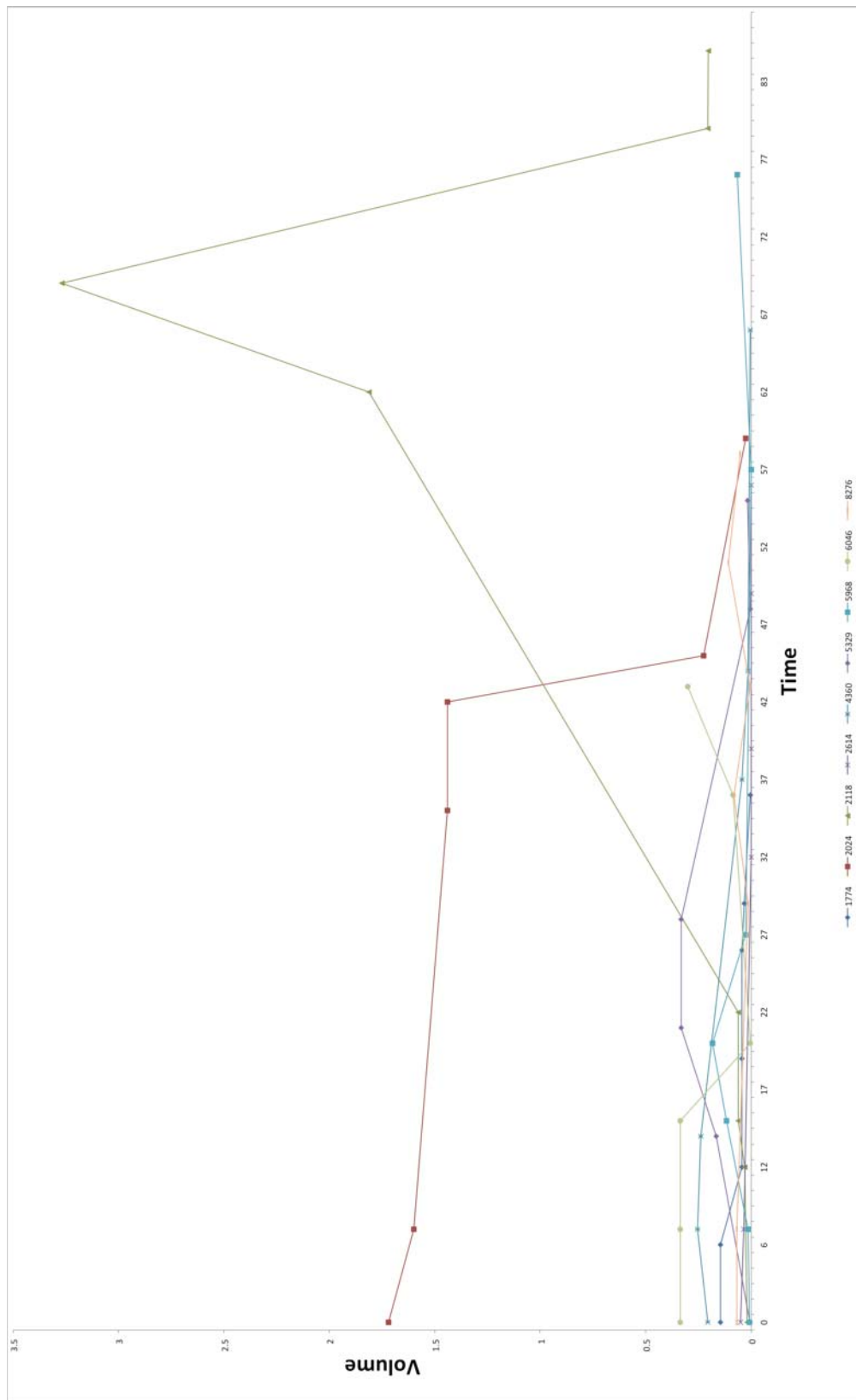


FIGURE 8.41: ASPECT RATIO OF GREATER THAN 2, VOLUME VERSUS TIME

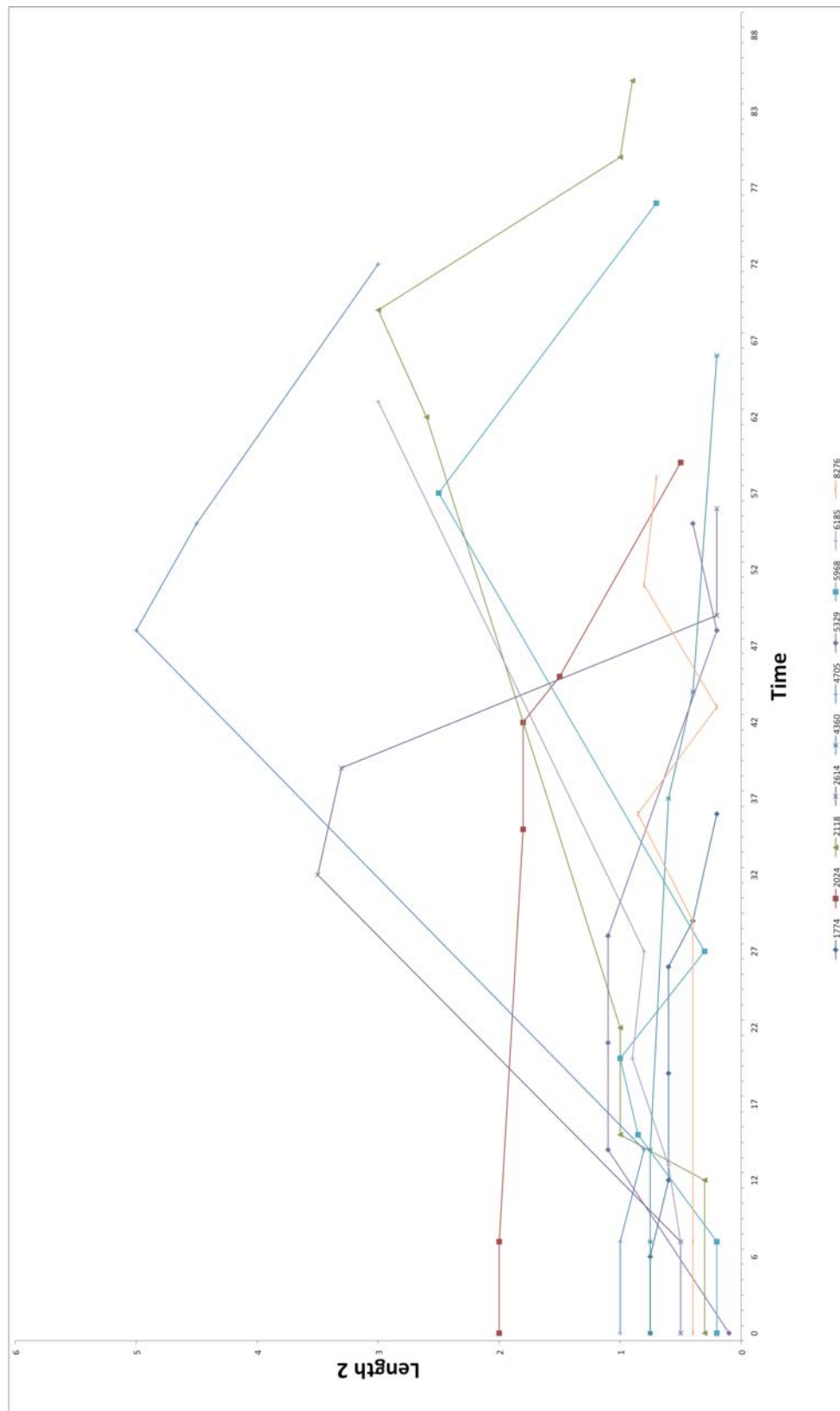


FIGURE 8.42: ASPECT RATIO OF GREATER THAN 2, LENGTH 2 VERSUS TIME

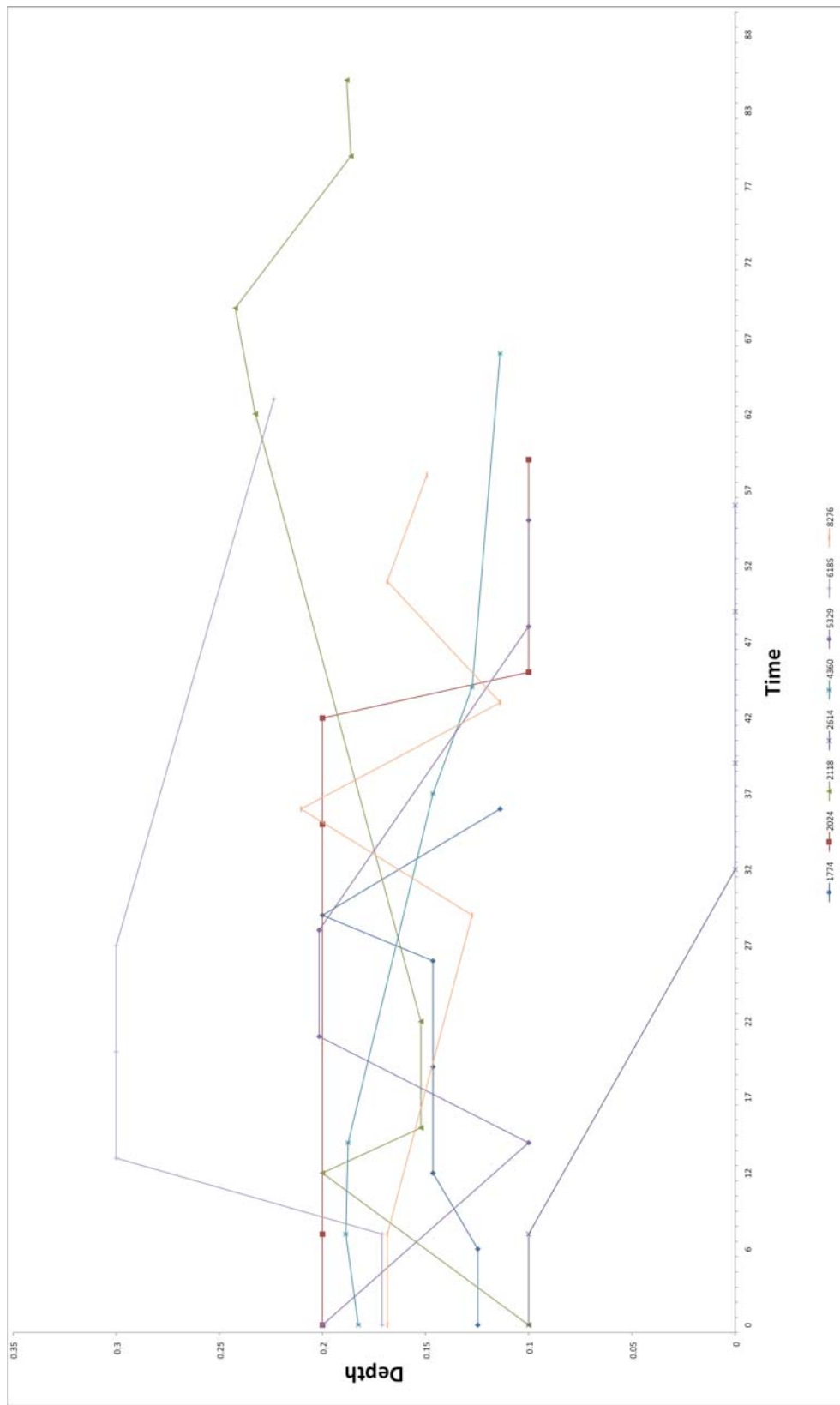


FIGURE 8.43: ASPECT RATIO OF GREATER THAN 2, DEPTH VERSUS TIME

8.5.1 DETERMINATION OF HEALED THRESHOLD

Because we categorized the variables based on aspect ratio, we have produced three neural-network models. The development of a theoretical, predictive model means that a difference exists between ideal and actual wound-healing parameters. Wound-care physicians consider a wound healed when the wound measures 0 cm. in length, width, and depth. Given that information, we never saw a 100%-healed wound in the data we received.

For the theoretical model, we have developed statistically supported assumptions that the determined healed threshold is based on the lower or upper limit of the respective input variable box plots. For example, if the input parameter is volume, we assume that the 25% percentile is healed. Similarly, if the input parameter is granulation, we would use the upper limit, 75% as the healed, or ideal, parameter. We repeated this process for each input variable and developed an ideal set of input variables. We then fed this ideal set of inputs into the designed neural network, which output a numerical value as time to heal. This single output, rather than a measurement of 0 cm. in length, width, and depth, represents a wound's stage in the healing process. We have observed, hypothesized, and supported the theory that a healing wound has asymptotic properties, and, as the wound heals, its asymptotic curve will approach the value of zero. However, Figure 8.44 shows a graph of time versus wound size (generically) approaching an asymptote of zero. One of the primary issues with using a measurement of 0 x 0 x 0 cm. is that the asymptote may take a long time to reach zero or may never reach zero.

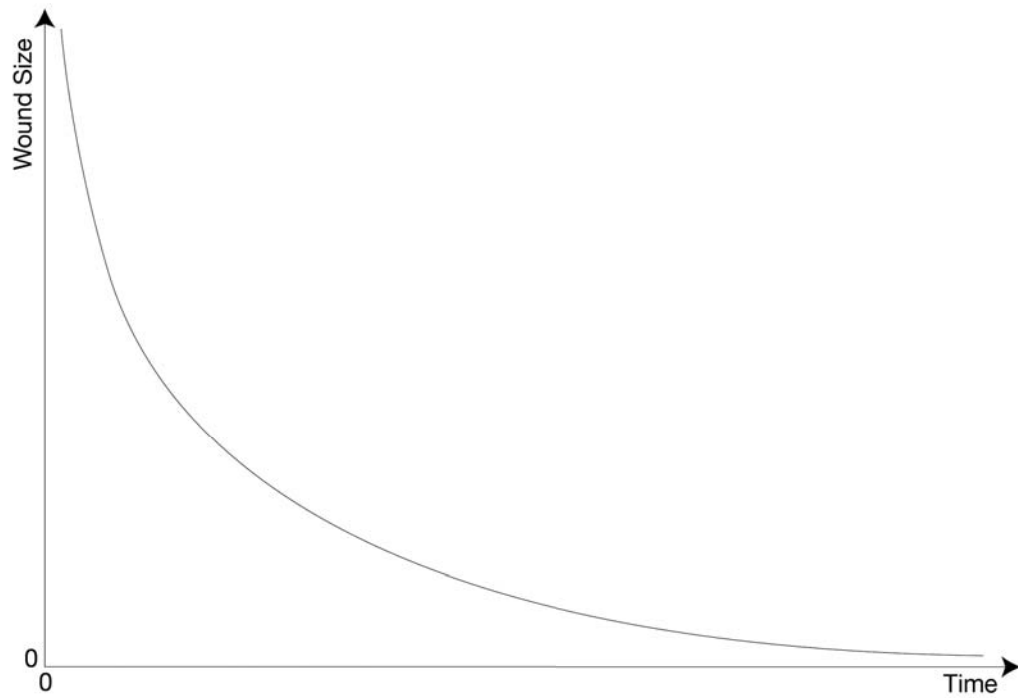


FIGURE 8.44: WOUND-HEALING TRAJECTORY APPROACHING AN ASYMPTOTE OF 0

8.5.1.1 Aspect Ratio of Less Than 1: Volume

To design and develop a model using volume calculations, we performed similar data cleaning based on the volumetric parameter. We eliminated outliers based on the upper whisker. We also used the box plot in Figure 8.45 to determine the lower quartile value for the ideal data set.

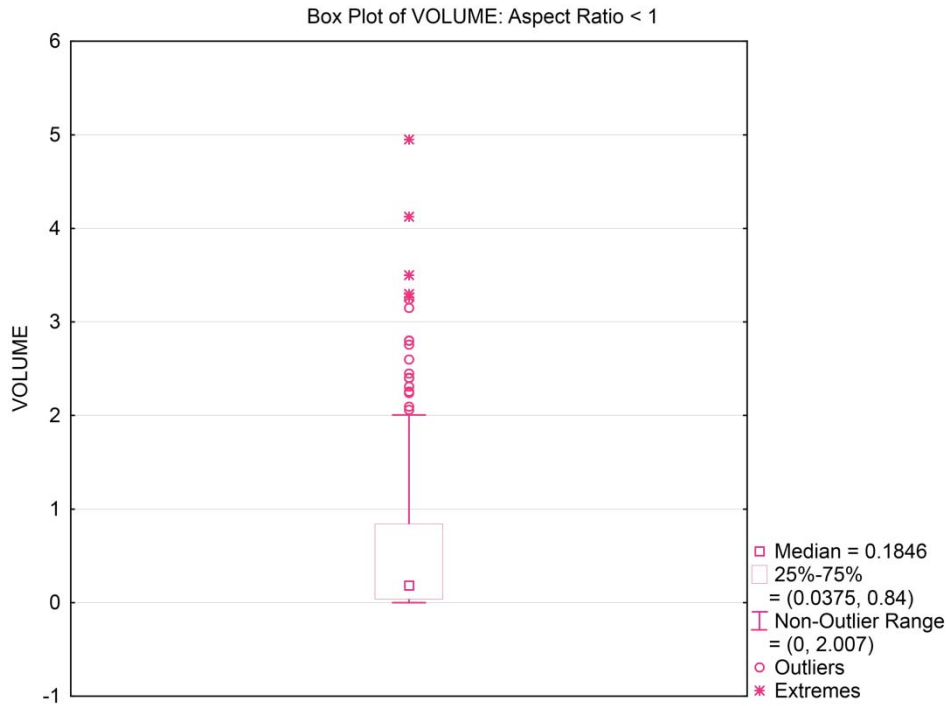


FIGURE 8.45: VOLUME BOX PLOT FOR AN ASPECT RATIO OF 1

Table 8.17 gives the numeric values of the lower and upper quartiles from the preceding box plot.

TABLE 8.17: COMPUTATION OF INDEPENDENT VARIABLES FOR LOWER AND UPPER WHISKERS OF BOX PLOTS

Independent Variable	Lower Quartile	Upper Quartile
Volume	0.0375	0.84
Granulation Tissue	0	100

Using the lower or upper limits of the box plots to determine the threshold of healed versus not healed wounds assisted us in deciding which input variables of the network were relevant. The two input variables deemed relevant showed variability between their 25th and 75th quartiles and was the calculated volume of the wound and granulation tissue.

TABLE 8.18: NEURAL-NETWORK PREDICTION VARIABLES AND PARAMETERS

Variables	Parameter/Options	
Number of input variables	2	
Input variables	Volume, granulation	
Output variable	Time remaining	
	Number of hidden layers	1
	Number of nodes in Hidden layer 1	1
	Number of epochs	7,000
	Step size for gradient descent	0.001
	Weight change momentum	0.01
	Error tolerance	0.001
	Weight decay	0

We tested and compared the theory by developing two neural-network models. The first model contained all independent variables, including volume, granulation, yellow necrotic tissue, slough, right Doppler reading, prealbumin, and albumin. The second model contained just two independent variables: volume and granulation. The difference in determining the threshold for time to heal was virtually equal. The first model produced a threshold value of 27.47. Table 8.18 shows the parameters of the first neural-network model, including the values for the hidden layers of the first neural-network model for both the inputs and the output.

TABLE 8.19: NEURAL-NETWORK PARAMETERS, ASPECT RATIO LESS THAN 1

	Input Layer		
Hidden Layer 1	Volume	Granulation	Bias node
Node # 1	-2.31343465	0.179825194	-0.497878206
	Hidden Layer 1		
Output Layer	Node 1	Bias Node	
Output Node	-1.473236968	-0.198861936	

Table 8.20 presents the results based on the training and validation scoring report. The average error using volume and granulation as the independent inputs resulted in ± 0.026 days.

TABLE 8.20: TRAINING- AND VALIDATION-DATA SCORING REPORT

Training-Data Scoring			Validation-Data Scoring		
Total sum of squared errors	RMS Error	Average Error	Total sum of squared errors	RMS Error	Average Error
139,660.7864	23.827	0.023	73096.16	26.3847	0.02645

Based on the information from the neural network and using the lower quartile of the volume variable and the upper quartile value of granulation, the predicated value of time to heal returned a predicted value of 27.96, or 28 days.

8.5.1.2 Aspect Ratio of Less Than 1: Length 1, Length 2, and Depth

Similarly, we produced a neural-network model to determine whether we could improve the accuracy of the model using the individual wound characteristics rather than a calculated input, such as volume. Table 8.21 to Table 8.24 provide the details of this revised neural-network model for the individual and calculated inputs. By using more independent input variables, we have lowered the number of hidden layers and the number of epochs are fewer than those of the previous model in Table 8.17 through Table 8.20. However, the most noticeable difference between the two models is the accuracy of the validation data. The earlier model had an average error of ± 0.26 days, whereas the model in Table 8.21 and Table, using more independent variables, returns an average error of ± 0.34 days. This discrepancy indicates that a neural-network model may be more reliable and robust when it uses raw independent variables, such as Length 1, Length 2, and depth, rather than a calculated independent variable, such as volume. The predicted healed threshold for this model was calculated at 28.858 days.

TABLE 8.21: COMPUTATION OF INDEPENDENT VARIABLES FOR LOWER AND UPPER WHISKERS OF BOX PLOTS

Independent Variable	Lower Quartile	Upper Quartile
Length 1	0.50	2.0
Length 2	0.60	2.4
Depth	0.10	0.20
Granulation tissue	0	100

TABLE 8.22: NEURAL-NETWORK PREDICTION VARIABLES AND PARAMETERS

Variables		Parameter/Options	
Number of input variables	4	Number of hidden layers	1
Input variables	Length 1, Length 2, Depth, Granulation	Number of nodes in Hidden Layer 1	3
Output variable	Time remaining	Number of epochs	100
		Step size for gradient descent	0.001
		Weight change momentum	0.1
		Error tolerance	0.007
		Weight decay	0

TABLE 8.23: NEURAL-NETWORK PARAMETERS, ASPECT RATIO OF LESS THAN 1

Input Layer						
Hidden Layer 1	Length 1	Length 2	Depth	Granulation	Bias Node	
Node 1	0.126943	-1.20982	-1.785782	0.8097	0.042952	
Node 2	-0.8225	0.7417	0.03296	0.8035	0.49139	
Node 3	1.06202	-0.9927	-0.5586	-0.2470	0.43752	
Hidden Layer 1						
Output Layer	Node 1		Node 2	Node 3	Bias Node	
Output Node	-0.699716628		0.249217775	-0.8221	-0.19055	

TABLE 8.24: TRAINING- AND VALIDATION-DATA SCORING REPORT

Training Data Scoring			Validation Data Scoring		
Total sum of squared errors	RMS Error	Average Error	Total sum of squared errors	RMS Error	Average Error
137963.8469	23.6816	0.5239	72217.08746	26.2256	0.03359

The predicted value for the threshold of time is 28.858 days.

8.5.1.3 Aspect Ratio of Greater Than 1 and Less Than 2: Volume

Similar to the method described in Section 8.5.1.1, the method in this section the same with the exception of a different set of testing data. Figure 8.46, Table 8.25, and Table 8.26 are the parameters for the neural-network model for Group 2.

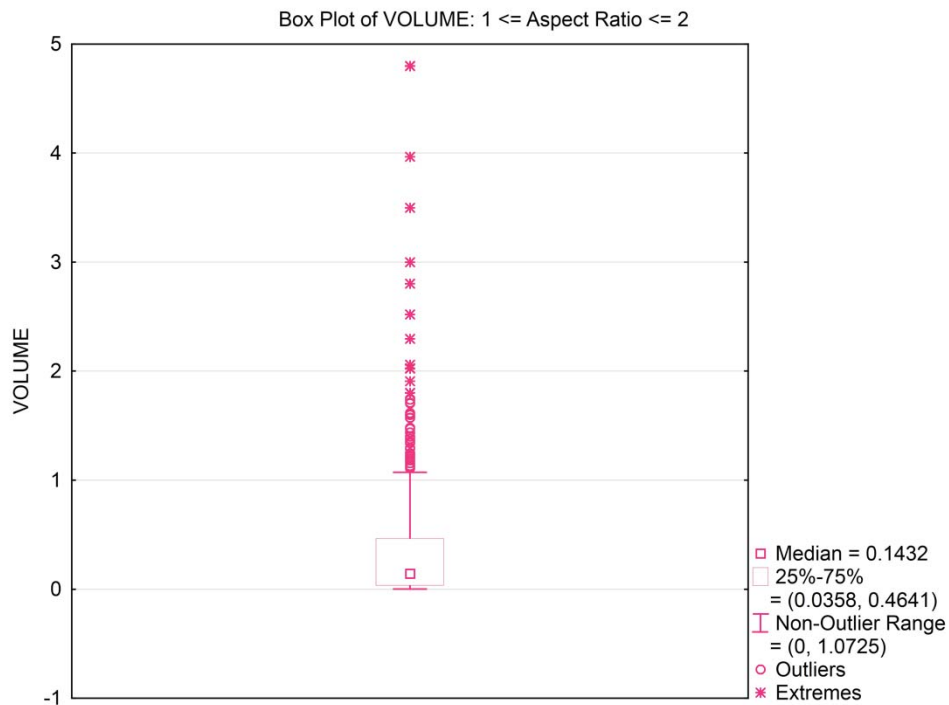


FIGURE 8.46: VOLUME BOX PLOT FOR ASPECT RATIO OF 2

TABLE 8.25: COMPUTATION OF INDEPENDENT VARIABLES FOR LOWER AND UPPER WHISKERS OF BOX PLOTS

Independent Variable	Lower Quartile	Upper Quartile
Volume	0.035833	0.4641
Granulation tissue	0	100
Yellow necrotic	0	10

TABLE 8.26: NEURAL-NETWORK PREDICTION VARIABLES AND PARAMETERS, FOR AN ASPECT RATIO GREATER THAN 1 AND LESS THAN 2

Variables		Parameter/Options	
Number of input variables	2	Number of hidden layers	2
Input variables	Volume, granulation, Yellow necrotic	Number of nodes in Hidden Layer 1	1
		# Nodes in HiddenLayer-1	1
Output variable	Time remaining	Number of epochs	6500
		Step size for gradient descent	0.001
		Weight-change momentum	0.02
		Error tolerance	0.001
		Weight decay	0

Table 8.27 is the neural network parameters for Group 2. Similarly, Table 8.27 states the numerical values of input and output hidden layer nodes.

TABLE 8.27: TRAINING- AND VALIDATION-DATA SCORING REPORT

Training-Data Scoring		Validation-Data Scoring		
Total sum of squared errors	RMS Error	Total sum of squared errors	RMS Error	Average Error
166836.5852	23.66 0.025	76008.91744	24.368	0.0126

TABLE 8.28: NEURAL-NETWORK PARAMETERS, ASPECT RATIO OF GREATER THAN 1 AND LESS THAN 2

	Input Layer			
Hidden Layer 1	Volume	Granulation	Yellow Necrotic	Bias Node
Node 1	-4.784279092	-0.41192969	-1.027211039	0.677571236
	Hidden Layer 1			
Output Layer	Node 1	Bias Node		
Node 1	-29.84249145	12.57158369		
	Hidden Layer 2			
Output Layer	Node 1	Bias Node		
Output Node	-0.690697574	-0.54806653		

The predicted value for the threshold of time is 33.118 days.

8.5.1.4 Aspect Ratio Greater Than 1 and Less Than 2: Length 1, Length 2, Depth

Unlike the neural network model presented in Section 8.5.1.3, figure, Figure 8.48, and Figure 8.49 and tables 8.Table 8.29, Table 8.30, and 8.31 describe the neural-network model using length 1, length 2, depth, and granulation, rather than volume, as the inputs.

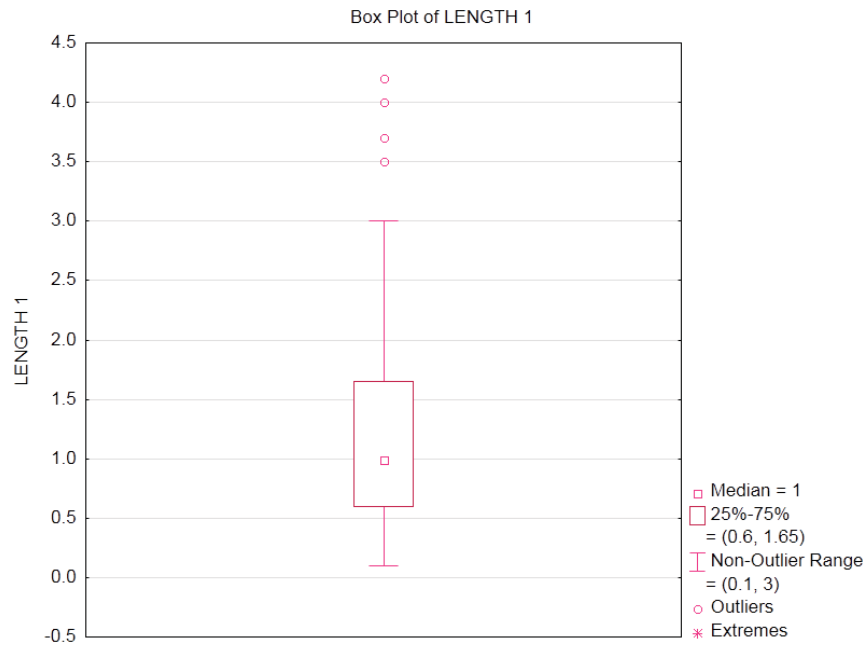


FIGURE 8.47: LENGTH 1 BOX PLOT FOR ASPECT RATIO GREATER THAN 1 AND LESS THAN 2

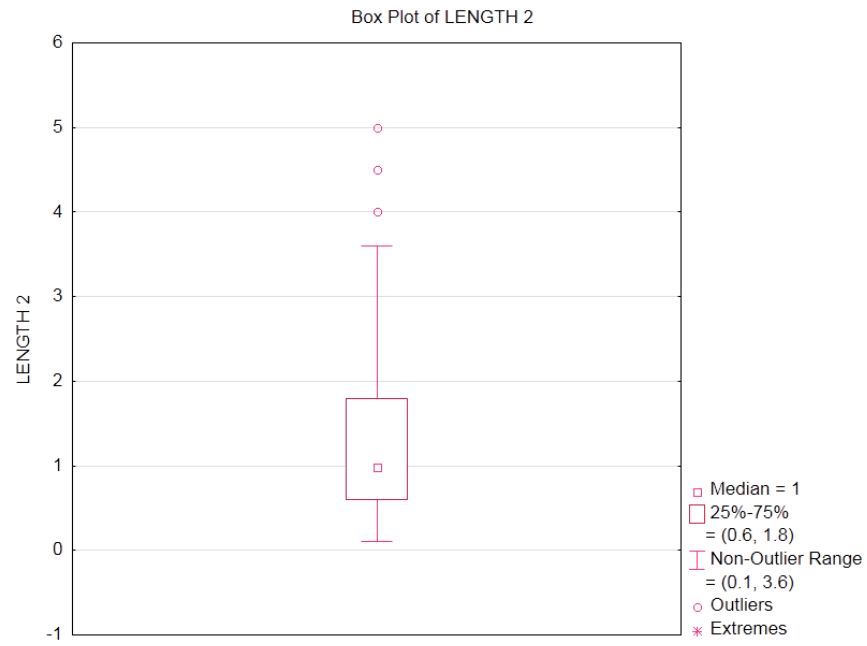


FIGURE 8.48: LENGTH 2 BOX PLOT FOR ASPECT RATIO GREATER THAN 1 AND LESS THAN 2

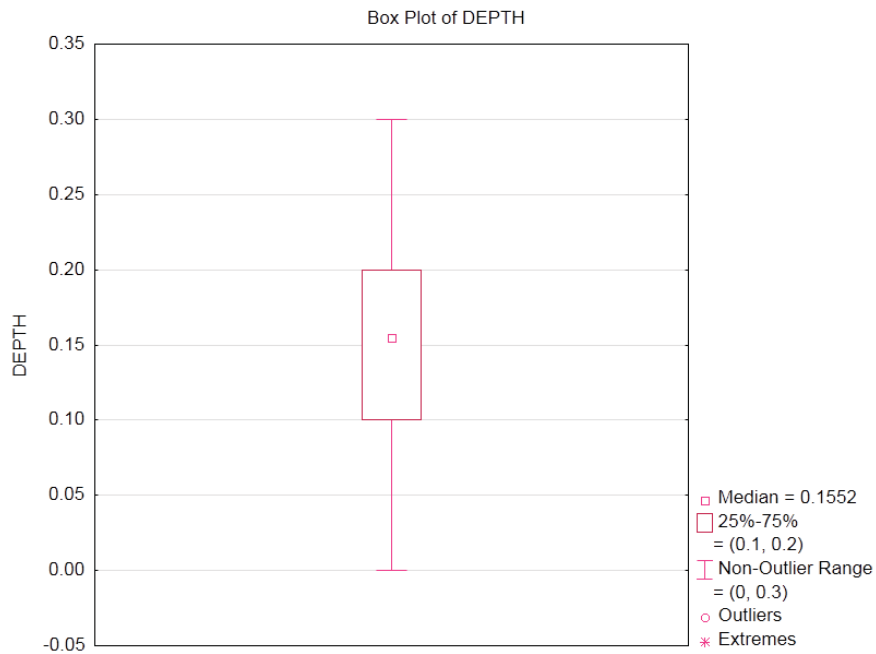


FIGURE 8.49: DEPTH BOX PLOT FOR ASPECT RATIO OF GREATER THAN 1 AND LESS THAN 2

TABLE 8.29: COMPUTATION OF INDEPENDENT VARIABLES FOR LOWER AND UPPER WHISKERS OF BOX PLOTS

Independent Variable	Lower Quartile	Upper Quartile
Length 1	0.60	1.65
Length 2	0.60	1.80
Depth	0.10	0.20
Granulation tissue	0	100

TABLE 8.30: NEURAL-NETWORK PREDICTION VARIABLES AND PARAMETERS

Variables	Parameter/Options	
Number of input variables	4	
Input Variables	Length 1, Length 2, Depth, Granulation	
Output Variable	Time Remaining	
	Number of hidden layers	1
	# Nodes in HiddenLayer-1	10
	# Epochs	800
	Step size for gradient descent	0.10
	Weight change momentum	0.60
	Error tolerance	0.01

The “healed threshold” when the $1 \leq \text{aspect ratio} \leq 2$ with four independent variables is 32.32 days.

TABLE 8.31: TRAINING AND VALIDATION DATA SCORING REPORT

Training Data Scoring			Validation Data Scoring		
Total sum of squared errors	RMS Error	Average Error	Total sum of squared errors	RMS Error	Average Error
158528.8208	23.06460	0.20083	76484.559	24.4445	0.01695

8.5.1.5 Aspect Ratio > 2: Volume

Similarly, Figure 8.50, Table 8.32, Table 8.33, Table 8.34, and Table 8.35 are the neural network model parameters and output that describe the model specific to Group 3 using volume, granulation tissue, and yellow necrotic tissue as inputs.

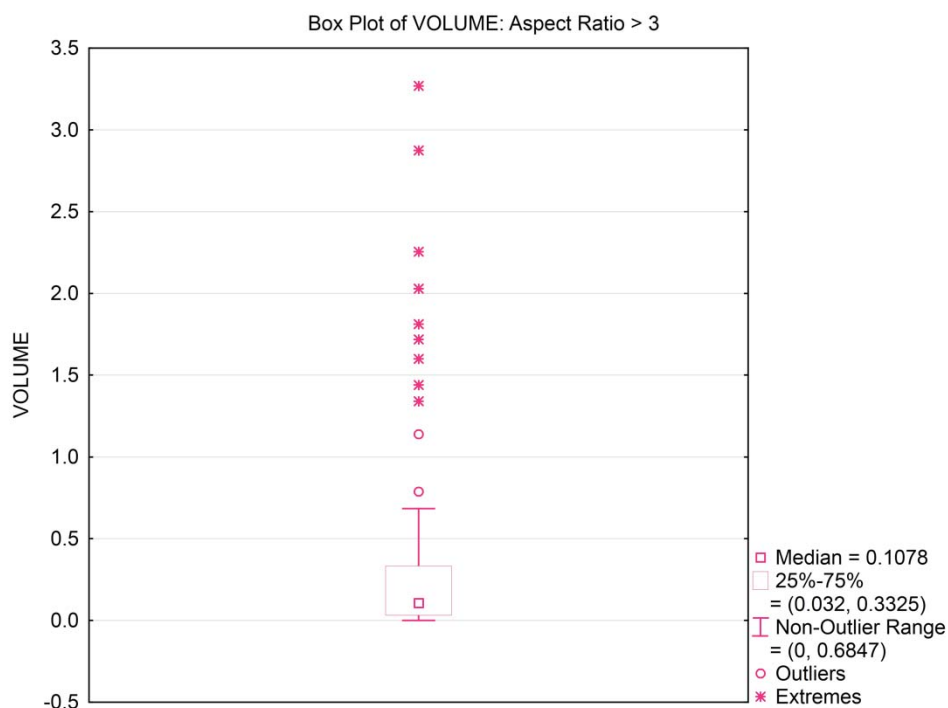


FIGURE 8.50: VOLUME BOX PLOT FOR ASPECT RATIO=3

TABLE 8.32: COMPUTATION OF INDEPENDENT VARIABLES FOR LOWER AND UPPER WHISKERS OF BOX PLOTS

Independent Variable	Lower Quartile	Upper Quartile
Volume	0.0320	0.3325
Granulation Tissue	0	100
Yellow Necrotic	0	10

TABLE 8.33: NEURAL NETWORK PREDICTION VARIABLES AND PARAMETERS, $1 < \text{ASPECT RATIO} < 2$

Variables	Parameter/Options		
# Input Variables	2	# Hidden layers	2
Input Variables	Volume, Granulation, Yellow Necrotic	# Nodes in HiddenLayer-1	1
		# Nodes in HiddenLayer-1	1
Output Variable	Time Remaining	# Epochs	365
		Step size for gradient descent	0.001
		Weight change momentum	0
		Error tolerance	0.001
		Weight decay	0

TABLE 8.34: NEURAL NETWORK PARAMETERS, $1 \leq \text{ASPECT RATIO} \leq 2$

Input Layer				
Hidden Layer # 1	Volume	Granulation	Yellow Necrotic	Bias Node
Node # 1	-0.990118719	-0.720849937	-0.121392742	-0.348850913

Hidden Layer # 1		
Output Layer	Node # 1	Bias Node
Node #1	1.710329786	3.805476422

Hidden Layer # 2		
Output Layer	Node # 1	Bias Node
Output Node	-0.658233027	0.041009775

Table 8.35 is the neural network training and validation data outputs for aspect ratio Group 3. The predicted value for the threshold of Time is 29.97 days.

TABLE 8.35: TRAINING AND VALIDATION DATA SCORING REPORT

Training Data Scoring			Validation Data Scoring		
Total sum of squared errors	RMS Error	Average Error	Total sum of squared errors	RMS Error	Average Error
38404.54498	25.73222352	-0.50	12382.60388	22.255	0.013

8.5.1.6 Aspect Ratio >_2: Length 1, Length 2, Depth

Similar to the previous box plots, Figure 8.51, Figure 8.52, and Figure 8.53 correlate to numerical data in Table 8.36 regarding the ideal set of wound parameter values. Additionally, Table 8.37 and Table 8.38 are the parameters for the neural network and the respective hidden layer node values.

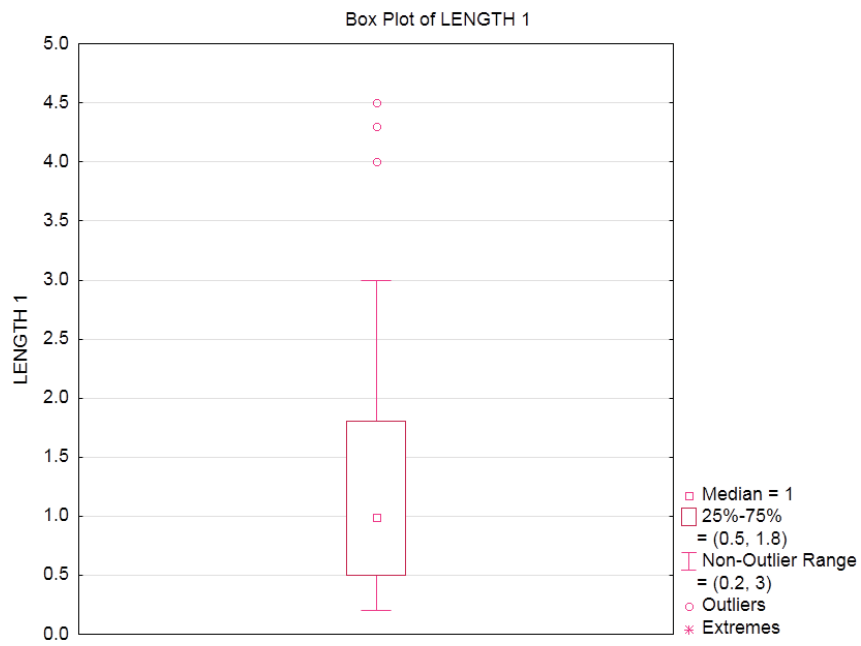


FIGURE 8.51: LENGTH 1 BOX PLOT FOR ASPECT RATIO > 2

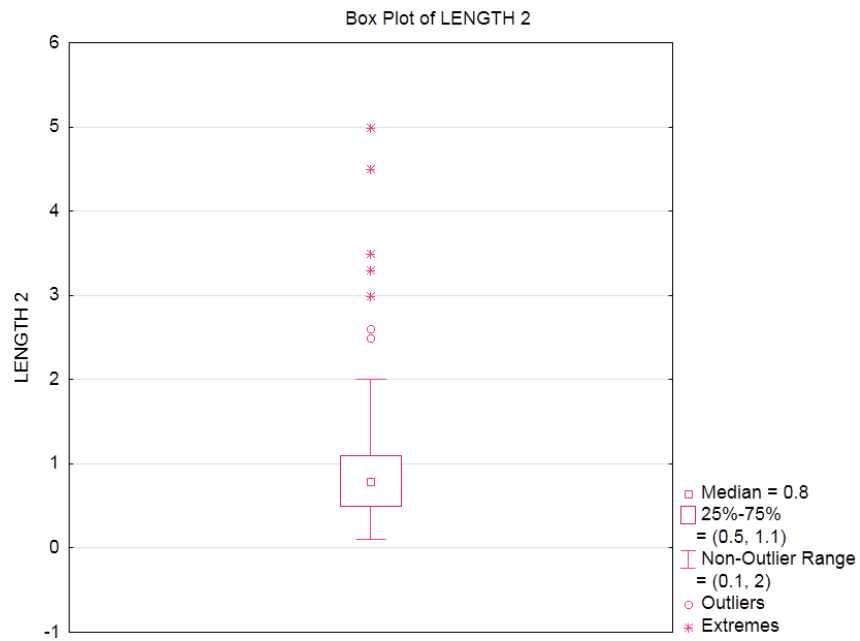


FIGURE 8.52: LENGTH 2 BOX PLOT FOR ASPECT RATIO > 2

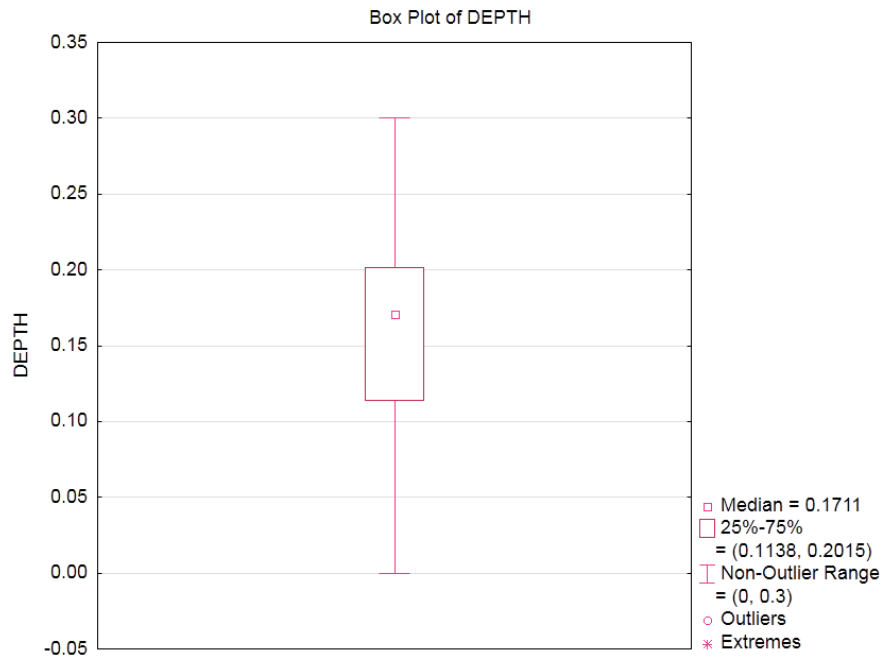


FIGURE 8.53: DEPTH BOX PLOT FOR ASPECT RATIO OF GREATER THAN 2

TABLE 8.36: COMPUTATION OF INDEPENDENT VARIABLES FOR LOWER AND UPPER WHISKERS OF BOX PLOTS

Independent Variable	Lower Quartile	Upper Quartile
Length 1	0.50	1.8
Length 2	0.50	1.1
Depth	0.1138	0.2015
Granulation tissue	0	100

TABLE 8.37: NEURAL NETWORK PREDICTION VARIABLES AND PARAMETERS

Variables		Parameters/Options	
Number of input variables	4	Number of hidden layers	1
Input variables	Length 1, Length 2, depth, granulation	Number of nodes in Hidden Layer 1	11
Output variable	Time remaining	Number of epochs	8000
		Step size for gradient descent	0.36
		Weight change momentum	1
		Error tolerance	0.001
		Weight decay	0

The healed threshold, when the aspect ratio is greater than 2, with four independent variables is 12.27 days.

TABLE 8.38: TRAINING- AND VALIDATION-DATA SCORING REPORT

Training Data Scoring			Validation Data Scoring		
Total sum of squared errors	RMS error	Average error	Total sum of squared errors	RMS error	Average error
5195.663598	9.464692	2.026675	29648.30695	34.43737	0.00669

8.6 SUMMARY

Table 8.39 presents a summary of the predicted threshold to calculate an estimated time to heal using volume.

TABLE 8.39: SUMMARY OF PREDICTED THRESHOLD VALUES (DAYS) TO CALCULATE TIME TO HEAL

Aspect Ratio of Less Than 1	Aspect Ratio of 1 to 2	Aspect Ratio of Less Than 2
27.96	33.12	29.97

Table 8.40 presents a summary of the predicted threshold to calculate an estimated time to heal using Length 1, Length 2, and depth.

TABLE 8.40: SUMMARY OF PREDICTED THRESHOLD VALUES (DAYS) TO CALCULATE TIME TO HEAL

Aspect Ratio of Less Than 1	Aspect Ratio of 1 to 2	Aspect Ratio of Less Than 2
28.858	32.32	12.27

Although the corresponding values of Table 8.39 and Table 8.40 are similar, the major difference is in the context of the algorithm. We have concluded that the behavior of the algorithms using volume as an input — that is, the calculated input — does not accurately reflect the change in time to heal. We attribute this inaccuracy to the large numerical value difference between the depth variable and the length 1 and length 2 variables. In other words, the depth variable is smaller than the length variables.

CHAPTER NINE WOUND-HEALING PREDICTIVE MODEL

CHAPTER 9

Wound-Healing Predictive Model

We now extend and apply the chosen modeling techniques of Chapter 7 to the healing statistical prediction model.

We have multiple predictive models for the data to compare and contrast the results and accuracy. We focused on nonlinear regression and neural networks. We pursued other regression models, such as multiple linear-regression predictive models, but the behavior of the data was too complex for linear regression. However, linear regression is a common predictive-modeling technique. As a comparison to nonlinear methods, we included the results.

9.1 MULTIPLE LINEAR REGRESSION

We developed one model using multiple linear regression. This model used the same predictive variables as the neural-network models. We developed the linear-regression model simply to compare the reliability of the linear-regression algorithm and how the number of predictor variables impacts the final linear algorithm.

The first regression model, including predictor variables Length 1, Length 2, depth, and granulation, is given by:

$$y(t) = 6.60 * L1 - 4.53 * L2 - 3.69 * D - 0.006 * G + 26.04 \quad (9.1)$$

Due to the complexity of the data, the behavior of the data is nonlinear. According to the model feedback, the linear-regression model does not fit the data well based on the statistics of model (Table 9.1).

TABLE 9.1: STATISTICS OF MULTIPLE LINEAR-REGRESSION MODEL (FOUR DEGREES OF FREEDOM)

	Value
Residual dF	597
R-squared	0.036
Standard deviation estimate	23.88
Residual SS	340305.3438

Using the R^2 statistic, we see that the data is not a good fit for a linear regression model. The average error for this model is approximately four days for the validation data. To determine the fit of the data, we evaluated the adjusted R^2 value and Mallows's C_p . In this model, $C_p = 0.036$, and $R^2_{adjusted} = 0.029$ reflecting a poor fit to the data.

TABLE 9.2: TRAINING- AND VALIDATION-DATA SCORING REPORT, MULTIPLE LINEAR REGRESSION (FOUR DEGREES OF FREEDOM)

Training Data Scoring			Validation Data Scoring		
Total sum of squared errors	RMS Error	Average Error	Total sum of squared errors	RMS Error	Average Error
340305.35	23.78	0.00	163820.42	25.20	3.78

9.2 NONLINEAR REGRESSION: SURVIVAL ANALYSIS

We employed the Cox regression method, which is commonly used to represent the amount of time to an event and, in this case, represents the time to heal. The Cox regression can accommodate both discrete and continuous measures of event times [122]. Cox regression models affect the covariates of the hazard rate but leave the baseline hazard rate, allowing us to evaluate the model when all the predictors are zero [123].

Using IBM's SPSS predictive analytics software, we modeled the data using Cox regression to determine a better predictive model than linear regression or regression trees. We developed two Cox regression models. The first model included all of the available covariates. The second model included the most common wound measurements across wound clinics.

Equation (9.2) is the Cox predictive model incorporating all the predictor variables. However, not every hospital and clinic collects this information. For a variety of reasons, there appears to be a

discrepancy in how to judge certain wound characteristics, such as the percentage of black or yellow necrotic tissue.

$$h(t) = [h_0(t)] * e^{(-0.433L1-0.359L2-7.009D+0.327U+0.002G-0.003YNT-0.003BNT+0.001S)} \quad (9.2)$$

Figure 9.1 through Figure 9.5 display the survival plots that result from survival analysis. Figure 9.1 shows the data when all of the predictors are at their mean values and the aspect ratios are the reference categories. The purpose of using the means of the predictor variables is to see on average how many wounds heal at a given time. When all predictor variables are average, a small percentage of people are healed within 30 days of obtaining treatment at a wound clinic (Figure 9.1). For chronic, nonhealing wounds, this reflection supports the theory that chronic wound healing takes a longer time to heal.

Figure 9.5 displays the same general characteristics of the data except it separates the data thereby aspect ratios. Figure 9.5 shows that the behavior of data with aspect ratios of 1 and 2 clearly differ from each other ($p=0.000$), whereas the data in aspect ratios 2 and 3 are more similar in behavior ($p=0.237$). Table 9.3 shows the covariate means.

TABLE 9.3: COVARIATE MEANS

	Mean
Length 1	1.370
Length 2	1.602
Depth	0.162
Undermining	0.003
Granulation	51.064
Yellow Necrotic Tissue	12.266
Black Necrotic Tissue	22.898
Slough	7.833

The focus of the nonlinear regression predictive model is to show the difference between linear, nonlinear, and neural-network modeling. Cox regression, simply a function of the baseline cumulative hazard, provides the ability to show the effect of time in a nonlinear format. Unlike neural networks, Cox regression outputs a respective nonlinear mathematical equation. Furthermore, we can evaluate the algorithm with only the baseline cumulative hazard and no predictors in the model. So, when all the predictor variables are zero, the Cox regression function

is equal to the baseline cumulative hazard. Unlike linear regression, in which the intercept is a fixed number, the intercept of the Cox regression is the baseline hazard function. Figure 9.6 shows the baseline cumulative hazard function as a curve that displays healing purely from the perspective of passing time. If the predictor variables have any effect on the model, including them in addition to the hazard function will shift the curve. If the predictor variables have little impact, the final Cox regression model will appear similar to the baseline hazard function. These graphs represent the percentage of wounds that are healed at a given time after the wound's initial treatment.

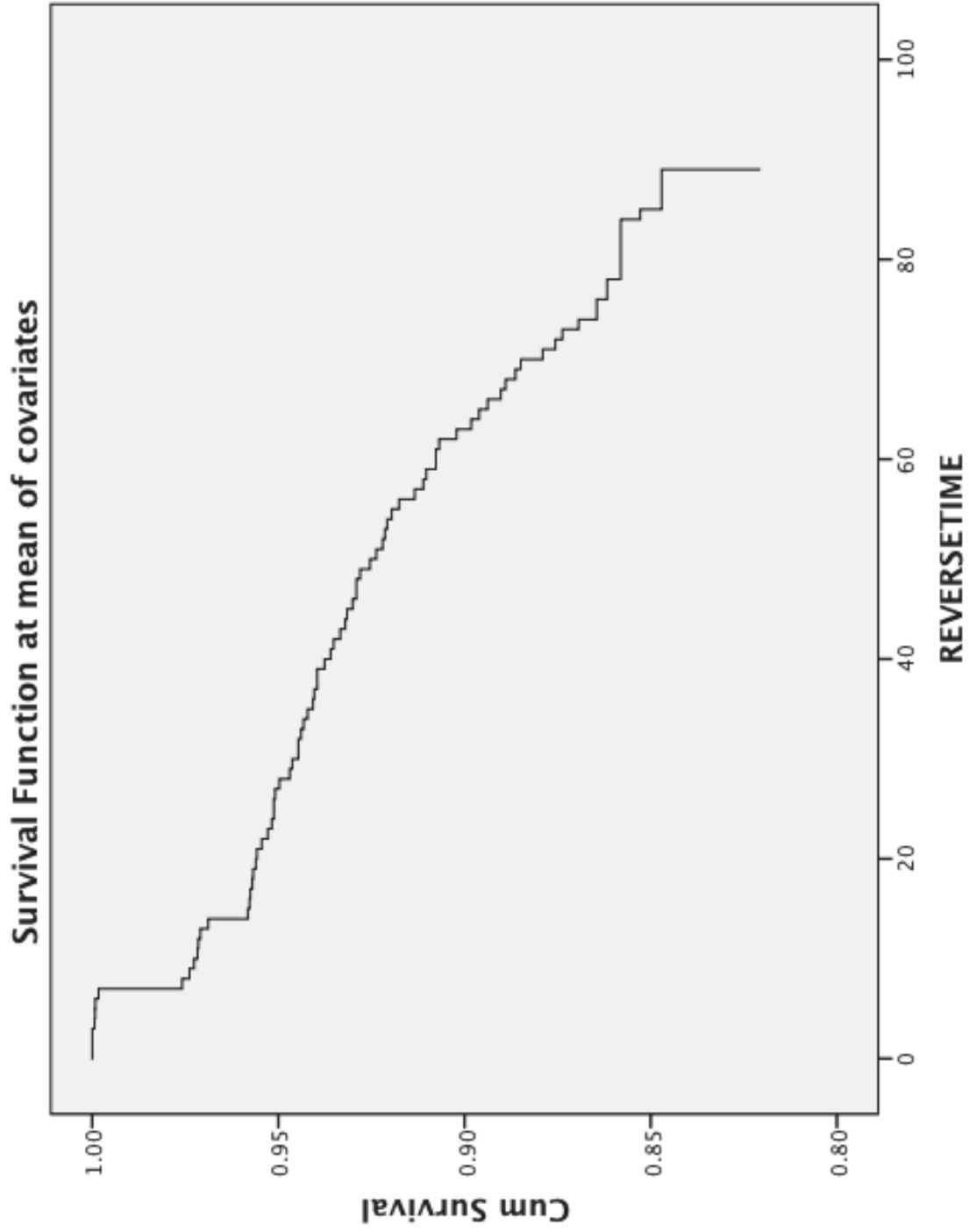


FIGURE 9.1: SURVIVAL FUNCTION AT MEAN OF COVARIATES

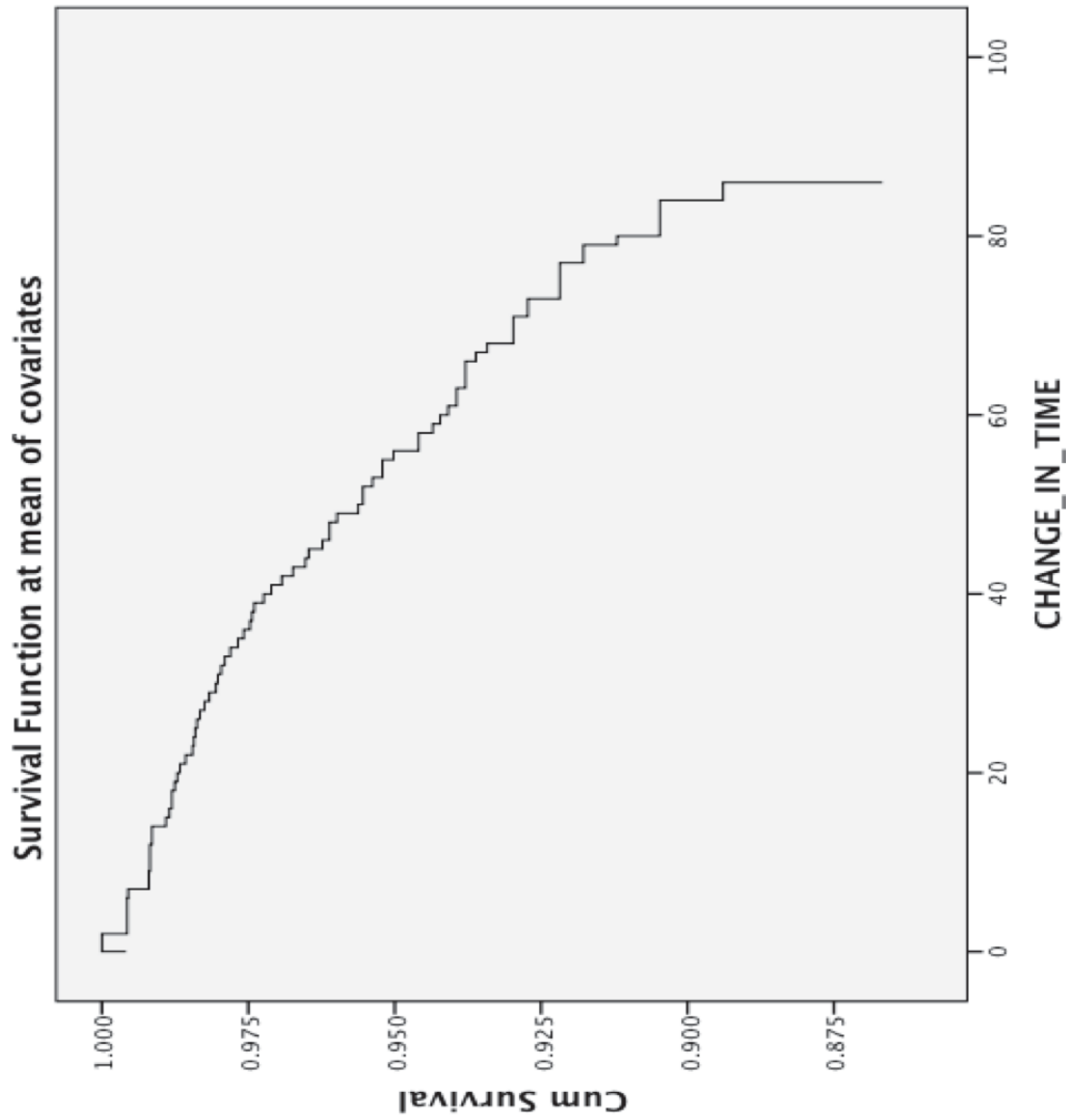


FIGURE 9.2: ONE MINUS SURVIVAL FUNCTION AT MEAN OF COVARIATES

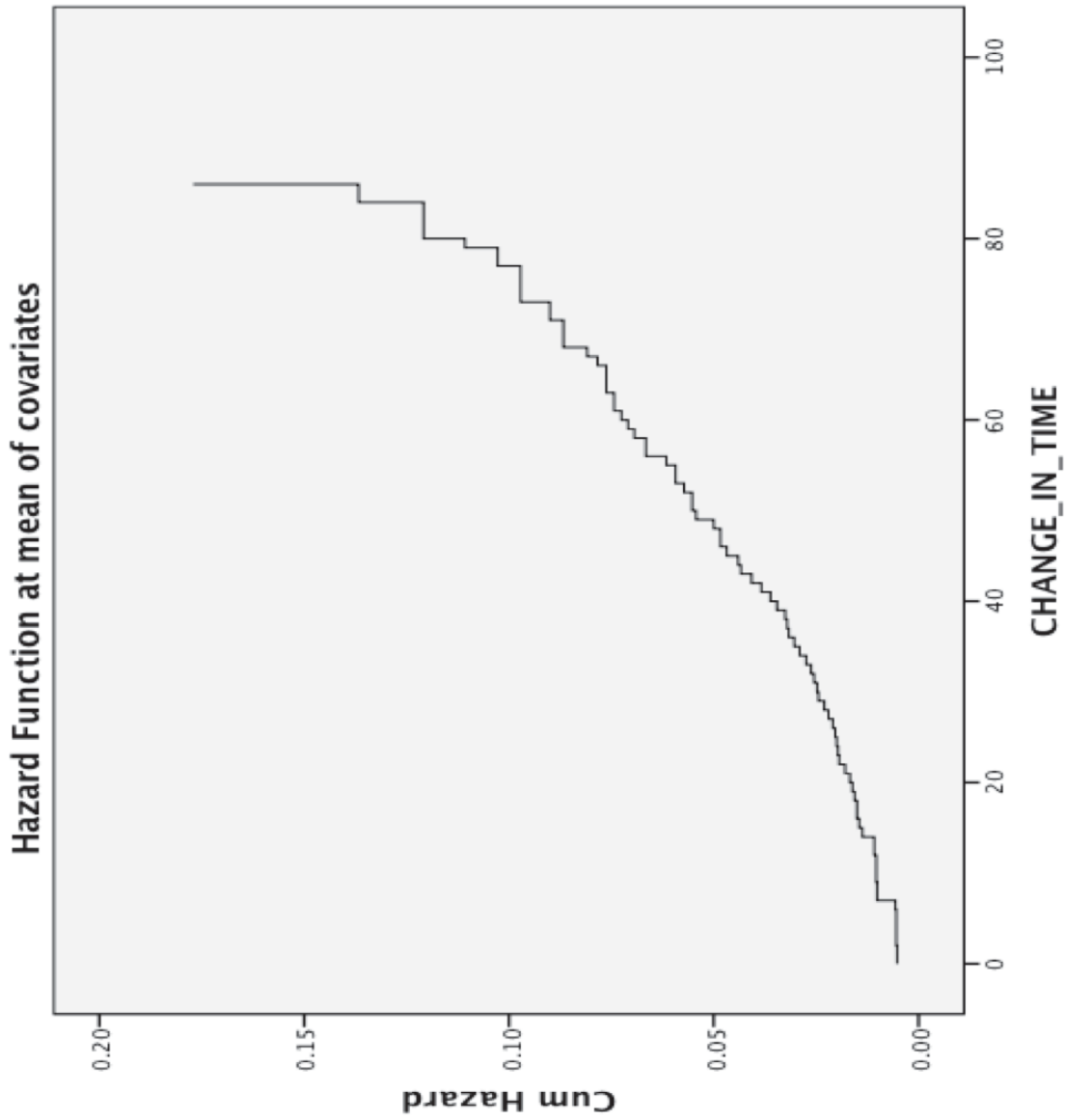


FIGURE 9.3: HAZARD FUNCTION AT MEAN OF COVARIATES

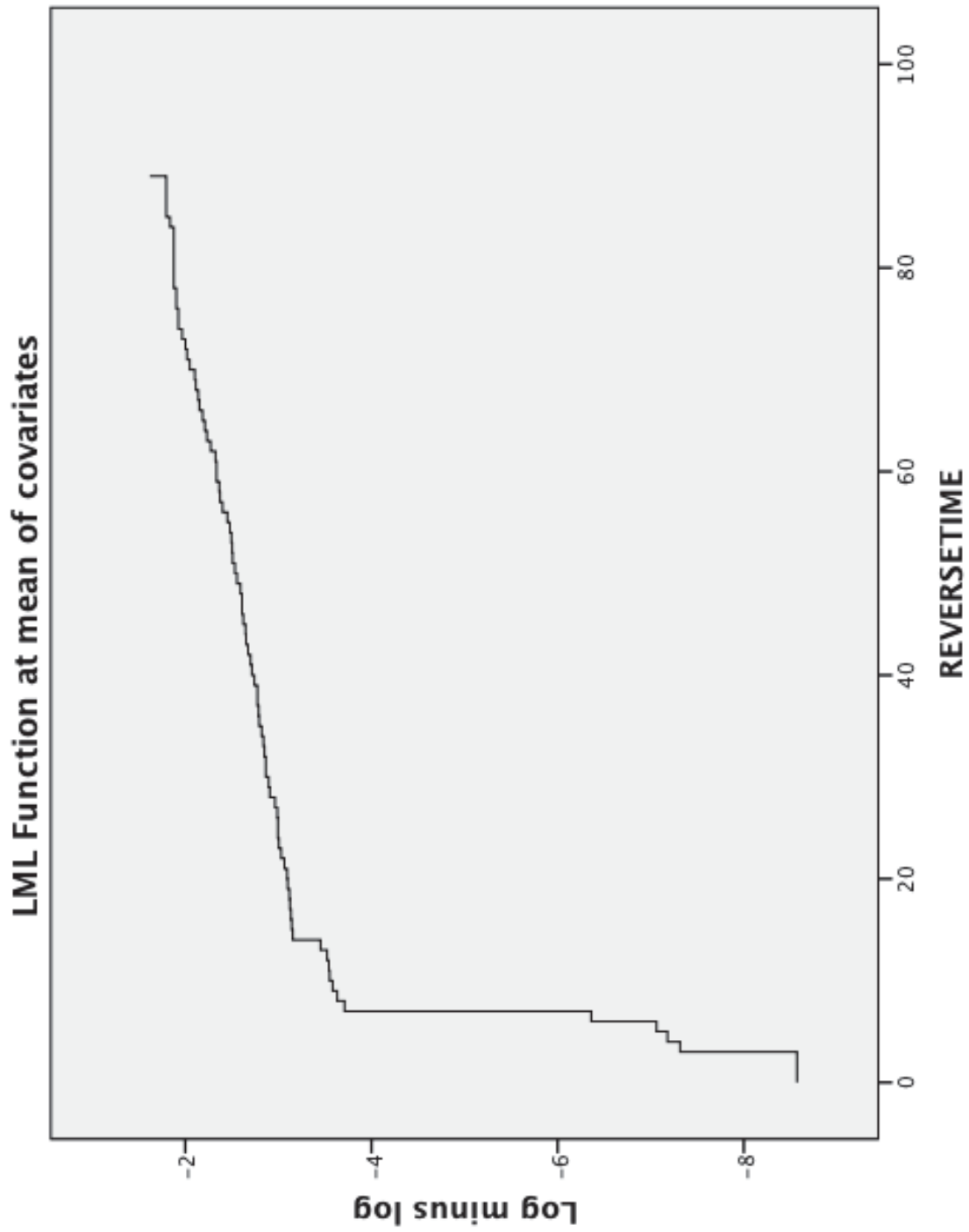


FIGURE 9.4: SURVIVAL FUNCTION AT MEAN OF COVARIATES

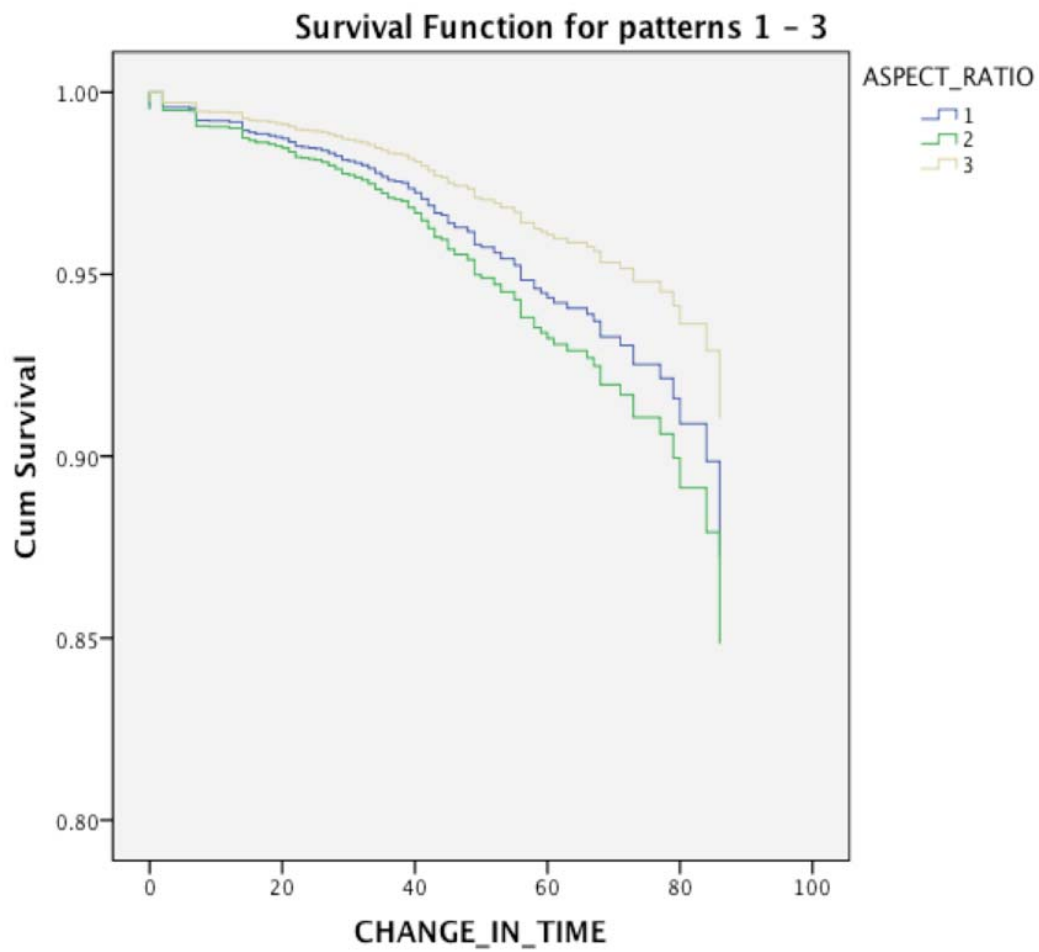


FIGURE 9.5: SURVIVAL FUNCTION DIFFERENTIATED BY ASPECT RATIOS

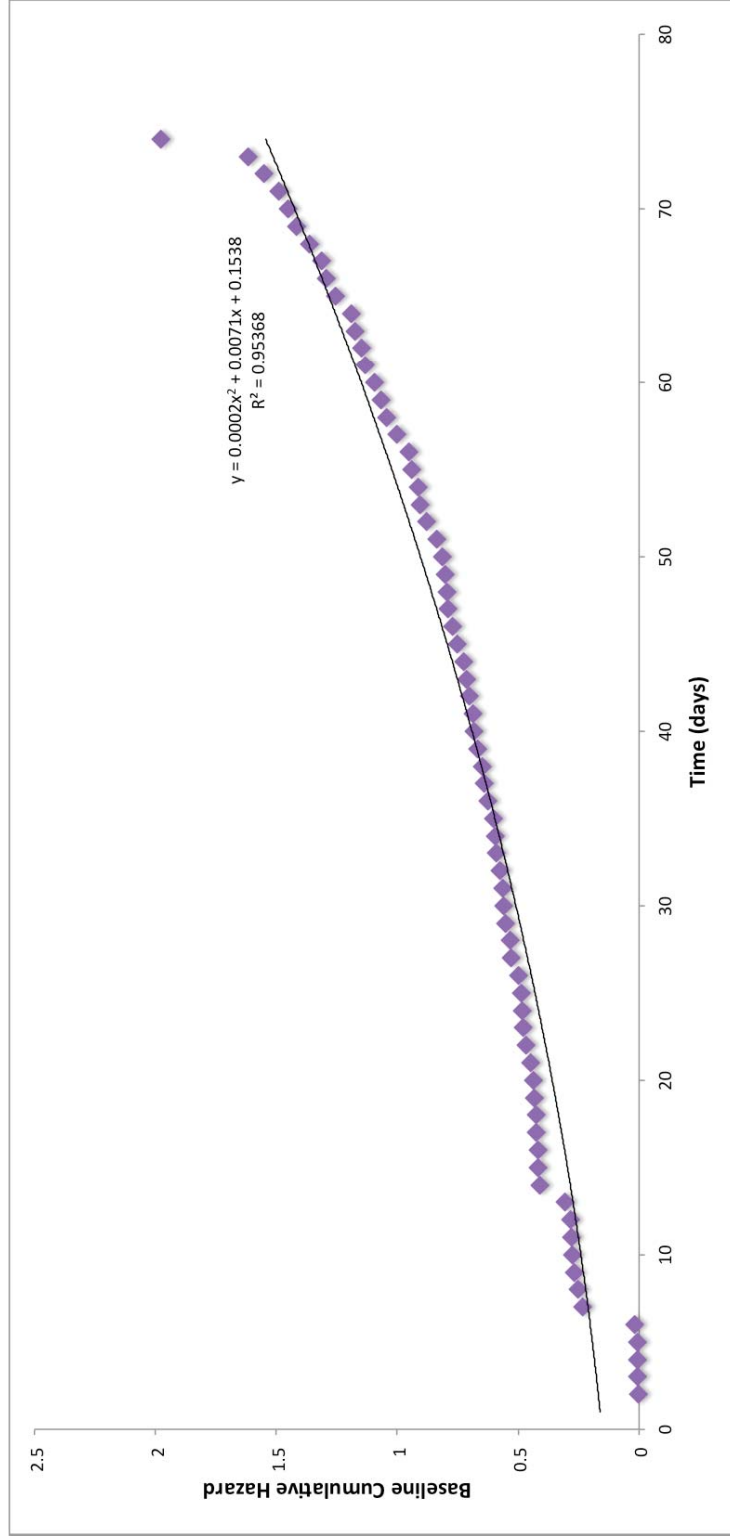


FIGURE 9.6: BASELINE CUMULATIVE HAZARD

To properly calculate the Cox regression, we need to include the value of the baseline cumulative hazard, $h_0(t)$, at time t . Table 9.5 is the survival table, which shows the value of $h_0(t)$ at every recognized time value. The survival column in Table 9.5 represents the percentage of wounds with average values of the predictor variables that have survived by time t that corresponds to the plot in Figure 9.1. This is the percentage of people of 100% who have survived up to the end of time interval t . This analysis indicates that chronic wounds take weeks and months to heal rather than days and reaffirms the findings in literature. The current study validates the challenge of predicting the time until chronic, nonhealing wound closure.

To determine the validity of the Cox regression model, we analyzed a number of factors that are associated with the quality of Cox regression output. Among these factors, the chi-square statistic and its significant level represent the probability of obtaining the chi-square statistic (366.016) given that the null hypothesis is true (Table 9.4). In the current case, the model is statistically significant because the p-value is less than 0.000.

TABLE 9.4: OMNIBUS TESTS OF MODEL COEFFICIENTS

-2 Log Likelihood	Overall (score)			Change From Previous Step			Change From Previous Block		
	Chi-square	df	Sig.	Chi-square	df	Sig.	Chi-square	df	Sig.
7368.974	366.016	8	.000	404.385	8	.000	404.385	8	.000

Each predictor variable in the equation has corresponding statistics to determine their relevance and impact on the final regression equation. Cox regression predictor variables have six pertinent statistics that help describe their relevance to the equation (Table 9.6). B predicts the dependent variable and the independent variable, and Exp(B) predicts the odds ratio for the predictors. Table 9.7 provides more details on these statistics. SE is the standard error associated with the algorithm coefficients. We use the standard error to test whether the parameters significantly differ from zero. Similarly, the Wald and significance values provide the Wald chi-square value and two-tailed p-value. The Wald statistic tests the null hypothesis. The significant value is the p-value that determines whether those variables are statistically significant. The p-value should be less than alpha — that is, 0.05. Through the analysis, we find that the undermining, granulation, yellow and black necrotic tissue, and slough values all have a p-value greater than 0.05. Thus, these coefficients are not statistically relevant to the regression algorithm.

TABLE 9.5: SURVIVAL TABLE

Time	Baseline Cumulative Hazard	At Mean of Covariates		
		Survival	SE	Cum
0	0.002	1.000	0.000	0.000
3	0.006	0.999	0.000	0.001
4	0.007	0.999	0.000	0.001
5	0.008	0.999	0.000	0.001
6	0.017	0.998	0.000	0.002
7	0.235	0.976	0.002	0.024
8	0.254	0.974	0.002	0.026
9	0.267	0.973	0.002	0.027
10	0.276	0.972	0.002	0.028
11	0.278	0.972	0.002	0.028
12	0.284	0.972	0.002	0.029
13	0.305	0.969	0.002	0.031
14	0.412	0.959	0.003	0.042
15	0.417	0.958	0.003	0.042
16	0.419	0.958	0.003	0.043
17	0.424	0.958	0.003	0.043
18	0.427	0.957	0.003	0.043
19	0.434	0.957	0.003	0.044
20	0.437	0.956	0.003	0.044
21	0.450	0.955	0.003	0.046
22	0.467	0.954	0.003	0.048
23	0.478	0.953	0.003	0.049
24	0.484	0.952	0.004	0.049
26	0.487	0.952	0.004	0.050
27	0.499	0.950	0.004	0.051
28	0.528	0.948	0.004	0.054
29	0.534	0.947	0.004	0.054
30	0.551	0.945	0.004	0.056
32	0.559	0.945	0.004	0.057
33	0.566	0.944	0.004	0.058
34	0.577	0.943	0.004	0.059
35	0.592	0.942	0.004	0.060
36	0.596	0.941	0.004	0.061
37	0.604	0.940	0.004	0.061
39	0.624	0.938	0.004	0.064
40	0.641	0.937	0.005	0.065
41	0.650	0.936	0.005	0.066
42	0.668	0.934	0.005	0.068
43	0.683	0.933	0.005	0.069
44	0.688	0.932	0.005	0.070
45	0.703	0.931	0.005	0.072
46	0.714	0.930	0.005	0.073

48	0.725	0.929	0.005	0.074
49	0.753	0.926	0.005	0.077
50	0.771	0.925	0.006	0.078
51	0.789	0.923	0.006	0.080
52	0.795	0.922	0.006	0.081
53	0.802	0.922	0.006	0.082
54	0.815	0.920	0.006	0.083
55	0.836	0.918	0.006	0.085
56	0.881	0.914	0.006	0.090
57	0.905	0.912	0.007	0.092
58	0.914	0.911	0.007	0.093
59	0.942	0.909	0.007	0.096
61	0.951	0.908	0.007	0.097
62	1.002	0.903	0.007	0.102
63	1.045	0.899	0.008	0.106
64	1.068	0.897	0.008	0.109
65	1.093	0.895	0.008	0.111
66	1.132	0.891	0.009	0.115
67	1.146	0.890	0.009	0.117
68	1.175	0.887	0.009	0.120
69	1.191	0.886	0.009	0.121
70	1.257	0.880	0.010	0.128
71	1.294	0.877	0.010	0.132
72	1.315	0.875	0.010	0.134
73	1.364	0.870	0.011	0.139
74	1.418	0.866	0.011	0.144
76	1.450	0.863	0.012	0.148
78	1.491	0.859	0.012	0.152
84	1.552	0.854	0.014	0.158
85	1.618	0.848	0.015	0.165
89	1.976	0.818	0.033	0.201

Table 9.7 shows the ratio of hazard rates for this predictive algorithm that includes all the variables versus the statistically significant variables. The ratio of hazard rates shows the respective constants associated with the regression algorithm, as well as the percentage change of each variable based on one unit of change. If $Exp_i(B) > 1$, the healing time decreases. If $Exp_i(B) < 1$, healing time increases for that predictor variable, and the healing time increases by that calculated percentage. Or, $Exp_i(B)$ is the ratio of hazard rates that are one unit apart on the predictor variable.

TABLE 9.6: VARIABLES IN THE EQUATION AND CORRESPONDING STATISTICS

	B	SE	Wald	df	Sig.	Exp(B)
Length_1	-0.433	0.111	15.304	1.000	0.000	0.648
Length_2	-0.359	0.090	15.757	1.000	0.000	0.698
Depth	-7.009	0.747	88.083	1.000	0.000	0.001
Undermining	0.327	0.460	0.507	1.000	0.476	1.387
Granulation	0.002	0.002	1.142	1.000	0.285	1.002
Yellow Necrotic Tissue	-0.003	0.003	1.184	1.000	0.276	0.997
Black Necrotic Tissue	-0.003	0.002	1.483	1.000	0.223	0.997
Slough	0.001	0.003	0.191	1.000	0.662	1.001

TABLE 9.7: RATIO OF HAZARD RATES

	Variable Constants		
	B	Exp(B)	Change (%)
Length 1	-0.433	0.648	35.17
Length 2	-0.359	0.698	30.17
Depth	-7.009	0.001	99.91
Granulation	0.327	1.387	-38.72
Undermining	0.002	1.002	-0.22
Yellow necrotic tissue	-0.003	0.997	0.30
Black necrotic tissue	-0.003	0.997	0.27
Slough	0.001	1.001	-0.13

The second model includes only those predictor variables — Length 1, Length 2, and depth — that are the most commonly recorded in wound clinics.

We have thus established a predictive model that uses only the most common wound characteristics given by:

$$h(t) = [h_0(t)] * e^{-0.0439L1-0.336L2-7.418D} \quad (9.3)$$

Unlike the previous model, which incorporated the calculated and assumed aspect ratios, this nonlinear model uses only the most commonly recorded wound characteristics as input variables in the equation. To establish the validity of using the Cox regression on the data, we analyzed the ratio of hazard rates that are one unit apart on the predictor [123]. Table 9.8 shows the ratio of hazard rates for the predictor variables and how they affect the healing time. Table 9.8 provides the information to determine the percent age of change if that predictor variable is equal to a specific value.

TABLE 9.8: RATIO OF HAZARD RATES

	Variable Constants		
	B	Exp(B)	Changed (%)
Length 1	-0.439	.644	35.55
Length 2	-0.336	.715	28.53
Depth	-7.418	.001	99.94

For every unit increase of a predictive variable, the percentage change equates to the effect that predictor variable has on the remaining healing time. If $Exp_i(B) > 1$, the healing time decreases. If $Exp_i(B) < 1$, healing time increases for that predictor variable and increases by that calculated percentage. In other words, for every additional increase of 1 cm. of Length 1, the healing rate slows, or increases, by 35.55%. Similarly, for Length 2, an increase of 1 cm. results in a 28.53% increase in healing time. Unlike Length 1 and Length 2, an increase in 1 cm. of depth results in a nearly 100% increase in healing time. In other words, Length 1 has a greater impact on remaining healing time and increases healing time more than does Length 2 for every one centimeter.

TABLE 9.9: COVARIATE MEANS

	Mean
Length_1	1.370
Length_2	1.602
Depth	0.162

Table 9.9 shows the covariate means for the model, including only the covariates of Length 1, Length 2, depth, and granulation. Figure 9.7 shows the survival functional plot of the four covariates from Table 9.9. Figure 9.8 depicts the cumulative survival estimate after the natural-log transformation that is applied to the estimate. The log-minus-log plot displays the log-minus-log of the survival function — that is, $\ln(-\ln(\text{survival}))$ — versus the survival time. Figure 9.9 shows the modified baseline cumulative hazard plot with the respective estimated nonlinear function for the covariates in Table 9.9. Table 9.10 displays the numerical baseline hazard values and the survival probabilities.

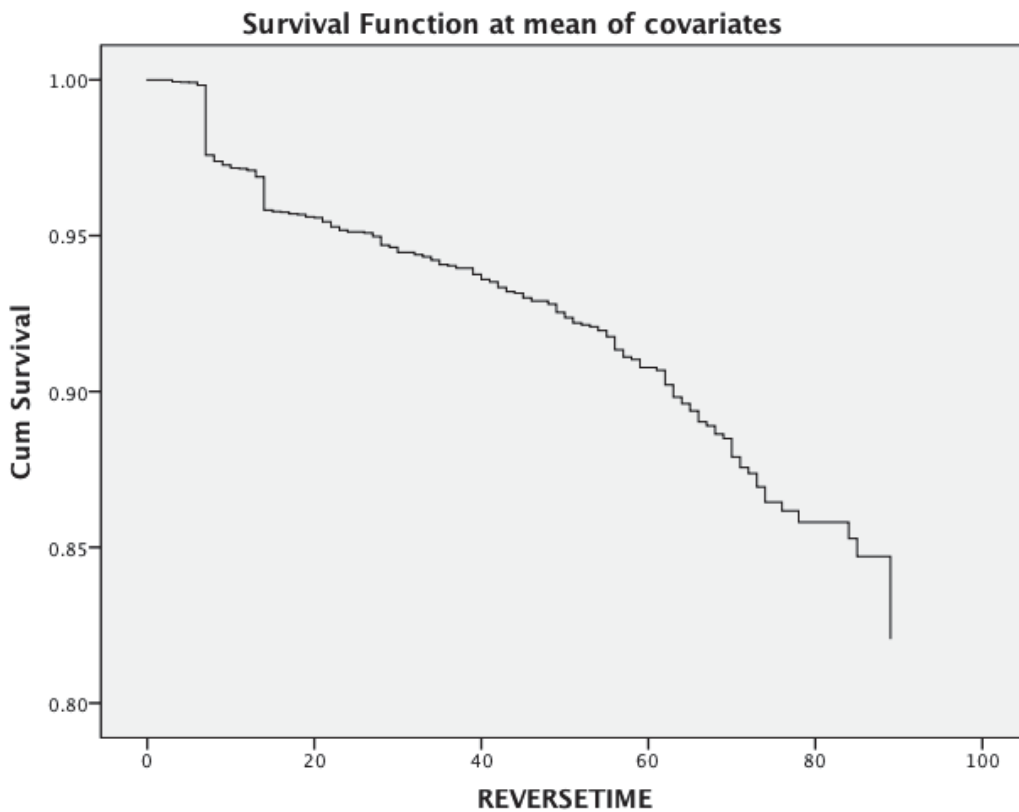


FIGURE 9.7: SURVIVAL FUNCTION AT MEAN OF COVARIATES

Figure 9.8 is important for understanding how the categorical predictors respond to the output of the Cox regression. The log (-log) plot represents a test of the main assumption of Cox regression and the proportional hazards. The assumption states that the ratio of the hazards should be the same across time for any two individuals.

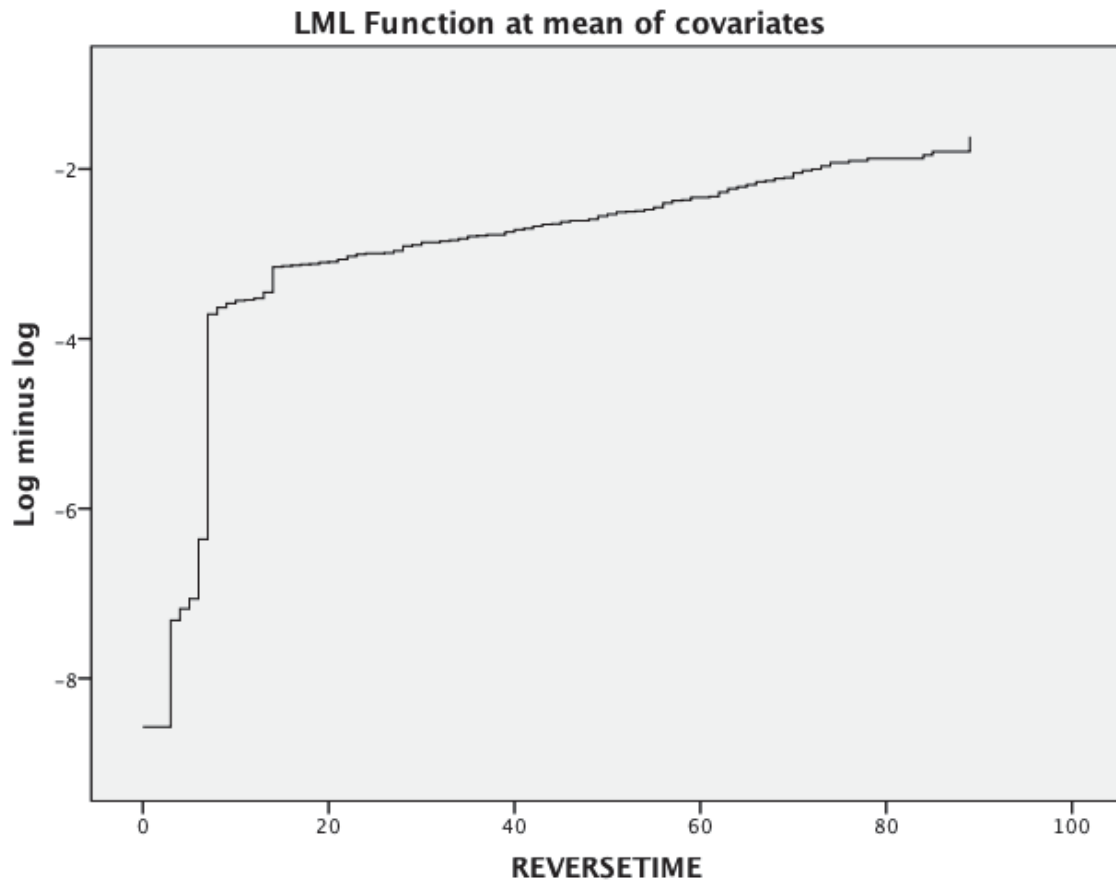


FIGURE 9.8: LOG-MINUS-LOG PLOT

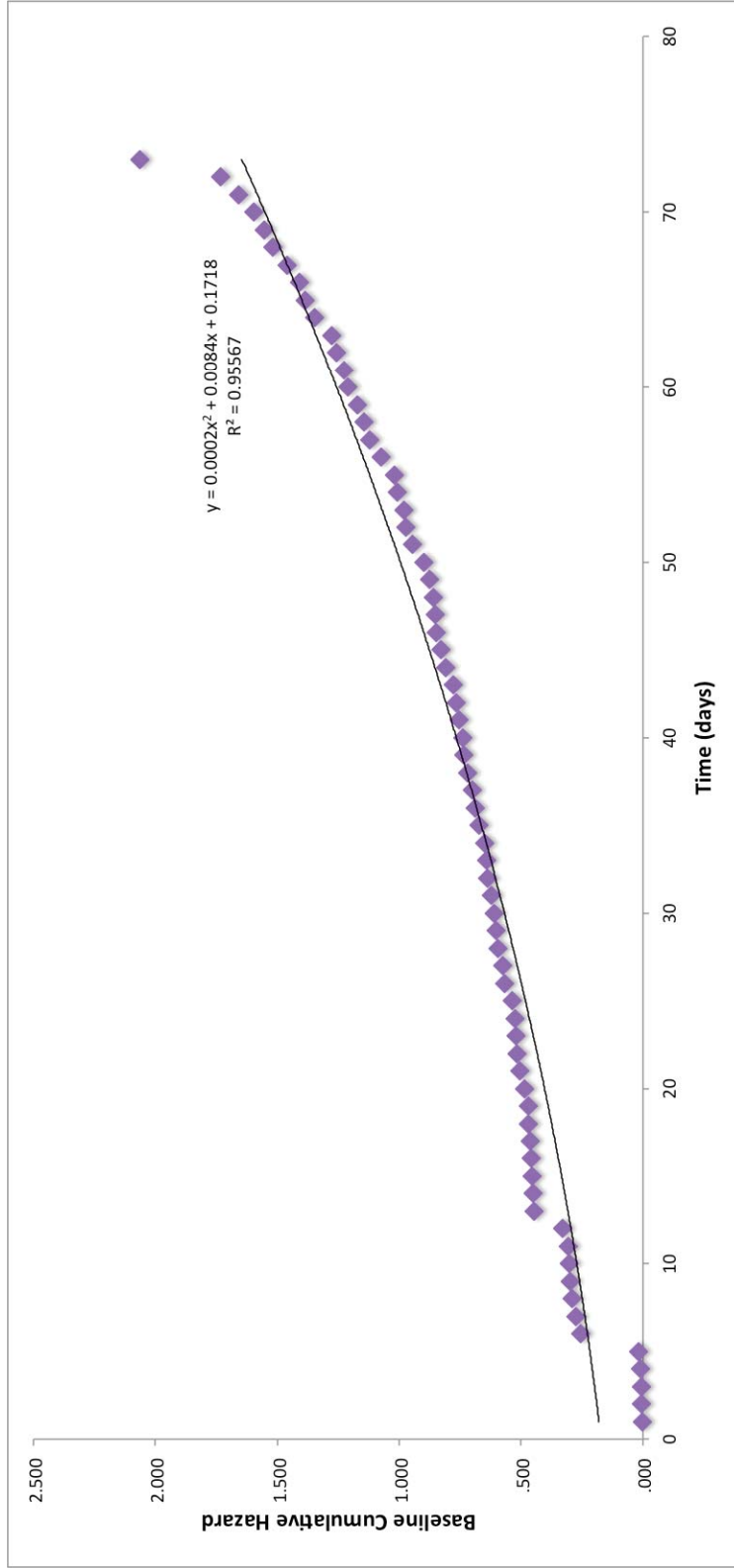


FIGURE 9.9: BASELINE CUMULATIVE HAZARD

TABLE 9.10: SURVIVAL TABLE

Time	Baseline	At mean of covariates		
	Cumulative	Survival	SE	Cum
0	0.002	1.000	0.000	0.000
3	0.007	0.999	0.000	0.001
4	0.008	0.999	0.000	0.001
5	0.009	0.999	0.000	0.001
6	0.018	0.998	0.000	0.002
7	0.255	0.976	0.002	0.024
8	0.276	0.974	0.002	0.026
9	0.289	0.973	0.002	0.028
10	0.299	0.972	0.002	0.029
11	0.301	0.972	0.002	0.029
12	0.308	0.971	0.002	0.029
13	0.330	0.969	0.002	0.032
14	0.445	0.958	0.003	0.043
15	0.450	0.958	0.003	0.043
16	0.453	0.958	0.003	0.043
17	0.458	0.957	0.003	0.044
18	0.461	0.957	0.003	0.044
19	0.469	0.956	0.003	0.045
20	0.472	0.956	0.003	0.045
21	0.486	0.954	0.003	0.047
22	0.504	0.953	0.003	0.048
23	0.516	0.952	0.003	0.049
24	0.522	0.951	0.004	0.050
26	0.525	0.951	0.004	0.050
27	0.538	0.950	0.004	0.052
28	0.569	0.947	0.004	0.055
29	0.576	0.946	0.004	0.055
30	0.594	0.945	0.004	0.057
32	0.602	0.944	0.004	0.058
33	0.610	0.943	0.004	0.058
34	0.621	0.942	0.004	0.060
35	0.637	0.941	0.004	0.061
36	0.641	0.940	0.004	0.062
37	0.650	0.940	0.004	0.062
39	0.672	0.938	0.005	0.064
40	0.690	0.936	0.005	0.066
41	0.699	0.935	0.005	0.067
42	0.719	0.933	0.005	0.069
43	0.734	0.932	0.005	0.070
44	0.739	0.932	0.005	0.071

45	0.756	0.930	0.005	0.072
46	0.767	0.929	0.005	0.074
48	0.779	0.928	0.005	0.075
49	0.809	0.925	0.005	0.078
50	0.828	0.924	0.006	0.079
51	0.847	0.922	0.006	0.081
52	0.854	0.921	0.006	0.082
53	0.861	0.921	0.006	0.083
54	0.875	0.920	0.006	0.084
55	0.897	0.918	0.006	0.086
56	0.945	0.913	0.006	0.091
57	0.971	0.911	0.007	0.093
58	0.980	0.910	0.007	0.094
59	1.010	0.908	0.007	0.097
61	1.020	0.907	0.007	0.098
62	1.074	0.902	0.007	0.103
63	1.120	0.898	0.008	0.107
64	1.144	0.896	0.008	0.110
65	1.171	0.894	0.008	0.112
66	1.212	0.890	0.009	0.116
67	1.227	0.889	0.009	0.118
68	1.259	0.886	0.009	0.121
69	1.275	0.885	0.009	0.122
70	1.345	0.879	0.010	0.129
71	1.385	0.876	0.010	0.133
72	1.408	0.874	0.010	0.135
73	1.460	0.869	0.011	0.140
74	1.518	0.865	0.011	0.146
76	1.552	0.862	0.012	0.149
78	1.596	0.858	0.012	0.153
84	1.660	0.853	0.013	0.159
85	1.731	0.847	0.015	0.166
89	2.063	0.821	0.030	0.198

9.3 NEURAL-NETWORK ANALYSIS

Neural networks enable us to create predictive models that are both accurate and robust. Neural networks are the most widely used of the predictive modeling methods because they have consistently been the most reliable. However, the limitation of using neural networks is that they do not provide the ability to know the black-box algorithm that they create. Instead, we base the accuracy of the model on statistical measures, such as the number of average errors. We can control the neural network using input parameters, such as the number of hidden layers, the number of nodes within those hidden layers, the number of epochs, and the step size of the gradient descent. With this control, we can produce predictive algorithms that are accurate to within five days. We can also verify the accuracy of the algorithms using corresponding lift charts, which assist in measuring the effectiveness of a predictive model. Lift charts use the ratio of the original data to the predictive data to analyze the accuracy of the overall model.

9.3.1 DATA ANALYSIS FOR DATA WITH ASPECT RATIO OF LESS THAN 1

For the data in this category, we created the corresponding neural network (Figure 9.10), using Length 1, Length 2, depth, and granulation as inputs, which have been established as the highest contributing inputs to the output, time to heal. Tables Table 9.11 and Table 9.12 provide the specifics of the neural network, the number of epochs necessary, and the accuracy of the model. Similarly, the lift charts (Figure 9.11) provide verification and support for the comparison of the neural network model's predictive performance to the baseline model with no predictors.

Figure 9.10 shows the neural network model with the respective weights of the hidden node. We show this network model to compare the inputs and the weights between the groups of aspect ratios. The foundation of Figure 9.10 is a multilayer perception neural network.

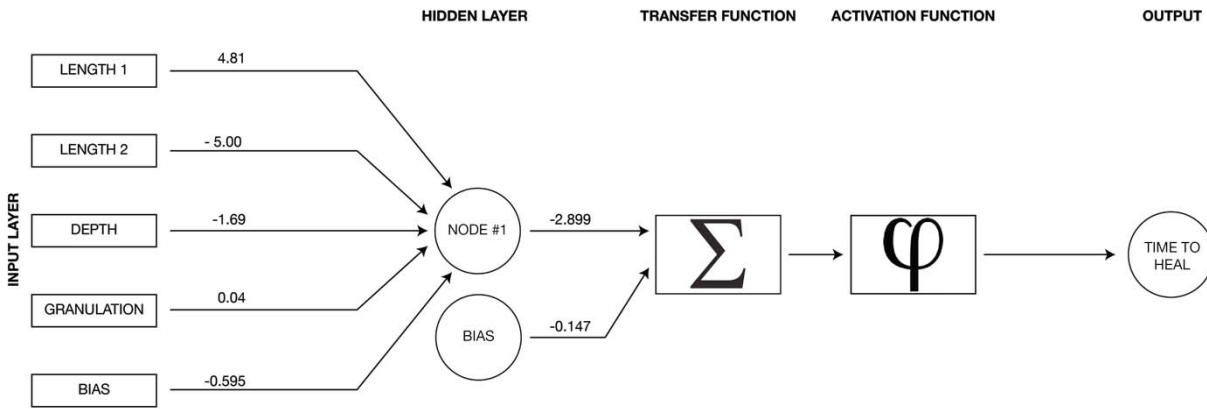


FIGURE 9.10: NEURAL-NETWORK MODEL FOR DATA WITH ASPECT RATIO OF LESS THAN 1

Table 9.11 shows the parameters of the neural-network model specific to Group 1, wounds with an aspect ratio less than 1.

TABLE 9.11: NEURAL-NETWORK PREDICTION VARIABLES AND PARAMETERS, ASPECT RATIO LESS THAN 1

Variables	Parameter/Options		
Number of input variables	4	Number of hidden layers	1
Input variables	Length 1, Length 2, depth, granulation	Number of nodes in Hidden Layer 1	1
Output variable	Time remaining	Number of epochs	200
		Step size for gradient descent	0.01
		Weight-change momentum	0.6
		Error tolerance	0.01
		Weight decay	0

Table 9.12 shows the training- and validation-data scoring for this network. The network analysis has returned accurate results with the average error for the training data of ± 1.61 days. The validation error is more accurate with ± 0.20 days of predictive accuracy.

TABLE 9.12: TRAINING- AND VALIDATION-DATA SCORING REPORT, ASPECT RATIO LESS THAN 1

Training-Data Scoring			Validation-Data Scoring		
Total sum of squared errors	RMS error	Average error	Total sum of squared errors	RMS error	Average error
129705.47	22.96	1.61	70953.89	26.00	0.20

Figure 9.11 and Figure 9.12 show the lift charts for the validation data set. These lift charts are based on the fitting from a linear-regression model that includes the time to heal and the set of predictor variables that describe the wound: Length 1, Length 2, depth, and granulation. The lift chart shows that the model's predictive performance is better than the baseline model due to the higher lift curve.

Lift Chart (Training Dataset)

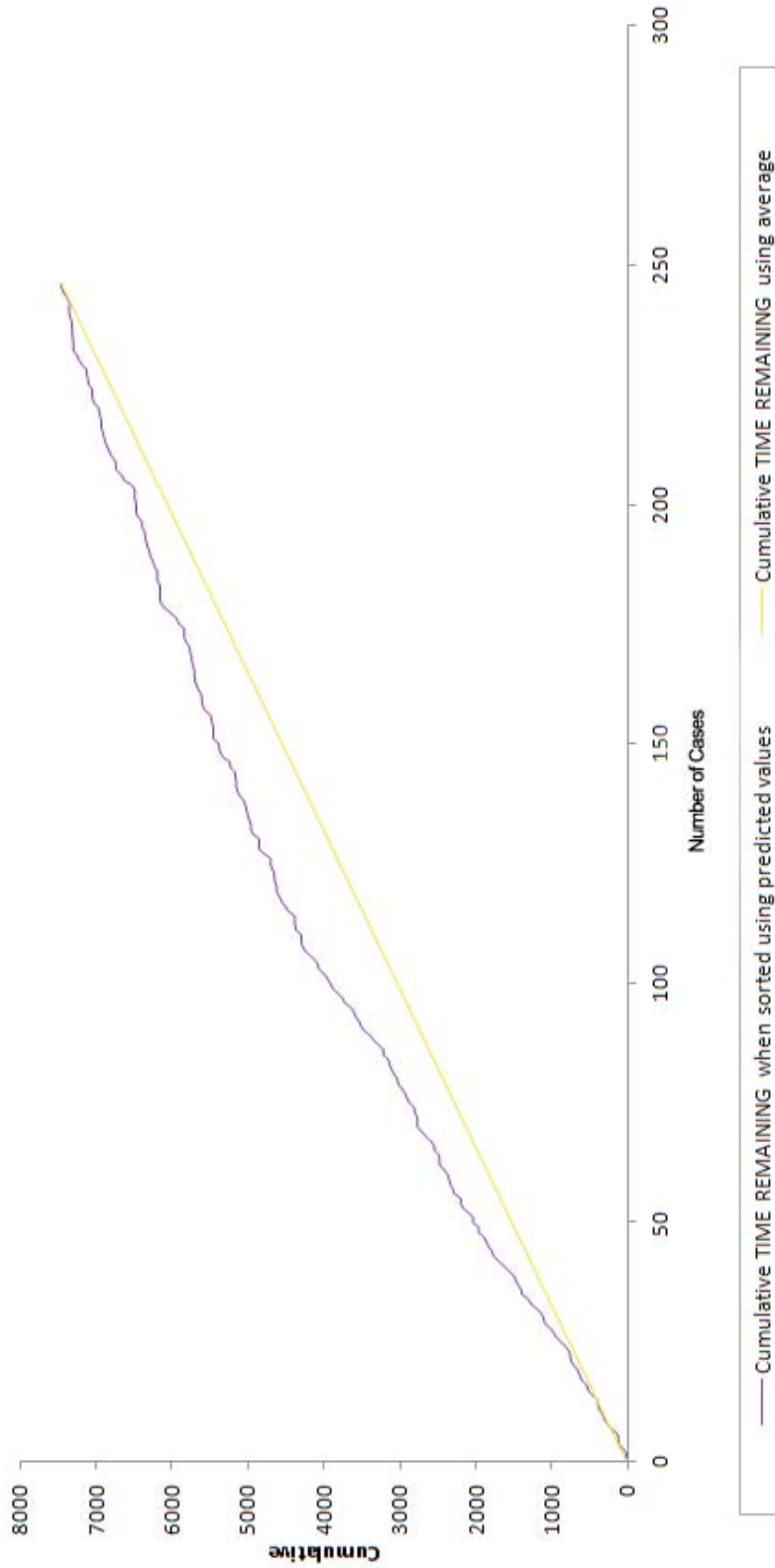


FIGURE 9.11: LIFT CHART FROM NEURAL-NETWORK MODEL FOR DATA WITH $AR < 1$, TRAINING DATASET

Lift Chart (Validation Dataset)

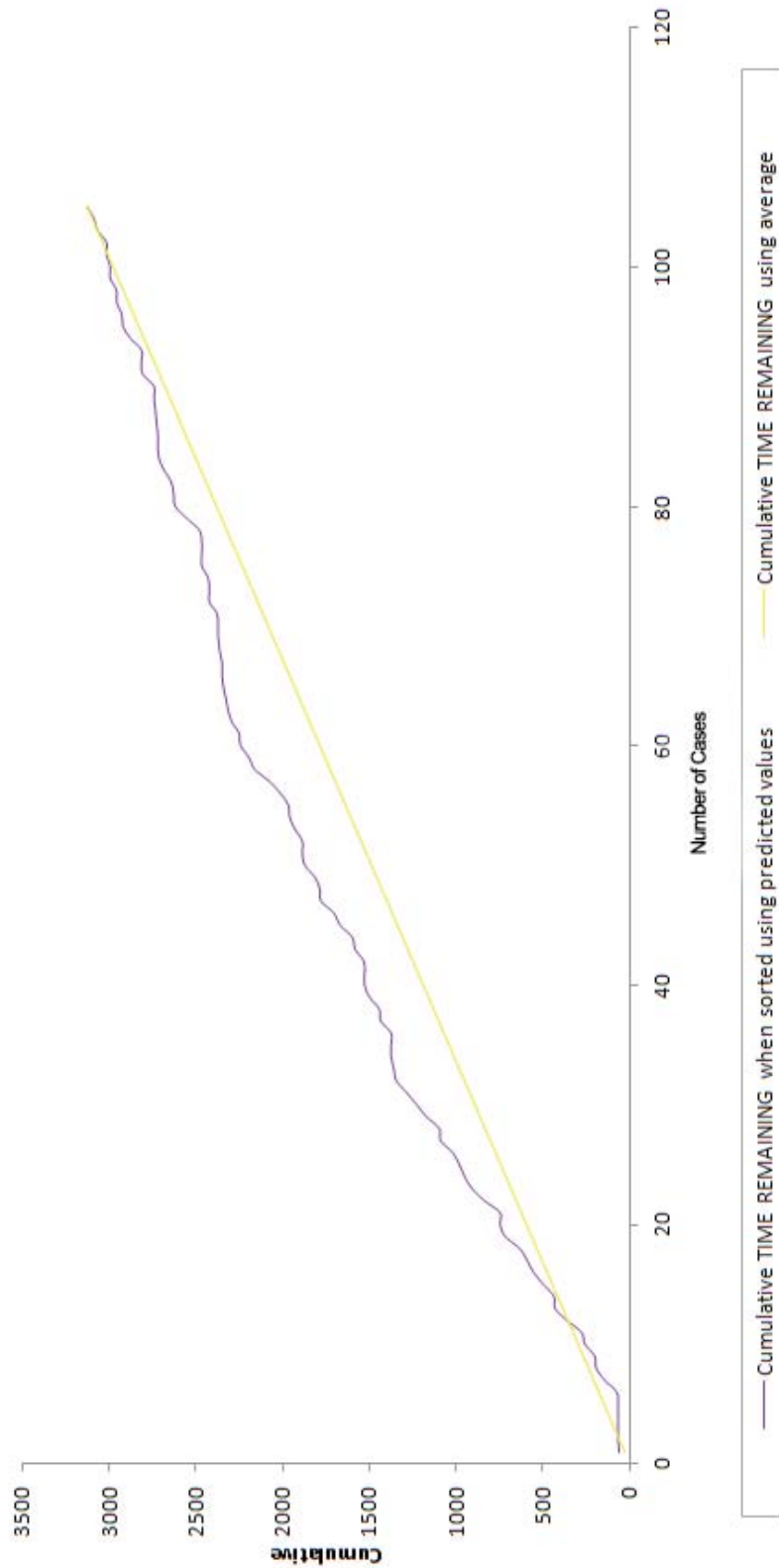


FIGURE 9.12: LIFT CHART FROM NEURAL-NETWORK MODEL FOR DATA WITH ASPECT RATIO OF LESS THAN 1, VALIDATION DATA SET

9.3.2 DATA ANALYSIS FOR COMBINED DATA OF ASPECT RATIO LESS THAN 1 AND RBMC DATA

Figure 9.13 shows the neural-network model for the combined data from both Vohra and RBMC. The purpose of combining the data was to determine whether the origin of the data had an effect on the neural-network model.

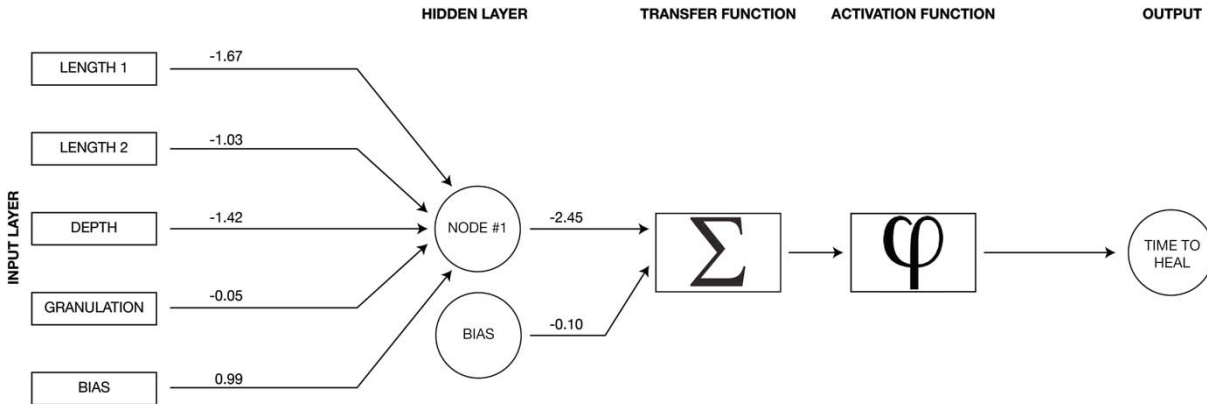


FIGURE 9.13: NEURAL NETWORK MODEL FOR DATA WITH AR < 1 AND RBMC

Table 9.13 shows the neural-network parameters for which we established the training and validation scoring.

TABLE 9.13: NEURAL-NETWORK PREDICTION VARIABLES AND PARAMETERS, ASPECT RATIO OF LESS THAN 1 AND RBMC

Variables	Parameter/Options		
Number of input variables	4	Number of hidden layers	1
Input variables	Length 1, Length 2, depth, granulation	Number of nodes in Hidden Layer 1	1
Output variable	Time remaining	Number of epochs	100
		Step size for gradient descent	0.01
		Weight-change momentum	0.15
		Error tolerance	0.01
		Weight decay	0

With an average error of ± 4.15 days between the theoretical and the actual outputs, the training-data scoring in this section is slightly less accurate than that of the neural-network in Section 9.31

However, the validation-data scoring was more precise with an average error of slightly less than ± 0.50 days.

TABLE 9.14: TRAINING- AND VALIDATION-DATA SCORING REPORT, ASPECT RATIO LESS THAN 1 AND RBMC

Training-Data Scoring			Validation-Data Scoring		
Total sum of squared errors	RMS error	Average error	Total sum of squared errors	RMS error	Average error
482383.73	34.13	4.15	178951.28	31.80	0.48

9.3.3 DATA ANALYSIS FOR DATA WITH ASPECT RATIO GREATER THAN 1 AND LESS THAN 2

Similarly, Figure 9.14 shows the neural-network model for Group 2, wounds that have an aspect ratio greater than 1 and less than 2.

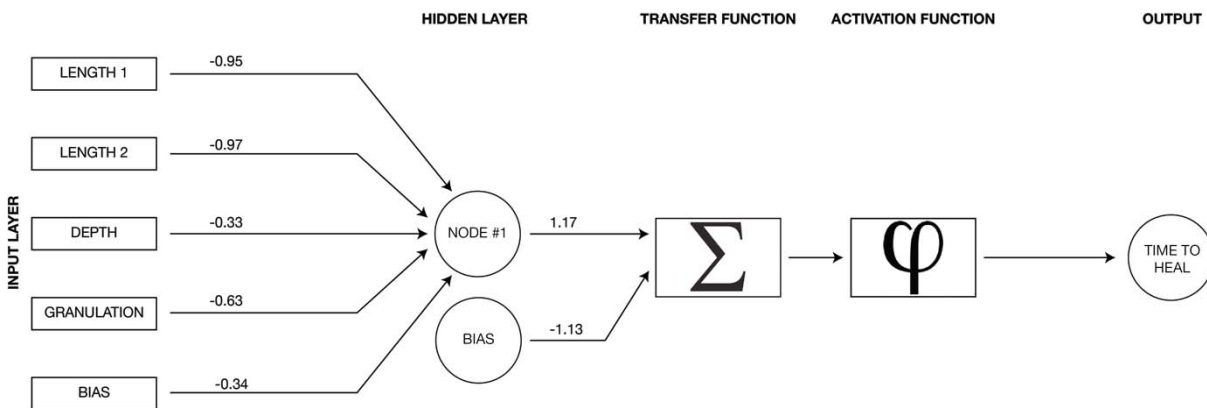


FIGURE 9.14: NEURAL-NETWORK MODEL FOR DATA WITH ASPECT RATIO GREATER THAN 1 AND LESS THAN 2

Table 9.15 shows the parameters for Group 2's neural-network model.

TABLE 9.15: NEURAL-NETWORK PREDICTION VARIABLES AND PARAMETERS,
ASPECT RATIO GREATER THAN 1 AND LESS THAN 2

Variables		Parameter/Options	
Number of input variables	4	Number of hidden layers	1
Input variables	Length 1, Length 2, depth, granulation	Number of nodes in Hidden Layer 1	1
Output Variable	Time Remaining	# Epochs	150
		Step size for gradient descent	0.01
		Weight change momentum	0.10
		Error tolerance	0.01
		Weight decay	0

Table 9.16 shows the training- and validation-scoring reports, revealing an average error of ± 0.14 and ± 0.53 days, respectively.

TABLE 9.16: TRAINING- AND VALIDATION-DATA SCORING REPORT,
ASPECT RATIO GREATER THAN 1 AND LESS THAN 2

Training-Data Scoring			Validation- Data Scoring		
Total sum of squared errors	RMS error	Average error	Total sum of squared errors	RMS error	Average error
170397.51	23.91	0.14	74061.73	24.05	0.53

9.3.4 DATA ANALYSIS FOR COMBINED DATA, ASPECT RATIO OF GREATER THAN 1 AND LESS THAN 2 AND RBMC DATA

Figure 9.15 depicts the neural network for the combined data of Group 2 from Vohra and RBMC. We used these neural network visualizations to compare how the combination of data from different origins affects the neural-network analysis. As this chapter shows, best-fit neural-network parameters have one hidden layer, one hidden node, and varying numbers of epochs and weight-change momentums.

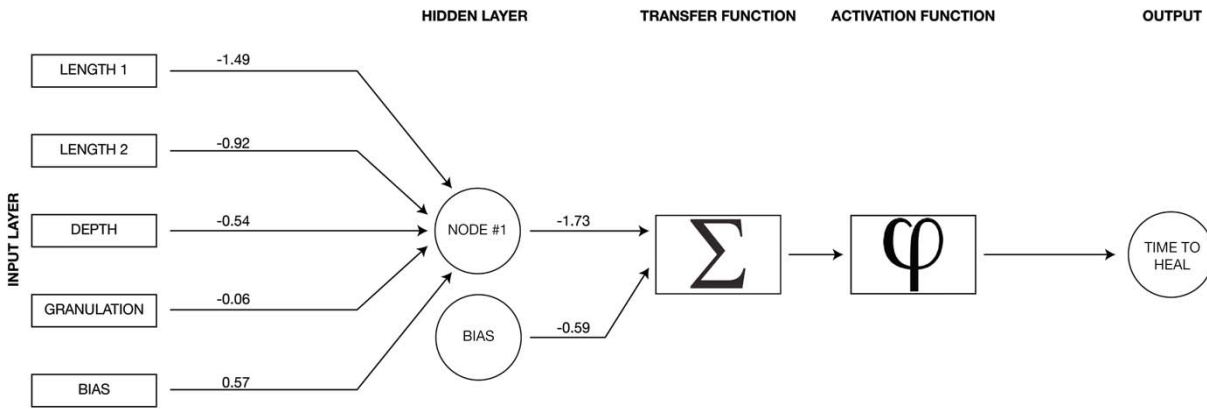


FIGURE 9.15: NEURAL NETWORK MODEL FOR DATA WITH $1 \leq \text{ASPECT RATIO} \leq 2$ AND RBMC

Table 9.17 shows the neural-network parameters for the neural network in Figure 9.15.

TABLE 9.17: NEURAL-NETWORK PREDICTION VARIABLES AND PARAMETERS, ASPECT RATIO GREATER THAN 1 AND LESS THAN 2 AND RBMC

Variables		Parameter/Options	
Number of input variables	4	Number of hidden layers	1
Input variables	Length 1, Length 2, depth, granulation	Number of nodes in Hidden Layer 1	1
Output variable	Time remaining	Number of epochs	100
		Step size for gradient descent	0.01
		Weight-change momentum	0.05
		Error tolerance	0.01
		Weight decay	0

Table 9.18 states the accuracy of this neural network's training- and validation-data scoring results. For this neural network, the training data scored an average error of ± 1.69 days, whereas the validation data scored ± 0.77 days.

TABLE 9.18: TRAINING- AND VALIDATION-DATA SCORING REPORT, ASPECT RATIO GREATER THAN 1 AND LESS THAN 2 AND RBMC

Training-Data Scoring			Validation-Data Scoring		
Total sum of	RMS error	Average	Total sum of squared	RMS	Average

squared errors		error	errors	Error	Error
505659.23	32.94	1.69	209347.23	32.35	0.77

These results bode well for this model's ability to predict an accurate time to heal given a reliable set of patient-demographic and wound-characteristic inputs.

9.3.5 DATA ANALYSIS FOR DATA WITH ASPECT RATIO GREATER THAN 2

Figure 9.16 presents the final neural-network model. To develop an accurate model for wounds with an aspect ratio greater than 2, the model needed more hidden nodes within its hidden-layer structure. Increasing the number of hidden nodes makes the neural network more complex than the previous models (Figure 9.16). Table 9.19 and Table 9.20 provide the interlayer connection weights for both the input and the output layers of this neural-network model.

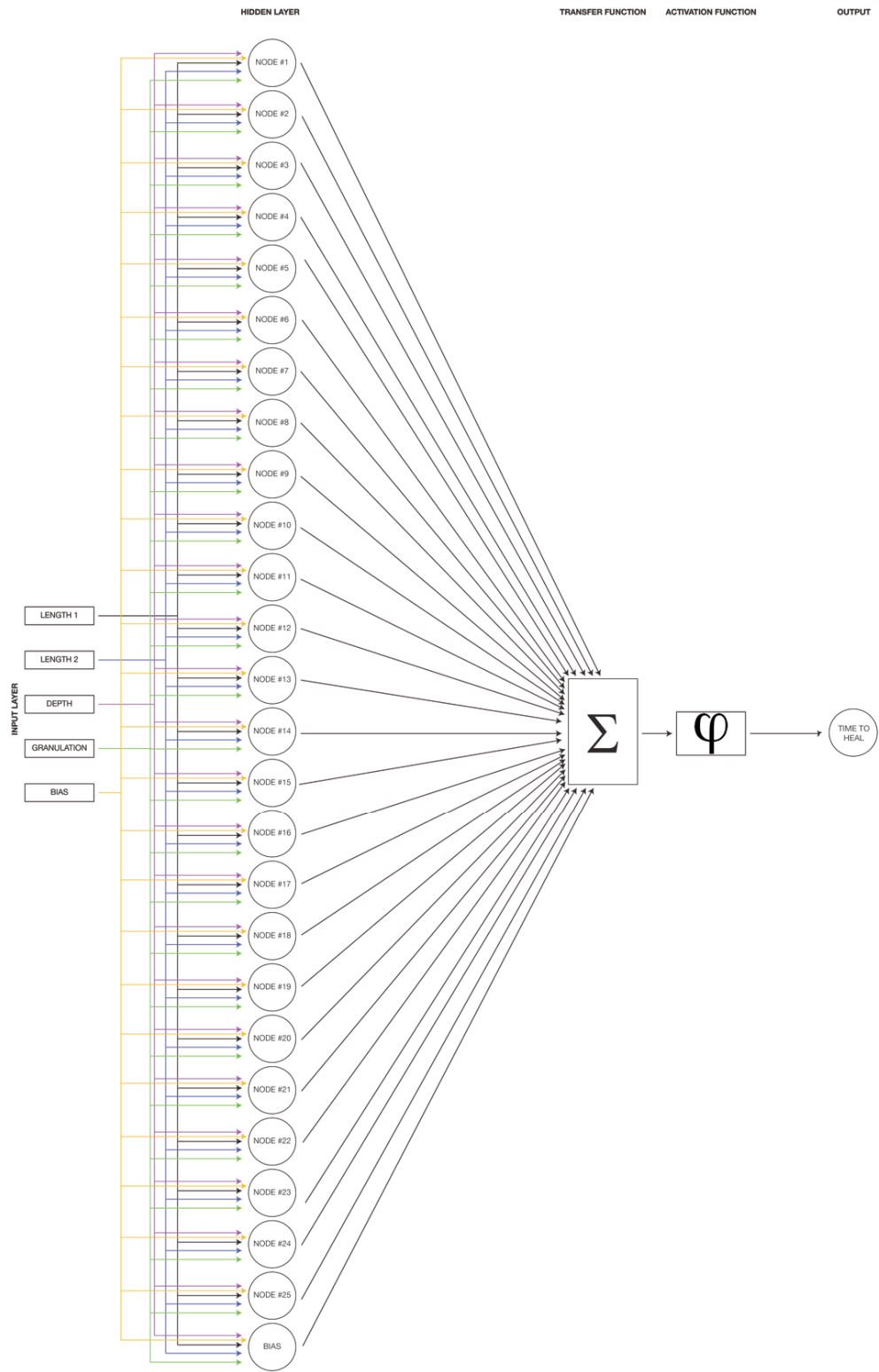


FIGURE 9.16: NEURAL-NETWORK MODEL FOR DATA WITH ASPECT RATIO 1 AND RBMC

TABLE 9.19: NEURAL-NETWORK PREDICTION, INTERLAYER CONNECTION WEIGHTS

Hidden Layer 1	Input Layer				
	Length 1	Length 2	Depth	Granulation	Bias Node
Node 1	-1.03	-0.62	-0.21	-0.46	0.06
Node 2	-0.89	0.67	-0.10	0.74	0.30
Node 3	0.79	-1.12	-0.37	-0.43	0.37
Node 4	-0.34	0.85	0.62	0.53	0.00
Node 5	-0.20	0.97	0.40	-0.83	0.21
Node 6	0.30	0.14	-0.25	-0.72	0.74
Node 7	-0.67	0.31	0.11	0.70	-0.81
Node 8	0.08	-0.91	-0.60	-0.58	-1.09
Node 9	-0.69	-0.39	-1.05	-0.76	-0.14
Node 10	0.55	-0.37	0.28	-0.70	-0.77
Node 11	-0.57	-0.89	0.16	-0.57	0.43
Node 12	0.21	0.73	-0.05	0.79	0.58
Node 13	0.16	-0.49	0.22	0.38	-0.12
Node 14	-0.97	0.82	-0.55	-0.14	-0.25
Node 15	0.28	1.06	-0.26	-1.04	-0.77
Node 16	0.92	-0.86	-0.68	0.16	0.22
Node 17	0.06	-0.32	-0.50	0.92	0.22
Node 18	-0.93	-0.70	-0.57	-0.19	0.66
Node 19	0.65	0.70	-0.55	-0.10	-0.38
Node 20	-0.27	-0.66	-0.30	-0.32	0.43
Node 21	0.31	-0.77	-0.29	-0.38	-0.47
Node 22	0.82	-0.61	0.39	0.44	-0.28
Node 23	0.05	-0.22	0.49	-0.42	-0.02
Node 24	0.07	-0.56	-0.67	0.81	-0.07
Node 25	-1.01	-0.04	0.15	0.27	-1.00

TABLE 9.20: NEURAL-NETWORK PREDICTION, OUTPUT-LAYER CONNECTION WEIGHTS

Hidden Layer 1	Output
Node 1	-0.21
Node 2	0.01
Node 3	0.73
Node 4	0.00
Node 5	-0.92
Node 6	0.21
Node 7	0.46
Node 8	-0.45
Node 9	0.83
Node 10	0.29
Node 11	0.19
Node 12	-0.29
Node 13	0.33
Node 14	0.03
Node 15	-0.81
Node 16	0.19
Node 17	0.47
Node 18	0.01
Node 19	0.16
Node 20	-0.34
Node 21	-0.09
Node 22	-0.24
Node 23	-0.27
Node 24	0.25
Node 25	-0.68
Bias Node	-0.40

Table 9.21 the neural network parameters, revealing 25 nodes within the hidden layer. However, unlike the previous models, the network experienced only 10 epochs, or iterations.

TABLE 9.21: NEURAL NETWORK PREDICTION VARIABLES AND PARAMETERS, ASPECT RATIO GREATER THAN 2

Variables		Parameter/Options	
Number of input variables	4	Number of hidden layers	1
Input variables	Length 1, Length 2, depth, granulation	Number of nodes in Hidden Layer 1	25
Output variable	Time remaining	Number of epochs	10
		Step size for gradient descent	0.01
		Weight-change momentum	1
		Error tolerance	0.01
		Weight decay	0

Table 9.22 shows the training- and validation-data scoring. Unlike the previous models, the best average error for Group 3 of chronic wounds was ± 5.69 days for training data and ± 4.02 days for validation data. This figure, on average, was a larger error than that of any of the previous neural-network models. We have hypothesized the primary reason behind this discrepancy is that the larger the aspect ratio, the more obscure the shape of the wound. This obscurity could result in nonuniform healing.

TABLE 9.22: TRAINING- AND VALIDATION DATA-SCORING REPORT, ASPECT RATIO GREATER THAN 2

Training-Data Scoring			Validation-Data Scoring		
Total sum of squared errors	RMS error	Average error	Total sum of squared errors	RMS error	Average error
29086.64	22.39	-5.69	21056.33	29.02	4.02

9.3.6 DATA ANALYSIS FOR COMBINED DATA WITH ASPECT RATIO GREATER THAN 2, RBMC DATA

Figure 9.17 depicts the final neural-network model. This model combines analysis of wounds with an aspect ratio greater than 2 and wound data from RBMC.

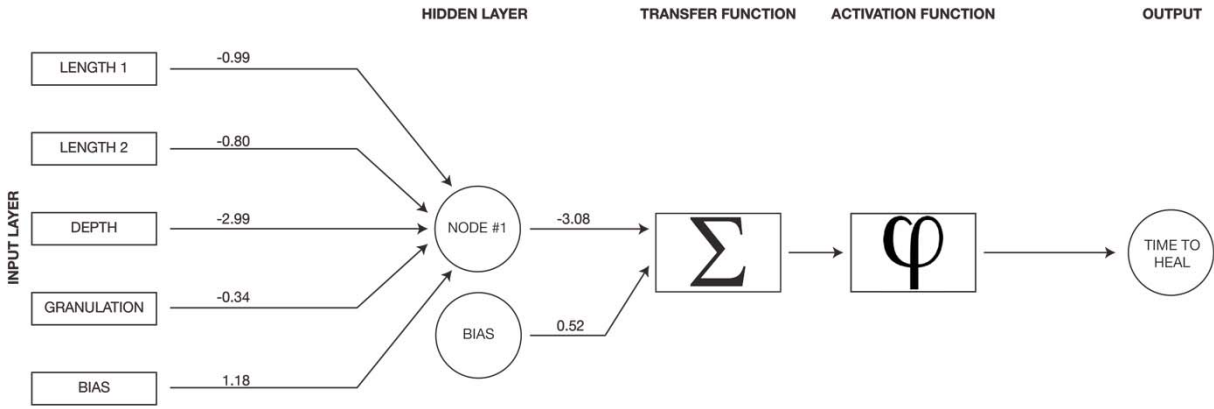


FIGURE 9.17: NEURAL-NETWORK MODEL FOR DATA WITH ASPECT RATIO GREATER THAN 2, RBMC

Table 9.23 provides the parameters for the final neural-network model.

TABLE 9.23: NEURAL-NETWORK PREDICTION VARIABLES AND PARAMETERS, ASPECT RATIO GREATER THAN 2, RBMC

Variables	Parameter/Options		
Number of input variables	4	Number of hidden layers	1
Input variables	Length 1, Length 2, depth, granulation	Number of nodes in Hidden Layer 1	1
Output variable	Time remaining	Number of epochs	145
		Step size for gradient descent	0.01
		Weight-change momentum	0.25
		Error tolerance	0.01
		Weight decay	0

Table 9.24 shows the training- and validation-data scoring, with an average error of ± 3.80 and ± 2.25 days, respectively.

TABLE 9.24: TRAINING- AND VALIDATION-DATA SCORING REPORT, ASPECT RATIO GREATER THAN 2, RBMC

Training-Data Scoring			Validation-Data Scoring		
Total sum of squared errors	RMS error	Average error	Total sum of squared errors	RMS error	Average error
321371.83	37.71	3.80	130663.77	36.70	-2.25

9.4 VALIDATION

To validate the accuracy of the models and methodology, we tested the models against respective data. From the neural-network models, we learned that it is possible to relatively accurately predict a time to heal. Within the context of the data and chronic-wound situation, the difference for these patients' time remaining to wound closure was insignificant, ranging from five to 10 days.

9.4.1 NONLINEAR REGRESSION: COX REGRESSION

The hazard function is a measure of the potential for the event to occur at a particular time, t , provided that the event did not occur yet. The greater the hazard function, the greater the potential and probability for the event to occur — in this case, for the wound to heal [98, 123]. A set of assumptions is made for each predictive-modeling technique. For the Cox proportional-hazards regression model, those assumptions include [99]:

- Independence of survival times among wounds within the data sample,
- A multiplicative, or nonlinear, relationship between the covariates and predictors and the hazard, and
- A calculated baseline hazard function at time t .

The Cox model is agnostic as the functional form of the baseline function. Cox regression in itself is inherently both semiparametric and nonparametric. It is semiparametric because $h_0(t)$ is nonparametric. However, because $h(t)$ is parametric, we specify an exponential shape, which is a mathematical consequence of assuming a proportional hazard over time. Theoretically, we expect a wound to start large and become smaller as time progresses. Although we theorized an exponential decline of the data over time, the baseline hazard function could have easily taken other graphical shapes. Unless we centered the data on the mean, or set it to zero, the baseline hazard graph simply shows the hazard rate when the predictors are at their mean level [99].

The survival function is the ratio of the hazard function and the baseline hazard function as given by:

$$\frac{h(t)}{h_0(t)} = e^{-0.0439L1-0.336L2-7.418D} \quad (9.4)$$

The baseline survival function was determined as a function of the baseline hazard function:

$$S_0(t) = e^{-H_0(t)} \quad (9.5)$$

The survival function as a constant power of the baseline survival function is given by:

$$S_i(t) = [S_0(t)]e^{-0.0439L1-0.336L2-7.418D} \quad (9.6)$$

The corresponding survival function for Wound 4917 (Figure 9.18) at the probability that survival is equal to zero is given by:

$$S_i(t) = 0.0002x^2 - 0.031x + 1.0751 @ S_i(t) = 0 \quad (9.7)$$

The approximate time to wound closure for Wound 4917 is 103 days.

The Cox proportional hazard model outputs a ratio rather than a time to heal. Therefore, to validate the use of this model, we calculated an alternative output as a function of the Cox proportional hazard. Thus, we verified the effectiveness of the model through the survival function, a function of the proportional hazard function. The survival function captures the probability that the wound will survive beyond time t . Through alternative calculations, we calculated the survival function of randomly selected wounds to determine whether the probability that the wound would survive corresponded with the actual recorded time of the patient visit. Figure 9.18 provides a visual example of the probability that this wound will survive until time t .

Each person's ability to heal a wound is unique. Therefore, it is nearly impossible to create a universal model to predict wound healing. However, with enough of a patient's retrospective data, demographics, and wound characteristics, we can develop a customized predictive model for that patient's wound. Figure 9.18 provides an example of a single wound's trajectory based on the Cox regression survival function. Using the approximated quadratic equation in Figure 9.18, we estimated that Wound 3381 would heal in approximately 62 days. The actual wound closure occurred in 56 days.

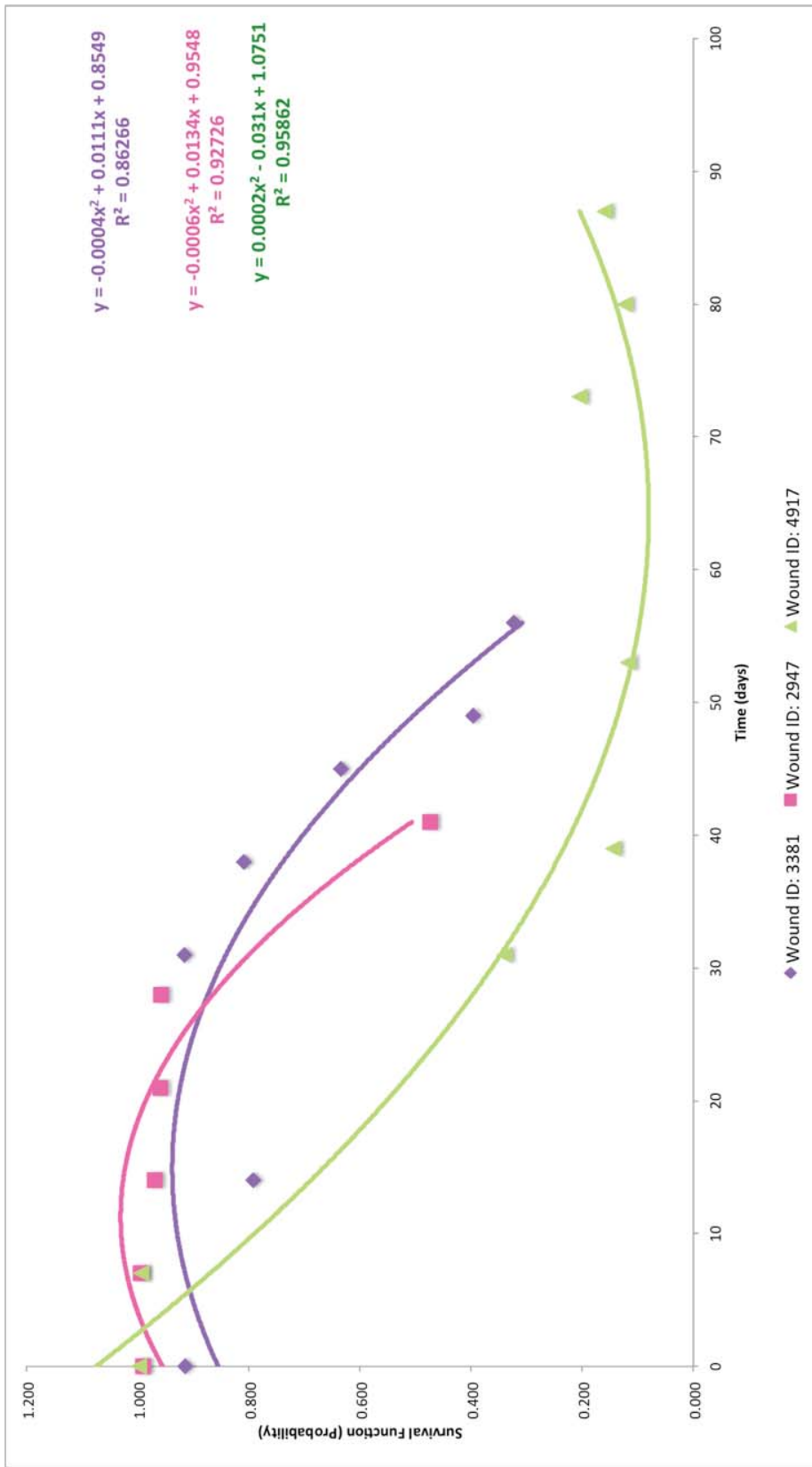


Figure 9.18: Example of Survival Function vs. Time for Sample Wounds (Variables: Length 1, Length 2, Depth, Granulation)

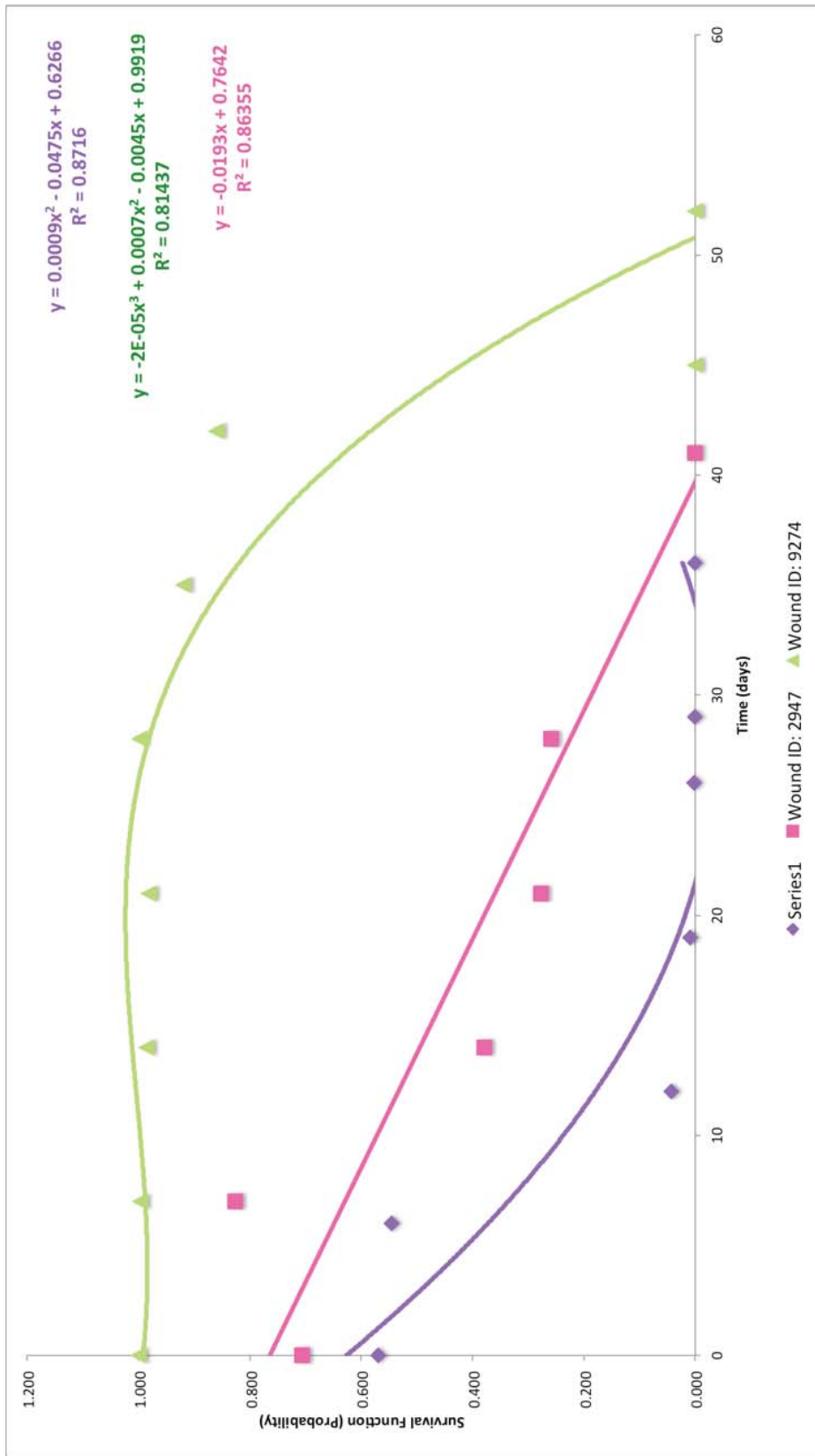


Figure 9.19: Example of Survival Function Versus Time for Sample Wounds (All Variables)

Similarly, in Figure 9.19, we show an example of three wounds and their respective survival function outputs. Unlike the outputs in Figure 9.18, more erratic behavior occurs with regard to curve fitting and shape within the survival functions that incorporate all the variables. More predictor variables appear to create more complex analysis to determine whether the wound survives until a specific time, t .

9.4.2 NEURAL NETWORKS

We developed a series of steps that supported the most robust algorithm we could design. We used correlation matrices and variable selection mechanisms to statistically determine the applicable predictor variables. To verify the validity of the neural network, we rely on the error of both the training and the validation data. We rely more on the feedback of the validation data in an attempt to not “overfit” the model to the training data. Table 9.25 provides a summary of the training and validation scoring from the original data, classified only by aspect ratio. Table 9.25 represents the data from Vohra.

TABLE 9.25: SUMMARY OF TRAINING- AND VALIDATION-DATA SCORING REPORT

Aspect Ratio 1					
Training-Data Scoring			Validation-Data Scoring		
Total sum of squared errors	RMS error	Average error	Total sum of squared errors	RMS error	Average error
129705.47	22.96	1.61	70953.89	26.00	0.20
Aspect Ratio 2					
Training-Data Scoring			Validation-Data Scoring		
Total sum of squared errors	RMS error	Average error	Total sum of squared errors	RMS error	Average error
170397.51	23.91	0.14	74061.73	24.05	0.53
Aspect Ratio 3:					
Training-Data Scoring			Validation-Data Scoring		
Total sum of squared errors	RMS error	Average error	Total sum of squared errors	RMS Error	Average error
29086.64	22.39	-5.69	21056.33	29.02	4.02

Table 9.26 categorizes the training and validation scoring reports by the data’s original aspect ratio with the data from RBMC. To validate the methodology, we first looked at the training data. The training data’s statistics reflect the fit of the network on 70% of the data. In this case, the training

error averages 3.21 days between the three classifications. Furthermore, the networks average better return on the validation data —approximately 30% of the original data with an average data of 0.56 days within the predicted value. All the validation-scoring reports show that the neural network is an accurate predictive modeling for the validation data.

TABLE 9.26: SUMMARY OF TRAINING- AND VALIDATION-DATA SCORING REPORT

Aspect Ratio 1					
Training-Data Scoring			Validation-Data Scoring		
Total sum of squared errors	RMS error	Average error	Total sum of squared errors	RMS error	Average error
482383.73	34.13	4.15	178951.28	31.80	0.48
Aspect Ratio 2:					
Training-Data Scoring			Validation Data Scoring		
Total sum of squared errors	RMS error	Average error	Total sum of squared errors	RMS error	Average error
505659.23	32.94	1.69	209347.23	32.35	0.77
Aspect Ratio 3					
Training-Data Scoring			Validation=Data Scoring		
Total sum of squared errors	RMS error	Average error	Total sum of squared errors	RMS error	Average error
321371.83	37.71	3.80	178951.28	31.80	0.48

RMS error within a neural-network analysis measures the difference between the predicted values by the model and the actual observed values. The RMS error is computed on the validation data. Because RMS error is difference between actual and predictive model values, the ideal RMS values should be small. The returned RMS error in Table 9.26 represents an average RMS error of 31.98, or approximately 32, days, a roughly four-week tolerance. Four weeks may seem like a long time for a wound to heal. However, it seems insignificant to those with chronic wounds that have lasted six to eight months.

We compared the predicted value to the actual value from the neural network analysis. Table 9.27 provides a sample of the validation scoring that occurs as part of the neural-network analysis. We notice that the percentage error ranges from 2.55% to 431% in this sample data. This range correlates to a difference range of two days to 12 weeks. The statistics in Table 9.25 and the large sum of the squared errors from the network analysis reinforce this feedback.

TABLE 9.27: SAMPLE VALIDATION SCORE

Predicted Value	Actual Value	Residual	Length 1	Length 2	Depth	Granulation	Percentage Error	Difference (Weeks)
40.64	98	57.356888	3.8	2.4	0.2	100	58.53	8.19
40.64	91	50.356888	3.8	2.4	0.2	100	55.34	7.19
49.38	21	-28.382882	4	2.7	0.3	100	135.16	-4.05
39.42	14	-25.420974	3.5	2	0.2	100	181.58	-3.63
75.96	56	-19.961683	5	3.8	0.5	100	35.65	-2.85
64.61	63	-1.605641	5	3.8	0.4	100	2.55	-0.23
27.00	117	90.004332	0.8	1	0.1	0	76.93	12.86
30.43	54	23.571859	0.6	1.2	0.2	0	43.65	3.37
30.10	40	9.901263	0.5	1	0.2	0	24.75	1.41
30.24	33	2.760344	0.8	1	0.2	0	8.36	0.39
26.56	5	-21.558464	0.4	0.7	0.1	0	431.17	-3.08
24.91	21	-3.908657	1.9	1	0	0	18.61	-0.56

CHAPTER TEN

MODEL VALIDATION AND VERIFICATION

CHAPTER 10

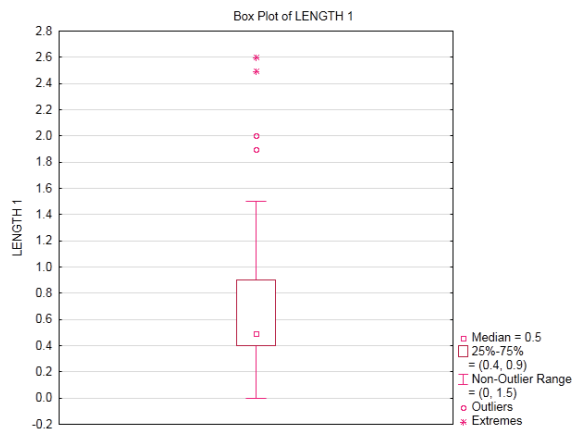
Model Validation and Verification

RBMC provided us with the opportunity to observe and collect original patient data. Ideally, the preference was the development of a universal algorithmic model to accommodate all wound clinics. However, with further insight and understanding of factors that contribute to day-to-day wound care, that task was not feasible with the current data set. This chapter discusses and verifies the methodology that we created and established from the data of Vohra and applies it to data collected from RBMC.

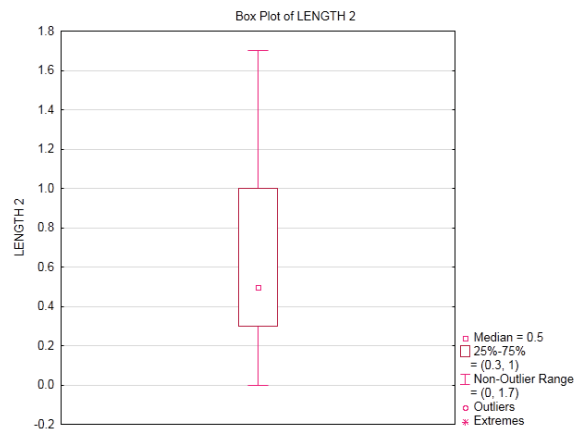
10.1 OVERVIEW

We used the data from RBMC to cross-validate the methodology on a new and unrelated set of data. This step allowed us to test the methods on an independent data sample and determine the validity of the processes and methodologies. Because we collected a smaller amount of data from RBMC than from Vohra, we were able to observe, converse, and record the necessary measurements through patient interaction and patient transcripts.

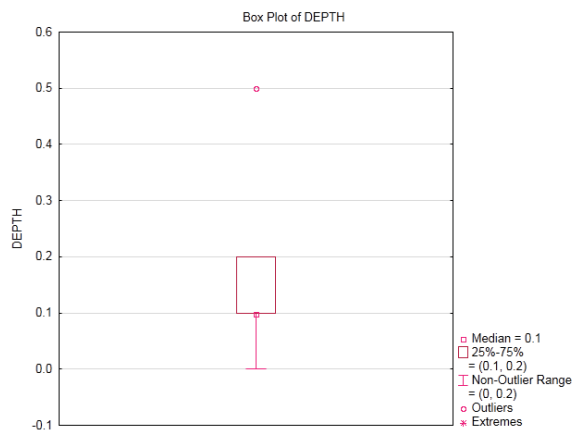
From the data summarized Figure 10.1, we determined the ideal wound-healing measurements and characteristics in Table 10.1. Table 10.1 shows the threshold of each variable. The combination of the independent variables shows when we consider the wound to be healed.



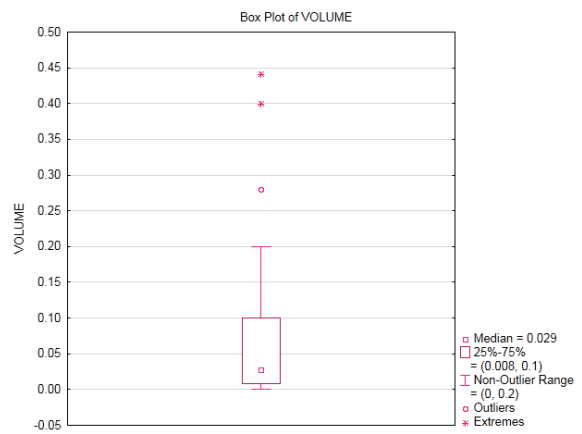
(A) LENGTH 1



(B) LENGTH 2



(C) DEPTH



(D) VOLUME

FIGURE 10.1: BOX PLOTS FOR RBMC DATA

TABLE 10.1: LOWER AND UPPER WHISKERS OF BOX PLOTS FOR RBMC DATA

Independent Variable	Lower Quartile	Upper Quartile
Length 1	0.40	0.90
Length 2	0.30	1
Depth	0.10	0.20
Granulation tissue	0	100

10.2 DATA COLLECTION

The data from RBMC was collected over multiple weeks. Similar to what occurs in other wound clinics, most RBMC patients have weekly or biweekly visits to care for their wounds. Although, the facility is extremely knowledgeable about how to efficiently treat wounds, staff may have difficulty in understanding patients' lifestyles. Nutrition plays a significant role in wound healing, and it is one of the most difficult factors to observe. Table 10.2 shows an example of a patient's wound that took 117 days to heal. Because these are chronic wounds, one of the assumptions for this study is that the first visit to a wound care clinic is $time = 0$, regardless of the length of time patients have had their wounds before their first appointments.

By performing similar analysis on the data from RBMC, the expected healing pattern for our validation data deviated little from the analysis results of the training data. Figure 10.2 through Figure 10.5 show the behavior of variables length 1, length 2, depth, and volume over time.

TABLE 10.2: SAMPLE PATIENT DATA

Wound ID	Time to					
	Heal	Length 1	Length 2	Depth	Volume	Black Necrotic
20002	117	0.8	1	0.1	0.08	0
20002	96	0.8	0.7	0.1	0.056	100
20002	89	0.6	1	0.2	0.12	100
20002	82	0.6	0.8	0.2	0.096	100
20002	68	0.6	0.8	0.2	0.096	100
20002	61	0.6	1.4	0.2	0.168	100
20002	54	0.6	1.2	0.2	0.144	100
20002	47	0.5	1	0.2	0.1	100
20002	40	0.5	1	0.2	0.1	100
20002	33	0.8	1	0.2	0.16	100
20002	26	0.5	1.2	0.2	0.12	100
20002	19	0.5	1.2	0.2	0.12	100
20002	5	0.4	0.7	0.1	0.028	100
20002	0	0	0	0	0	100

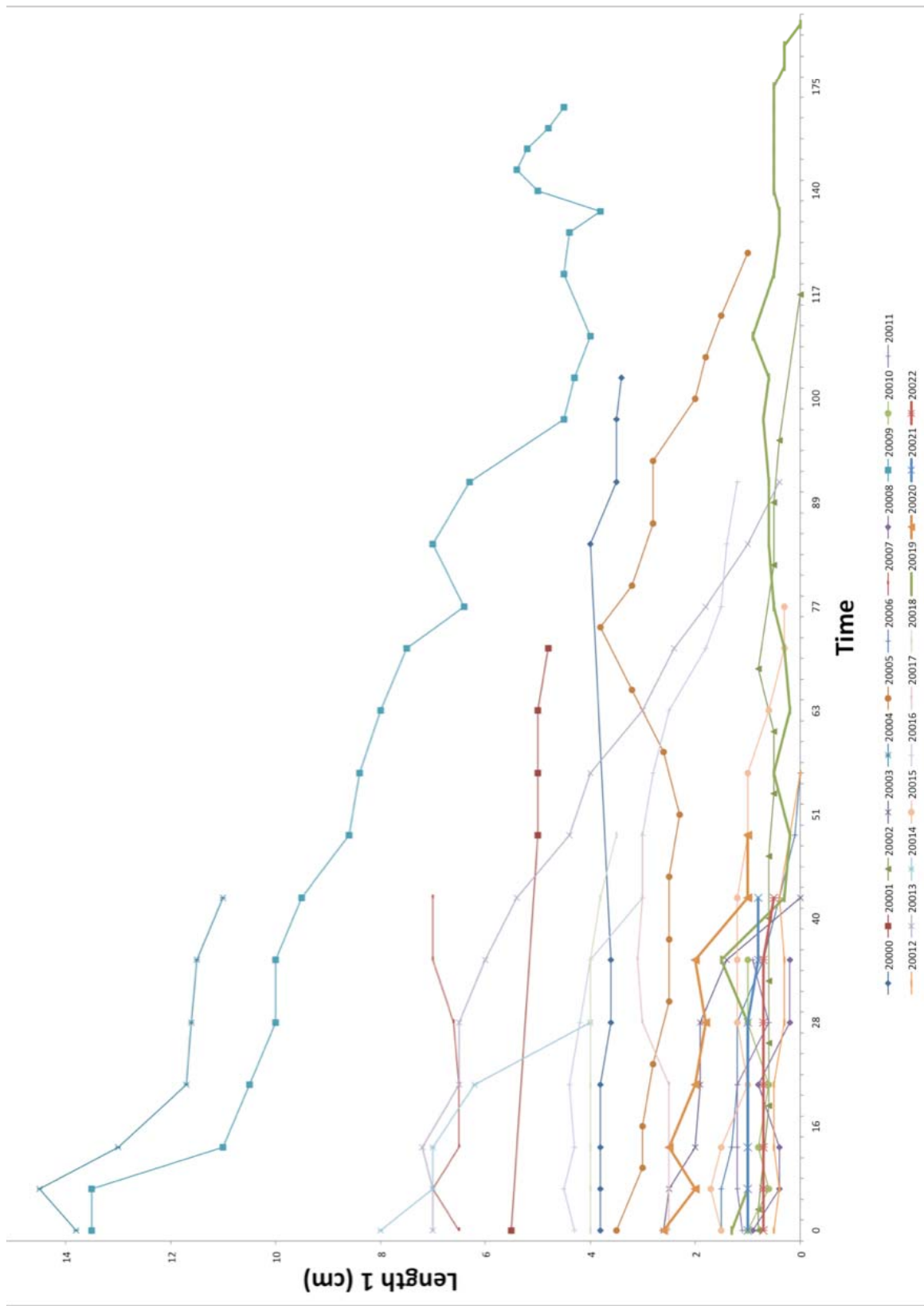


Figure 10.2: Length 1 Versus Time

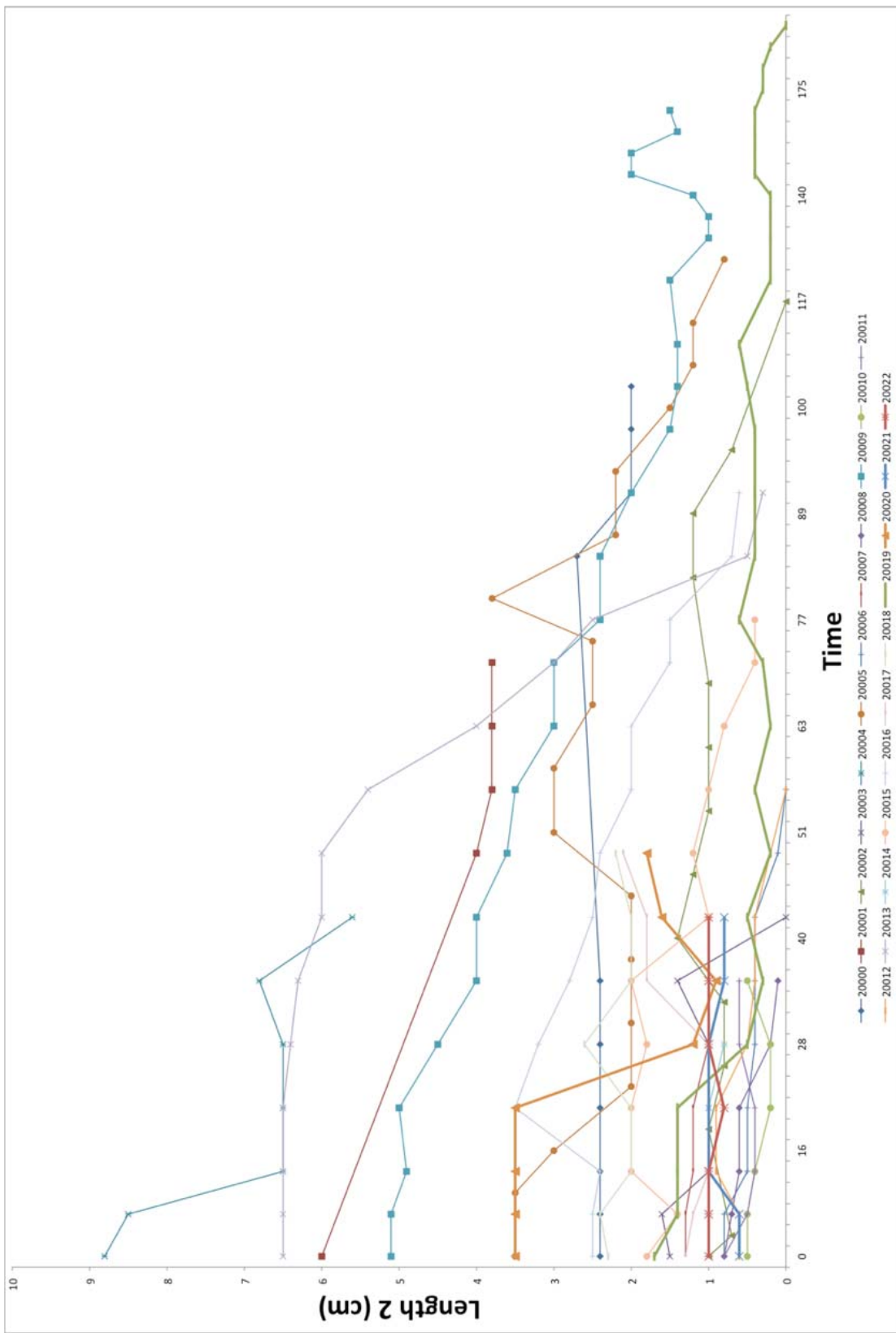


Figure 10.3: Length 2 Versus Time

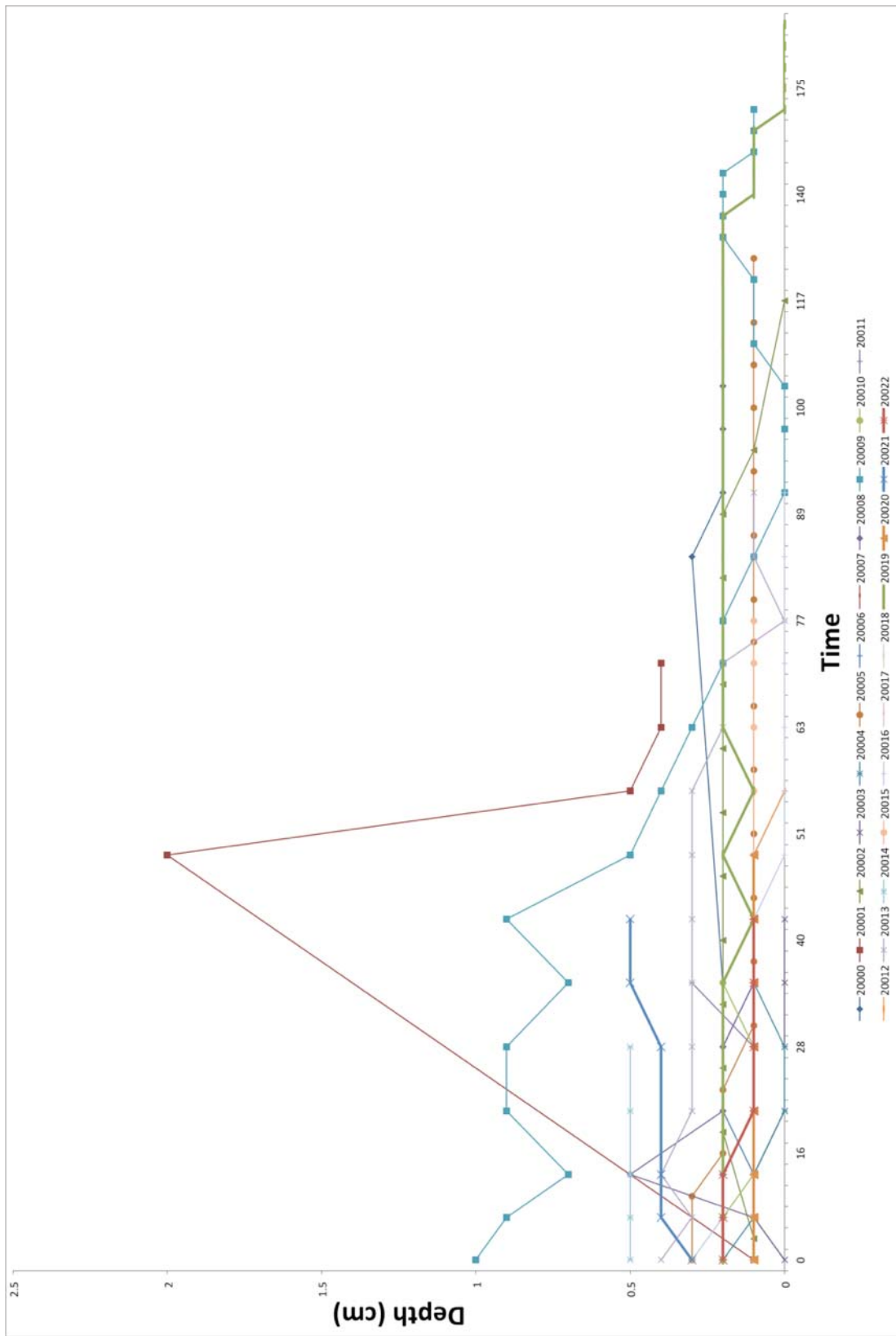


Figure 10.4: Depth Versus Time

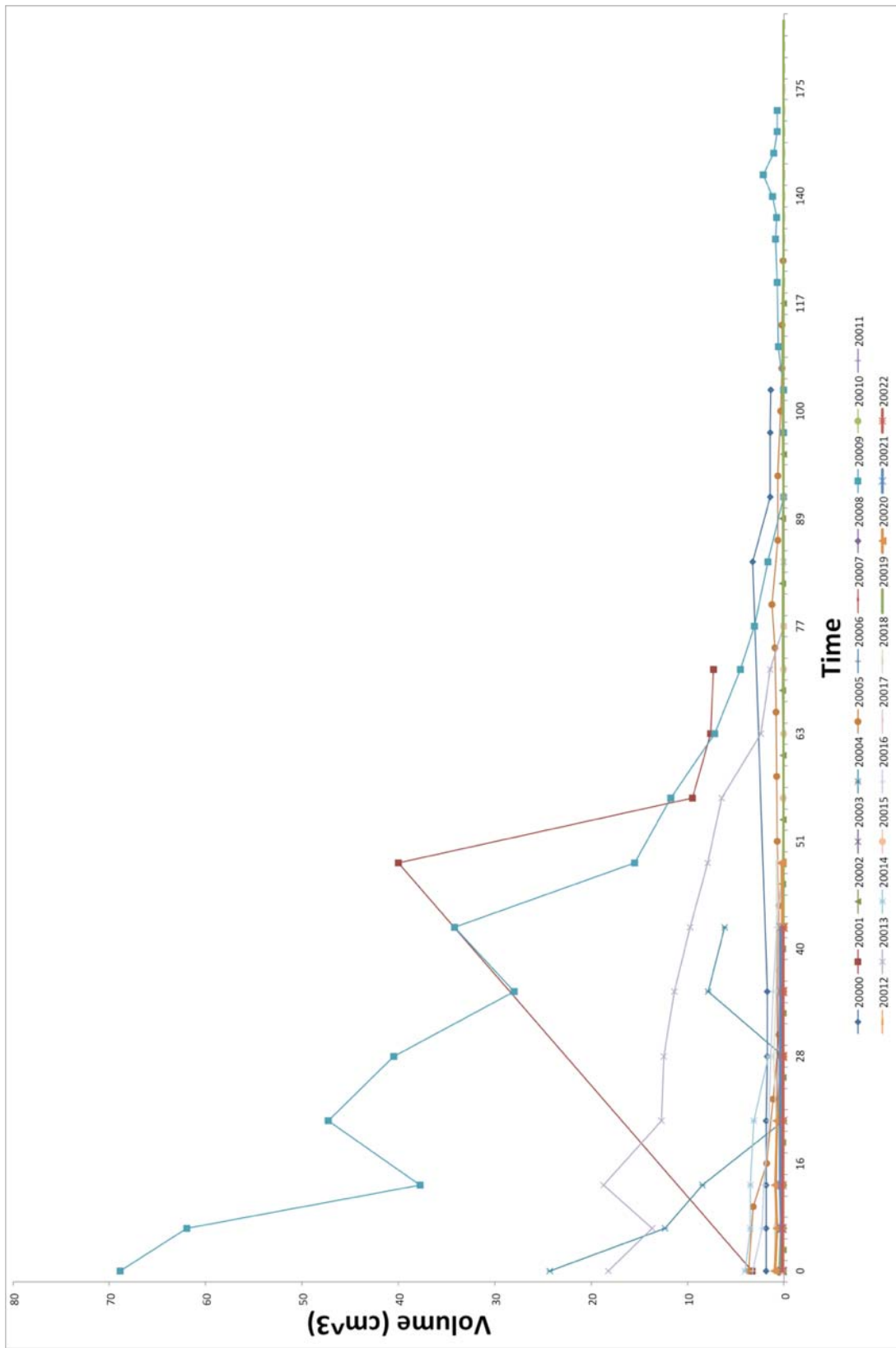


Figure 10.5: Volume Versus Time

10.3 THREE-DIMENSIONAL SURFACE PLOTS

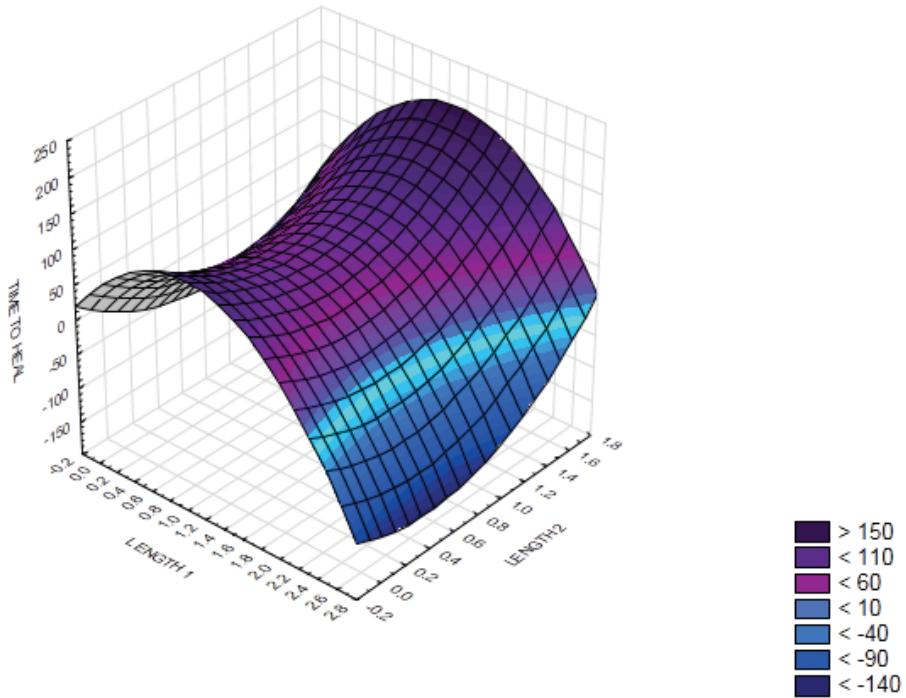
Three-dimensional surface plots help demonstrate the behavior and relationship among three variables and to determine the location of a combination of variables based on density and population. For this analysis, three-dimensional surface plots permit us to visually represent three variables of data and the relationships between them. For example, Figure 10.6 through Figure 10.8 display the relationship between Length 1 and Length 2 with time to heal. Figure 10.6 shows the relationship among the variables with the fit of a quadratic curve, and Figure 10.8 represents a linear relationship.

Surface plots and the combination of variables determine any patterns or similarities between the respective combinations. Table 10.3 shows the combination of variables per each group of surface plots.

TABLE 10.3: VARIABLE COMBINATIONS OF SURFACE PLOTS

Combination	Variables	Figures
1	Time to heal versus Length 1 and Length 2	Figure 10.6, 10.7, 10.8
2	Depth versus Length 1 and Length 2	10.3.1.1.1 10.9, 10.10, 10.11
3	Time to heal versus Length 2 and depth	10.12, 10.13, 10.14
	Depth versus Length 2 and depth	10.3.1.1.2 10.15, 10.16. 10.17

3D Surface Plot of TIME TO HEAL against LENGTH 1 and LENGTH 2
 $\text{TIME TO HEAL} = 25.3464 + 163.5587x - 121.2812y - 78.6008x^2 + 21.6706xy + 77.2009y^2$



3D Surface Plot of TIME TO HEAL against LENGTH 1 and LENGTH 2
 $\text{TIME TO HEAL} = 25.3464 + 163.5587x - 121.2812y - 78.6008x^2 + 21.6706xy + 77.2009y^2$

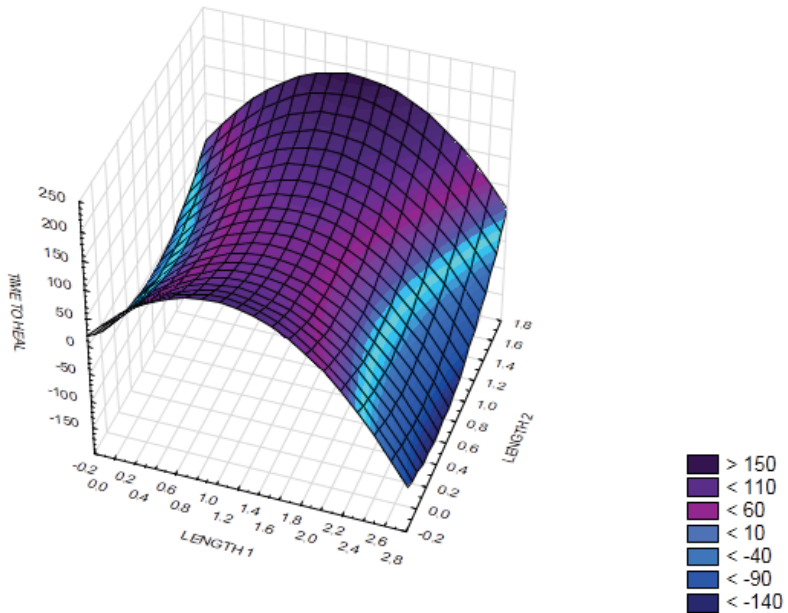


FIGURE 10.6: SURFACE PLOT: TIME TO HEAL AGAINST LENGTH 1, LENGTH 2 (QUADRATIC FIT)

3D Surface Plot of TIME TO HEAL against LENGTH 1 and LENGTH 2
 TIME TO HEAL = Spline

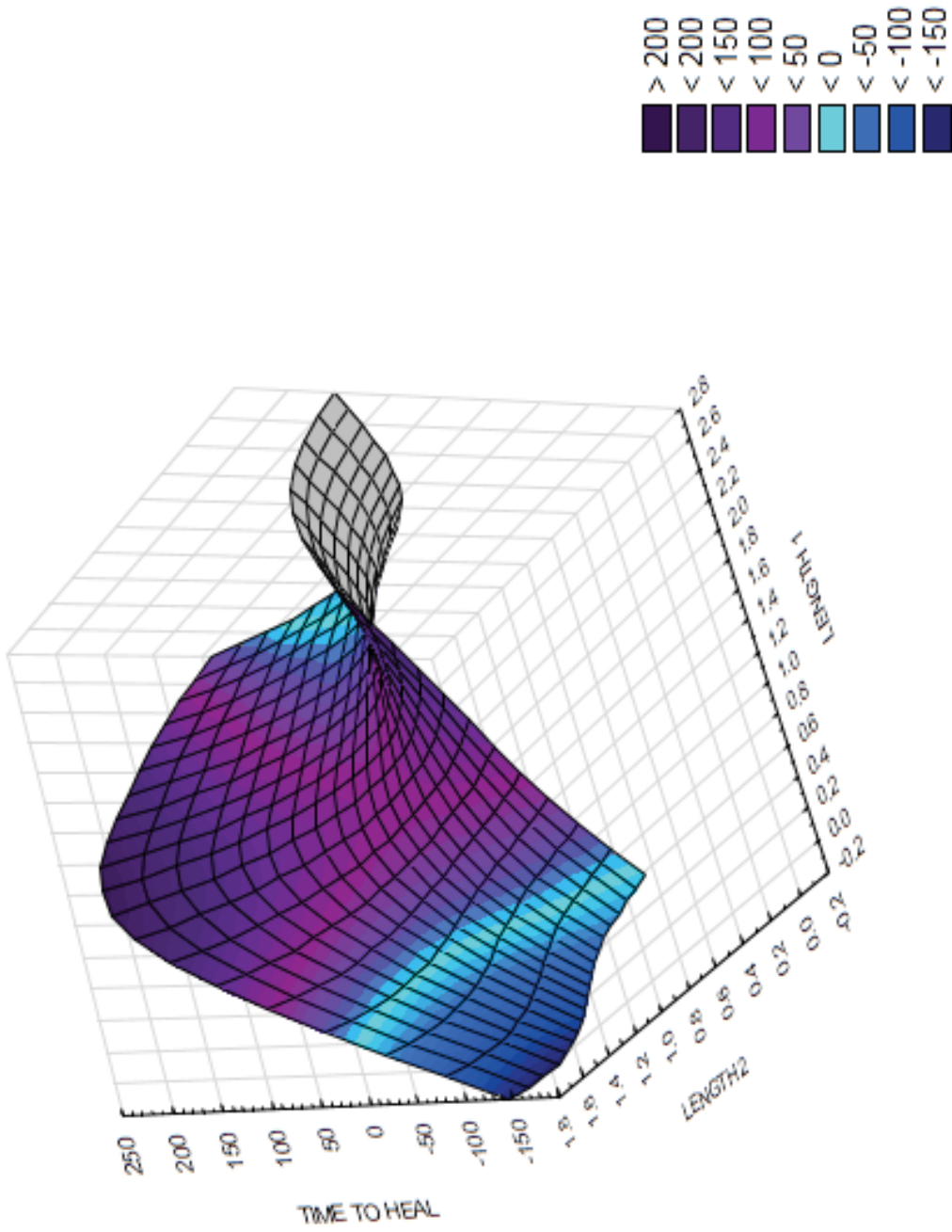


FIGURE 10.7: SURFACE PLOT: TIME TO HEAL AGAINST LENGTH 1, LENGTH 2 (SPLINE FIT)

3D Surface Plot of TIME TO HEAL against LENGTH 1 and LENGTH 2
 TIME TO HEAL = $38.328 - 3.9944 * x + 36.7784 * y$

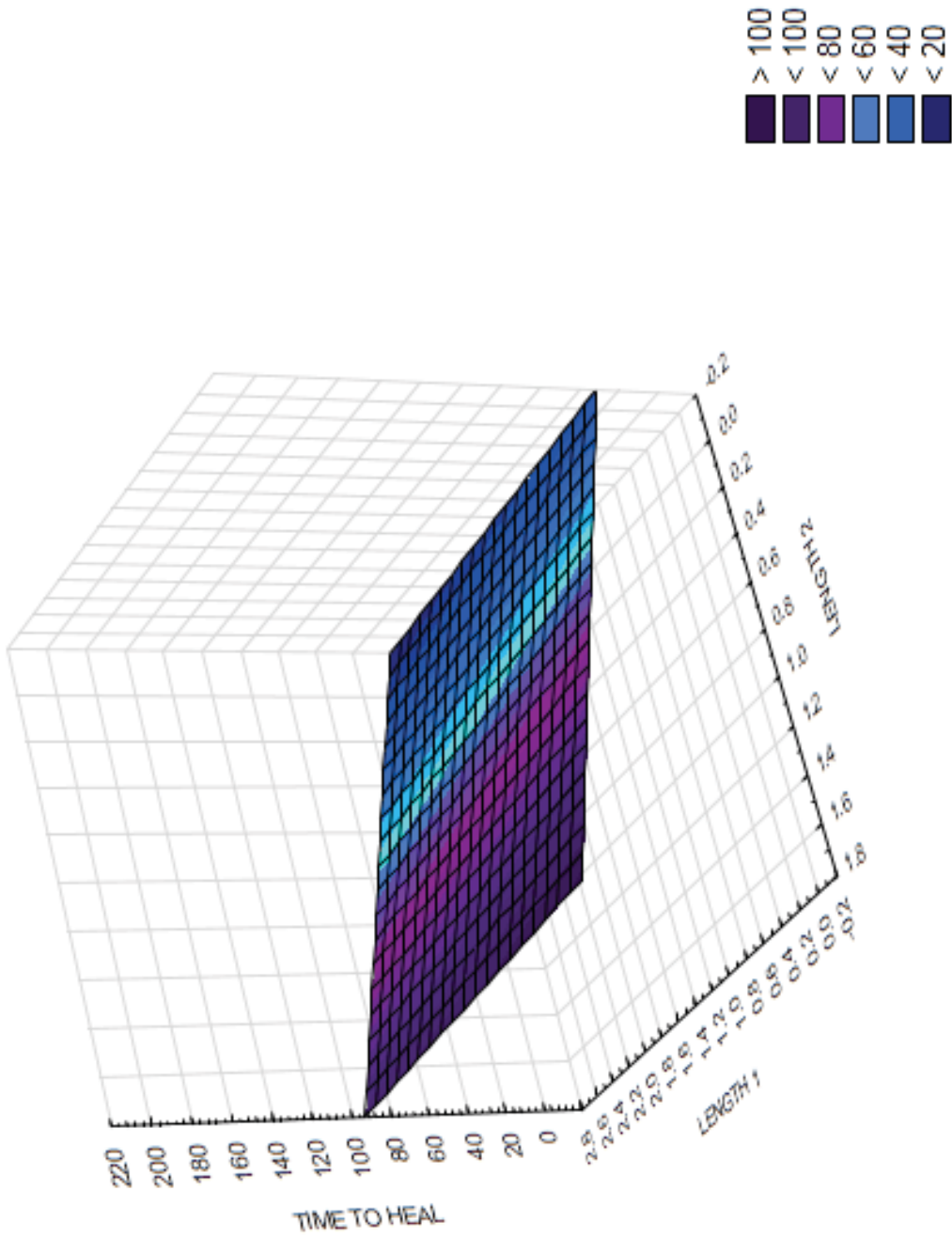


FIGURE 10.8: SURFACE PLOT: TIME TO HEAL AGAINST LENGTH 1, LENGTH 2 (LINEAR FIT)

3D Surface Plot of DEPTH against LENGTH 1 and LENGTH 2
 $DEPTH = 0.0639 + 0.1132x + 0.0737y - 0.0112x^2 - 0.1383xy + 0.0553y^2$

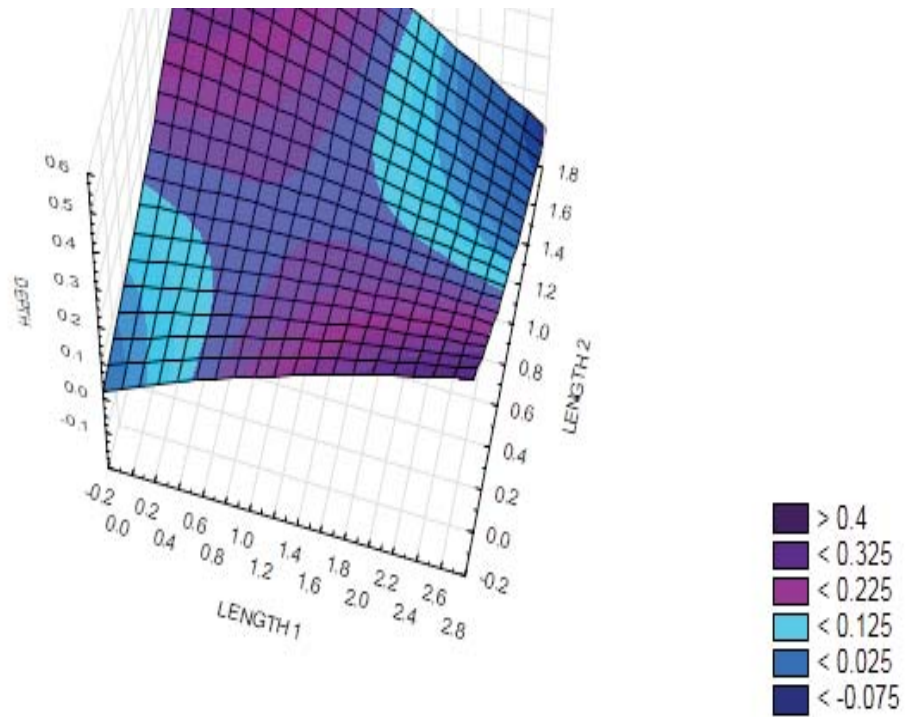
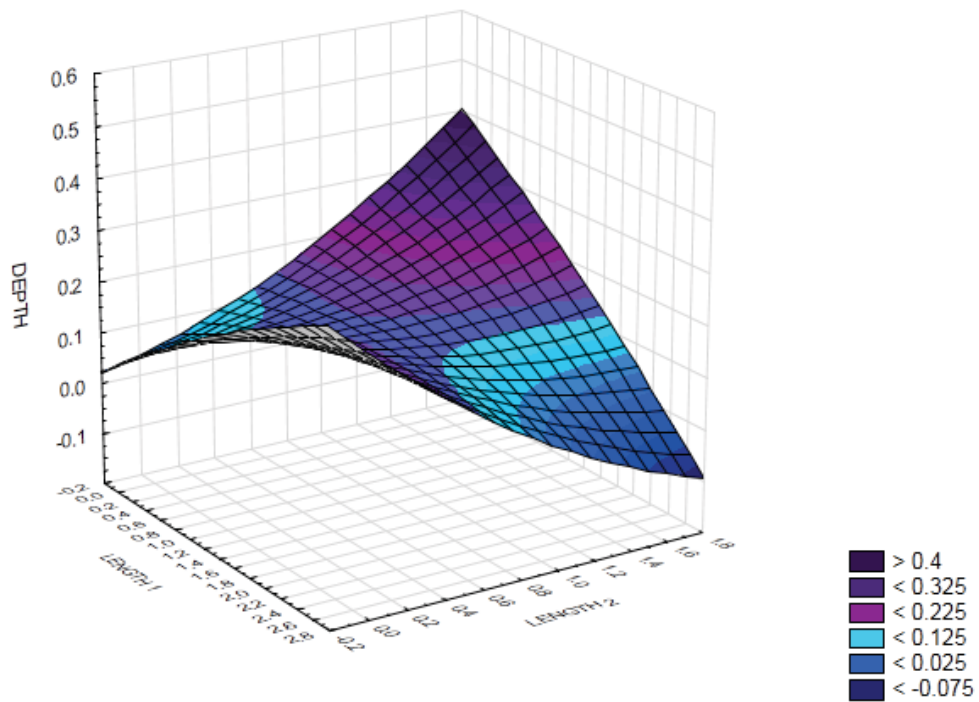


FIGURE 10.9: SURFACE PLOT: TIME TO HEAL AGAINST LENGTH 1, LENGTH 2 (QUADRATIC FIT)

3D Surface Plot of DEPTH against LENGTH 1 and LENGTH 2

$$\text{DEPTH} = 0.116 - 0.0448 * x + 0.0735 * y$$

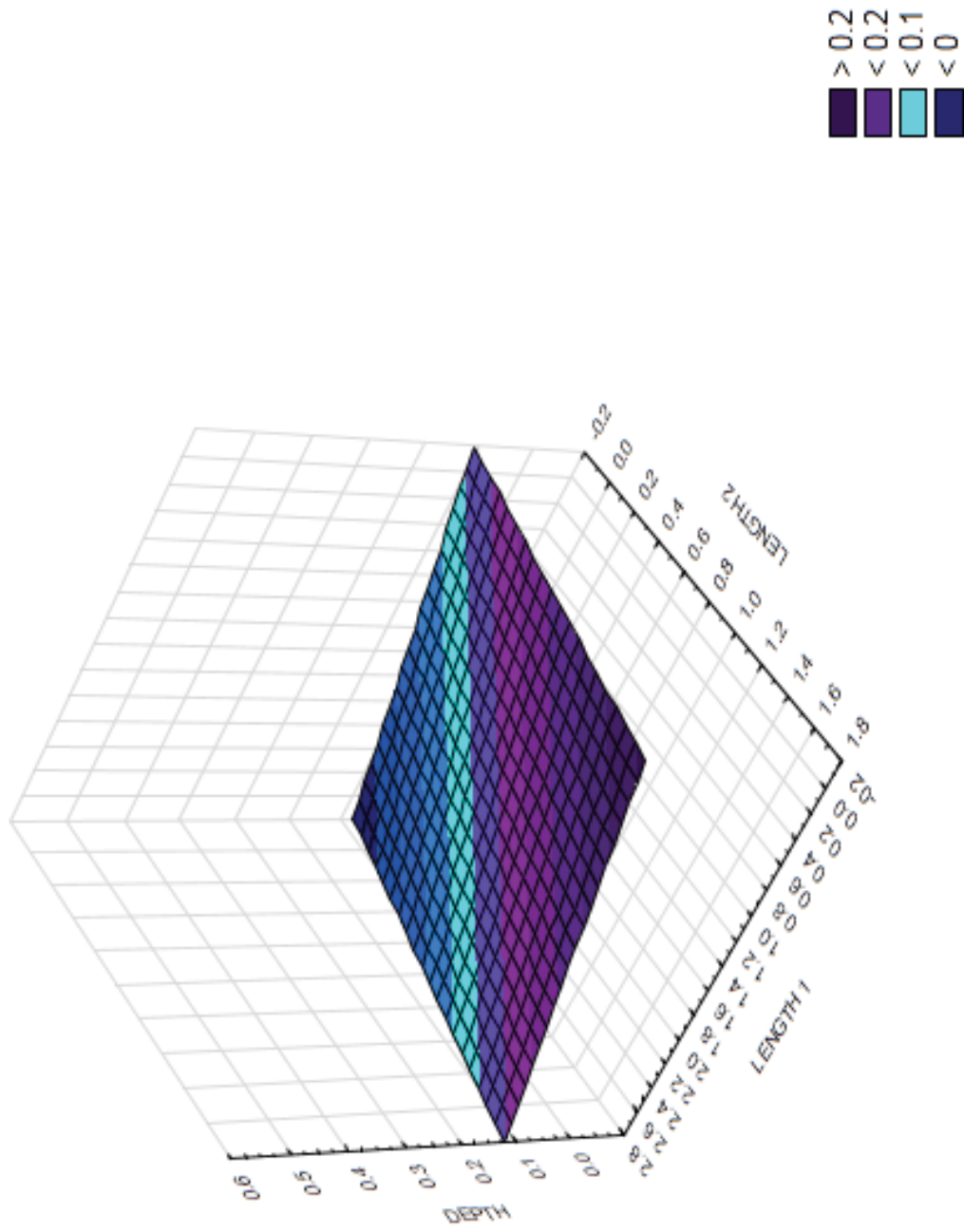


FIGURE 10.10: SURFACE PLOT: TIME TO HEAL AGAINST LENGTH 1, LENGTH 2 (SPLINE FIT)

3D Surface Plot of DEPTH against LENGTH 1 and LENGTH 2
 DEPTH = Spline

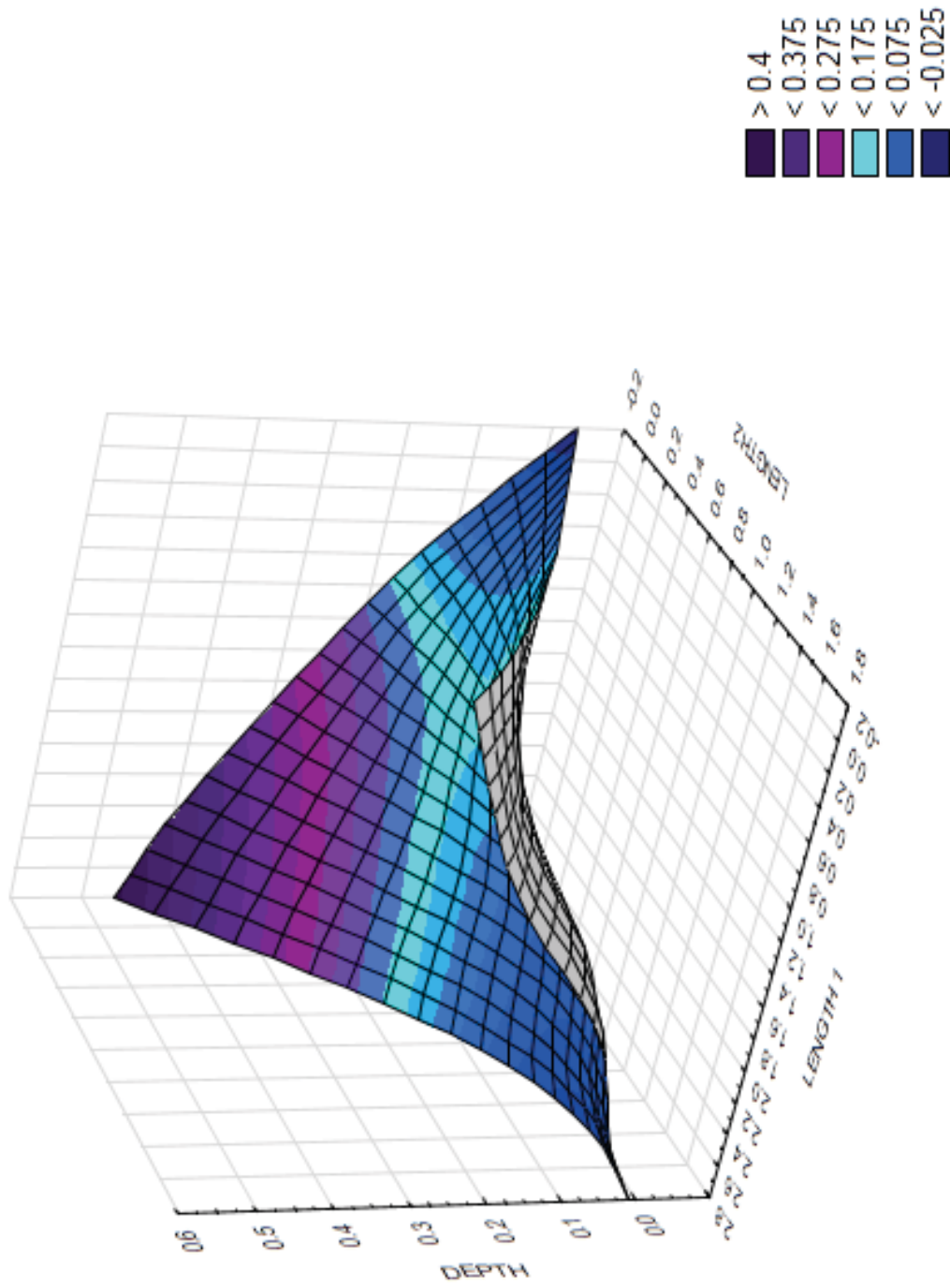


FIGURE 10.11: SURFACE PLOT: TIME TO HEAL AGAINST LENGTH 1, DEPTH (LINEAR FIT)

3D Surface Plot of TIME TO HEAL against LENGTH 1 and DEPTH

$$\text{TIME TO HEAL} = -4.0617 + 33.9564x + 438.1807y - 13.1835x^2x + 150.6536x^2y - 871.3826y^2y$$

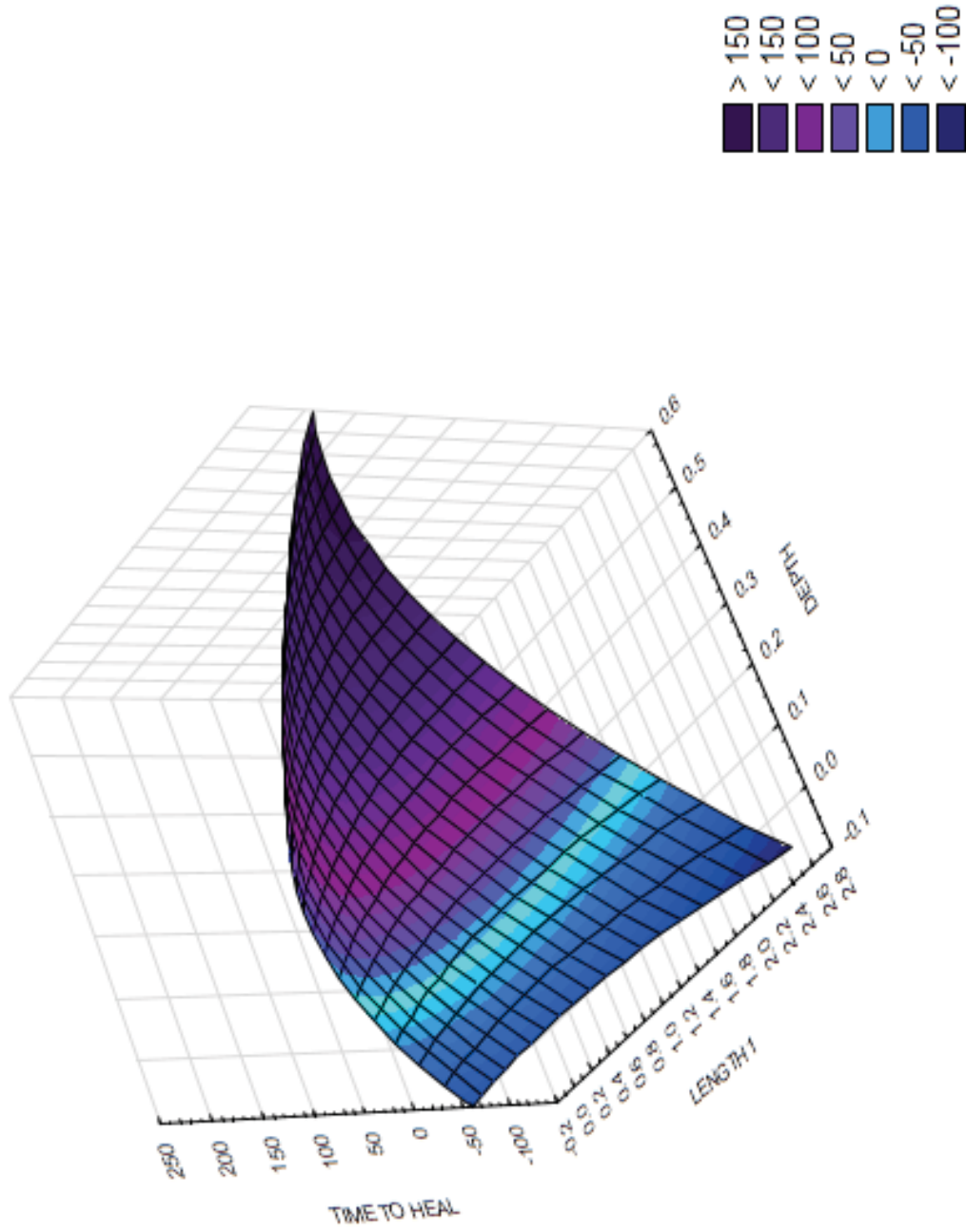


FIGURE 10.12: SURFACE PLOT: TIME TO HEAL AGAINST LENGTH 1, DEPTH (SPLINE FIT)

3D Surface Plot of TIME TO HEAL against LENGTH 1 and DEPTH
 TIME TO HEAL = Spline

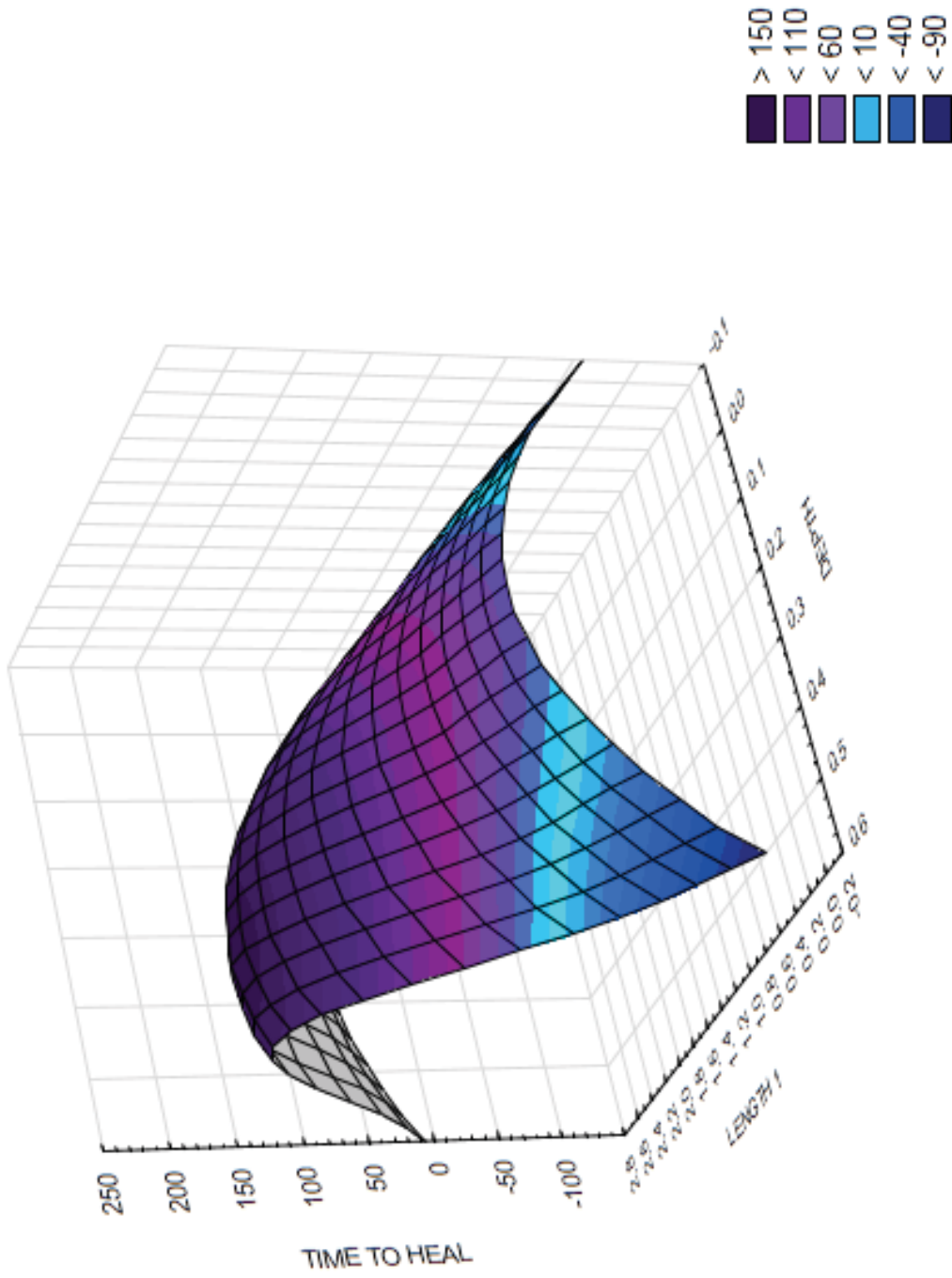


FIGURE 10.13: SURFACE PLOT: TIME TO HEAL AGAINST LENGTH 1, DEPTH (LINEAR FIT)

3D Surface Plot of TIME TO HEAL against LENGTH 1 and DEPTH
 $\text{TIME TO HEAL} = 10.3229 + 16.6138x + 280.6333y$

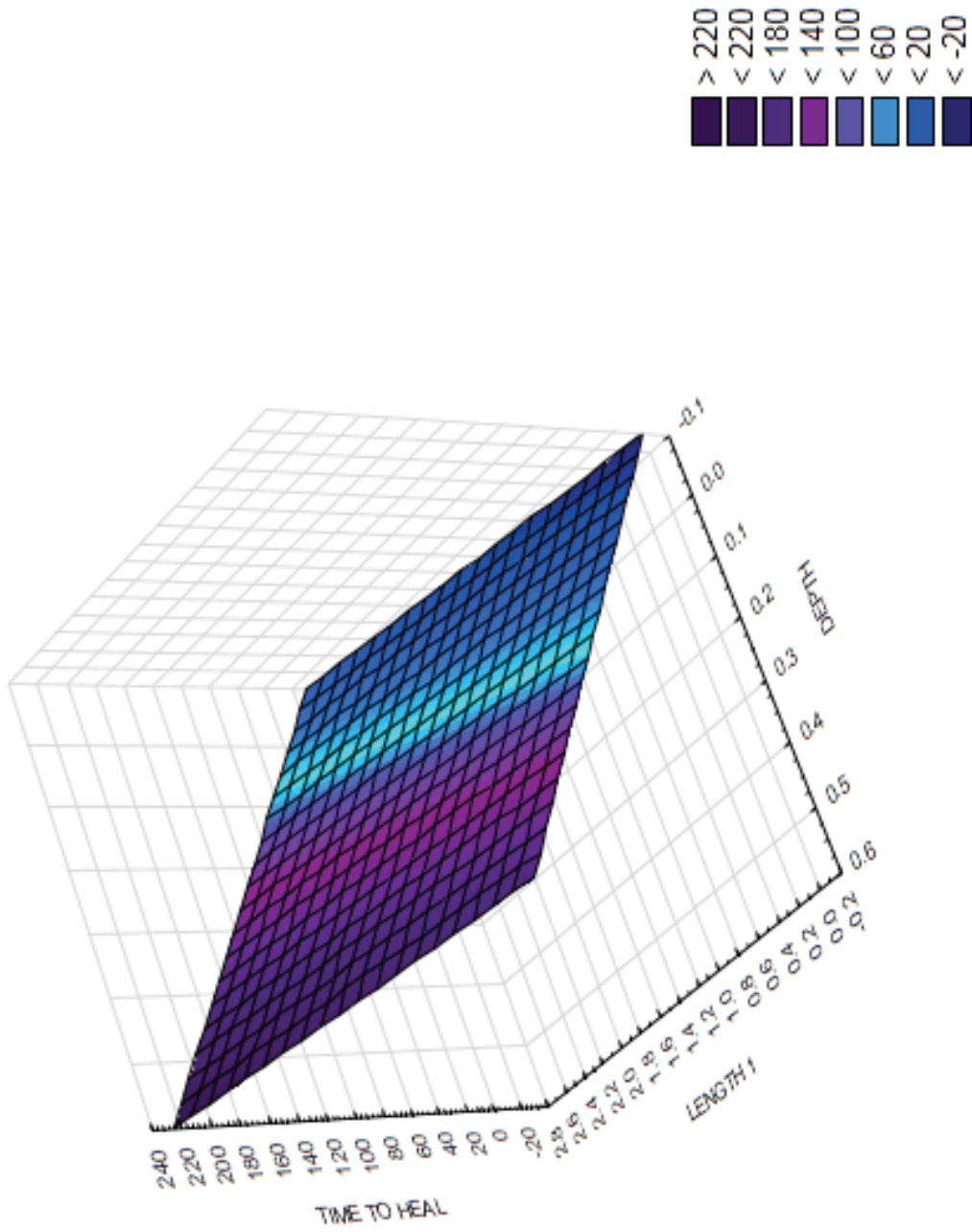


FIGURE 10.14: SURFACE PLOT: TIME TO HEAL AGAINST LENGTH 1, DEPTH (LINEAR FIT)

3D Surface Plot of TIME TO HEAL against LENGTH 2 and DEPTH

$$\text{TIME TO HEAL} = 6.9487 - 54.1337x + 665.0938y + 49.9416x^2 - 29.1442x^2y - 1137.8257y^2$$

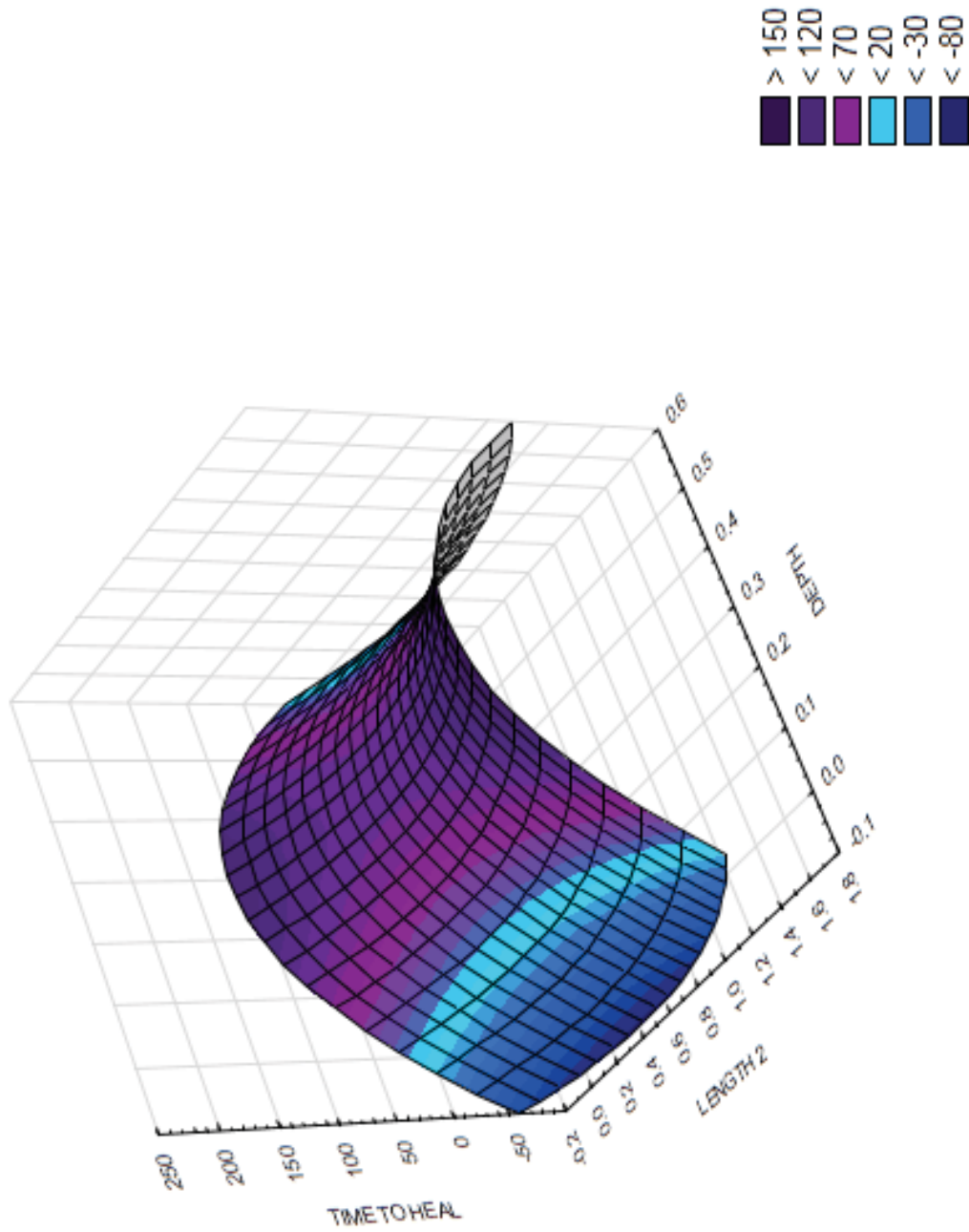


FIGURE 10.15: SURFACE PLOT: TIME TO HEAL AGAINST LENGTH 2, DEPTH (QUADRATIC FIT)

3D Surface Plot of TIME TO HEAL against LENGTH 2 and DEPTH
 TIME TO HEAL = Spline

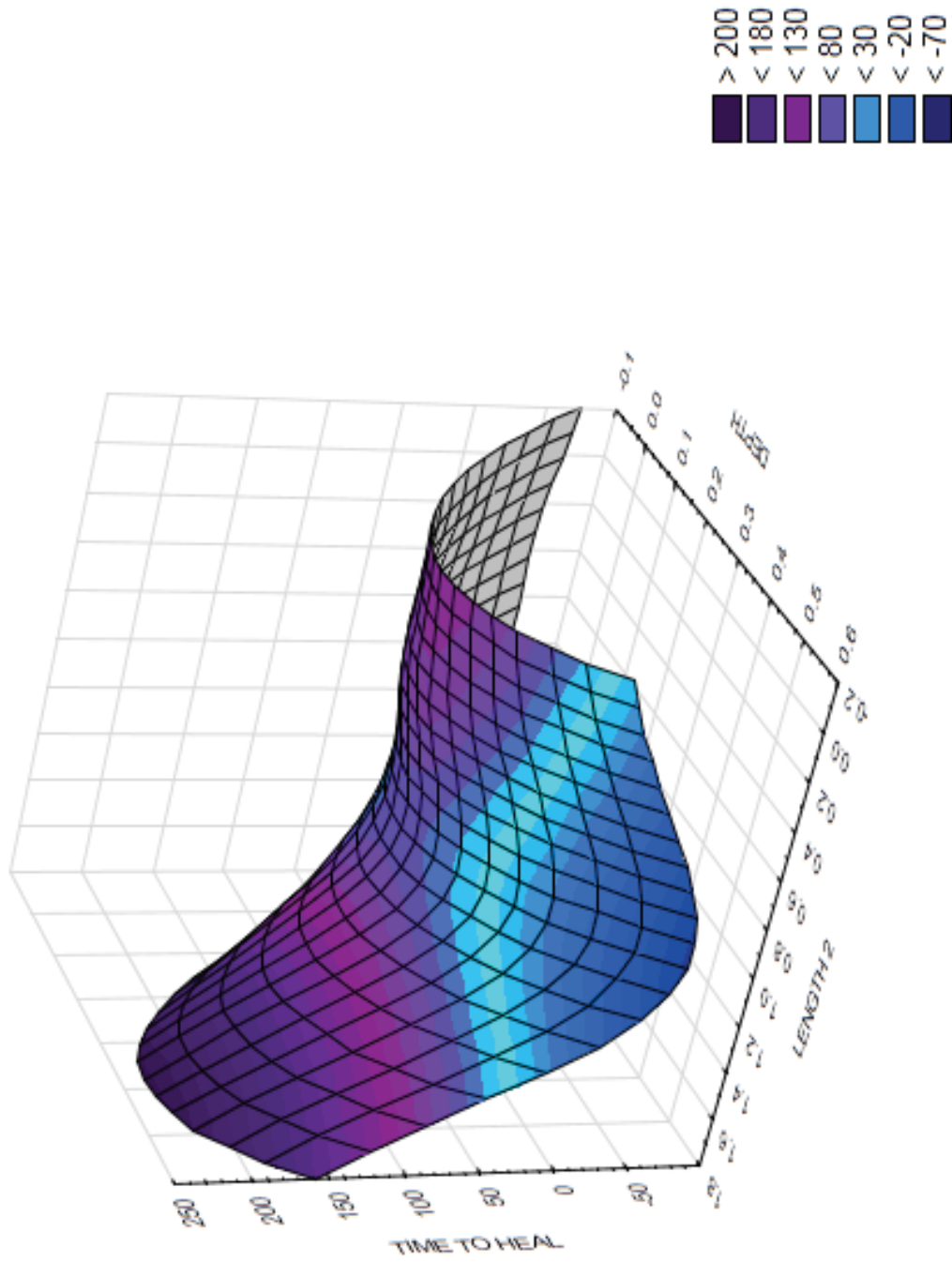


FIGURE 10.16: SURFACE PLOT: TIME TO HEAL AGAINST LENGTH 2, DEPTH (SPLINE FIT)

3D Surface Plot of TIME TO HEAL against LENGTH 2 and DEPTH
 $\text{TIME TO HEAL} = 10.4336 + 24.1022x + 252.2659y$

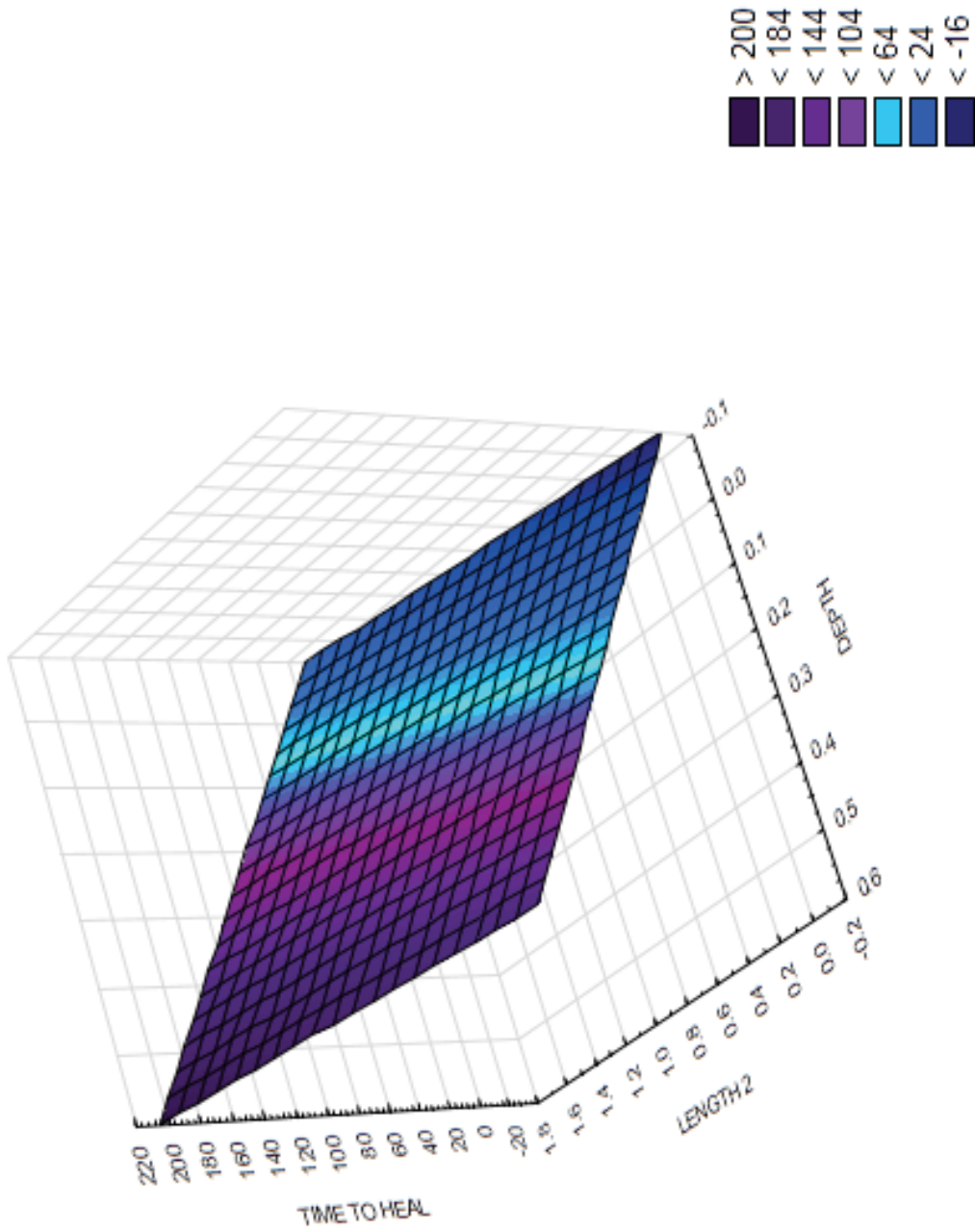


FIGURE 10.17: SURFACE PLOT: TIME TO HEAL AGAINST LENGTH 2, DEPTH (LINEAR FIT)

10.4 VALIDATING PREDICTIVE MODELS AND THE METHODOLOGY

10.4.1 MULTIPLE LINEAR-REGRESSION MODEL, RBMC

The multiple linear-regression models also showed predictive capabilities. Although the expectation for accuracy was greater for the neural-network model, the linear-regression model produced better predictive capabilities, resulting in approximately ± 5.55 -day accuracy.

TABLE 10.4: MULTIPLE LINEAR-REGRESSION MODEL VARIABLES, RBMC DATA

Variables	
Number of input variables	5
Input Variables	Length 1, Length 2, depth, granulation, black necrotic tissue
Output variable	Time remaining

TABLE 10.5: MULTIPLE LINEAR-REGRESSION MODEL PARAMETERS, RBMC DATA

Regression Model				
Input variables	Coefficient	Standard Error	p-value	SS
Constant term	-26.15	13.67	0.06	155107.69
Length 1	2.46	12.83	0.85	839.47
Length 2	52.12	19.34	0.01	3744.70
Depth	264.32	74.42	0.00	35630.03
Granulation	0.48	0.13	0.00	31331.90
Black necrotic tissue	-0.26	0.16	0.11	3488.11

The regression-model statistics include the degrees of freedom, standard deviation, and R^2 (Table 10.6). These statistics represent characteristics about this linear-regression model.

TABLE 10.6: MULTIPLE LINEAR-REGRESSION MODEL PARAMETERS, RBMC DATA

Input variables	Coefficient
Residual DF	46
R^2	0.56
Standard deviation estimate	36.14
Residual SS	60082.11

The corresponding data in Table 10.5 establishes the linear-regression predictive model (Equation(10.1)). This model produces an RMS error of 44.47 days and an average error of approximately ± 5.55 days (Table 10.7).

$$\text{Time to Heal} = 2.46(L1) + 52.12(L2) + 264.32(D) + 0.48(G) - 0.26(BN) - 26.15 \quad (10.1)$$

TABLE 10.7: TRAINING AND VALIDATION DATA SCORING REPORT FOR RBMC DATA

Training-Data Scoring			Validation-Data Scoring		
Total sum of squared errors	RMS error	Average error	Total sum of squared errors	RMS error	Average error
60082.11	33.99	0.00	43497.94	44.47	-5.55

10.4.2 NONLINEAR REGRESSION: COX PROPORTIONAL HAZARDS MODEL

The Cox Proportional hazard model assumes that enough data exists to train a regression model and have it understand the difference between a healed and an unhealed wound. With the data from RBMC, there is insufficient wound range for the model to understand and recognize what a healed-wound model. As a result, the survival function has a different shape from the curve using the feedback from the Vohra data (Figure 10.18).

Equation (10.2) describes the hazard function equation for the RBMC data. This function, similar to the analysis in Section 9.2, allows the calculation of the survival function to determine the individual wound-trajectory algorithms.

$$h(t) = [h_0(t)] * e^{0.037L1 - 0.0862 - 8.142D} \quad (10.2)$$

Table 10.8 and Table 10.9 provide the summary statistics of the ratio of hazard rates and the percentage change that equates to one unit of change per predictor variable.

TABLE 10.8: RATIO OF HAZARD RATES

	Variable Constants		
	B	Exp(B)	Changed (%)
Length 1	0.037	1.037	3.70
Length 2	-0.086	0.918	8.20
Depth	-8.142	0.000	0.00

TABLE 10.9: COVARIATE MEANS

	Mean
Length_1	3.632
Length_2	2.468
Depth	0.20

We lack sufficient data on healed wounds to accurately use the survival-function plot of the mean of the covariates to predict when a wound would heal.

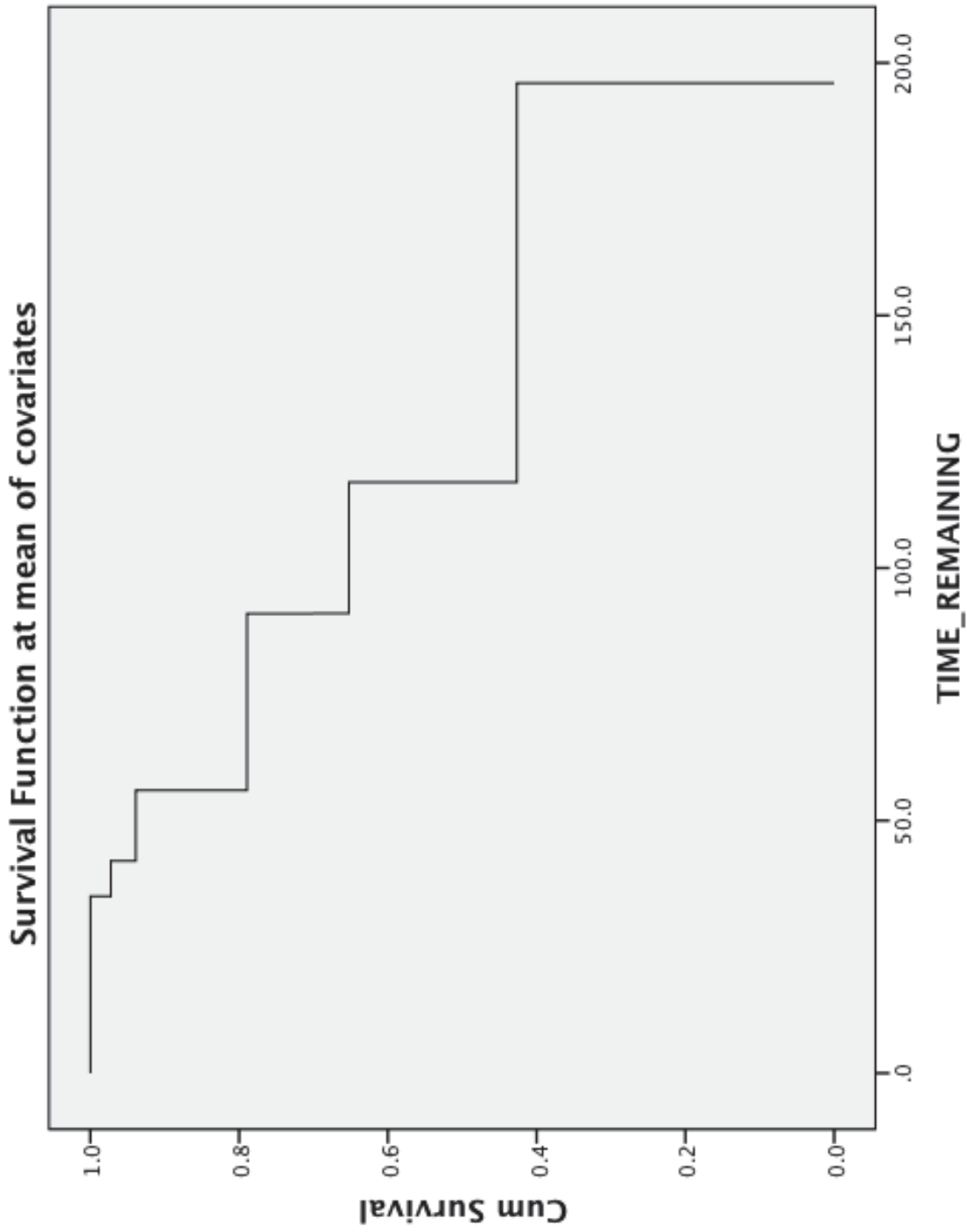


Figure 10.18: Survival Function at Mean of Covariates

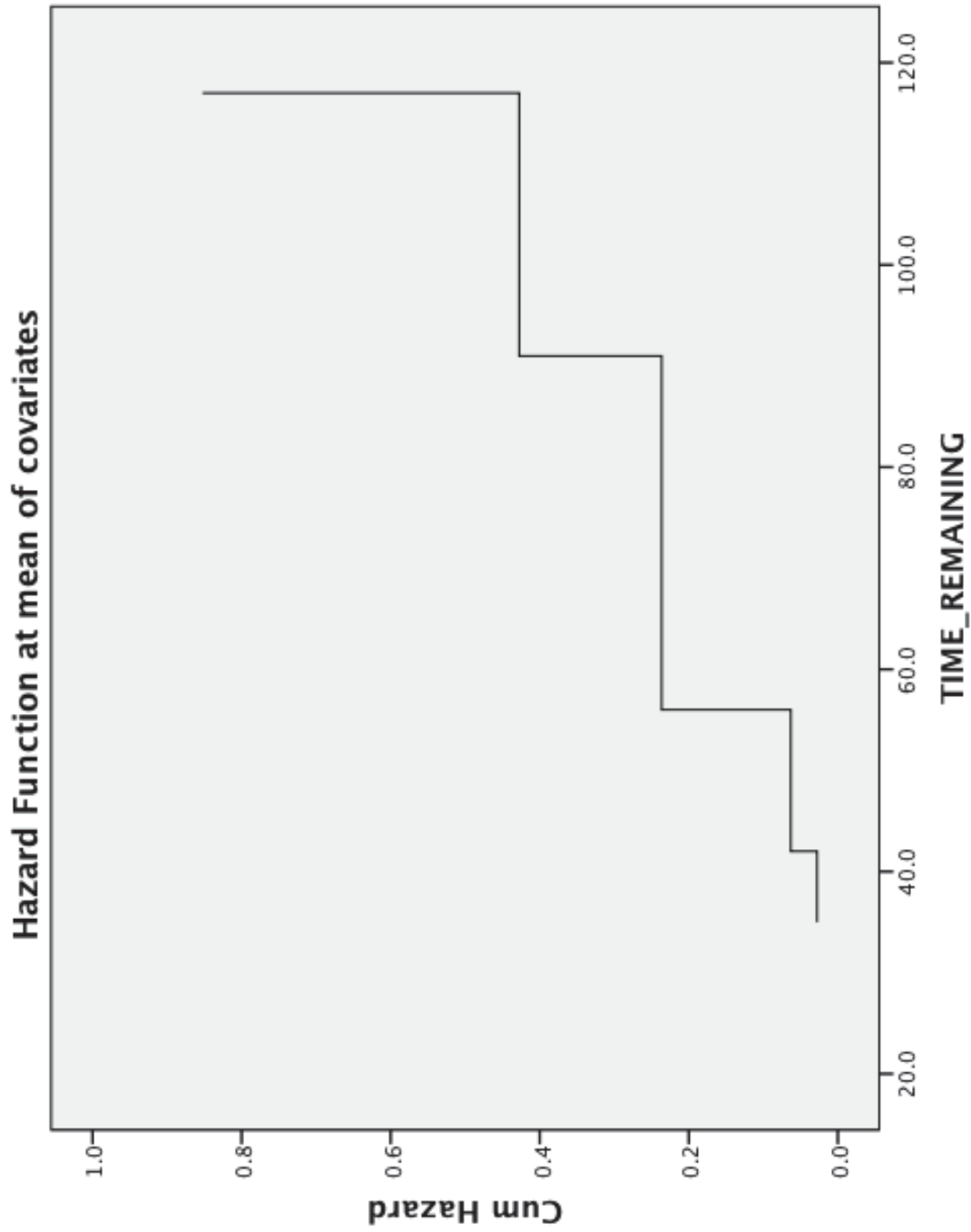


Figure 10.19: Hazard Function, RBMC

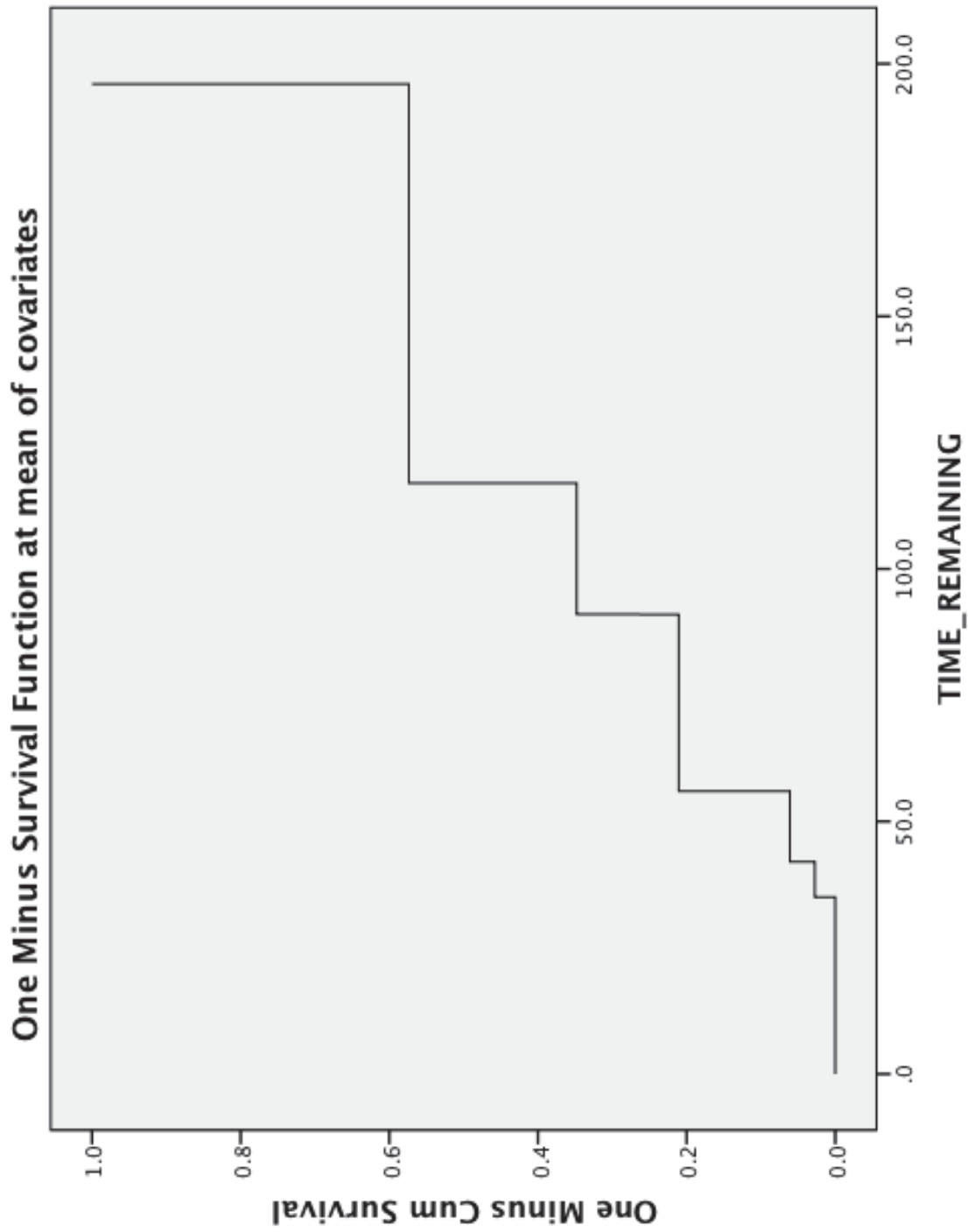


Figure 10.20: One Minus Survival Function at Mean of Covariates

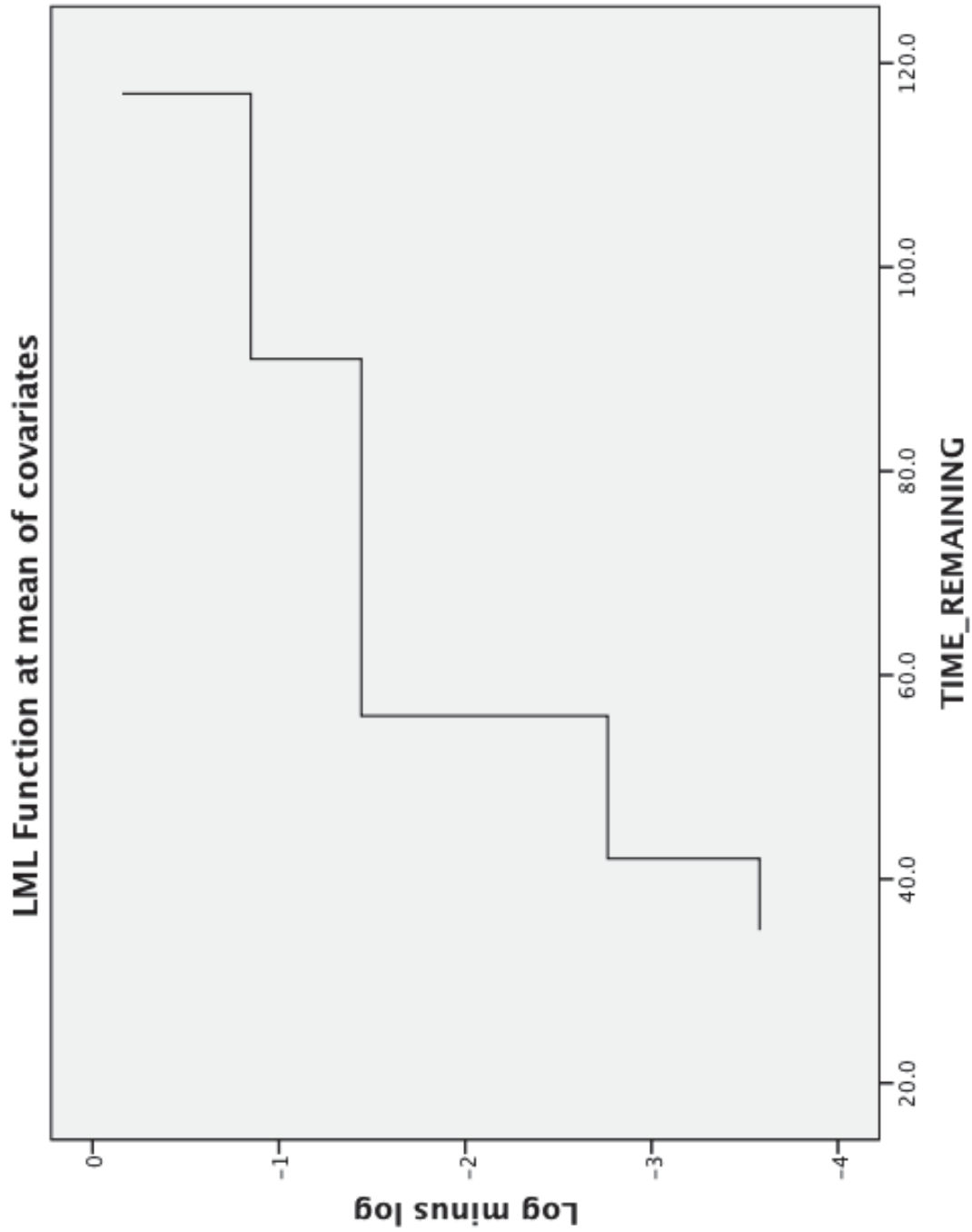


FIGURE 10.21: LOG MINUS LOG FUNCTION

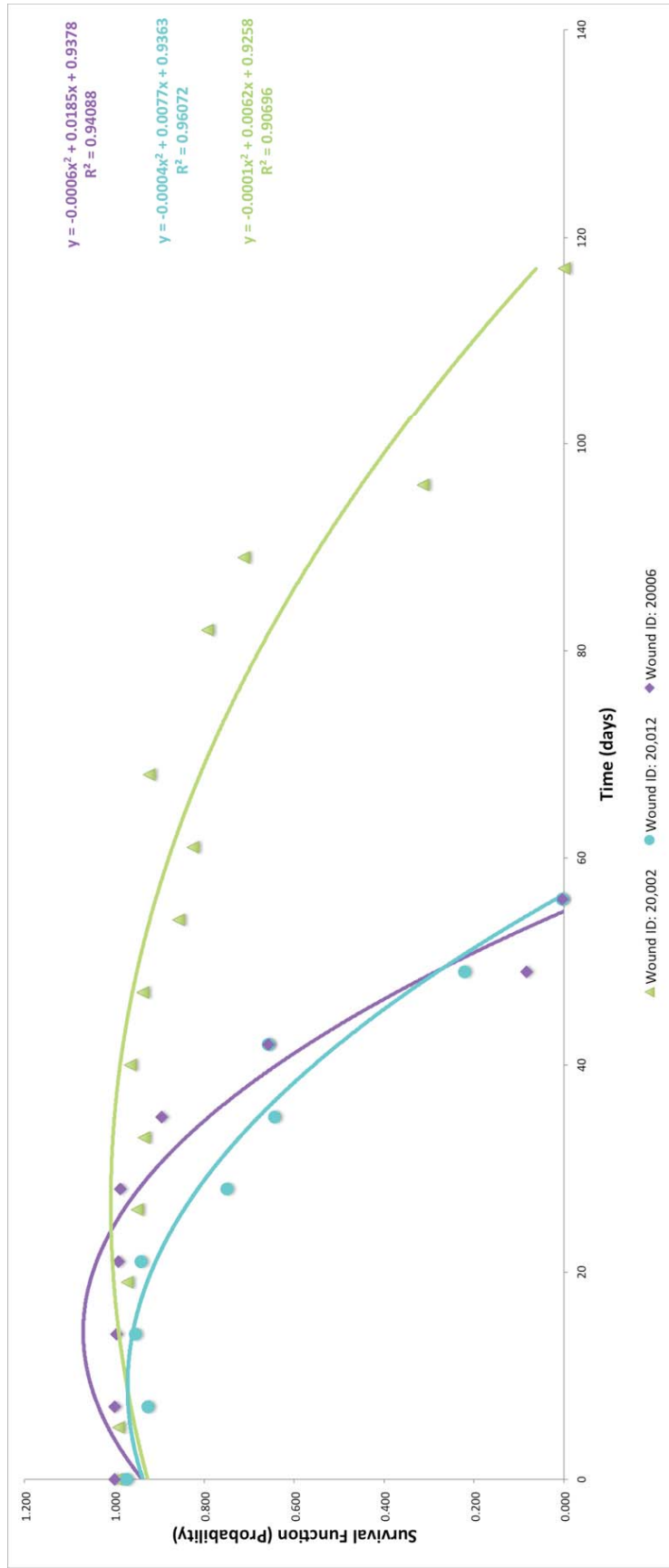


FIGURE 10.22: EXAMPLE OF SURVIVAL FUNCTION VS. TIME FOR SAMPLE WOUNDS (VARIABLES: L1, L2, D), RBMC

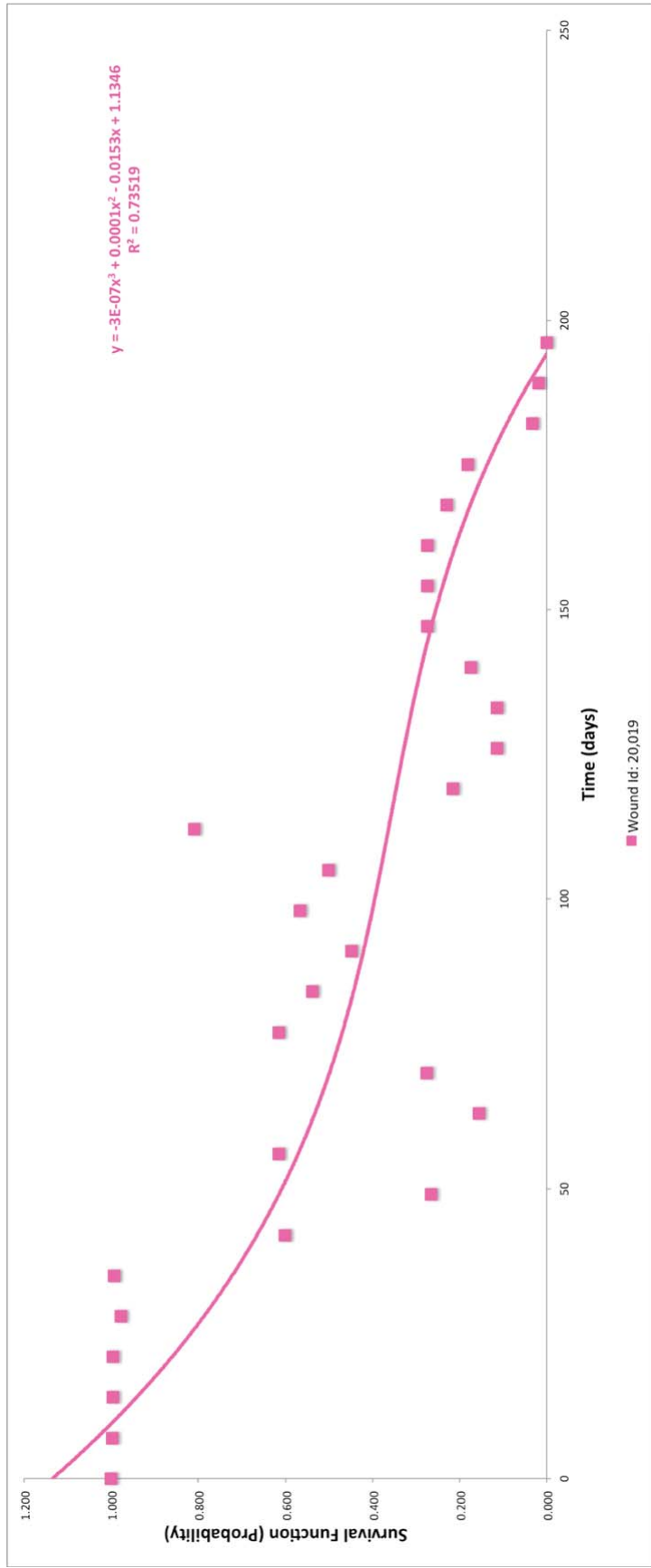


FIGURE 10.23: EXAMPLE OF SURVIVAL FUNCTION VS. TIME FOR SAMPLE WOUNDS (VARIABLES: L1, L2, D), RBMC

Similar to plots in Section 9.2, Figure 10.22 is a plot of three example wounds and their projected survival time. As model verification, we plotted the survival versus time for each wound. This plot allows us to approximate a regression equation for that wound and the time at which survival will equal zero. Figure 10.23 provides the graphical representation of the survival-function probability for one wound. We included this plot because it was the longest tracked wound that we have documented. Figure 10.23 shows the complexity of wound healing. Additionally, it represents typical and somewhat erratic behavior of wound healing and how factors can influence the healing time of a chronic wound. In many cases, wounds must become larger before they get smaller, which seems counterintuitive. Yet it emphasizes the complexity of the human body and the healing process.

We verified the methodology through the calculated numerical value of the survival function. The resulting outputs led each wound to have a set of survival-function outputs that correspond to their respective time, t . The data from Figure 10.22 shows how we arrived at the respective calculations and, ultimately, the regression equation.

Equation (10.3) expresses the ratio of the hazard function at time t to the baseline hazard function or the mean of the covariates. This ratio allows us to understand how a wound at time t changes compared with the hazard function when all predictive covariates are equal to zero.

$$\frac{h(t)}{h_0(t)} = e^{-3.451L1-1.508L2-1.299D} \quad (10.3)$$

The baseline survival function was determined as a function of the baseline hazard function:

$$S_0(t) = e^{-H_0(t)} \quad (10.4)$$

The survival function as a constant power of the baseline survival function is given by:

$$S_i(t) = [S_0(t)]^{e^{-3.451L1-1.508L2-1.299D}} \quad (10.5)$$

Table 10.10 documents the wound plotted in Figure 10.23 with the respective numerical values of the variables in equations 10.3, 10.4, and 10.5. Figure 10.23 is a plot of the survival function versus time in Table 8.6 versus Time (Column 2 in Table 10.10). Equation (10.6) yields the approximate regression equation for the best-fit line in Figure 10.23:

$$S_i(t) = (-3E - 07)x^3 + 0.0001x^2 - 0.0153x + 1.1346 @ S_i(t) = 0 \quad (10.6)$$

Solving Equation (10.6) at $S_i(t) = 0$ produces three roots. The only positive root is the wound's approximate healing day. The root of the equation represents the number of days since the wound was conceived at $t = 0$. For this patient's wound, the approximate day of healing is the 163rd day since the patient first visited a wound clinic. This calculation results in approximately a 17% error, or approximately four weeks.

$$Error = \frac{(estimate - actual)}{actual} = \frac{163 - 196}{196} = -.1684 \rightarrow -16.84\% \quad (10.7)$$

Although we would have preferred a smaller error, a tolerance of four weeks for a wound to heal is an adequate tolerance for an individual that would have had a wound for nearly six months. A number of factors contribute to wound healing, many of which only the patient can control.

TABLE 10.10: WOUND DATA THAT CORRESPONDS TO PLOT IN FIGURE 10.23

Wound Number	Time (Days)	Healed or Unhealed	Baseline Hazard Function	Exponent	Ratio of Hazard Function to Baseline Hazard	Survival Function
20019	0	0	0.01	0.001	0.074	1.000
20019	7	0	0.01	0.003	0.329	0.997
20019	14	0	0.01	0.003	0.329	0.997
20019	21	0	0.01	0.003	0.329	0.995
20019	28	0	0.01	0.012	1.279	0.978
20019	35	0	0.10	0.003	0.027	0.993
20019	42	0	0.22	0.147	0.667	0.601
20019	49	0	0.49	0.286	0.580	0.265
20019	56	0	0.86	0.086	0.100	0.615
20019	63	0	0.86	0.286	0.334	0.156
20019	70	0	0.86	0.174	0.204	0.276
20019	77	0	0.86	0.056	0.065	0.614
20019	84	0	0.86	0.053	0.062	0.538
20019	91	0	1.12	0.053	0.047	0.447
20019	98	0	1.12	0.038	0.034	0.566
20019	105	0	1.12	0.046	0.041	0.501
20019	112	0	1.12	0.014	0.012	0.810
20019	119	0	1.46	0.102	0.069	0.215
20019	126	0	1.46	0.143	0.098	0.114
20019	133	0	1.46	0.143	0.098	0.114
20019	140	0	1.46	0.116	0.079	0.174
20019	147	0	1.46	0.086	0.058	0.274
20019	154	0	1.46	0.086	0.058	0.274
20019	161	0	1.46	0.086	0.058	0.274
20019	168	0	1.46	0.097	0.067	0.229
20019	175	0	1.46	0.113	0.077	0.180
20019	182	1	2.19	0.226	0.103	0.033
20019	189	1	3.08	0.263	0.085	0.019
20019	196	1	3.08	1.000	0.325	0.000

10.4.3 NEURAL-NETWORK MODEL BASED ON DATA FROM RBMC

For this study, we analyzed 22 unique wounds with 240 documented visits. Because the model is a time-varying analysis, each wound had a minimum of five recorded clinic visits. For the data, the neural-network model that fits this data has an average validation-scoring error of ± 1.40 days, indicating that the model had accurate predictive capabilities. However, the RMS error was relatively high indicating that the data does not follow a specific pattern. A similarly high standard deviation of 53.12 days for the original output also results in a high RMS error. We attribute the high standard deviation and RMS to human inconsistencies that naturally occur in wound measurement. Table 10.11 shows these neural-network model parameters.

TABLE 10.11: NEURAL-NETWORK PREDICTION VARIABLES AND PARAMETERS, RBMC DATA

Variables		Parameter/Options	
Number of input variables	4	Number of hidden layers	1
Input variables	Length 1, Length 2, depth, granulation, black necrotic tissue	# Nodes in HiddenLayer-1	1
Output variable	Time remaining	Number of epochs	30
		Step size for gradient descent	0.01
		Weight-change momentum	0.6
		Error tolerance	0.01
		Weight decay	0

Table 10.12 shows the training- and validation-data scoring report. The average error for this model is ± 0.618 and ± 1.40 days for the training- and validation-data scoring, respectively.

TABLE 10.12: TRAINING- AND VALIDATION-DATA SCORING REPORT FOR RBMC DATA

Training-Data Scoring			Validation-Data Scoring		
Total sum of squared errors	RMS error	Average error	Total sum of squared errors	RMS error	Average error
70405.461	36.796	-0.6177	46119.47495	45.786	1.4025

The study at RBMC validates the methodology for developing a model for the prediction of wound healing. Through the verification and validation, we found that it is difficult to develop one algorithmic model for all wound clinics due to the extensive number of factors that contribute to wound healing. Chapter 11 will further discuss this topic.

CHAPTER ELEVEN ANALYSIS OF WOUND COMPUTATIONAL MODELS

CHAPTER 11

Analysis of Wound Computational Models

The ability to predict when chronic wounds heal is a challenging task. Many chronic wounds become chronic because of a number of uncontrollable factors. Factors that influence the length of time to heal include age, weight, family history, nutrition, and compliance of the patient. Physicians cannot control many — if any — of these factors. With that understanding, the objective is to find the best course of treatment to efficiently heal and close the wound. Wound clinics differ greatly from each, providing an eye-opening experience on the quality of patient care.

11.1 IMPLICATIONS

The purpose of this research and study was to design and develop predictive models to estimate the time to heal for chronic wounds. Our research hypothesized that a predictive model and algorithm could be accurate and robust, provided that the predictor variables were independent of each other. This dissertation resulted in four distinct contributions: 1) Methodologies to design, develop, and implement predictive models to estimate chronic wound healing; 2) Linear, nonlinear, and neural network predictive algorithms to estimate time to heal for chronic wounds; 3) Using CAD to create a three-dimensional model of a patient's wound to better calculate surface area and volume; and 4) Routine chronic wound management from an engineering perspective for wound-care clinics.

The methodology was created to develop more effective processes to track, monitor, and predict time to heal for chronic, nonhealing wounds. The overall methodology in Figure 7.1 shows the inconsistencies and limitations of current predictive methods for chronic wounds. What has since

materialized from the original hypothesis were smaller, parallel subprocesses that could assist in chronic wound-care tracking and predictive capabilities.

Subprocesses include better understanding the limitations of the technology infrastructure, better integration and more consistent incorporation of digital imaging, and the ability to use mathematical algorithms to assist in approximating the time to wound closure. We further focused on how to understand, clean, and use large data sets to develop robust and accurate predictive algorithms.

To reach the stage of algorithm development, the raw data of wounds had to be unidentified and cleaned. Vohra's EMR system unidentified data before this study began, but we had to develop a coding and patient unidentification process for the data set from RBMC. With thousands of wound measurements, we developed mini processes and coding structures to ensure the quality and thoroughness of the data (Figure 8.3 and Figure 8.4). The mini code explorations allowed us to better understand the data for statistical exploration. Additionally, we developed processes and coding structures (Figure 8.11) to properly analyze the surface areas of wounds. Image analysis and boundary-detection algorithms provided a more realistic analysis and measurement of wounds than human measurement. Image integration in wound clinics with the right image-analysis software can also provide a more accurate measurement in the percentage change from week to week for chronic wounds than human measurement can provide. The processes and methods in the clinics must be efficient, more routine, and better standardized in their wound-photography practices.

Before the visits to these wound clinics, we assumed that the incorporation of tools such as digital camera would be an easy adaptation. However, no modification proved easy. Clinics provide a specific amount of time to each patient, have a limited number of nurses, and have technology restrictions. Many of these clinics must focus on efficiency and patient care rather than wound photography. Unfortunately, there appears to be a discrepancy with regard to the value of properly performed wound photography and its contribution to patient and wound information.

From an engineering and processes perspective, those wound clinics that incorporated photographs in the patient record lacked the proper tools and procedures to correctly integrate photos with patient wound tracking. A major issue with wound photographs is how to centralize patients' photographs and EMRs. When hospitals began to migrate from paper records to electronic medical records, most hospitals used one EMR system for every department. Unfortunately, one EMR system does not meet the needs of all departments, including wound-care

departments. For example, wound-care clinics must record dimensions and qualitative visual information about the wound. Descriptive analyses about the wound's color, density, and bacteria provide insight into the health of both the wound and the patient.

Further, clinicians measure the progress of wounds, especially chronic wounds, by their size and change in size from week to week. For example, the size of a wound from week could decrease by as little as 0.25 cm. However, anyone measuring the wound could come up with a slightly different measurement; staff members in wound clinics have their own methods of measuring wounds. Thus, digital image processing and analysis become more important. However, a lack of consistency exists in wound photography. Photography issues include blurriness, external flash, lack of a ruler, or even a skewed perspective (Figure 11.1). Clinics can nevertheless correct these issues by providing staff members with proper training. A more serious issue, however, is that wound clinics lack wound-care statistics in their EMR systems and thus cannot connect wound photographs with patient records. This problem in turn makes it difficult for clinicians compare, monitor, and analyze changes in the wound, such as size and color, over weeks or months. These inefficiencies have led wound photography to be a hindrance rather than a help.

One of the goals of this research was to properly determine the appropriate wound parameters and characteristics for predicting the time to heal for chronic wounds. Each wound clinic we visited contributed different insights on standard practice and patient care. Through site observation, we gained knowledge about what clinics require, how they report wounds conditions, and how many moving components contribute to how they treat nonhealing wounds. Two of the four clinic sites, Tufts and Morganti, enabled us to become familiar with wound-care clinic practice. We used the other two sites, RBMC and Vohra, for both content knowledge and physical data collection and acquisition.

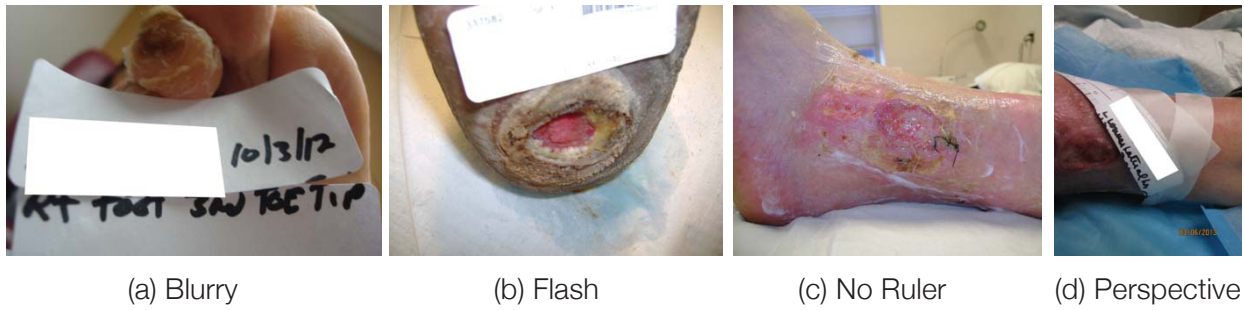


FIGURE 11.1: VARIOUS IMAGING ISSUES

We conceived this research under the assumption that the inputs to the algorithm would include a variety of inputs ranging from patient demographics to wound characteristics to patient health history. Unfortunately, that assumption proved incorrect. Instead, we received most of the data from the Vohra clinic rather than the hospitals. Unlike the hospitals, Vohra has its own proprietary wound-tracking database that allowed clinicians to document patient progress through a customized EMR system. With this tool, clinicians could sort, filter, and organize patient data based on the requirements for wound characteristics. As a result, we were able to obtain data for thousands of patients and thousands of wounds. Through multiple discussions and analysis, physicians at Vohra assisted us in determining the proper wound data based on their experience and clinician expertise.

The ability of people to acquire patient data from medical facilities has given rise to a number of patient privacy laws. This limitation worked against us in the collection of data. Vohra could provide us only information about patient wounds, not patient demographics. The lack of access to patient demographics was a limitation of the study, which Section 11.2 further discusses. However, we were able to build a solid, robust, and accurate model based only on wound characteristics.

We designed the algorithms in three phases. The first phase required us to determine the relevant inputs that the predictive model would include. The second phase required us to determine which predictive-modeling techniques best fit the data. The third phase required us to create a methodology that modeled wounds from two-dimensional images to three-dimensional models.

To determine the relevant inputs, we used statistical analysis to verify and confirm which covariates were significant to the development of the model. We used box plots to find the upper and lower limits for each covariate. We used correlation plots to determine variables of linearity. We also used correlation heat maps to establish independence between covariates and statistical analysis to

determine the relationships among each of the predictor variables and the output. This analysis led us to what we hypothesized: that the size of the wound has the greatest impact on the time to heal.

This statistical validation of the respective covariates showed that, despite the federal government's procedural standardization and regulations, little consistency exists across various clinics in the collection of patient data. This fact makes it difficult to create a universal algorithm for chronic wounds based on a characteristic such as the arterial, venous, or diabetic etiology of a wound. From an engineering perspective, the recorded information differs among clinics. In other words, the data that we received from Vohra included the dimensions of the wound, the percentage of characteristics such as granulation and necrotic tissue, blood flow, and nutrition. The only common patient statistics that all four clinics consistently collected were the dimensions of the wound and the granulation of the wound. This limitation added a level of unexpected complexity to the analysis.

We chose to explore multiple-regression, nonlinear-regression, and neural-network modeling techniques for compelling reasons. Linear regression is the simplest form of predictive modeling. Due to the complexity of the human body and the challenge of abnormal healing, we predicted that the behavior of the data would not follow a linear relationship. We did, however, believe that we needed to understand and analyze the data in the context of multiple linear regression. We explored and ultimately developed a linear model to compare the fit of the data with that of the other modeling techniques. We chose nonlinear regression because it includes foundation algorithms, such as exponential, quadratic, and logarithmic behaviors. We determined the best nonlinear-regression model would be based on the Cox regression algorithm.

Cox regression aids survival-time and time-to-event analysis. Unlike linear regression, Cox regression assumes entirely independent data points. As a result, we structured the data with one set of parameters for each wound, allowing us to focus only on whether the wound had healed by the completion of the study. We chose neural-network modeling because it is the most complex technique for analyzing the behavior of the data to predict the time to heal. Unfortunately, unlike the previous two modeling techniques, the final output is not a mathematical equation but a set of equation parameters. Comparing these modeling techniques using the same set of data provided insight into the overall behavior of chronic wound healing.

We used three data sets to evaluate the theory that the time to heal primarily depends on the size and surface area of a chronic wound. Chapter 6 discusses the sample data set that we initially acquired for preliminary study. We used this data set to test the behavior of the data and how chronic wounds heal over time. For this preliminary examination, we had less information about the patients and their wounds. Unlike the larger set of data, this preliminary data set did not come from a wound clinic but from other sources. However, this data set allowed us to perform initial regression and neural-network analysis to see whether we could establish credible algorithms using only the inputs of Length 1, Length 2, and depth. This study supported the belief that we could accurately predict the time to heal using mathematical algorithms.

The survival analysis and corresponding Cox regression proved to be a substantially better fit than the multiple linear-regression analysis. Using past literature and logic reasoning, we estimated that a chronic wound, regardless of the length of time it takes to heal, should reflect an exponential decline in behavior. Cox regression assumes that the behavior of the data follows an exponential decline and shows the relationship between the function, the analysis, and all the covariates. Through analysis, Cox regression enables us to examine the survival time of chronic wounds. The Cox regression analysis results in graphs that show the probability that the wound is healed at a given time t . Cox regression analysis not only provides a mathematical algorithm, but also validates the idea that only specific covariates truly affect the survival time of a chronic wound. Similarly, the descriptive statistics of the Cox model and corresponding coefficients validate how the behaviors of each of the variables affect the algorithm. Section 9.2 shows how each covariate affects the output. In other words, every time Length 1 increases by 1 cm., healing time increases by approximately 35%. Understanding how the variables affect the output is important in understanding how a unit of change affects the output using Cox regression. By understanding the effect of each variable, we can better predict the time to heal based on the change in surface area and dimensions and how each predictor variable affects the output.

Additionally, Cox-regression equations differ depending on whether they include covariates. We further analyzed this theory in the development of the second Cox regression model, which includes Length 1, Length 2, and depth. We included these variables because they are the most common predictors we collected across all wound clinics and because we theorized that these covariates had the greatest effect on the time left to heal. More important, Cox regression provides equations to validate the hypothesis of predicting time to heal.

The Cox proportional hazard model depends on the baseline hazard function and its corresponding coefficients of the respective covariates. Cox regression reinforces the notion that the probability a chronic wound will survive until a specific time t and thus translates it to patient benefits. Regardless of whether a patient has one wound, two wounds, or five wounds, each wound has a unique healing trajectory. Cox regression allows the mass customization of predictive models for wounds based on the patient's retrospective data (figures 9.18 and 9.19). We have created personalized wound-healing trajectories for the patients and their respective wounds. Cox regression models can also predict the best-fit regression equation and an estimated time to closure of a wound. Under these circumstances and with this data, this model was the most credible that we could create.

We conjectured that the neural-network model, unlike the previous two models, would perform better if we categorized wounds based on their initial aspect ratio. Aspect ratios provided interpretive information about the shape of each wound, relative to the first record of Length 1 and Length 2. Aspect ratios also allowed us to make certain generalizations. For example, the neural-network models showed that most wounds have aspect ratios of 1 to 2, representing Length 1 and Length 2, respectively. This aspect ratio, however, did not appear to affect the total sum of squared errors or the RMS error in either the training or the validation scoring. Sorting this data, however, provided us with a general understanding of the behavior of wounds with specific aspect ratios. For example, we observed that the wounds with aspect ratios of 1 to 2 got larger and then smaller over time rather than simply becoming smaller.

Neural networks provided us a framework for developing reliable, predictive models for chronic wounds and their time to heal. However, the development of a universal model was difficult without the ability to use patient demographics as additional factors within the algorithms. For various reasons, a number of observations supported the theory of an improbable universal predictive model. We observed human discrepancy across clinics that resulted in inconsistency with wound measurement and other factors.

We also investigated the difference in clinicians' wound-measuring techniques and a clinician and computerized wound-boundary determination. Clinicians have only the tools that the facilities provide. For most clinicians, these tools may include only a paper ruler. Given these facts, the accuracy and consistency of measurements from wound to wound can produce only so much information. We then investigated whether high-quality photographs of wounds with a ruler could provide more information about the size and shape of the wound. Thus, we developed a

combination of tools, subprocesses, and an overall methodology that produced a precise wound boundary and, ultimately, a three-dimensional virtual model of the wound.

Three-dimensional imaging and analysis provides us with more detail pertaining to the object of interest — in this case, chronic wounds. Using a combination of the Adobe Photoshop image-manipulation program, the ImageJ image-analysis program, and Matlab programming, we extracted the pixel location of the wound boundary over time. Through these tools, we were able to precisely determine the wound boundary, create a matrix of the location of the wound boundary using pixel coordinates, and import them as a three-dimensional spline in Solidworks. The spline provided the shape and dimensions of the surface area of the wound, which in turn allowed us to extrapolate the shape and create a three-dimensional model (Figure 8.25).

In addition to developing accurate predictive models for chronic wound-healing time, we also pursued the development of precise three-dimensional models and representations of chronic wounds. The original premise of pursuing three-dimensional modeling of wounds was to determine whether the volume of a wound is a better indicator of wound-healing time than superficial surface area. By building three-dimensional models of wounds, we discovered that we could more precisely calculate the volume of a wound rather than estimating an approximate shape, such as a rectangle or an ellipse. Unfortunately, without the ability to streamline the process of acquiring the boundary of the wound and modeling it in Solidworks, the creation of a three-dimensional model is cumbersome and tedious. Although we can create three-dimensional models of wounds in real time, the process lacks sufficient automation to be efficient in a clinical setting. Regardless of the real-time factor, the development of a three-dimensional wound model could assist clinicians in better determining the underlying shape of a chronic wound and provide insight into how the wound heals. Chapter 8 shows that we can produce an accurate representation for the wound and successfully calculate the change in volume over time. This ability could lead to better, more efficient algorithms that assist in the evaluation and diagnosis of chronic wounds.

In parallel with the development of three-dimensional wound models, we also investigated the use of thermal imaging. We based the decision to include thermal imaging in the research on the fact that the wounds had consistently higher temperatures than the surrounding tissue and the fact that the change in temperature over time could indicate healing or nonhealing of wounds. We collected the thermal-imaging data with the idea that average wound temperature would be a predictor variable within the algorithms, alongside predictors such as length and depth. With the few wounds that we were able to track over a short time, we discovered that the temperature did appear to

change. However, without more data over a longer time, it is unknown whether this change was due to healing or to the tolerance of the thermal imager. Unfortunately, we could not collect enough data to substantiate the idea that the temperature of a wound differs from that of the surrounding tissue. We included the work with the thermal imager because we believe the relationship between the temperature of a chronic wound and time could affect the healing trajectory of the time to heal. We strongly believe this avenue of research is worth additional exploratory analysis, especially with a more accurate thermal-imaging camera.

Any of the predictive models indicates that it is possible to determine the difference between a healed and nonhealed wound through computational analysis. To arrive at that conclusion was more complex than simply classifying this variable as healed or nonhealed. The preprocessing of the data included statistical analysis using box plots, correlation plots, and heat maps to support the conclusion and determination of the modified healing threshold for each variable. Most wound-care physicians we met throughout the research would agree that a healed wound measures 0 x 0 x 0 cm and allow no other definition of a healed wound. In this case, a discrepancy arises between medicine and engineering. Using this measurement, the healed threshold is not possible from an algorithmic point of view. Instead, we used a reasonable threshold that produced accurate enough algorithms in comparison with actual wound data.

We based the predictive models on the wounds themselves using the underpinning of survival analysis and Cox regression (figures 9.18 and 9.19). Using the principles and assumptions of Cox regression modeling, we analyzed the data set, which allowed us to construct the base algorithms (equations 9.3 and 10.2) in parallel with the base hazard function. This algorithmic development allowed us to then calculate the alternative survival function. The survival-function plot versus time to wound closure provided us the necessary graphical representation to estimate the corresponding trend line (figures 10.22 and 10.23) of the prospective wound. By fitting a spline to the wound-survival data, we determined and predicted when the wound will heal by solving for x in the spline algorithm at $S_i(t) = 0$. The solution to x is the predicted time to heal. This solution represents the number of days from conception — that is, from the first visit to the wound clinic, $t = 0$ — to the predicted day of fully healed or the time in days when the probability that the wound would survive is zero.

11.2 ASSUMPTIONS AND LIMITATIONS

With the current study, the assumptions pertain primarily to the data and data collection. We have two primary groups of data, from Vohra and data RBMC: Data Set A and Data Set B, respectively. We performed the data acquisition in different ways but with similar assumptions for the two sets.

Data Set A includes the data we received that had already been unidentified. We received the data in its rawest form, which included wound characteristics we previously discussed with the company. Although we requested corresponding patient demographics to accompany the wound information, federal HIPAA regulations prevented us from obtaining patient demographics and unidentifiable patient information for this data set. Because Data Set A was larger than Data Set B, we had to build the predictive models using Data Set A. We assumed that patient demographic data does not have an effect on the time to heal for chronic wounds.

We were able to collect and control the data in Data Set B. Before collecting data, we had assumed that wound clinics would record patient demographics, such as age, weight, medical history, and nutrition. Unfortunately, patient demographics that we collected in the wound clinic limited the data set, and the assumption was incorrect. We collected only the patients' ages and blood pressure. We did not have access to the patients' entire medical records.

In general, we also assumed that all clinics required clinicians to know the same standard measuring techniques, minimizing human variability and error in wound measurements. This assumption was unrealistic. All of the clinics we visited stated that the accuracy of their wound measurements depends on who performs those measurements. Clinicians have their own ways of measuring and methods of interpreting the wound boundary. This assumption and limitation are inherent components of predictive modeling and analysis of chronic wounds. Variability in wound measurement and interpretation will continue until clinics perform wound measurements using digital image processing and analysis.

For the current study, we assumed that patient demographic did not have a substantial effect on the time to heal for chronic wounds. However, after assessing literature and expert opinion, we believe that this assumption is incorrect. We recommend that future studies include patient demographics in the predictive models to ensure the robustness of the algorithms.

CHAPTER TWELVE CONCLUSIONS AND FUTURE WORKS

CHAPTER 12

Conclusions and Future Works

12.1 CONCLUSION

The research in this dissertation has extended far beyond the expectation of just developing a predictive model to estimate time to heal for chronic, nonhealing wounds. We established a process for using and integrating both still and thermal photography in wound clinics. We advanced and refined a method for developing a three-dimensional model of a chronic wound, and we contributed mass customized methods for creating predictive algorithms for patients' chronic wound-healing trajectories. These processes enable wound clinics and patients to establish trends and connections using retrospective and current data. The model in this research gives an estimated time to heal for patients' chronic wounds rather than using a wait-and-see approach.

By comparing three predictive-modeling techniques, we have concluded that linear regression is not a good fit for measuring chronic wound healing. The models of survival analysis and neural networks enable a better understanding and analysis of the behavior of chronic wounds. These models improve predictive capabilities from both survival analysis and neural networks. Survival analysis and neural networks were equally accurate, but, unlike the survival-analysis technique, neural networks produced large standard errors and standard deviations. Survival analysis initially depends on the set of covariates at $time = 0$ and the length of time that the wound has existed. It also includes the wound's healing trajectory to predict the final time to heal. Thus, we believe that survival analysis is better than neural networks in accurately predicting time to heal.

The results show that survival analysis allows a more comprehensive and more customized method of producing more accurate and robust predictive algorithms. Part of this reasoning relates to the lack of patient demographics and inconsistent wound data across clinics. The models use

only the provided predictor variables. The analysis also considers redundancy in the covariates, which can lead to unstable algorithms.

This research proposes models and methods to predict chronic wound-healing time. By integrating consistency and technology into best practices, wound-care clinics can integrate real-time predictive modeling into daily practice. We seek to contribute to improving predictive capabilities and timing expectations for patients that suffer from chronic, nonhealing wounds.

12.2 FUTURE WORK

Future work includes promotion of certain goals for wound-care clinics in the United States. These goals include a better understanding of standard care; more consistent integration of technology, such as hybrid digital cameras; and more refined predictive models that include patient demographics and additional wound-predictor variables. We also hope that future research will refine the prototype model by adding parameters that clinicians have defined as pertinent to better enhance the predictability of the model.

The comparison and analysis of theoretical versus actual implementation of overall standard wound-care practice represent a branch of research. The practice in wound-care clinics do not follow mandates from state and federal authorities. Further research would provide a better understanding of the difference between theoretical guidelines and actual practice. The next steps pertaining to further investigation into standardizing routine chronic-wound management and operating procedures in wound-care clinics are:

- To understand regulations pertaining to the inclusion or exclusion of patient data in a patient record and documentation on the information that wound clinics must collect; To understand how to adapt the regulations to geographic locations and the economic stability of the clinic; and
- To develop routine chronic-wound-management assessment tools and processes that can be integrated in real-time clinic settings that better streamline chronic-wound assessment.

This research regarding routine chronic wound management found variability among clinics in techniques such as wound photography. We suggest a more comprehensive study regarding routine chronic-wound management and evidence-based best practices at various-sized wound clinics in different locations. We also suggest collection of consumer insights regarding the logistics, operations, and infrastructure of these facilities to create more efficient wound-care clinics. We also recommend an attempt to better integrate technology, which includes wound

EMRs and training on measuring and photographing wounds. The next steps for integrating real-time imaging into wound care clinics are:

- To develop a consistent and detailed training standard operating procedure and program to instruct clinicians in wound photography;
- To develop a set of digital-camera specifications for photographing wounds; and
- To develop a wound-care-specific EMR system that uses cloud-based computing to store patient records and images.

As the cost of technology decreases, more research could focus on the use of thermal imaging and surface-heat analysis in chronic wound care. We believe that the temperature difference between a chronic wound and the surrounding tissue could have an effect on better predicting time to heal. With more consistent integration in clinical practice, thermography could become an indicator of wound-healing trajectory.

Future work also includes more comprehensive predictive models using a larger variety of data from multiple sources. Future work should include a more comprehensive set of predictor variables that include both patient and wound demographics. A more inclusive algorithm may lead to a universal chronic-wound-healing predictive algorithm. Prospective work could also explore incorporating treatments within a predictive model to determine whether a treatment is healing a wound or failing to heal a wound. This work would involve a better understanding of how chronic-wound-care treatments affect the healing trajectory of nonhealing wounds. This work would include patient demographics for each chronic wound, the use of a greater variety of data sources, and further exploration of the qualitative wound characteristics on wound health and wound-healing trajectories.

APPENDIX

APPENDIX A: PRELIMINARY STUDY RAW DATA

Width (cm)	Height (cm)	Depth (cm)	Weeks to Heal Based on Surface Area (cm ²)	Weeks to Heal = Ellipsoid (cm ³)	Weeks to Heal Natural Log (Cm)	Width Ln	Height Ln	Depth Ln	Weight
8	12	2	24	50.3	3.18	3.92	2.08	2.48	0.69
8	4	1	12	8.4	2.48	2.13	2.08	1.39	0.00
12	12	2.4	52	90.5	3.95	4.51	2.48	2.48	0.88
3	0.7	1.5	2	0.8	0.69	-0.19	1.10	-0.36	0.41
8	6	3.5	18	44.0	2.89	3.78	2.08	1.79	1.25
12	8	2.1	30	52.8	3.40	3.97	2.48	2.08	0.74
5	8	1.5	11	15.7	2.40	2.75	1.61	2.08	0.41
3	3	1.5	3	3.5	1.10	1.26	1.10	1.10	0.41
6	6	2.3	8	21.7	2.08	3.08	1.79	1.79	0.83
8	8	2.5	24	41.9	3.18	3.73	2.08	2.08	0.92
3.5	3	2.5	4	6.9	1.39	1.93	1.25	1.10	0.92
4	2.5	4	5	10.5	1.61	2.35	1.39	0.92	1.39
3	0.4	1	1	0.3	0.00	-1.16	1.10	-0.92	0.00
6	6	2	9	18.8	2.20	2.94	1.79	1.79	0.69
12	8	1.1	12	27.6	2.48	3.32	2.48	2.08	0.10
6	3	1.1	4	5.2	1.39	1.65	1.79	1.10	0.10
6	4	1.1	5	6.9	1.61	1.93	1.79	1.39	0.10
8	6	1	10	12.6	2.30	2.53	2.08	1.79	0.00
4	4	1	3	4.2	1.10	1.43	1.39	1.39	0.00
6	6	2	13	18.8	2.56	2.94	1.79	1.79	0.69
8	6	1.5	10	18.8	2.30	2.94	2.08	1.79	0.41
4	4	1.3	3	5.4	1.10	1.69	1.39	1.39	0.26
6.5	2.7	0.8	3.5	3.7	1.26	1.30	1.87	0.99	-0.22
2.5	2.4	0.6	0.9	0.9	-0.11	-0.06	0.92	0.88	-0.51
6	4	1.3	7.8	8.2	2.05	2.10	1.79	1.39	0.26
6	4.3	2.2	14.2	14.9	2.65	2.70	1.79	1.46	0.79
5	3.5	0.5	2.2	2.3	0.78	0.83	1.61	1.25	-0.69
16	12	2.8	134.4	140.7	4.90	4.95	2.77	2.48	1.03
7	4.5	0.3	2.4	2.5	0.88	0.91	1.95	1.50	-1.20
2	0.5	0.3	3.0	0.1	1.10	-2.54	0.69	-0.69	-1.20
7.5	3.6	2	8.0	14.1	2.08	2.65	2.01	1.28	0.69
10	8	1	7.5	20.9	2.01	3.04	2.30	2.08	0.00
10	7	2	8.5	36.7	2.14	3.60	2.30	1.95	0.69
3	2	0.2	3.5	0.3	1.25	-1.16	1.10	0.69	-1.61
8	10	2.4	9.5	50.3	2.25	3.92	2.08	2.30	0.88
6.5	5.5	1.3	7.0	12.2	1.95	2.50	1.87	1.70	0.26
6	4.5	1.5	6.5	10.6	1.87	2.36	1.79	1.50	0.41

APPENDIX B: RARITAN AY MEDICAL CENTER AFFILIATION AGREEMENT

EDUCATIONAL AFFILIATION AGREEMENT

THIS AGREEMENT is made February 25, 2013 by and between **NORTHEASTERN UNIVERSITY** having a business address at 360 Huntington Avenue, Boston, Massachusetts 02115 (hereafter "School"), and **RARITAN BAY MEDICAL CENTER, A NEW JERSEY NONPROFIT CORPORATION**, having a business address at 530 New Brunswick Avenue, Perth Amboy, New Jersey 08861 (hereafter "Agency").

WHEREAS, Agency owns and operates hospitals in Perth Amboy and Old Bridge, New Jersey, which provide acute care services to its patients, including wound care; and

WHEREAS, School educates students enrolled in its Mechanical and Industrial Engineering Department, through didactic and research, to enable those students to obtain advanced degrees; and

WHEREAS, Agency and School desire to enter into an Agreement to enable students to engage in research activities at Agency as part of their advanced degree program;

NOW, THEREFORE, in consideration of the mutual promises and covenants contained herein, the parties agree as follows:

1. DEFINITIONS

For purpose of this Agreement, the following terms shall have the meanings ascribed hereto:

1.1 **Agreement**. "Agreement" shall mean this Educational Affiliation Agreement and any amendments hereto.

1.2 **Clinical Experience**. "Clinical Experience" shall mean that portion of Student research requested by School and performed at Agency that has been approved by Agency's Institutional Review Board and other appropriate medical staff committee(s).

1.3 **Faculty**. "Faculty" shall mean the person(s) employed or retained by School and serving as supervisor(s)/instructor(s) for Students under this Agreement.

1.4 **Student**. "Student" shall mean an individual enrolled in the School and who intends to conduct research at Agency.

2. TERM AND TERMINATION

2.1 The Term of this Agreement shall be for one (1) year commencing on February 25, 2013 and ending on February 24, 2014.

2.2 Agency shall have the right to terminate this Agreement at any time for any material breach hereof by School, or in the event Agency determines that the safety of any patient, employee, physician, or any other individual would be in jeopardy by continuing this Agreement.

2.3 At its sole discretion, Agency may immediately remove and terminate the participation of any Student who fails to comply with applicable Agency policies and procedures, or whose performance or actions are determined to be detrimental to the proper functioning of Agency.

2.4 School shall have the right to terminate this Agreement at any time for any material breach hereof by Agency.

3. RESPONSIBILITIES OF AGENCY

3.1 Agency shall provide Clinical Experiences, if available, for Students that fulfill the curriculum requirements of the School's advanced degree program.

3.2 Agency shall designate those units or areas within Agency in which Students may be exposed for their Clinical Experience.

3.3 Agency shall orient Faculty who will come to the Agency, and Students, to Agency, including policies and procedures applicable to their conduct during the Clinical Experience.

3.4 In the event that the Agency participates in more than one Educational Affiliation Agreement at any one time, Agency shall determine priorities for the use of Agency facilities and services.

3.5 Agency, through appropriate staff, shall be responsible for the oversight of all patient care activities.

3.6 Prior to the Clinical Experience, Agency shall approve the number of Students, the dates of attendance, and the areas to be involved in the Clinical Experience.

4. RESPONSIBILITIES OF SCHOOL

4.1 School shall be solely responsible for the planning and implementation of the research program, including but not limited to academic administration, curriculum content and programming, faculty appointments and administration, requirements for Student admission, promotion and graduation, and maintenance of all Student records and reports.

4.2 Any proposed change in an approved Clinical Experience must be approved in writing by Agency's Institutional Review Board.

4.3 School shall be responsible for the instruction and evaluation of all Students as well as the determination of all grades or degrees to be awarded Students for their participation in this Clinical Experience.

4.4 During the Clinical Experience, on-site Faculty and Students shall comply with applicable policies and procedures of Agency, including but not limited to those relating to patient confidentiality.

4.5 Both during and after the Clinical Experience, Faculty and Students shall not breach the confidential nature of any patient information with which they may have access during the Clinical Experience. Faculty and Students further agree to comply with all federal and state laws regarding the confidential nature of patient medical records and any other form of patient information. School shall ensure that Faculty and Students participating in any Clinical Experience sign a confidentiality agreement reasonably acceptable to Agency prior to participating in any Clinical Experience.

4.6 School shall ensure that all Students and Faculty have completed and filed certifying documents with School, prior to the commencement of any Clinical Experience, assuring that each meet the following health or health-related requirements:

(a) initial physical examination, and annually thereafter;

(b) Rubella, Rubeola, and Varicella - proof of positive titers or documentation of immunity in writing from a licensed physician;

(c) PPD - initial step 2 and current within one year, and a Mantoux test annually thereafter; anyone testing positive require a current chest x-ray;

(d) Hepatitis B vaccine status - either declined, in progress, or completed (a titer of immunity is recommended);

(e) any other health requirements established by Agency for its own employees;

(f) respiratory mask and fit testing on all Students and Faculty (Agency shall identify the type of mask utilized at Agency); and

(g) criminal background check verifying no criminal record.

4.7 Prior to each Clinical Experience, School shall submit in writing to Agency a list of Students and Faculty verifying that they have met all of the health, training, and any other requirements set forth in this Agreement.

4.8 School shall provide all Students and Faculty who are to be sent to the Agency training in the following areas: OSHA Hazardous Communication Standard, Fire/Electrical Safety, Infection Control, Body

Mechanics, Safe Waste Disposal, OSHA Blood Borne Pathogens, Agency HIPAA Notice of Privacy Practices, Corporate Compliance. This training shall be provided before a Students or Faculty are sent to Agency. Students shall complete Agency's on-line resource guide. Agency will assist in this training if requested by School.

4.9 School shall ensure that Students understand they are not entitled to wages or any benefits for their activities during the Clinical Experience with Agency and are not employees of Agency at any time while assigned for this Clinical Experience.

4.10 School shall ensure that Students understand that any medical treatment, emergency or otherwise, required by any Student for injuries incurred during Clinical Experience will be covered through said Student's personal health insurance plan or through is or her own resources.

4.11 School shall advise Students that Students bear the cost of all transportation, meals and lodging related to this Clinical Experience.

4.12 School shall keep and maintain all records and reports on the Students' Clinical Experience.

5. GENERAL PROVISIONS

5.1 Student Uniforms and Identification

All Students shall wear the uniform of School, if any. All Students shall wear a name tag identifying themselves by name and as a student of School, and shall introduce themselves to all patients as students.

5.2 Insurance. Both parties shall maintain, at a minimum, the following insurance, and provide the other with a Certificate of Insurance evidencing this coverage at or prior to the commencement of this Agreement, and prior to the expiration of any such policies of insurance.

General liability	\$1,000,000 per claim; \$3,000,000 annual aggregate
Professional liability	\$1,000,000 per claim; \$3,000,000 aggregate

Workers' Compensation Statutory

School shall ensure that all Students and Faculty are covered by a policy of professional liability insurance in the amount set forth above. Such insurance shall be with a company or companies reasonably satisfactory to the other party, or through a program of self-insurance or other risk financing mechanism reasonably acceptable to the other party, or any combination thereof. Should School's policy or policies of insurance be of the claims-made type, School shall assume liability for all future claims presented and arising out of the acts or missions of School, its employees, Faculty, and Students under this Agreement. A Certificate of Insurance evidencing

these coverages shall be provided to each party upon execution of this Agreement and prior to the expiration of each policy of insurance.

5.3 Relationship between the Parties. This Agreement shall in no way be interpreted as creating an agency or employment between the parties. Faculty and Students shall not be construed as employees or agents of Agency.

5.4 Governing Law. This Agreement shall be deemed to have entered into and completely performed in the State of New Jersey. The interpretation and enforcement of this Agreement shall be governed by laws of the State of New Jersey, without regard to its choice of law provisions.

5.5 Severability. The invalidity or unenforceability of any provision of this Agreement shall not affect the validity or enforceability of any other provision.

5.6 Amendments. Any amendments to this Agreement shall be effective only if in writing and signed by both parties.

5.7 Waiver. No waiver of a breach of any provision of this Agreement shall be construed to be a waiver of any breach of any other provision. No delay in acting with regard to any breach of any provision of this Agreement shall be construed to be a waiver of such breach.

5.8 Gender. Any noun or pronoun used in this Agreement shall be construed in the masculine, feminine, or neuter as its sense and use may require.

5.9 Assignment. Neither party shall have the right to assign this Agreement, and any attempted or purported assignment shall be null and void.

5.10 Captions. Captions contained in this Agreement are inserted only as a matter of convenience and in no way define, limit, or extend the scope or intent of this Agreement or any provision hereof.

5.11 Notices. Any notice required to be given by this Agreement shall be deemed to have been made on the date received if sent via Certified Mail, Return Receipt Requested, or recognized overnight courier with verification of receipt, addressed as set forth below, or to any other address designated by the party by notice consistent with this section:

If to Agency:

Raritan Bay Medical Center
530 New Brunswick Avenue
Perth Amboy, New Jersey 08861
Attn: President/CEO

If to School:

Northeastern University
360 Huntington Avenue
Boston, Massachusetts 02115
Attn:

5.12 No Construction Against Drafting Party. Both parties acknowledge and agree that each of them and their counsel have had an opportunity to review this agreement, and that this agreement shall not be construed against one party merely because that party prepared this agreement.

5.13 Entire Agreement. This Agreement constitutes the entire agreement of the parties with respect to this subject matter.


5.14 Authority to Bind. The individuals signing on behalf of their respective institutions represent and warrant that they have the authority to enter into this Agreement.

IN WITNESS WHEREOF, the parties hereto have executed this Agreement by their duly authorized representatives.

Raritan Bay Medical Center

By: Thomas G. Shanahan
Title: Sr. Vice President/CFO

Northeastern University

By: 
Title: Treasurer

Approved as to Form

NB 2/28/13



CERTIFICATE OF LIABILITY INSURANCE

DATE (MM/DD/YYYY)
03/04/2013

THIS CERTIFICATE IS ISSUED AS A MATTER OF INFORMATION ONLY AND CONFERS NO RIGHTS UPON THE CERTIFICATE HOLDER. THIS CERTIFICATE DOES NOT AFFIRMATIVELY OR NEGATIVELY AMEND, EXTEND OR ALTER THE COVERAGE AFFORDED BY THE POLICIES BELOW. THIS CERTIFICATE OF INSURANCE DOES NOT CONSTITUTE A CONTRACT BETWEEN THE ISSUING INSURER(S), AUTHORIZED REPRESENTATIVE OR PRODUCER, AND THE CERTIFICATE HOLDER.

IMPORTANT: If the certificate holder is an ADDITIONAL INSURED, the policy(ies) must be endorsed IF SURRENDER IS WAIVED, subject to the terms and conditions of the policy, certain policies may require an endorsement. A statement on this certificate does not confer rights to the certificate holder in lieu of such endorsement(s).

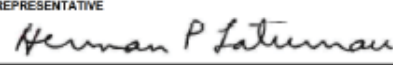
PRODUCER Fred C. Church, Inc. 41 Wellman Street Lowell, MA 01851 (800) 225-1866	CONTACT NAME: Jeanne Pitts, CIC, CSR PHONE (A/C, No, Ext): 978 3227262 FAX (A/C, No): (978) 454-1866 E-MAIL: jpitts@fredochurch.com ADDRESS:																					
INSURED Northwestern University 122 St. Stephen Street Boston, MA 02115-5000	<table border="1"> <thead> <tr> <th colspan="2">INSURER(S) AFFORDING COVERAGE</th> <th>NAIC #</th> </tr> </thead> <tbody> <tr> <td>INSURER A:</td> <td>Twin City Fire Insurance Co.</td> <td>29469</td> </tr> <tr> <td>INSURER B:</td> <td>United Educators Insurance, a Reciprocal Risk Retention Group</td> <td>10020</td> </tr> <tr> <td>INSURER C:</td> <td></td> <td></td> </tr> <tr> <td>INSURER D:</td> <td></td> <td></td> </tr> <tr> <td>INSURER E:</td> <td></td> <td></td> </tr> <tr> <td>INSURER F:</td> <td></td> <td></td> </tr> </tbody> </table>	INSURER(S) AFFORDING COVERAGE		NAIC #	INSURER A:	Twin City Fire Insurance Co.	29469	INSURER B:	United Educators Insurance, a Reciprocal Risk Retention Group	10020	INSURER C:			INSURER D:			INSURER E:			INSURER F:		
INSURER(S) AFFORDING COVERAGE		NAIC #																				
INSURER A:	Twin City Fire Insurance Co.	29469																				
INSURER B:	United Educators Insurance, a Reciprocal Risk Retention Group	10020																				
INSURER C:																						
INSURER D:																						
INSURER E:																						
INSURER F:																						

COVERAGES CERTIFICATE NUMBER: 25011 REVISION NUMBER:

THIS IS TO CERTIFY THAT THE POLICIES OF INSURANCE LISTED BELOW HAVE BEEN ISSUED TO THE INSURED NAMED ABOVE FOR THE POLICY PERIOD INDICATED. NOTWITHSTANDING ANY REQUIREMENT, TERM OR CONDITION OF ANY CONTRACT OR OTHER DOCUMENT WITH RESPECT TO WHICH THIS CERTIFICATE MAY BE ISSUED OR MAY PERTAIN, THE INSURANCE AFFORDED BY THE POLICIES DESCRIBED HEREIN IS SUBJECT TO ALL THE TERMS, EXCLUSIONS AND CONDITIONS OF SUCH POLICIES. LIMITS SHOWN MAY HAVE BEEN REDUCED BY PAID CLAIMS.

INSR LTR	TYPE OF INSURANCE	ADDL SUBR INSR WVD	POLICY NUMBER	POLICY EFF (MM/DD/YYYY)	POLICY EXP (MM/DD/YYYY)	LIMITS
B	GENERAL LIABILITY <input checked="" type="checkbox"/> COMMERCIAL GENERAL LIABILITY <input type="checkbox"/> CLAIMS-MADE <input checked="" type="checkbox"/> OCCUR <input checked="" type="checkbox"/> Auto Liability Included <input checked="" type="checkbox"/> Liquor Liability Included GEN'L AGGREGATE LIMIT APPLIES PER: <input checked="" type="checkbox"/> POLICY <input type="checkbox"/> PRO-JECT <input type="checkbox"/> LOC		BLX201200062800	7/1/2012	7/1/2013	EACH OCCURRENCE \$ 750,000 DAMAGE TO RENTED PREMISES (EA OCCURRENCE) \$ 750,000 MED EXP (Any one person) \$ PERSONAL & ADV INJURY \$ Included GENERAL AGGREGATE \$ 3,000,000 PRODUCTS - COMP/OP AGG \$ Included
	AUTOMOBILE LIABILITY <input type="checkbox"/> ANY AUTO <input type="checkbox"/> ALL OWNED AUTOS <input type="checkbox"/> SCHEDULED AUTOS <input type="checkbox"/> HIRED AUTOS <input type="checkbox"/> NON-OWNED AUTOS					COMBINED SINGLE LIMIT (EA ACCIDENT) \$ BODILY INJURY (Per person) \$ BODILY INJURY (Per accident) \$ PROPERTY DAMAGE (Per accident) \$
B	<input checked="" type="checkbox"/> UMBRELLA LIAB <input checked="" type="checkbox"/> OCCUR <input checked="" type="checkbox"/> EXCESS LIAB <input type="checkbox"/> CLAIMS-MADE DED <input checked="" type="checkbox"/> RETENTION \$ 1,000,000		GLX201200062800	7/1/2012	7/1/2013	EACH OCCURRENCE \$ 40,000,000 AGGREGATE \$ 40,000,000
A	WORKERS COMPENSATION AND EMPLOYERS' LIABILITY ANY PROPRIETOR/PARTNER/EXECUTIVE OFFICER/OWNER EXCLUDED? <input type="checkbox"/> Y/N (Mandatory in NH) If yes, describe under DESCRIPTION OF OPERATIONS below	N/A	08WECVT0708	3/15/2013	3/15/2014	WC STATUTORY LIMITS OTH-ER E.L. EACH ACCIDENT \$ 1,000,000 E.L. DISEASE - EA EMPLOYEE \$ 1,000,000 E.L. DISEASE - POLICY LIMIT \$ 1,000,000
B	Professional Liability		LPO201200062800	7/1/2012	7/1/2013	Limited Professional Liability, Claims Made; 1,000,000 Each Claim; 2,000,000 Annual Aggregate

DESCRIPTION OF OPERATIONS / LOCATIONS / VEHICLES (Attach ACORD 101, Additional Remarks Schedule, if more space is required)
RE-Servence of Insurance for PhD Student, Jessica Chin observation research at RBMC
Professional Liability includes coverage for Students

CERTIFICATE HOLDER Raritan Bay Medical Center 530 New Brunswick Avenue Perth Amboy, NJ 08861	CANCELLATION SHOULD ANY OF THE ABOVE DESCRIBED POLICIES BE CANCELLED BEFORE THE EXPIRATION DATE THEREOF, NOTICE WILL BE DELIVERED IN ACCORDANCE WITH THE POLICY PROVISIONS. AUTHORIZED REPRESENTATIVE 
--------------------------------------------------------------------------------------------------------------	----------------------------------------------------------------------------------------------------------------------------------------------------------------------------------------------------------------------------------------------------------------------------------------------------------------

Client # 4996 Mt # 25011 Cert Holder # 45811 © 1988-2010 ACORD CORPORATION. All rights reserved.
ACORD 25 (2010/05) The ACORD name and logo are registered marks of ACORD



APPENDIX C: VOHRA WOUND CARE PHYSICIANS DATA AGREEMENT

Data Use Agreement For Disclosure of a Limited Data Set For Research Purposes

This Data Use Agreement For Disclosure of a Limited Data Set For Research Purposes (the "Agreement") is made and entered into this 28th day of February, 2013, and is effective on the date of the last signature below by and among Vohra Health Services, P.A., Vohra Wound Physicians of FL, LLC, Vohra Wound Physicians of IL, S.C., Vohra Wound Physicians of NY, PLLC and Vohra Wound Physicians of CA, P.C. (collectively, the "Covered Entity") and Jessica Chin, PhD Candidate ("Recipient") (collectively "the Parties").

WHEREAS:

WHEREAS, Covered Entity maintains certain confidential protected health information that Recipient desires to use for research purposes permitted under 45 CFR § 164.514(e) of the Privacy Rule (defined below); and

WHEREAS, prior to Covered Entity releasing any confidential protected health information to Recipient, the Privacy Rule (defined below) requires the Parties to enter into a data use agreement as defined in 45 CFR § 164.514(e)(4) pursuant to which Recipient agrees to certain restrictions on the use and disclosure of such information.

NOW, THEREFORE, intending to be legally bound and for and in consideration of the mutual covenants contained herein, and for other good and valuable consideration, the receipt and sufficiency of which are hereby acknowledged, the Parties hereto agree as follows:

1. **RECITALS.** The Recitals above are true and correct and are incorporated herein by reference as if fully set forth below.

2. **ACCESS TO DATA.** Covered Entity shall provide Recipient with a Limited Data Set (defined below) of Protected Health Information ("PHI") that contains the minimum necessary data for the research project. A description of the data files provided by Covered Entity to Recipient is attached hereto as Exhibit A. Under no circumstances shall Covered Entity be required under this Agreement to provide Recipient with any information that does not qualify as part of a Limited Data Set.

3. **DEFINITIONS.** Except as otherwise defined herein, any and all capitalized terms in this Agreement shall have the definitions set forth in the Health Insurance Portability and Accountability Act of 1996 ("HIPAA") and the regulations promulgated thereunder including, without limitation, the federal privacy standards as contained in 45 CFR Part 160 and Part 164, Subparts A and E (the "Privacy Rule") and the federal security standards as contained in 45 CFR Part 160 and Part 164, Subparts A and C (the "Security Rule").

3.1 Limited Data Set, as defined in the Privacy Rule at 45 CFR § 164.514(e)(2), is PHI that may include certain specific identifiers and must exclude other direct identifiers in the PHI about the individual or about relatives, employers, or household members of the individual. A Limited Data Set may include if needed for the purpose of the research: (1) dates (e.g., admission, discharge, and service dates, dates of birth and death); and (2) five-digit zip codes and state, county, city, and precinct, but not any other postal address information. A limited data set must exclude the following direct identifiers of an individual and his or her relatives, employer(s), and household members: (i) name; (ii) postal address information (except town or city, state and zip code which are permitted); (iii) telephone numbers; (iv) fax numbers; (v) electronic mail addresses; (vi) social security numbers; (vii) medical record numbers; (viii) health plan beneficiary numbers; (ix) account numbers; (x) certificate/license numbers; (xi) license plate numbers and other vehicle identifiers and serial numbers; (xii) device identifiers and serial numbers; (xiii) Web Universal Resource Locators (URLs); (xiv) Internet Protocol (IP) address numbers; (xv) biometric identifiers including finger and voice prints; and (xvi) full-face photographic images and any comparable images. In the event of any conflict between this description and the definition set forth in the Privacy Rule, the Privacy Rule definition will govern.

3.2 The following terms shall also have the meanings given to them in the Privacy Rule: Covered Entity, Individual, PHI, and Required by Law.

4. **AUTHORIZED PARTIES.** The Recipient is the primary responsible person for the research project described in paragraph 5 below and persons under her direct supervision (each individually an "Authorized Party" and collectively, the "Authorized Parties"), are authorized to use the Limited Data Set or any part of it on behalf of Recipient. Recipient shall ensure that any Authorized Party agrees to abide by the terms of this Agreement. Recipient agrees that access to the Limited Data Set covered by this Agreement shall be limited to the minimum amount of data and minimum number of individuals necessary to achieve the research purpose stated in Section 5 below.

5. **PERMITTED USE.** Recipient agrees and shall ensure that any Authorized Party agrees to use the Limited Data Set only for the purposes of the following research project, except as required by law: Investigating a Framework for Modeling and Analysis for Wound Progression.

If Recipient publishes or utilizes in any form the research project and/or the results thereof, then Recipient shall include the name of Covered Entity, Christopher Leonard, D.O., Director of Medical Informatics and EHR Development, and Shark Bird, M.D., Chief Medical Officer, as providers of some or all of the data used by Recipient in the research project.

6. **RESTRICTIONS ON USE.**

6.1 Recipient agrees that it will not use or further disclose the Limited Data Set or any information contained therein other than as permitted by this Agreement or as otherwise required by law.

6.2 Recipient shall use appropriate safeguards to prevent any use or disclosure of the Limited Data Set or any information contained therein other than as specified in this Agreement. To the extent that Recipient receives, creates, maintains or transmits Electronic PHI, Recipient shall use appropriate administrative, physical and technical safeguards that reasonably and appropriately protect the confidentiality, integrity, and availability of any Electronic PHI.

6.3 Recipient shall not use the information contained in the Limited Data Set to identify or contact the individuals to whom the information pertains.

6.4 Recipient shall ensure that any agent or subcontractor to whom it provides the Limited Data Set agrees to the same restrictions and conditions that apply to the Recipient and Authorized Parties under this Agreement. Recipient shall terminate its agreement with any agent or subcontractor to whom it provides the Limited Data Set if such agent or subcontractor fails to abide by any material term of such agreement.

6.5 Recipient shall comply with applicable state and local security and privacy laws to the extent that they are more protective of the individual's privacy than the HIPAA Privacy Rule and Security Rule.

7. **REPORTING.** Recipient agrees to report to Covered Entity any use or disclosure of the Limited Data Set not provided for by this Agreement of which Recipient or any Authorized Party becomes aware, or any Security Incident of which it becomes aware. Such reporting shall take place within ten (10) calendar days of Recipient or Authorized Party becoming aware of the unauthorized use or disclosure.

8. **OWNERSHIP.** Recipient and Covered Entity each agree that Covered Entity retains all ownership rights to the Limited Data Set and that Recipient does not obtain any right, title, or interest in any of the data furnished by Covered Entity to Recipient as part of the Limited Data Set. Recipient shall not sell, rent, lease, loan, disclose, use or reuse any of the information contained in the Limited Data Set except as specified in this Agreement or except as Covered Entity may authorize in writing.

9. **TERMINATION.**

9.1 This Agreement shall be effective on the Effective Date set forth above and shall continue as long as Recipient retains the Limited Data Set.

9.2 Recipient may terminate this Agreement by returning or destroying the Limited Data Set and providing written verification of this to the Covered Entity.

9.3 Should the Covered Entity become aware of a pattern of activity or practice on the part of Recipient that constitutes a material breach of this Agreement, the Covered Entity shall have the right to summarily terminate this Agreement.

9.4 This Agreement is valid only if the data being provided meets the definition of a "Limited Data Set" as specified in HIPAA. Both Parties believe that the data does meet this definition. If, subsequent to implementation of this Agreement, either Party becomes aware that the data provided by Covered Entity to Recipient exceeds the definition of a Limited Data Set as defined in 45 CFR § 164.514(e)(2), this Agreement shall be terminated, and Recipient agrees to follow the Covered Entity's directions with respect to the return or destruction of the Limited Data Set. In this event, the Parties agree to make reasonable efforts to devise alternative means of providing the Limited Data Set to recipient in compliance with HIPAA.

10. MISCELLANEOUS

10.1 Recipient agrees to mitigate, to the extent feasible and allowed by law, any harmful effect that is known or becomes known to Recipient that arises from a use or disclosure of the Limited Data Set by Recipient or any Authorized Party in violation of this Agreement, the Privacy Rule, or the Security Rule.

10.2 Within five (5) calendar days of a written request by Covered Entity, Recipient shall allow Covered Entity to conduct a reasonable inspection of Recipient's facilities, systems, books, records, agreements, and policies and procedures relating to the use or disclosure of the Limited Data Set for the purpose of determining Recipient's compliance with the terms of this Agreement. Any failure of Covered Entity to inspect or to detect or notify Recipient of an unsatisfactory practice does not constitute acceptance of the practice by Covered Entity or a waiver of any remedy or right Covered Entity has under the Agreement or applicable law.

10.3 When Covered Entity reasonably concludes that an amendment to this Agreement is necessary to comply with applicable law, Covered Entity shall notify Recipient in writing of the proposed modification(s) ("Legally-Required Modifications"). Covered Entity shall request Recipient's written approval in the form of an amendment to this Agreement at the time of notification. Recipient shall have thirty (30) days to sign the amendment and return it to Covered Entity. Recipient's rejection of a Legally Required Modification is grounds for termination of this Agreement by Covered Entity on at least thirty (30) days' prior written notice to Recipient.

10.4 Recipient shall comply with the requirements of 45 CFR Sections 164.524 (Access of Individuals to PHI), 164.526 (Amendment of PHI) and 164.528 (Accounting of Disclosures of PHI) as directed by Covered Entity.

10.5 Any ambiguity in this Agreement relating to the use and disclosure of the Limited Data Set by Recipient shall be resolved in favor of a meaning that further protects the privacy and security of the information.

10.6 This Agreement may be executed by facsimile signature and by either of the Parties in counterparts. A fax of a signature page signed by a party hereto shall be as valid and binding as an original thereof. If multiple counterparts of this Agreement are executed, each shall be deemed an original, but all such counterparts shall constitute one (1) and the same instrument.

10.7 This Agreement may not be assigned by Recipient without the prior written consent of Covered Entity.

10.8 This Agreement has been executed and delivered in, and shall be interpreted, construed, and enforced pursuant to and in accordance with the laws of the State of Florida only, without regard to conflict of laws principles. Venue for any action arising out of or relating to this Agreement shall be in Broward County, Florida.

10.9 The Parties hereto agree and stipulate that the original of this Agreement, including the signature page, may be scanned and stored in a computer database or similar device, and that any printout or other output readable by sight, the reproduction of which is shown to accurately reproduce the original of this document, may be used for any purpose just as if it were the original, including proof of the content of the original writing.

10.10 This Agreement, and any exhibits, constitutes the entire agreement between the Parties hereto with respect to its subject matter and there are no other representations, understandings or agreements, whether written or oral, between the Parties relating to such subject matter.

[Signature page immediately follows]

IN WITNESS WHEREOF, the parties hereto have executed this Agreement as of the date first written above.

COVERED ENTITY

Vohra Health Services, P.A.
Vohra Wound Physicians of FL, LLC
Vohra Wound Physicians of IL, LLC
Vohra Wound Physicians of NY, PLLC
Vohra Wound Physicians of CA, P.C.

By: _____
Christopher Leonard, D.O., Authorized Agent

Date: _____

RECIPIENT



Jessica Chin, PhD Candidate

Date: February 28, 2013

APPENDIX D: THERMACAM S65 TECHNICAL SPECIFICATIONS

ThermaCAM® S65 Technical Specifications

Imaging Performance	
Thermal	
Field of view/min focus distance	24° x 18° / 0.3 m
Spatial resolution (IFOV)	1.3 mrad
Electronic zoom function	2, 4, 8, interpolating
Focus	Automatic or manual
Digital image enhancement	Normal and enhanced
Detector type	Focal plane array (FPA) uncooled microbolometer, 320 x 240 pixels
Spectral range	7.5 to 13 µm
Thermal sensitivity @ 50/60Hz	0.08° C at 30° C
Visual	
Built-in digital video	640 x 480 pixels, full color
Image Presentation	
Viewfinder	Built-in high-resolution color LCD (1FT)
Video output	4" LCD with integrated remote control RS 170 EIA/NTSC or CCIR/PAL
External display	Built-in high-resolution color LCD (1FT)
Measurement	
Temperature ranges	-40° C to +120° C (-40° F to +248° F), Range 1 0° C to +500° C (+32° F to +932° F), Range 2 +350° C to +1500° C (+662° F to +2732° F), Range 3 Up to +2000° C (+3632° F), optional
Accuracy (% of reading)	± 2° C or ± 2%
Measurement modes	Up to 10 movable spots. Automatic temperature difference (Δ) and placement and reading of maximum and minimum temperatures. Up to 5 movable circle areas or boxes. Up to 2 isotherms. Line profile.
Emissivity corrections	Variable from 0.1 to 1.0 or select from listings in pre-defined material list
Measurement features	Automatic corrections based on user input for reflected ambient temperature, distance, relative humidity, atmospheric transmission, and external optics
Optics transmission correction	Automatic, based on signals from internal sensors
Image Storage	
Type	Removable CompactFlash (256 MB) memory card; built-in Flash memory (100 images); built-in RAM memory for burst and A/V recording
File format - THERMAL	Standard JPEG; 14 bit thermal measurement data included
File format - VISUAL	Standard JPEG inked with corresponding thermal image
Voice annotation of images	Input via supplied Bluetooth® wireless headset up to 30 seconds of digital voice clip per image stored with image
Text annotation of images	Predefined by user and stored with image
System Status Indicator	
LCD display	Shows status of battery and storage media. Indication of power, communication and storage modes.
Power Source	
Battery type	Li-Ion, rechargeable, field-replaceable
Battery operating time	2 hours continuous operation
Charging system	In camera (AC adapter or 12V from car) or 2 bay intelligent charger
External power operation	AC adapter 110/220 VAC, 50/60Hz or 12V from car (cable with standard plug optional)
Power saving	Automatic shutdown and sleep mode (user-selectable)
Environmental	
Operating temperature range	-15° C to +50° C (5° F to 122° F)
Storage temperature range	-40° C to +70° C (-40° F to 158° F)
Humidity	Operating and storage 10% to 95%, non-condensing
Encapsulation	IP 54 IEC 529
Shock	Operational: 25G, IEC 68-2-29
Vibration	Operational: 2G, IEC 68-2-6
Physical Characteristics	
Weight	2.0 kg (4.4 lbs) w/battery and top handle (includes remote control, LCD, video camera and laser) 1.4 kg (3.1 lbs) excluding battery and handle
Size	100mm x 120mm x 220 mm (3.9" x 4.7" x 8.7") camera only
Tripod mounting	1/4" - 20

ThermaCAM S65 System Includes:	
IR camera with visual camera, Laser LocatIR, remote with LCD display	
High-output multi-LED target light	
Bluetooth® wireless headset	
Carrying case, lens cap, shoulder strap, hand strap	
User manual (multilingual)	
Batteries (2)	
Power supply	
Battery charger	
FireWire® (IEEE 1394) cable	
Video cable with RCA plug	
USB cable	
S-video cable	
256 MB CompactFlash card	
ThermaCAM QuickView™ software	
Lenses (optional)	
Field of view/ minimum focus distance	3X Telescope (7" x 5.3"/4m) 2X Telescope (12" X 9"/1.2m) 0.5X Wide angle (45° x 34"/0.1m) 0.3X Wide angle (80° x 64"/0.1m) 200 µm Close-up (64mm x 48mm/150mm) 100 µm Close-up (34mm x 25mm/80mm) 50 µm Close-up (15mm x 11mm/19mm) Wearable Optics/Heads-up Display
Interfaces	
Firewire output (IEEE 1394)	Real-time digital transfer of radiometric thermal images or digital video (DV) out
USB / RS232	Image (thermal and visual), measurement data, voice and text transfer to PC
IrDA	Two-way data transfer from laptop, PDA
Remote control	Removable handle with redundant controls and LCD
Laser LocatIR	
Classification type	Class 2 Semiconductor AlGaInP Diode Laser: 1 mW/635 nm (red)



APPENDIX E: MATLAB CODE, DATA CLEANING

CHANGE THE DATE

```
%% Start with a clean slate
clear all;
close all;
clc;

%% Import Excel Data
data = csvread('rawdata.csv');
[r,c] = size(data);

%% Row Number

for count=1:r
    data(count,16)=count;
end

%% Calculate Difference in Patient Visits (Days)

y=0;

for x=1:r
    if x < r
        y = x+1;
    end

    row = data(x,16);           %ROW Number
    newrow = data(y,16);       %Next ROW Number

    if data(row,3) == 0;       %Determines First Patient Visit
        start = data(row,2);  %Set "Patient first visit"
    end

    wound_id = data(row,1);    %Finds first instance of Wound ID
    wound_check = data(newrow,1); %Finds every subsequent Wound with
    the same Wound_ID

    next = data(newrow,2);     %Determines the Subsequent Patient
    Visits

    while wound_id == wound_check & newrow <= r %Loop that finds the
    difference between visits for EACH patient

        next = data(newrow,2);
        diff = next - start;

        data(newrow,17)=diff;

        newrow = newrow + 1;
        if newrow < r+1
            wound_check = data(newrow,1);
        end
    end
end
```

```

    end

end

%% Write to CSV File
csvwrite ('changeintime.csv', data);

CLEAN DATA
%% Start with a clean slate
clear all;
close all;
clc;

%% Import Excel Data
data_cleaning = csvread('cleaned_triple_minus_ones.csv');
[r,c] = size(data_cleaning);

%% Length A: Cleaned

row = 1;

for count=1:r
    if data_cleaning(count,4) <= 4.5
        for col=1:c
            length_a_cleaned(row,col) = data_cleaning(count,col);
        end
        row = row + 1;
    end
end

[r,c] = size(length_a_cleaned);

%% Write to CSV File
csvwrite ('cleaned_length_a.csv', length_a_cleaned);

%% Length B: Cleaned

row = 1;

for count=1:r
    if length_a_cleaned(count,5) <= 5.5
        for col=1:c
            length_b_cleaned(row,col) = length_a_cleaned(count,col);
        end
        row = row + 1;
    end
end

[r,c] = size(length_b_cleaned);

%% Write to CSV File
csvwrite ('cleaned_length_b.csv', length_b_cleaned);

```

TRAINING AND TESTING DATA FOR MISSING DEPTH VALUES

```
%% Start with a clean slate
clear all;
close all;
clc;

%% Import Excel Data
data = csvread('cleaned_length_b.csv');
[r,c] = size(data);

%% Separation of Training and Testing Data to Determine Missing Depth Values

row = 1;

for count=1:r
    if data(count,6) == -1

        for col=1:c
            testing_depth(row,col) = data(count,col);
        end
        row = row + 1;
    end

end

row = 1;

for count=1:r

    if data(count,6) > -1

        for col=1:c
            training_depth(row,col)=data(count,col);
        end
        row = row + 1;
    end
end

%% Write to CSV File
csvwrite ('training_depth.csv', training_depth);
csvwrite ('testing_depth.csv',testing_depth);
```

CLEANING DUPLICATES

```
%% Start with a clean slate
clear all;
close all;
clc;

%% Import Excel Data
cleaned = csvread('N_CleanedDataW_Duplicates.csv');
[r,c] = size(cleaned);

%% Clean Duplicates (Round 1)
```

```

row = 1;
newrow = 2;
row2 = 1;

r_temp=1;
f_row=1;

while row<=r
    if cleaned(row,1) == cleaned(newrow,1) && cleaned(row,2) ==
cleaned(newrow,2)
        for c_temp=1:16
            temp(r_temp,c_temp)=(cleaned(row,c_temp)+cleaned(newrow,c_temp))/2;
            int_cleaned(f_row, c_temp) = temp(r_temp, c_temp);
        end

        f_row = f_row+1;
        r_temp=r_temp+1;

        if row < r
            row = row+1;
            newrow = row+1;
        end
    else

        for col=1:16
            int_cleaned(f_row,col)=cleaned(row,col);
        end

        f_row=f_row+1;
    end

    row = row+1;

    if row<r
        newrow=row+1;
    end
end

```

```

%% Size of Int_Cleaned Matrix
[r,c] = size(int_cleaned);

```

```

%% Clean Duplicates (Round 2)

```

```

row = 1;
newrow = 2;
row2 = 1;

r_temp=1;
f_row=1;

while row<=r
    if int_cleaned(row,1) == int_cleaned(newrow,1) && int_cleaned(row,2) ==
int_cleaned(newrow,2)
        for c_temp=1:16

```



```

temp(r_temp,c_temp)=(int_cleaned(row,c_temp)+int_cleaned(newrow,c_temp))/2;
    final_cleaned(f_row, c_temp) = temp(r_temp, c_temp);
end

f_row = f_row+1;
r_temp=r_temp+1;

if row < r
    row = row+1;
    newrow = row+1;
end
else
    for col=1:16
        final_cleaned(f_row,col)=int_cleaned(row,col);
    end

    f_row=f_row+1;
end

row = row+1;

if row<r
    newrow=row+1;
end
end

%% Size of Int_Cleaned Matrix
[r,c] = size(final_cleaned);
%% Export to CSV
csvwrite('O_CleanedData_NO_Duplicates.csv',final_cleaned);

```

DELETE SINGLE-VISIT WOUNDS

```
%% Start with a clean slate
clear all;
close all;
clc;

%% Import Excel Data
cleaned = csvread('P_DeleteSingles.csv');
[r,c] = size(cleaned);

%% Create Completely Cleaned Matrix

row = 1;

for x=1:r
    if cleaned(x,4) == 1
        for col=1:c
            final(row,col)=cleaned(x,col);
        end
        row = row+1;
    end
end

%% 100% Cleaned Matrix
csvwrite('100_Percent_Cleaned_Data.csv',final);
```

FIND WOUNDS WITH MORE THAN FIVE VISITS

```
%% Start with a clean slate
clear all;
close all;
clc;

%% Import Excel Data
data = csvread('AB_DataWithElimDupl.csv');
[r,c] = size(data);

%%

start_row = 1;
check_row = 2;
count = 1;
new_row=1;
cc=0;

while check_row < r

    wound_id = data(start_row,1);
    if start_row < r
        wound_check = data(check_row,1);
    end

    while wound_id == wound_check;
```

```

    check_row = check_row+1;
    count = count+1;
    wound_check = data(check_row,1);

end

% count
% start_row

if count > 6

    rr = start_row;

    while cc < count
        for col=1:c
            new_data(new_row,col)=data(rr,col);
        end

        new_row = new_row+1;
        rr = rr+1;
        cc = cc+1;
    end

    cc = 0;

end

count = 1;

start_row = check_row;

if start_row < r

    check_row = start_row+1;
end

end

%% No Duplicates
csvwrite('AC_GreaterThan6Visits.csv',new_data);

```

TRANSPOSE DATA BASED ON ASPECT RATIO

```
%% Start with a clean slate
clear all;
close all;
clc;

%% Import Excel Data
AR1 = csvread('AH_AspectRatio1.csv');
[AR1_r,AR1_c] = size(AR1);

AR1_volume = csvread('AH_UniqueAspectRatio1.csv');
[AR1_new_r,AR1_new_c] = size(AR1_volume);

%% Make New Data Matrix Internal Zero Cells = 999
for x=2:AR1_new_r
    for y=2:AR1_new_c
        AR1_volume(x,y) = 999;
    end
end

%% Make New Matrix for L1, L2, D

for x=1:AR1_new_r
    for y=1:AR1_new_c
        AR1_L1(x,y) = AR1_volume(x,y);
        AR1_L2(x,y) = AR1_volume(x,y);
        AR1_D(x,y) = AR1_volume(x,y);
    end
end

%% AR1_Volume

row = 2;
data_row = 1;

col_of_time = 2;

while row <= AR1_new_r

    wound = AR1(data_row,1);
    wound_unique = AR1_volume(row,1);

    while wound == wound_unique

        time = AR1(data_row,6);
        volume = AR1(data_row,10);

        while AR1_volume(1,col_of_time) ~= time && col_of_time < AR1_new_c
            col_of_time = col_of_time+1;
        end

        t = AR1_volume(1,col_of_time);
```

```

    if t == time
        AR1_volume(row,col_of_time) = AR1(data_row,10);
    end

    data_row = data_row+1;

    if data_row <= AR1_r
        wound = AR1(data_row,1);

    else
        break
    end

end

    row = row+1;
    col_of_time = 2;

end

%% AR1_L1

row = 2;
data_row = 1;

col_of_time = 2;

while row <= AR1_new_r

    wound = AR1(data_row,1);
    wound_unique = AR1_L1(row,1);

    while wound == wound_unique

        time = AR1(data_row,6);

        while AR1_L1(1,col_of_time) ~= time && col_of_time < AR1_new_c
            col_of_time = col_of_time+1;

        end

        t = AR1_L1(1,col_of_time);

        if t == time
            AR1_L1(row,col_of_time) = AR1(data_row,7);
        end

        data_row = data_row+1;

        if data_row <= AR1_r
            wound = AR1(data_row,1);

```

```

else
    break
end

end

row = row+1;
col_of_time = 2;

end

%% AR1_L2

row = 2;
data_row = 1;

col_of_time = 2;

while row <= AR1_new_r

wound = AR1(data_row,1);
wound_unique = AR1_L2(row,1);

while wound == wound_unique

time = AR1(data_row,6);

while AR1_L2(1,col_of_time) ~= time && col_of_time < AR1_new_c
    col_of_time = col_of_time+1;

end

t = AR1_L2(1,col_of_time);

if t == time
    AR1_L2(row,col_of_time) = AR1(data_row,8);
end

data_row = data_row+1;

if data_row <= AR1_r
    wound = AR1(data_row,1);

else
    break
end

end

row = row+1;
col_of_time = 2;

```

```

end

%% AR1_D

row = 2;
data_row = 1;

col_of_time = 2;

while row <= AR1_new_r

    wound = AR1(data_row,1);
    wound_unique = AR1_D(row,1);

    while wound == wound_unique

        time = AR1(data_row,6);

        while AR1_D(1,col_of_time) ~= time && col_of_time < AR1_new_c
            col_of_time = col_of_time+1;
        end

        t = AR1_D(1,col_of_time);

        if t == time
            AR1_D(row,col_of_time) = AR1(data_row,9);
        end

        data_row = data_row+1;

        if data_row <= AR1_r
            wound = AR1(data_row,1);

        else
            break
        end

    end

    row = row+1;
    col_of_time = 2;

end

%% Transposed Matrix Based on Aspect Ratio
csvwrite('AI_AspectRatioMatrix1_Volume.csv',AR1_volume);
csvwrite('AI_AspectRatioMatrix1_L1.csv',AR1_L1);
csvwrite('AI_AspectRatioMatrix1_L12.csv',AR1_L2);
csvwrite('AI_AspectRatioMatrix1_D.csv',AR1_D);

```

TIME REMAINING

```
%% Start with a clean slate
clear all;
close all;
clc;

%% Import Excel Data
data = csvread('AL_ToFindTimeRemaining.csv');
[r,c] = size(data);

%% Find Time Remaining

row = 1;
next_row = 2;
count = 1;
t_x=2;
t = 1;

while row < r

    start = data(row,3);
    start_time = data(row,6);
    next = data(next_row,3);
    time(1,1) = start_time;

    while next ~= 0

        if data(next_row,3)
            time(t_x,1) = data(next_row,6);
            t_x = t_x+1;
        end

        if next_row == r
            break
        else
            next_row = next_row+1;
            next = data(next_row,3);
        end

    end

end

t_x = t_x - 1;

while row < next_row
    data(row, 7) = time(t_x,1);

    row = row+1;
    t_x = t_x-1;
end

if next_row == r
    data(next_row,7) = 0;
end
```



```
next_row = row+1;
t_x = 2;

end

%% Transposed Time to Heal
csvwrite('AL_TimeRemaining.csv',data);
```

APPENDIX F: MATLAB CODE, IMAGE ANALYSIS AND EDGE DETECTION

```
%% Start with a clean slate
clear all;
close all;
clc;

%% Import Excel Data
rgb = imread('wound_rgb-2.tif');
% binary = imread('patient2_wound_binary_w_measurements.tif');
% binary = imread('patient11_wound_binary_w_measurement.tif');
% binary = imread('patient2_wound_binary_w_measurements.tif');
binary = imread('patient4_wound_outline.tif');

%% RGB Matrix
binary_imR = squeeze(binary(:,:,1));
binary_imG = squeeze(binary(:,:,2));
binary_imB = squeeze(binary(:,:,3));

%% Edge Detection
sob = edge(binary_imB, 'sobel');
figure, imshow(sob)

can = edge(binary_imB, 'canny');
figure, imshow(can)

%% BW Perimeter

x = 1;
new_x = 1;

BW2 = bwperim(sob);

[r c] = size(BW2);

for row = 2:r
    for col=1:c
        if BW2(row,col) > 0
            contour = bwtraceboundary(BW2, [row, col], 'W', 8,50,'clockwise');

            if(~isempty(contour))

                [c_r, c_c] = size(contour);

                while contour(x,1) > 0 && x < c_r

                    new(new_x, 1) = contour(x,1);
                    new(new_x, 2) = contour(x,2);
                    new(new_x, 3) = 0;

                    x = x+1;
                    new_x = new_x+1;

                end
            end
        end
    end
end
```

```

        x=1;

    end
end
end
end

%% Reduction of Points
new_x = 1;
next_x = 2;

final_x = 1;

copy = new;

[r c] = size(new);

while new_x < r

    start(1,1) = new(new_x,1);
    start(1,2) = new(new_x,2);

    while next_x < r
        check(1,1) = new(next_x,1);
        check(1,2) = new(next_x,2);

        if isequal(start,check)
            new(next_x,1) = 0;
            new(next_x,2) = 0;
        end

        next_x = next_x + 1;
    end

    new_x = new_x + 1;
    next_x = new_x + 1;
end

%% Cleaned Final Matrix

row = 1;

while x < r

    if new(x,1) ~= 0

        final(row,1) = new(x,1);
        final(row,2) = new(x,2);
        final(row,3) = 0;

        row = row+1;

    end

    x = x+4;

```

```
end

%% Image Verification

copy_image = BW2;
row = 1;

[r c] = size(copy_image);
[rr cc] = size(final);

for x=1:rr
    x_point = final(x,1);
    y_point = final(x,2);

    copy_image(x_point, y_point) = 1;
end

figure, imshow(copy_image);
figure, imshow(can);
```

REFERENCES

REFERENCES

1. Merriam-Webster Medical Dictionary. *Dictionary and Thesaurus - Merriam-Webster Online*. Trauma - Definition and More from the Free Merriam-Webster Dictionary 2011; Available from: <http://www.merriam-webster.com/dictionary/trauma>.
2. Bryant, R. and D. Nix, *Acute and chronic wounds* 2006: Mosby.
3. Cooper, D.M., *Acute & Chronic Wounds: Nursing Management, in Assessment, Measurement, and Evaluation: Their Pivotal Roles in Wound Healing*, Ruth Bryant RN MS CWOCN, Editor 2000, Mosby. p. 558.
4. Mayo Clinic. *Wound / Ostomy Care*. 2013 [cited 2013 June 13]; Available from: <http://mayoclinichealthsystem.org/locations/mankato/medical-services/wound-and-ostomy-care>.
5. Dallam, L., et al., *Pressure ulcer pain: assessment and quantification*. Journal of Wound Ostomy & Continence Nursing, 1995. **22**(5): p. 211.
6. Lammers, R.L., D.L. Hudson, and M.E. Seaman, *Prediction of traumatic wound infection with a neural network-derived decision model* 1*. The American journal of emergency medicine, 2003. **21**(1): p. 1-7.
7. Pecoraro, R., G. Reiber, and E. Burgess, *Pathways to diabetic limb amputation. Basis for prevention*. Diabetes Care, 1990. **13**(5): p. 513.
8. Steed, D.L., et al., *Guidelines for the prevention of diabetic ulcers*. Wound Repair and Regeneration, 2008. **16**(2): p. 169-174.
9. Lavery, L.A., et al., *Diabetes-related lower-extremity amputations disproportionately affect Blacks and Mexican Americans*. Southern medical journal, 1999. **92**(6): p. 593.
10. Lavery, L.A., *Discussion: Off-Loading the Diabetic Foot for Ulcer Prevention and Healing*. Plastic and Reconstructive Surgery, 2011. **127**: p. 257S.
11. Severens, J.L., et al., *The cost of illness of pressure ulcers in The Netherlands*. Advances in skin & wound care, 2002. **15**(2): p. 72.
12. Netherlands, H.C.o.t., *The Hague: Health Council of the Netherlands*. Pressure Ulcers, 1999. **Publication 1999/23**.
13. Gordon, M.D., et al., *Review of evidenced-based practice for the prevention of pressure sores in burn patients*. Journal of Burn Care & Research, 2004. **25**(5): p. 388.

14. Kuhn, B. and S. Coulter, *Balancing the pressure ulcer cost and quality equation*. Nursing economic\$, 1992. **10**(5): p. 353.
15. Boulton, A.J.M., et al., *Comprehensive foot examination and risk assessment*. Diabetes Care, 2008. **31**(8): p. 1679.
16. Bansal, C., et al., *Decubitus ulcers: a review of the literature*. International journal of dermatology, 2005. **44**(10): p. 805-810.
17. American Podiatric Medical Association, I. *Diabetic Wound Care*. 2012 [cited 2013 June 20]; Available from: <http://www.apma.org/Learn/FootHealth.cfm?ItemNumber=981>.
18. National Institute of Health. *National Diabetes Statistics, 2011*. 2011 [cited 2011 April 16]; Available from: <http://diabetes.niddk.nih.gov/dm/pubs/statistics/ - Amputations>.
19. Bharara, M., et al., *Diabetes and landmine related amputations: a call to arms to save limbs*. International Wound Journal, 2009. **6**(1): p. 2-3.
20. Kruse, I. and S. Edelman, *Evaluation and treatment of diabetic foot ulcers*. Clinical Diabetes, 2006. **24**(2): p. 91.
21. Cardinal, M., D.E. Eisenbud, and D.G. Armstrong, *Wound shape geometry measurements correlate to eventual wound healing*. Wound Repair and Regeneration, 2009. **17**(2): p. 173-178.
22. Barone, S., A. Paoli, and A. Razionale, *Assessment of chronic wounds by three-dimensional optical imaging based on integrating geometrical, chromatic, and thermal data*. Proceedings of the Institution of Mechanical Engineers, Part H: Journal of Engineering in Medicine, 2011. **225**(2): p. 181-193.
23. Ranachowska, C., et al., *Diagnostic imaging of the diabetic foot*. Nuclear Medicine Review, 2010. **13**(1): p. 18-17.
24. Neidrauer, M. and E.S. Papazoglou, *Optical Non-invasive Characterization of Chronic Wounds*. Bioengineering Research of Chronic Wounds, 2009: p. 381-404.
25. Berry, C., D.R. Murdoch, and J.J.V. McMurray, *Economics of chronic heart failure*. European Journal of Heart Failure, 2001. **3**(3): p. 283-291.
26. Flynn, C., *Finite element models of wound closure*. Journal of Tissue Viability, 2010. **19**(4): p. 137-149.
27. Reddy, M., S.S. Gill, and P.A. Rochon, *Preventing pressure ulcers: a systematic review*. JAMA: the journal of the American Medical Association, 2006. **296**(8): p. 974.
28. University Health Care Center. *Wound Care: Information for You from your Healthcare Team*. 2011 [cited 2011 April 4]; Available from: http://www.upstate.edu/pated/document/dry_sterile_dressing.pdf.
29. United States Government Accountability Office. *Baby Boom Generation: Retirement of Baby Boomers Is Unlikely to Precipitate Dramatic Decline in Market Returns, but Broader Risks Threaten Retirement Security*. 2006 [cited 2013 June 24]; Available from: <http://www.gao.gov/assets/260/250908.html>.

30. Pruchno, R., *Not Your Mother's Old Age: Baby Boomers at Age 65*. The Gerontologist, 2012. **52**(2): p. 149-152.
31. Sen, C.K., et al., *Human skin wounds: a major and snowballing threat to public health and the economy*. Wound Repair and Regeneration, 2009. **17**(6): p. 763-771.
32. Supp, D.M. and S.T. Boyce, *Engineered skin substitutes: practices and potentials*. Clinics in dermatology, 2005. **23**(4): p. 403-412.
33. St-Supery, V., et al., *Wound Healing Assessment: Does the Ideal Methodology for a Research Setting Exist?* Annals of plastic surgery, 2011. **67**(2): p. 193.
34. Cutler, N.R., et al., *Comparison of quantitative methodologies to define chronic pressure ulcer measurements*. Decubitus, 1993. **6**(6): p. 22.
35. Keast, D.H., et al., *Contents*. Wound Repair and Regeneration, 2004. **12**: p. s1-s17.
36. Thomas, D.R., *Existing Tools: are they meeting the challenges of Pressure ulcer healing?* Advances in wound care: the journal for prevention and healing, 1997. **10**(5): p. 86.
37. Chin, J., A. Zeid, and S. Kamarthi, *Investigating A Framework For Modeling And Analysis For Wound Progression* in ASME 2012 International Mechanical Engineering Congress & Exposition 2012: Houston, Tx.
38. Neidrauer, M.T., *Assessment of chronic wounds using in vivo diffuse near infrared spectroscopy*, 2010, Drexel University.
39. Gefen, A., *Bioengineering Research of Chronic Wounds: A Multidisciplinary Study Approach* 2009: Springer Verlag.
40. Thomas, A.C. and A.B. Wysocki, *The healing wound: a comparison of three clinically useful methods of measurement*. Decubitus, 1990. **3**(1): p. 18.
41. Langemo, D., et al., *Measuring wound length, width, and area: which technique?* Advances in skin & wound care, 2008. **21**(1): p. 42.
42. Majeske, C., *Reliability of wound surface area measurements*. Physical Therapy, 1992. **72**(2): p. 138-141.
43. Bulstrode, C., A. Goode, and P. Scott, *Stereophotogrammetry for measuring rates of cutaneous healing: a comparison with conventional techniques*. Clinical science (London, England: 1979), 1986. **71**(4): p. 437.
44. Mayrovitz, H.N. and L.B. Soontupe, *Wound areas by computerized planimetry of digital images: accuracy and reliability*. Advances in skin & wound care, 2009. **22**(5): p. 222.
45. Chen, M.H., et al., *Development of a thermal and hyperspectral imaging system for wound characterization and metabolic correlation*. Johns Hopkins APL technical digest, 2005. **26**(1): p. 67.
46. Albouy, B., Y. Lucas, and S. Treuillet. *3D Modeling from Uncalibrated Color Images for a Complete Wound Assessment Tool*. in Engineering in Medicine and Biology Society, 2007. EMBS 2007. 29th Annual International Conference of the IEEE. 2007.
47. Malian, A., A. Azizi, and F. Van Den Heuvel, *MEDPHOS: a new photogrammetric system for medical measurement*. Proceedings of the XXth ISPRS International archives of

- photogrammetry, remote sensing, and spatial information sciences, Istanbul, Turkey, 2004: p. 12-23.
48. Plassmann, P. and T. Jones, *MAVIS: a non-invasive instrument to measure area and volume of wounds. Measurement of Area and Volume Instrument System*. Medical engineering & physics, 1998. **20**(5): p. 332.
 49. Medline, *Wound and Skin Care Reference Guide* 2009, Mundelein: Medline Industries.
 50. Ankrom, M.A., et al., *Pressure-related deep tissue injury under intact skin and the current pressure ulcer staging systems*. Advances in skin & wound care, 2005. **18**(1): p. 35.
 51. Liu, X., et al., *Wound measurement by curvature maps: a feasibility study*. Physiological Measurement, 2006. **27**: p. 1107.
 52. Ahn, C. and R. Salcido, *Advances in wound photography and assessment methods*. Advances in skin & wound care, 2008. **21**(2): p. 85.
 53. Jones, B. and P. Plassmann, *Digital infrared thermal imaging of human skin*. Engineering in Medicine and Biology Magazine, IEEE, 2002. **21**(6): p. 41-48.
 54. Jones, B.F., *A reappraisal of the use of infrared thermal image analysis in medicine*. Medical Imaging, IEEE Transactions on, 1998. **17**(6): p. 1019-1027.
 55. Romanelli, M., et al., *Technological advances in wound bed measurements*. Wounds, 2002. **14**(2): p. 58-66.
 56. Krouskop, T.A., R. Baker, and M.S. Wilson, *A noncontact wound measurement system*. Journal of Rehabilitation Research and Development, 2002. **39**(3): p. 337-346.
 57. Ruminski, J., et al., *Thermal parametric imaging in the evaluation of skin burn depth*. Biomedical Engineering, IEEE Transactions on, 2007. **54**(2): p. 303-312.
 58. Crenshaw, R.P. and L.M. Vistnes, *A decade of pressure sore research: 1977-1987*. J Rehabil Res Dev, 1989. **26**(1): p. 63-74.
 59. Sapico, F.L., et al., *Quantitative microbiology of pressure sores in different stages of healing*. Diagnostic microbiology and infectious disease, 1986. **5**(1): p. 31-38.
 60. Seiler, W. and H. Strehlein, *Recent findings on decubitus ulcer pathology: implications for care*. Geriatrics, 1986. **41**(1): p. 47.
 61. European Pressure Ulcer Advisory Panel and National Pressure Ulcer Advisory Panel *Prevention of Pressure Ulcers: Quick Reference Guide*. 2009. 8-10.
 62. Lait, M.E. and L.N. Smith, *Wound management: a literature review*. Journal of clinical nursing, 1998. **7**(1): p. 11-17.
 63. SHEA, J.D., *Pressure sores classification and management*. Clinical Orthopaedics and Related Research, 1975. **112**: p. 89.
 64. Lazarus, G.S., et al., *Definitions and guidelines for assessment of wounds and evaluation of healing*. Wound Repair and Regeneration, 2002. **2**(3): p. 165-170.
 65. Bergin, S. and P. Wraight, *Silver based wound dressings and topical agents for treating diabetic foot ulcers*. Cochrane Database Syst Rev, 2006. **1**.

66. Stromberg, K., et al., *Regulatory concerns in the development of topical recombinant ophthalmic and cutaneous wound healing biologics*. Wound Repair and Regeneration, 2002. **2**(3): p. 155-164.
67. Robson, M.C., *WOUND INFECTION: A Failure of Wound Healing Caused by an Imbalance of Bacteria*. Surgical Clinics of North America, 1997. **77**(3): p. 637-650.
68. Kujath, P. and A. Michelsen, *Wounds From physiology to wound dressing*. Deutsches Arzteblatt International, 2008. **105**(13): p. 239.
69. Clark, J.J., *Wound repair and factors influencing healing*. Critical Care Nursing Quarterly, 2002. **25**(1): p. 1-12.
70. Brissett, A.E. and D.B. Hom, *The effects of tissue sealants, platelet gels, and growth factors on wound healing*. Current opinion in otolaryngology & head and neck surgery, 2003. **11**(4): p. 245-250.
71. Hooper, B.J. and M.P. Goldman, *Primary dermatologic care* 1999: Mosby.
72. Leopold, J.R., *Clinical Manager, MSN APRN CWCN CDE, Morganti Wound Care Center*, J. Chin, Editor 2012.
73. Wicke, C., et al., *Aging influences wound healing in patients with chronic lower extremity wounds treated in a specialized wound care center*. Wound Repair and Regeneration, 2009. **17**(1): p. 25-33.
74. The Wound Healing Society, *Wound Care Guidelines*. Wound Repair and Regeneration, 2006(December 2006): p. 29.
75. Rennert, R., et al., *Standardization of wound photography using the wound electronic medical record*. Advances in skin & wound care, 2009. **22**(1): p. 32-38.
76. Nada Kecelj-Leskovec MD, M., et al., *Measurement of venous leg ulcers with a laser-based three-dimensional method: Comparison to computer planimetry with photography*. Wound Repair and Regeneration, 2007. **15**(5): p. 767-771.
77. Defloor, T., et al., *Statement of the European Pressure Ulcer Advisory Panel--Pressure ulcer classification*. J WOCN, 2005. **32**: p. 302-306.
78. Albouy, B., Y. Lucas, and S. Treuillet. *3d Modeling from uncalibrated color images for a complete wound assessment tool*. 2007. IEEE.
79. Papazoglou, E.S., et al., *Image analysis of chronic wounds for determining the surface area*. Wound Repair and Regeneration, 2010. **18**(4): p. 349-358.
80. Sugama, J., et al., *A study of the efficiency and convenience of an advanced portable Wound Measurement System (VISITRAKTM)*. Journal of clinical nursing, 2007. **16**(7): p. 1265-1269.
81. Halstead, L.S., et al., *Teleassessment compared with live assessment of pressure ulcers in a wound clinic: a pilot study*. Advances in skin & wound care, 2003. **16**(2): p. 91-96.
82. Salmhofer, W., et al., *Wound teleconsultation in patients with chronic leg ulcers*. Dermatology, 2005. **210**(3): p. 211-217.

83. Pocket Professions, I. *WoundSmart - The Professional Wound Care Documentation Tool*. 2013; Available from: <https://itunes.apple.com/us/app/woundsmart-professional-wound/id548016466?mt=8>.
84. Havelin, R. *Wound Analyzer*. 2013; Available from: <https://itunes.apple.com/us/app/pressure-wound-analyzer/id449564315?mt=8>.
85. McDonald, H. and F. Alpert. *Predicting consumer innovative behavior using alternative theories and likelihood measures: a longitudinal study*. 2011. American Marketing Association.
86. Tufts Medical Center. *Vascular, Wound, and Hyperbaric Center*. 2013 [cited 2013 March]; Available from: <http://www.tuftsmedicalcenter.org/OurServices/SpecialServicesandCenters/CenterforWoundHealing/>.
87. Nemeth, M.E., S. Sprigle, and A. Gajjala, *Clinical Usability of a Wound Measurement Device*. 2010.
88. Santamaria, N., F. Ogce, and A. Gorelik, *Healing rate calculation in the diabetic foot ulcer: Comparing different methods*. Wound Repair and Regeneration, 2012.
89. Cardinal, M., et al., *Early healing rates and wound area measurements are reliable predictors of later complete wound closure*. Wound Repair and Regeneration, 2008. **16**(1): p. 19-22.
90. Han, J. and M. Kamber, *Data mining: concepts and techniques*2006: Morgan Kaufmann.
91. Dayton, C.M., *Logistic regression analysis*. Stat, 1992: p. 474-574.
92. Shmueli, G., N.R. Patel, and P.C. Bruce, *Data mining for business intelligence: Concepts, techniques, and applications in Microsoft Office Excel with XLMiner*2010: Wiley.
93. Sherrod, P.H., *Nonlinear regression analysis program*, 2005, Version.
94. Beaumont, R., *An Introduction to Statistics: Survival Analysis 1*, 2010.
95. Fox, J., *Cox Proportional-Hazards Regression for Survival Data*, 2002: Appendix to An R and S-PLUS Companion to Applied Regression.
96. Benítez-Parejo, N., M.M. Rodríguez del Águila, and S. Pérez-Vicente, *Survival analysis and Cox regression*. Allergologia et Immunopathologia, 2011. **39**(6): p. 362-373.
97. Jr., L.H. and J. Hossain, *Logistic Regression & Survival Analysis*, 2008.
98. IBM. *Cox-Regression*. 2011 [cited 2013 April 12]; Available from: http://publib.boulder.ibm.com/infocenter/spsstat/v20r0m0/index.jsp?topic=%2Fcom.ibm.spss.statistics.cs%2Fcoxregression_table.htm.
99. Mason, C. *Cox Proportional Hazard Models*. 2005.
100. Haykin, S.S., et al., *Neural networks and learning machines*. Vol. 3. 2009: Prentice Hall.
101. Chen, W.S. and Y.K. Du, *Using neural networks and data mining techniques for the financial distress prediction model*. Expert Systems with Applications, 2009. **36**(2): p. 4075-4086.

102. Tzeng, F.-Y. and K.-L. Ma. *Opening the black box-data driven visualization of neural networks*. in *Visualization, 2005. VIS 05. IEEE*. 2005. IEEE.
103. Frontline Solvers. *XLMiner Capabilities Overview*. 2013 [cited 2013 February 20]; Available from: <http://www.solver.com/xlminer-capabilities-overview>.
104. Rengier, F., et al., *3D printing based on imaging data: review of medical applications*. International journal of computer assisted radiology and surgery, 2010. **5**(4): p. 335-341.
105. Alabama Corporate Extension System (Alabama A&M and Auburn Universities), *Explanation of the LAB Color Space*, 2013, Alabama A&M and Auburn University: http://www.aces.edu/dept/fisheries/education/pond_to_plate/documents/ExplanationoftheLABColorSpace.pdf.
106. <http://www.linocolor.com>. *CIE Lab Color Space*. 2013 [cited 2013 April 24, 2013]; Available from: <http://www.linocolor.com>.
107. Lupo, J. and R. Balcerak. *The physical basis of thermal imaging*. 2000.
108. Cayless, M. and A.M. Marsden, *Lamps and lighting: a manual of lamps and lighting*1983: Hodder Arnold.
109. Bharara, M., et al., *Wound Inflammatory Index: A Proof of Concept Study to Assess Wound Healing Trajectory*. Journal of Diabetes Science and Technology, 2010. **4**(4): p. 773-779.
110. Roback, K., *Vormerötning fr diagnos av begynnande fotproblem vid diabetes: Metodöversikt samt fröksanvöndning av fotindikatorn SpectraSole Pro 1000*. 2009.
111. Roback, K., *An overview of temperature monitoring devices for early detection of diabetic foot disorders*. Expert Review of Medical Devices, 2010. **7**(5): p. 711-718.
112. Montgomery, D.C., G.C. Runger, and N.F. Hubele, *Engineering Statistics*2004, New York, NY: John Wiley & Sons. 461.
113. Posthauer, M.E. *Albumin and Pre-albumin: Are They Markers of Nutritional Status in Wound Management?* 2011 [cited 2013 March 14]; Available from: <http://www.woundsource.com/blog/albumin-and-pre-albumin-are-they-markers-nutritional-status-wound-management>.
114. Nutrition 411. *Albumin as an Indicator of Nutritional Status*. 2011 [cited 2013 March 10]; Available from: Albumin as an Indicator of Nutritional Status.
115. Fausett, L., *Fundamentals of Neural Networks: Architectures, Algorithms, and Applications*1994, Upper Saddle River, New Jersey: Prentice-Hall, Inc.
116. Collins, T.J., *ImageJ for microscopy*. Biotechniques, 2007. **43**(1 Suppl): p. 25-30.
117. Research Services Branch, *ImageJ: Image Processing and Analysis in Java*, N.I.o.N.D.a.S. National Institute of Mental Health, Editor 2012: Washington D.C.
118. ImageJ. *Technical Proposal*. 2009 [cited 2013 April 9]; Available from: <http://developer.imagej.net/proposal>.
119. Maini, R. and H. Aggarwal, *Study and comparison of various image edge detection techniques*. International Journal of Image Processing (IJIP), 2009. **3**(1): p. 1-11.

120. Dassault Systemes. *ScanTo3D Overview*. 2013 [cited 2013 April 25]; Available from: http://help.solidworks.com/2012/English/SolidWorks/ScanTo3D/c_Scanto3d_overview.htm.
121. Rusu, R.B. and S. Cousins. *3d is here: Point cloud library (pcl)*. in *Robotics and Automation (ICRA), 2011 IEEE International Conference on*. 2011. IEEE.
122. Boston University. *Cox Proportional Hazards Regression Analysis*. 2013 [cited 2013 April 18]; Available from: http://sph.bu.edu/otlt/MPH-Modules/BS/BS704_Survival/BS704_Survival6.html.
123. Swain, S., *Personal Communication*, J. Chin, Editor 2013.

© Copyright 2013 by Jessica Selina Cho Chin
All Rights Reserved